Probabilistic Optimization of Vibrational Systems under Stochastic Excitation Containing Extreme Forcing Events

by

Han Kyul Joo

S.M., Massachusetts Institute of Technology (2014)

Submitted to the Department of Mechanical Engineering
in partial fulfillment of the requirements for the degree of

Doctor of Philosophy in Mechanical Engineering

at the

MASSACHUSETTS INSTITUTE OF TECHNOLOGY

June 2017

Signature redacted

Author .....
Department of Mechanical Engineering
Mar 16, 2017

Signature redacted

Certified by .....
Themistoklis P. Sapsis
Associate Professor of Mechanical and Ocean Engineering
Thesis Supervisor

Signature redacted

Accepted by .....
Rohan Abeyaratne
Quentin Berg Professor of Mechanics
Chairman, Committee on Graduate Students

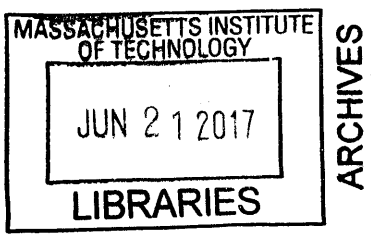

Probabilistic Optimization of Vibrational Systems under Stochastic Excitation Containing Extreme Forcing Events

by

Han Kyul Joo

Submitted to the Department of Mechanical Engineering
on Mar 16, 2017, in partial fulfillment of the
requirements for the degree of
Doctor of Philosophy in Mechanical Engineering

Abstract

For the past few decades there has been an increased interest for efficient quantification schemes of the response statistics of vibrational systems operating in stochastic settings with the aim of providing optimal parameters for design and/or operation. Examples include energy harvesting configurations from ambient vibrations and stochastic load mitigation in vibrational systems. Although significant efforts have been made to provide computationally efficient algorithms for the response statistics, most of these efforts are restricted to systems with very specific characteristics (e.g. linear or weakly nonlinear systems) or to excitations with very idealized form (e.g. white noise or deterministic periodic). However, modern engineering applications require the analysis of strongly nonlinear systems excited by realistic loads that have radically different characteristics from white noise or periodic signals. These systems are characterized by essentially non-Gaussian statistics (such as bimodality of the probability distributions, heavy tails, and non-trivial temporal correlations) caused by the nonlinear characteristics of the dynamics, the correlated (non-white noise) structure of the excitation, and the possibility of non-stationary forcing characteristics (intermittency) related to extreme events.

In this thesis, we first address the problem of deriving semi-analytical approximations for the response statistics of strongly nonlinear systems subjected to stationary, correlated (colored) excitation. The developed method combines two-times moment equations with new non-Gaussian closures that reflect the underlying nonlinear dynamics of the system. We demonstrate how the proposed approach overcomes the limitations of traditional statistical linearization schemes and can approximate the statistical steady state solution. The new method is applied for the analysis of bistable energy harvesters with mechanical and electromagnetic damping subjected to correlated excitations. It allows for the computation of semi-analytical expressions for the non-Gaussian probability distributions of the response and the temporal correlation functions, with minimal computational effort involving the solution of a low-dimensional optimization problem. The method is also assessed in higher-dimensional

problems involving linear elastic rods coupled to a nonlinear energy harvester.

In the second part of this thesis, we consider the problem of mechanical systems excited by stochastic loads with non-stationary characteristics, modeling extreme events. Such excitations are common in many environmental settings and they lead to heavy-tailed probability distribution functions. For both design and operation purposes it is important to efficiently quantify these high-order statistical characteristics. To this end, we apply a recently developed approach, the probabilistic decomposition-synthesis (PDS) method. Under suitable but sufficiently generic assumptions, the PDS method allows for the probabilistic and dynamic decoupling of the regime associated with extreme events from the "background" fluctuations. Using this approach we derive fully analytical formulas for the heavy tailed probabilistic distribution of linear structural modes subjected to stochastic excitations containing extreme events. The derived formulas can be evaluated with very small computational cost and are shown to accurately capture the complicated heavy-tailed and asymmetrical features in the probability distribution many standard deviations away from the mean. We finally extend the scheme to quantify the response statistics of nonlinear multi-degree-of-freedom systems under extreme forcing events, emphasizing again accurate heavy-tail statistics.

The developed scheme is applied for the design and optimization of small mechanical attachments that can mitigate and suppress extreme forcing events delivered to a primary system. Specifically, we consider the suppression of extreme impacts due to slamming in high speed craft motion via optimally designed nonlinear springs/attachments. The very low computational cost for the quantification of the heavy tail structure of the response allows for direct optimization on the nonlinear characteristics of the attachment. Based on the results of this optimization we propose a new asymmetric nonlinear spring that far outperforms optimal cubic springs and tuned mass dampers, which have been used in the past. Accuracy of the developed method is illustrated through direct comparisons with Monte-Carlo simulations.

Thesis Supervisor: Themistoklis P. Sapsis
Title: Associate Professor of Mechanical and Ocean Engineering

Acknowledgments

I would like express my greatest appreciation to Prof. Themistoklis Sapsis who served as my thesis supervisor. He is truly an excellent mentor with sharp insights. Themis always tried to draw a bigger picture not only for the research but also for the entire phd life. His inputs were invaluable and helped me succeed and win through whenever I stand at the crossroads of my career. I'll never forget the very first moment I started working with him for the PhD research, and I am very much proud of being one of the first graduate students in his group.

I would also like to acknowledge my PhD committee, Prof. Nicholas Patrikalakis and Prof. Konstantin Turitsyn, for their valuable feedback and constructive advice on my research. They have taken significant amount of time directing my research toward the right path. It is my sincere honor to have them as my committee members. I am also very grateful for my former undergraduate advisor in Japan, Prof. Takashi Maekawa, for his endless cares and supports. Needless to mention, all the academic foundations that I acquired while I was working with him have served as a significant backbone on the way to PhD. I would like to also thank administrative assistants at mechanical engineering department, Ms. Barbara Smith, Ms. Leslie Regan, and Ms. Joan Kravit, for their warm support.

I would like to take this opportunity to thank all those who have interacted and worked with me at MIT. Especially I would like to acknowledge members of SAND lab, Jocelyn Kluger, Mustafa Mohamad, Zhong Yi Wan, Saviz Mowlavi, Dr. Will Cousins, Dr. Hessam Babaee, and Dr. Mohammad Farazmand for being useful resources whenever I faced difficulties. In particular, I would like to thank Mustafa for tons of hours we spent together for technical discussions. I would like to thank many peers I met in Boston including but not limited to Dongkwan Kim, Dr. Alan Gye hyun Kim, Dr. Donghun Kim, Sucheol Shin, Hyung Won Chung, Kyungyong Choi, Junghyun Lee, Joohyun Seo, Siwon Choi, Anna Lee, So Yeon Lim, Barom Yang, Dr. Grace Han, Ingon

Lee, Jongwoo Lee, and many others. Countless social interactions with fried chickens and beers are unforgettable memories.

I would like to share my special thanks to all my friends, mentors, colleagues. Especially I would like to acknowledge the class of 2017 members, Doojoon Jang, Minkyun Noh, Heejin Ahn, Hyundo Lee, Hyeonyu Kim, Jeonyoon Lee, Keunhwan Pack, Hyunho Kim, and Dr. Junghee Park, for the unforgettable precious memories. Also I would thank Dong Hoon Yi, Byung Gu Cho, Soon Ju Choi, Byungjin Koo, Dr. Jiyoun Chang and all other members of KGSAME and KGSA. I'll miss you all.

I cannot complete the acknowledgment without mentioning Taegu Noh, who I spent most of my time together at college. Thank you for your warm cares. Also I would like to acknowledge many of my high school friends, YongRak Jang, Yejoon Chung, Euijun Noh, Seungho Choi, Jaehoon Song, Kyojun Chu, Jaeyoon Lee, Joon Woo Baek, Dooyeon Cho, Sunghwan Kim, Ji Seok Park, and many others. Thank you all for the supports, and wish you the best of luck for all of your careers.

Last but not least, I would like to thank my father, Jaejung Joo, my mother, Hoeun Oh, and my younger sister, Hanna Joo, who have been extremely supportive and caring all the time throughout my life. I love you.

The PhD research has been funded by the Kwanjeong Educational Foundation (2012-2014), a Samsung Scholarship (2014-2017) and the MIT Energy Initiative with support under the grant 'Nonlinear Energy Harvesting From Broad-Band Vibrational Sources By Mimicking Turbulent Energy Transfer Mechanisms'.

Contents

List of Figures

Chapter 1

Introduction

1.1 Background and Motivation

For the past few decades there has been an increased interest for efficient quantification schemes of the response statistics of vibrational systems operating in stochastic settings with the aim of providing optimal parameters for design and/or operation. Examples include energy harvesting configurations from ambient vibrations and stochastic load mitigation in vibrational systems. Although significant efforts have been made to provide computationally efficient algorithms for the response statistics, most of these efforts are restricted to systems with very specific characteristics (e.g. linear or weakly nonlinear systems) or to excitations with very idealized form (e.g. white noise or deterministic periodic). However, modern engineering applications require the analysis of strongly nonlinear systems excited by realistic loads that have radically different characteristics from white noise or periodic signals. These systems are characterized by essentially non-Gaussian statistics (such as bimodality of the probability distributions, heavy tails, and non-trivial temporal correlations) caused by the nonlinear characteristics of the dynamics, the correlated (non-white noise) structure of the excitation, and the possibility of non-stationary forcing characteristics (intermittency) related to extreme events. These are apparent in the ocean engineering environment where for instance it has been repeatedly reported that extreme and rare ocean waves can lead to cargo damage or cargo loss, capsizing of ships and, in catastrophic situation,

injuries on human beings [12, 84, 152].

The inevitable uncertainty introduced through the stochastic character of the excitation and/or the uncertainty of the parameters, can be adequately captured through a probabilistic perspective, and therefore significant efforts have been made to provide statistical and probabilistic characteristics of the response. The Fokker-Planck-Kolmogorov (FPK) equation provides complete statistical description of the response probability density function [155, 45, 43]. However, analytical solutions for the steady state pdf of the FPK equation is only available for very few systems. Moreover, FPK equation cannot easily handle stochastic excitations other than the Gaussian white noise [25]. For systems under correlated excitations, one can utilize the joint response-excitation pdf scheme to obtain the complete description of response statistics [126, 153, 27]. However, the large computational cost associated with solving high-dimensional transport equations hinders the applicability.

In order to lower the computational cost, semi-analytical schemes have been developed. Among them, the most popular scheme is the statistical linearization method which replaces the nonlinear equations of motion with a linear set by minimizing the statistical difference [24, 22]. The accuracy of this approach relies on the assumption of the Gaussian distribution for the response. Therefore, in cases where the actual response statistics deviate from Gaussian, the application of statistical linearization is less straightforward and often not very successful [73, 122, 137]. An alternative scheme is to derive moment equations that describe the evolution of response statistical moments [125, 19, 14]. The challenge however with moment equations arises again if the system contains strong nonlinearities, in which case one needs to apply appropriate closures to truncate the infinite system of moment equations. Gaussian closure schemes provide in many cases sufficiently accurate response statistics [66]. However, if the system is essentially nonlinear, non-Gaussian closure techniques should be utilized [33, 34, 54] in which case it is not always straightforward on how to choose the closure parameters [31].

Apart of the technical challenges associated with the strong nonlinearities, the assumption for stationary stochastic excitation is often not sufficient for representing uncertainty associated with transient events, such as extreme forcing events. Important examples include ocean waves with extreme magnitude (i.e. freak and rogue waves [112, 105]), slamming loads in high speed crafts, vehicles hitting deep potholes, and ice loads acting on offshore structures [85]. Such intermittent rare and extreme forcing events have been represented as identically distributed independent impulses arriving at random times, and accordingly studies on the response statistics under Poisson white noise gained a growing attention. Generalized FPK equation or Kolmogorov-Feller (KF) equation is the governing equation which provides the evolution of response pdf under Poisson white noise. However, the exact analytical solution for the statistical steady state probability density function is only available under special conditions [151]. Alternative methodologies such as path integral method [82, 65, 8] and the stochastic averaging method [161, 160] have also been developed, but solving the FP or KF equations is often very expensive even for low dimensional systems [40].

1.2 Research Objectives

In this work, we first develop a moment equation closure minimization (MECC) method for the parsimonious approximation of the steady state statistical structure of strongly nonlinear systems, subjected to correlated excitations. The approach relies on the derivation of moment equations that describe the dynamics governing the two-time statistics. These are combined with a non-Gaussian pdf representation for the joint response-excitation statistics. We then derive a closure scheme which we formulate in terms of a consistency condition involving the second order statistics of the response, the closure constraint. A similar condition, the dynamics constraint, is also derived directly through the moment equations. These two constraints are formulated as a low-dimensional minimization problem with respect to unknown parameters of the

representation, the minimization of which imposes an interplay between the dynamics and the adopted closure. This method will allow the semi-analytical representation of the two-time, non-Gaussian structure of the solution as well as the joint statistical structure of the response-excitation over different time instants.

We then apply the developed approach to analyze the response statistics of essentially nonlinear vibrational systems under correlated stochastic excitations. These are important for a variety of applications such as energy harvesting and stochastic forcing mitigation. We demonstrate the effectiveness of the method through bistable nonlinear energy harvesters with mechanical and electromagnetic damping and we show that the results compare favorably with direct Monte-Carlo Simulations. The method is also demonstrated in higher dimensional systems such as a continuous elastic rods coupled to nonlinear elements. The developed method is one of the main building blocks for analyzing the response of systems under stationary stochastic excitation containing rare and extreme events that we study next.

Specifically, the next topic involves the statistical quantification of systems subjected to statistically non-stationary excitations. In particular, we characterize the complex, heavy-tailed probability distribution functions describing the response and its local extrema for structural systems subjected to random forcing that includes extreme events. The approach is based on the probabilistic decomposition-synthesis method where we decouple rare events regimes from the background fluctuations. The result of the analysis has the form of a semi-analytical approximation formula for the pdf of the response and the pdf of the local extrema. For special limiting cases (lightly damped or heavily damped systems), the analysis provides fully analytical approximations. We also demonstrate how the method can be applied to higher dimensional structural systems through a two-degrees-of-freedom structural system undergoing rare events due to intermittent forcing. The derived formulas can be evaluated with very small computational cost and are shown to accurately capture the complicated heavy-tailed and asymmetrical features in the probability distribution many standard deviations

away from the mean, through comparisons with expensive Monte-Carlo simulations.

In the last part of this thesis we focus on the quantification and optimization of the response statistics of general nonlinear multi-degree-of-freedom systems under extreme forcing events, emphasizing accurate heavy-tail statistics. This is a direct extension of the previous semi-analytical scheme applied to linear multi-degree-of-freedom systems under stochastic excitations containing extremes, where we decomposed rare events from background fluctuations by the probabilistic decomposition-synthesis technique. We appropriately adapt the developed scheme for the nonlinear case and then apply it to the design and optimization of small attachments that can mitigate and suppress extreme forcing events delivered to a primary system. We apply the framework for the suppression of extreme responses on prototype ocean engineering systems: *the suspended seat* and *the suspended seat-deck* problem in a high speed craft in rough seas. The suppression is performed via optimal attachments through parametric optimization by minimization of the forth-order moments of the response. We also perform design optimization on the nonlinear characteristics of the attachment (employing a general, assymetric piecewise linear from) and propose a new design that far outperforms optimal cubic energy sink and tuned mass dampers. We emphasize that the proposed optimization scheme is practically infeasible with traditional methods due to the large computational cost. Feasibility is achieved through the developed quantification framework for extreme event statistics. For all steps of the analysis accuracy of the estimation method is illustrated through direct comparisons with Monte-Carlo simulations.

1.3 Thesis Organization

The thesis is organized as follows. In chapter 2, we provide a survey of probabilistic computational methods for stochastic dynamical systems. Definitions, derivations, and applications with appropriate references are provided for a selected number of

topics. In chapter 3, we present the formulation of the moment equation copula closure (MECC) method for nonlinear systems under correlated excitations [69] . Applications of the MECC method are illustrated in chapter 4 considering a bistable nonlinear oscillator. Generalized examples such as the continuous undamped elastic rod are also considered, and the results are compared with direct Monte-Carlo simulations. In chapter 5, we provide the characterization of complex, heavy-tailed probability distribution functions describing the response and its local extrema for structural systems subjected to random forcing that includes extreme events [68]. In chapter 6, the developed computational framework is applied on the probabilistic design and optimization of ocean structures subjected to stochastic excitation containing extreme forcing events [67]. In chapter 7, we conclude the thesis with recommendations for future work.

Chapter 2

Survey of Probabilistic Computational Approaches for Stochastic Dynamical Systems

In a variety of systems uncertainty in the dynamics and system parameters plays a very important role and therefore a deterministic consideration can be very restrictive when it comes to the analysis of the response or optimization of the operation. Furthermore, the co-existence of stationary stochastic excitations and rare and extreme forcing events make the deterministic model even harder to describe the underlying response statistics. The probabilistic perspective can provide such information but the numerical treatment of the associated stochastic equations is a challenging task. In this chapter, we first provide an overview of various uncertainty quantification methods for stochastic dynamical systems.

2.1 Fokker-Planck-Kolmogorov Equation

The first method is the Fokker-Planck-Kolmogorov (FPK) equation (or forward diffusion equation) which can provide the complete statistical description of the response probability density function [144]. Described by a linear parabolic partial differential equation, the FPK equation governs the diffusion of probability in state space, which is analogous to the heat equation. The foundation of the the theory has been built by Rayleigh [117] and Fokker [49], and the solution of FPK equation has been widely studied.

The externally forced linear systems under the white noise have considered in [88] for the complete solution of FPK equation. Solutions of FPK equation for the first order nonlinear systems under Gaussian white noise are investigated [25, 143], especially by means of Fourier and Laplace transformation approach [7], eigenfunction expansion method [6], and a method based on the group theory [16]. The steady state solutions of FPK equation for nonlinear multi-degree-of-freedom systems under Gaussian white noise are studied in [26, 83, 23]. The stationary pdf of a specific set of single-degree-of-freedom systems under parametric and external Gaussian white noise has studied in [44]. More extensive reviews on the solution of FPK equation can be found in [98, 144, 155] and references there in.

One advantage of the FPK equation is that the drift and diffusion coefficients can be directly connect to the parameters of the dynamical systems [136, 140]. Although the analysis is based on the assumption of Gaussian excitation with no correlation, the FPK equation provides a convenient theoretical framework to treat nonlinear random vibrations. In this section, we provide the summary of FPK equation by describing the evolution of probability density function for one-dimensional and multi-dimensional stochastic processes. In the later part of this section, we provide examples to derive steady state probability density functions considering first and second order differential equations.

2.1.1 Derivation of FPK Equation

Let us first consider the one-dimensional stochastic process X_t whose stochastic differential equation is given by [136]

$$dX_t = \mu(X_t, t)dt + \sigma(X_t, t)dW_t, \tag{2.1}$$

where $\mu(X_t, t)$ indicates the drift term, $\sigma(X_t, t)$ indicates the diffusion term, and W_t is the standard Wiener process. Here the FPK equation that describes the transient probability density function $f(x, t)$ of the one dimensional random variable X_t is given by

$$\frac{\partial}{\partial t}f(x,t) = -\frac{\partial}{\partial x}\left[\mu(x,t)f(x,t)\right] + \frac{\partial^2}{\partial x^2}\left[D(x,t)f(x,t)\right], \tag{2.2}$$

where $D(x, t) = \sigma^2(x, t)/2$.

One-dimensional FPK equation can be generalized for the multi-dimensional (i.e. N-dimensional) stochastic process $\mathbf{X}_t$ whose stochastic differential equation in matrix form is given by [136, 113]

$$d\mathbf{X}_t = \boldsymbol{\mu}(\mathbf{X}_t, t)\, dt + \boldsymbol{\sigma}(\mathbf{X}_t, t)\, d\mathbf{W}_t, \tag{2.3}$$

where $\boldsymbol{\mu}(\mathbf{X}_t, t)$ indicates the N-dimensional drift term, $\boldsymbol{\sigma}(\mathbf{X}_t, t)$ is a N by M matrix describing the diffusion term, and $\mathbf{W}_t$ is the M-dimensional standard Wiener process. The FPK equation which describes the transient probability density function $f(\mathbf{x}, t)$ of the N-dimensional random vector $\mathbf{X}_t$ can be expressed by

$$\frac{\partial f(\mathbf{x},t)}{\partial t} = -\sum_{i=1}^{N}\frac{\partial}{\partial x_i}\left[\mu_i(\mathbf{x},t)f(\mathbf{x},t)\right] + \frac{1}{2}\sum_{i=1}^{N}\sum_{j=1}^{N}\frac{\partial^2}{\partial x_i\,\partial x_j}\left[D_{ij}(\mathbf{x},t)f(\mathbf{x},t)\right], \tag{2.4}$$

where

$$D_{ij}(\mathbf{x},t) = \sum_{k=1}^{M} \sigma_{ik}(\mathbf{x},t)\sigma_{jk}(\mathbf{x},t). \tag{2.5}$$

In order to illustrate the treatment of FPK equation in the context of random vibrations, we provide examples in the following subsections. These will complete the description of how the FPK equation can be obtained and solved for the stationary probability density function by considering first order and second order differential equations [136, 144].

2.1.2 Application on First Order Differential Equations

We consider the following first order stochastic differential equation with respect to $x(t)$, subject to the Gaussian white noise.

$$\frac{dx(t)}{dt} + g(x(t)) = \alpha\dot{W}(t), \quad x(0) = x_0. \tag{2.6}$$

where $g(\cdot)$ is an arbitrary nonlinear function of $x(t)$ and α is a positive constant describing the intensity of the white noise. The above equation can be converted into the Itō stochastic equation:

$$dx_t = -g(x_t)dt + \alpha dW_t. \tag{2.7}$$

Based on the one-dimensional FPK equation formulated in equation (2.2), the transient probability density function $f(x,t)$ can be obtained by

$$\frac{\partial f(x,t)}{\partial t} = \frac{\partial}{\partial x}[g(x)f(x,t)] + \frac{1}{2}\alpha^2\frac{\partial^2 f(x,t)}{\partial x^2}, \tag{2.8}$$

where $f(x,0;x_0) = \delta(x - x_0)$ and $\delta(\cdot)$ indicates Dirac Delta function. In the case where the diffusion coefficient and the drift coefficient are independent of time (i.e. $\mu(x,t) = \mu(x)$ and $\sigma(x,t) = \sigma(x)$), there exists a stationary probability density

function $f_{st}(x)$,

$$f_{st}(x) = \lim_{t\to\infty} f(x,t), \tag{2.9}$$

which does not depend on time. In this case, by letting $\frac{\partial f}{\partial t} = 0$, the FPK equation can be reduced to

$$\frac{\partial}{\partial x}[g(x)f_{st}(x)] + \frac{1}{2}\alpha^2\frac{\partial^2 f_{st}(x)}{\partial x^2} = 0. \tag{2.10}$$

Note that $g(x)$ does not depend on time. We can rewrite the equation as

$$\frac{\partial}{\partial x}\left\{g(x)f_{st}(x) + \frac{1}{2}\alpha^2\frac{\partial f_{st}(x)}{\partial x}\right\} = 0. \tag{2.11}$$

The direct integration of the equation gives

$$f_{st}(x) = \frac{1}{C}\exp\left[-\frac{2}{\alpha^2}\int_0^x g(z)dz\right], \tag{2.12}$$

where C is just a normalization constant.

$$C = \int_{-\infty}^{\infty}\exp\left[-\frac{2}{\alpha^2}\int_0^y f(z)dz\right]dy. \tag{2.13}$$

2.1.3 Application on Second Order Differential Equations

More intuitive examples in the context of random vibrations can be found in second order differential equations which describe dynamical systems subject to stochastic excitations. Here we consider a nonlinear single-degree-of-freedom system excited by the Gaussian white noise.

$$\frac{d^2x(t)}{dt^2} + \beta\frac{dx(t)}{dt} + g(x(t)) = \dot{W}(t), \tag{2.14}$$

where β is the damping coefficient, $g(\cdot)$ indicates an arbitrary nonlinear function of x and $\dot{W}(t)$ is a zero mean Gaussian white noise whose intensity is set to be 2α. This

equation can be converted into

$$\frac{dX_1}{dt} = X_2(t), \tag{2.15}$$

$$\frac{dX_2}{dt} = -\beta X_2(t) - g(X_1(t)) + \dot{W}(t), \tag{2.16}$$

where we assumed

$$X_1 = X(t), \tag{2.17}$$

$$X_2 = \frac{dX(t)}{dt}. \tag{2.18}$$

Based on the formulation in equation (2.4), the FPK equation that describes the evolution of response pdf can be derived as follows.

$$\begin{aligned}\frac{\partial}{\partial t} f(x_1, x_2, t) = & -\frac{\partial}{\partial x_1}\left[x_2 f(x_1, x_2, t)\right] \\ & + \frac{\partial}{\partial x_2}\left[\left(\beta x_2 + g(x_1)\right) f(x_1, x_2, t)\right] + \alpha \frac{\partial^2}{\partial x_2^2} f(x_1, x_2, t).\end{aligned} \tag{2.19}$$

By assuming that the response pdf is independent of time $\frac{\partial f}{\partial t} = 0$, the stationary joint probability density function $f_{st}(x_1, x_2)$ satisfies

$$\alpha \frac{\partial^2}{\partial x_2^2} f_{st}(x_1, x_2) - \frac{\partial}{\partial x_1}\left[x_2 f_{st}(x_1, x_2)\right] + \frac{\partial}{\partial x_2}\left[\left(\beta x_2 + g(x_1)\right) f_{st}(x_1, x_2)\right] = 0. \tag{2.20}$$

The above equation can be solved numerically using standard finite-element or finite-difference methods to obtain the stationary joint probability density function.

We have formulated the FPK equation for one-dimensional and multi-dimensional stochastic processes, and provided some demonstrations involving first and second order differential equations subject to the Gaussian white noise in order to derive the steady state pdf solution of the FPK equation. We would like to emphasize that the transient solution of the FPK equation has been characterized by the time dependency and nonstationarity, however in general, such nonstationary solutions

cannot be obtained in explicit form. Only the exact steady state solutions for a specific set of FPK equations associated with second-order nonlinear differential equations are available under Gaussian white noise excitations. Especially for multi-degree-of freedom systems, the exact solutions of FPK equations are not readily available and therefore the use of FPK equations is often inefficient. Consequently, alternative approximate approaches are developed in order to deal with such difficulties.

2.2 Statistical Linearization

In nonlinear stochastic vibration problems, the statistical linearization method (also known as stochastic linearization) [144, 122, 137] is by and large the most popular approach. As a direct extension of the harmonic linearization technique, this method can be applied to multi-degree-of-freedom systems subject to either stationary or nonstationary excitations [98]. The basic concept of the statistical linearization is to replace the original nonlinear equation of motion with an equivalent linear equation, which can be treated analytically, by minimizing the statistical difference between those two equations.

This idea was initially introduced by Booton [18] and Kazakov [73, 74], and further improved by many other researchers in the context of nonlinear stochastic control systems [129, 11, 150], nonlinear structural dynamics [24, 22], nonlinear offshore structures [95], and random vibrations on multidimensional systems [141, 2, 64]. In this section we provide an overview of the method with a general nonlinear single-degree-of-freedom system under stationary stochastic excitation with broadband spectral density, and then consider a cubic nonlinearity as a specific example. Additional examples and applications of statistical linearization can be found in [144, 136, 140, 122] and references therein.

2.2.1 Derivation of the Equivalent Linear Equation

To illustrate the basic idea, we consider the following second order differential equation which describes a single-degree-of-freedom system excited by a stationary stochastic process $y(t)$ [136].

$$\ddot{x}(t) + g(x(t), \dot{x}(t)) = y(t), \tag{2.21}$$

where $g(\cdot)$ is an arbitrary nonlinear function that depends on x and $\dot{x}$. With the statistical linearization, we approximate the above governing equation with an equivalent linear equation in the form of

$$\ddot{x}(t) + \beta_e \dot{x}(t) + k_e x(t) = y(t), \tag{2.22}$$

where β_e and k_e are equivalent linear damping coefficient and stiffness, respectively. These quantities will be chosen such that the (second order) statistical differences between equation (2.21) and equation (2.22) are minimized. We demonstrate how these parameters are determined systematically. We let the difference of equation (2.21) and equation (2.22) as

$$\epsilon(t) = \beta_e \dot{x}(t) + k_e x(t) - g(x(t), \dot{x}(t)). \tag{2.23}$$

Note that the difference $\epsilon(t)$ is also a stochastic process and therefore the statistical minimization is performed in terms of the mean squared of the error.

$$E[\epsilon^2] = \lim_{T\to\infty} \frac{1}{T} \int_0^T \epsilon^2(\tau) d\tau. \tag{2.24}$$

Parameters β_e and k_e will be determined such that the following equation is satisfied.

$$E[\epsilon^2] = \min \left\{ E\left[\{\beta_e \dot{x}(t) + k_e x(t) - g(x(t), \dot{x}(t))\}^2 \right] \right\}. \tag{2.25}$$

The minimization will be performed with respect to β_e and k_e, and this can be computed by their gradients,

$$\frac{\partial}{\partial \beta_e} E[\epsilon^2] = 0, \tag{2.26}$$

$$\frac{\partial}{\partial k_e} E[\epsilon^2] = 0. \tag{2.27}$$

This leads

$$\beta_e E\left[\dot{x}^2(t)\right] + k_e E\left[x(t)\dot{x}(t)\right] - E\left[\dot{x}(t)g(x,\dot{x})\right] = 0, \tag{2.28}$$

$$k_e E\left[x^2(t)\right] + \beta_e E\left[x(t)\dot{x}(t)\right] - E\left[x(t)g(x,\dot{x})\right] = 0. \tag{2.29}$$

Hence we have

$$\beta_e = \frac{E\left[x^2(t)\right] E\left[\dot{x}(t)g(x,\dot{x})\right] - E\left[x(t)\dot{x}(t)\right] E\left[x(t)g(x,\dot{x})\right]}{E\left[x^2(t)\right] E\left[\dot{x}^2(t)\right] - \left\{E\left[x(t)\dot{x}(t)\right]\right\}^2}, \tag{2.30}$$

$$k_e = \frac{E\left[\dot{x}^2(t)\right] E\left[x(t)g(x,\dot{x})\right] - E\left[x(t)\dot{x}(t)\right] E\left[\dot{x}(t)g(x,\dot{x})\right]}{E\left[x^2(t)\right] E\left[\dot{x}^2(t)\right] - \left\{E\left[x(t)\dot{x}(t)\right]\right\}^2}. \tag{2.31}$$

We observe that β_e and k_e are expressed by the moments, or the expectations of stochastic responses in terms of $x(t)$ and $\dot{x}(t)$. This indicates that in order to perform the statistical linearization, we need to have the estimation of the response statistics for the stochastic nonlinear system in advance. Indeed, if the probability distribution for the response is known in advance there is no point for approximating nonlinear equations into linear ones. This is the main difficulty associated with the statistical linearization approach.

One can resolve this difficulty by assuming the response $x(t)$ as a Gaussian process. We note that if we had a linear time-invariant system and the excitation is a stationary stochastic process with Gaussian distribution, the response process also follows the Gaussian distribution. If we have a nonlinear system, and its response distribution does not deviate far from the Gaussian, Gaussian process approximation can still hold, however, if the system is essentially nonlinear (i.e. bimodal systems), the performance of statistical linearization decreases significantly. For example, the statistical linearization works reliably for systems with unimodal potential function, i.e. response close to Gaussian. However, when the response is essentially non-Gaussian, e.g. as it is the case for a double-well oscillator, the application of statistical linearization is less straightforward and involves the ad-hoc selection of shape parameters for the

response statistics [31]. We demonstrate how the Gaussian process approximation can be applied along with the statistical linearization.

2.2.2 Application on Second Order Differential Equation

Let's consider the following nonlinear single-degree-of-freedom system with cubic stiffness excited by a correlated stochastic force [136].

$$\ddot{x} + \lambda\dot{x} + kx + cx^3 = y, \tag{2.32}$$

where λ indicates the damping coefficient, k is the linear stiffness and c is the cubic stiffness. We assume that the excitation has a power spectral density of $S_{yy}(\omega)$ and is known in advance. Following the analysis in equation (2.31), we obtain

$$\beta_e = \lambda, \tag{2.33}$$

$$k_e = \frac{kE\left[x^2\right] + cE\left[x^4\right]}{E\left[x^2\right]}. \tag{2.34}$$

As we have discussed previously, those quantities ($E\left[x^2\right]$ and $E\left[x^4\right]$) require the probability distribution of the stochastic unknown response $x(t)$. In this case, the potential function of the system is given by

$$U = \frac{1}{2}kx^2 + \frac{1}{4}cx^4, \tag{2.35}$$

which is the unimodal function in which case the response pdf does not deviate far from Gaussian structure. Hence we can apply the Gaussian process approximation following the Isserli's Theorem.

$$E\left[x^4\right] = 3\left(E\left[x^2\right]\right)^2. \tag{2.36}$$

Then we have

$$k_e = k + 3cE\left[x^2\right]. \tag{2.37}$$

Based on the approximation, we can obtain the response spectral density function of the equivalent linear system.

$$S_{xx}(\omega) = \frac{S_{yy}(\omega)}{|-\omega^2 + \beta_e(j\omega) + k_e|^2}. \tag{2.38}$$

We note that the response spectral density is expressed in terms of given excitation spectral density, which indicates the statistical linearization method can be applicable on correlated excitations. Integration of the spectral density function yields the variance.

$$\sigma_x^2 = \int_{-\infty}^{\infty} S_{xx}(\omega)d\omega, \tag{2.39}$$

$$= \int_{-\infty}^{\infty} \frac{S_{yy}(\omega)}{|-\omega^2 + \beta_e(j\omega) + k_e|^2}d\omega, \tag{2.40}$$

$$= \int_{-\infty}^{\infty} \frac{S_{yy}(\omega)}{|-\omega^2 + \lambda(j\omega) + k + 3\,c\,\sigma_x^2|^2}d\omega. \tag{2.41}$$

We note that k_e in the right hand side of the above equation also depends on the unknown variance σ_x^2 as in equation (2.37). This unknown variance can be obtained by solving the nonlinear equation.

$$\sigma_x^2 - \int_{-\infty}^{\infty} \frac{S_{yy}(\omega)}{|-\omega^2 + \lambda(j\omega) + k + 3\,c\,\sigma_x^2|^2}d\omega = 0. \tag{2.42}$$

Statistical linearization method has served as one of the most popular approximation schemes for the response statistics quantification due mainly to its simplicity and its adaptability to multi-degree-of-freedom cases. However, as we have pointed out, the accuracy of the solution heavily depends on the structure of the response probability distribution and in case it deviates far from Gaussian, the reliability of the estimate is not guaranteed. Furthermore, if the excitation contains extreme forcing events within

the stochastic excitation, the accuracy of the solution significantly decreases in the heavy-tail regimes even for the nonlinear systems whose core probability distribution is close to Gaussian.

This is because the statistical linearization method relies on the minimization of the mean square error, in other words, the second order statistics [144]. Thus the approximation of the response statistics higher than second order statistics may not be reliable. Inaccuracy of the statistical linearization estimates has been reported in many articles, ranging from the Duffing oscillator under Gaussian white noise [57], to various nonlinear damping models subject to Gaussian white noise [130], to the Van der Pol oscillator with Gaussian white noise [163].

2.3 Moment Equations

Another computational approach developed to quantify the response statistics is the moment equations method, which describes the evolution of the the joint response-excitation statistical moments or the response statistical moments [125, 19, 14] depending on the nature of the stochastic excitation. Especially in the stochastic nonlinear vibration problems, response moment equations form an infinite hierarchy, and generally exact solutions are not possible [98]. Thus the challenge with moment equations arises if the equation of motion of the system contains nonlinear terms. This is the well known closure problem, which consists of approximately replacing the infinite hierarchy of equations with a finite set of lower order moments. This is the main notorious difficulty associated with the moment equations approach.

Among various closure techniques, the Gaussian closure scheme [66] is the simplest approach along this line in that it assumes the response to be close to Gaussian distributed. With the assumption of Gaussian distribution, all the higher order of cumulants can be expressed in terms of lower order of moments enabling us to close the moment equations [157]. It should be noted that the application of the Gaussian closure scheme to the moment equations may lead to the exactly same results with those obtained from the statistical linearization approach with Gaussian process approximation [144]. Gaussian closure scheme has been studied widely in the context of nonlinear systems under random vibrations (either Gaussian [32] or non-Gaussian [66]) and nonlinear liquid sloshing under stochastic excitations [61]. However, the assumption of Gaussian is not adequate if the response distribution deviates far from the Gaussian structure.

As an alternative, non-Gaussian closure schemes have also been developed in order to take into account the nonlinear structure of the response probability distribution [62, 53, 156]. In most cases, these nonlinear approaches may offer some improvement compared with the stochastic linearization approach applied to nonlinear systems but

the associated computational cost is considerably larger [109]. This is because the complexity of the moment equations dramatically increases as the order of closure increases [33, 34, 92]. For strongly nonlinear systems, such as bistable systems, these improvements can be very small.

2.3.1 Derivation of Moment Equations

In this section, we demonstrate how the moment equations can be obtained. One of the most general ways of obtaining moment equations is by applying the Itō formula [37] to the following function

$$h(\mathbf{X}) = X_1^{k_1}(t)\, X_2^{k_2}(t)\, X_3^{k_3}(t) \ldots X_n^{k_n}(t), \tag{2.43}$$

and by taking the ensemble averages. Thus the moment equations can be directly obtained as the following equation [144]:

$$\frac{d}{dt} E\left[h(\mathbf{X})\right] = \sum_i E\left[a_i(\mathbf{X}) \frac{\partial h(\mathbf{X})}{\partial X_i}\right] + \frac{1}{2} \sum_l \sum_{i,j} E\left[b_{il}(\mathbf{X}) b_{jl}(\mathbf{X}) \frac{\partial^2 h(\mathbf{X})}{\partial x_i \partial x_j}\right]. \tag{2.44}$$

As an illustrative purpose, we consider the nonlinear first order differential equation subject to the Gaussian white noise [136].

$$\dot{x}(t) + x(t) + c x^3(t) = \dot{W}(t). \tag{2.45}$$

where c is the nonlinear stiffness and $\dot{W}(t)$ indicates Gaussian white noise. Based on the formulation given in equation (2.44), by letting

$$h(y) = y^k, \tag{2.46}$$

and since $n = 1$, we have

$$a_1 = -(x + cy^3), \tag{2.47}$$

$$b_{11} = 1, \tag{2.48}$$

$$\frac{dh}{dy} = ky^{k-1}, \tag{2.49}$$

$$\frac{d^2h}{dy^2} = k(k-1)y^{k-2}. \tag{2.50}$$

where $k_1 = k$ and $k_2 = k_3 = ... = k_n = 0$. Plugging above equations into equation (2.44), we obtain

$$\dot{m}_k(t) = -km_k(t) - k\,c\,m_{k+2}(t) + \frac{1}{2}k(k-1)m_{k-2}, \tag{2.51}$$

Here k takes any positive integers $k = 1, 2...$, and we have used the notation of $m_k(t) = E\left[Y^k(t)\right]$. For example, we will have

$$\dot{m}_1(t) = -m_1(t) - c\,m_3(t), \tag{2.52}$$

$$\dot{m}_2(t) = -2m_2(t) - 2c\,m_4(t) + 1, \tag{2.53}$$

$$\vdots$$

We note that the equation for moment $m_k(t)$ contains unknown higher order moment $m_{k+2}(t)$. In this way, an infinite set of moment equations will be generated, and to this end an appropriate closure scheme should be applied.

2.3.2 Various Closure Schemes

As previously discussed, moment equations cannot be explicitly solved in general due to the existence of infinite number of higher order moments. Hence the approximate solutions are derived based on numerous closure techniques, i.e. the central moment closure, Gaussian closure, cumulant closure, and non-Gaussian closure. In this section, we briefly introduce some of the most popular techniques [144, 98].

Central Moment Closure

Central moment closure assumes that all central moments of orders higher than k are set to be zero and can be discarded from the moment equations:

$$E\left[(X_1(t) - E[X_1(t)])^{k_1} (X_2(t) - E[X_2(t)])^{k_2} ... (X_n(t) - E[X_n(t)])^{k_n}\right] = 0, \quad (2.54)$$

where $k_1 + k_2 + ... + k_n > k$. In this way, one can discard certain higher central moments so that the moment equations can be exactly solved. The method works well especially for weakly non-Gaussian processes.

Gaussian Closure

This technique is based on the assumption that $X_1(t), X_2(t), ...X_n(t)$ obey the Gaussian distribution. In this way, the first two moments ($m_1(t)$ and $m_2(t)$) uniquely define the probability distribution, and hence all higher moments, $m_k(t)$ where $k > 2$, can be determined. For $k \geq 1$,

$$E\left[(X_1(t) - E[X_1(t)]) (X_2(t) - E[X_2(t)]) ... (X_{2k-1}(t) - E[X_{2k-1}(t)])\right] = 0, \quad (2.55)$$

and

$$E\left[(X_2(t) - E[X_2(t)]) \dots (X_{2k}(t) - E[X_{2k}(t)])\right] = \sum E\left[(X_{a_1}(t) - E[X_{a_1}(t)]) \dots (X_{a_{2k}}(t) - E[X_{a_{2k}}(t)])\right]. \quad (2.56)$$

Here the summation can be considered as the permutation of $2k$ elements of k pairs, and it has $\frac{(2k)!}{2^k k!}$ terms. For the simple case of $X(t)$, where $n = 1$, the above equations reduce to

$$E\left[\{X(t) - E[X(t)]\}^k\right] = \frac{k!}{2^{k/2}(\frac{k}{2})!}\sigma^k(t), \qquad k = 2, 4, 6, \dots \quad (2.57)$$

$$= 0, \qquad k = 1, 3, 5, \dots \quad (2.58)$$

where $\sigma^2(t)$ is the variance of the stochastic process $X(t)$. Based on this, we can obtain the approximation for 3rd and 4th order moments:

$$m_3(t) = E\left[\{X(t) - E[X(t)]\}^3\right] + 3m_1(t)m_2(t) - 2m_1^3(t), \quad (2.59)$$

$$m_4(t) = E\left[\{X(t) - E[X(t)]\}^4\right] + 4m_1(t)E\left[\{X(t) - E[X(t)]\}^3\right] + 6m_1^2(t)m_2(t) - 5m_1^4(t). \quad (2.60)$$

Assuming zero mean $m_1(t) = E[X(t)] = 0$ and variance $\sigma^2(t)$, the above equations further reduce to

$$m_3(t) = 0, \quad (2.61)$$

$$m_4(t) = 3\{m_2(t)\}^2. \quad (2.62)$$

Cumulant Closure

Similar to the central moment closure, the cumulant closure technique close the moment equations by assuming that the cumulants of higher than k-th order are zero. In order for that, we first require the relation connecting ordinary moments and cumulants of the stochastic process $X(t)$. We summarize the relation between ordinary moments and cumulants for first three orders. Readers are refered to [140] and references therein for the computation of cumulants.

$$E[X] = \lambda_1(X), \tag{2.63}$$

$$E[X^2] = \lambda_2(X) + (\lambda_1(X))^2, \tag{2.64}$$

$$E[X^3] = \lambda_3(X) + 3\lambda_1(X)\lambda_2(X) + (\lambda_1(X))^3. \tag{2.65}$$

where λ_k indicates the k-th order cumulant. In this way, the higher order moments can be approximated by the lower order moments where cumulants with higher than certain order will set to be zero. This is a very important approach for the analysis of nonlinear vibrational systems. Its most important drawback is the lack of stability of the moment equations which can lead to negative variance and other moments that should be strictly positive (i.e. we may end up with moments which are not associated to a pdf).

2.4 Perturbation Method

An alternative approach to compute the response statistics for the nonlinear stochastic system is the perturbation approach. In this technique, we treat the stochastic system in a similar manner as a deterministic one as the idea comes from the classical theory of ordinary differential equations. One should be noted that perturbation method can be applied only if the nonlinearity is sufficiently small so that the solution can be expanded in powers of small parameter ϵ [136, 98].

The perturbation approach was first adopted by Crandall [35] in his work for the estimation of response moments of nonlinear multi-degree-of-freedom systems under stationary Gaussian excitations. Symmetric and asymmetric nonlinear systems under stationary stochastic excitations are considered in [133], and systems with nonlinear damping have been considered in [36, 76]. The response of the Duffing oscillator has been studied for stationary stochastic excitations [97] and for nonstationary stochastic excitations [139].

We note that the perturbation method is particularly beneficial in case one has polynomial nonlinearities. This method can be useful for the derivation of power spectral densities, however it might not be the case for the derivation of response probability density function due to the non-Gaussian structure of the higher order terms. In this section we introduce the applicability of perturbation approach on the single-degree-of-freedom system under stationary stochastic excitations [144].

2.4.1 Application on Second Order Differential Equation

We consider a nonlinear second order differential equation describing the motion of single-degree-of-freedom system under stochastic excitation as follows.

$$\ddot{x}(t) + \alpha\dot{x}(t) + \beta x(t) + \epsilon g(x, \dot{x}) = y(t), \tag{2.66}$$

where α is the damping coefficient, β is the linear stiffness, $g(\cdot)$ is an arbitrary nonlinear function of x and $\dot{x}$, and we let $\epsilon \ll 1$. Also the excitation $y(t)$ is considered to be a stationary Gaussian stochastic process. What perturbation method does is that it expands the solution $x(t)$ in terms of powers of ϵ,

$$x(t) = x_0(t) + \epsilon x_1(t) + \epsilon^2 x_2(t) + ... \tag{2.67}$$

We plug above expansion into equation (2.66), and all terms of same order (with respect to ϵ) will be equated.

$$O(1) \qquad \ddot{x}_0(t) + \alpha\dot{x}_0(t) + \beta x_0(t) = y(t), \tag{2.68}$$

$$O(\epsilon) \qquad \ddot{x}_1(t) + \alpha\dot{x}_1(t) + \beta x_1(t) = -g(x_0, \dot{x}_0), \tag{2.69}$$

$$O(\epsilon^2) \qquad \ddot{x}_2(t) + \alpha\dot{x}_2(t) + \beta x_2(t) = -g'_{x_0}(x_0, \dot{x}_0)x_1(t) - g'_{\dot{x}_0}(x_0, \dot{x}_0)\dot{x}_1(t), \tag{2.70}$$

$$\vdots$$

where g'_{x_0} indicates the derivative of $g(x, \dot{x})$ with respect to x evaluated at $x(t) = x_0(t)$, similarly $g'_{\dot{x}_0}$ indicates the derivative of $g(x, \dot{x})$ with respect to x evaluated at $\dot{x}(t) = \dot{x}_0(t)$. In this way the nonlinear stochastic equation in equation (2.66) has been reduced to a set of linear equations, which we are now able to solve. The impulse response of the left hand side of the linear equations can be obtain by

$$h(t) = \mathrm{FT}^{-1}\left\{\frac{1}{(j\omega)^2 + \alpha(j\omega) + \beta}\right\}, \tag{2.71}$$

where FT^{-1} indicates the inverse Fourier transform. We can write the steady state solution.

$$x_0(t) = h(t) * y(t) = \int_0^\infty h(\tau) y(t-\tau) d\tau, \tag{2.72}$$

$$x_1(t) = -h(t) * g(x_0, \dot{x}_0) = -\int_0^\infty h(\tau) g(x_0(t-\tau), \dot{x}_0(t-\tau)) d\tau, \tag{2.73}$$

$$\vdots$$

where $*$ indicates the convolution operator. Once each of these linear equations has been solved, by using equation (2.67) we can compute the response statistics. For example, the mean of the response becomes

$$E[x(t)] = E[x_0(t)] + \epsilon E[x_1(t)] + \epsilon^2 E[x_2(t)] + ..., \tag{2.74}$$

$$= \int_0^\infty h(\tau) E[y(t-\tau)] d\tau - \epsilon \int_0^\infty h(\tau) E[g(x_0(t-\tau), \dot{x}_0(t-\tau))] d\tau + O(\epsilon^2). \tag{2.75}$$

As one can notice, the computational difficulty associated with the perturbation method is that its complexity increases dramatically as we go to higher order moments.

2.5 Stochastic Averaging Method

Another class of techniques for the approximate solutions to the nonlinear stochastic systems is the stochastic averaging method. Stochastic averaging method is a technique to average the stochastic response with respect to the rapidly varying processes to obtain the averaged stochastic differential, and it serves as a powerful tool for predicting the response statistics. In general the stochastic averaging technique consists of two steps [144]: the first step is to average out the terms independent from the stochastic forcing, and the second step is to approximate the terms which depend on the stochastic forcing. In this case, the stochastic forcing can be anything, from correlated broad-band process to Gaussian white noise.

One of the advantages of stochastic averaging method is that it often reduces the dimensionality of the problem by significantly simplifying the solution procedures [98]. Different versions of reviews on the stochastic averaging method have been reported [62, 123, 161, 160]. In particular, this approach has been further classified into three distinct groups depending on the derivation [144]: the first group is the classical stochastic averaging (CSA) method [143, 17, 77], the second group is the stochastic averaging method of energy envelope (SAMEE) [143, 121, 162, 118], and the third group is the higher order approximation of CSA method [140, 132, 21, 131]. It has been noted that for systems with linear stiffness the first two groups become equivalent. We note that further details regarding each method can be found in [144] and references therein. In the following subsection, we consider the classical stochastic averaging approach and illustrate the derivation procedure with the single-degree-of-freedom system under stochastic excitation.

2.5.1 Application on Second Order Differential Equation

We consider the nonlinear single-degree-of-freedom system whose equation of motion is given by

$$\ddot{x}(t) + \omega_0^2 y(t) + \epsilon^2 g(x, \dot{x}) = \epsilon y(t), \tag{2.76}$$

where ω_0^2 is the stiffness of the system, and the parameter ϵ indicates the relative strength of the nonlinear term. y indicates the stationary stochastic excitation. We then convert the above differential equation into a set of equations for x and $\dot{x}$. Since the stochastic responses are rapidly fluctuating with respect to time, we adopt the following transformation:

$$x(t) = a(t)\cos\left[\omega_0 t + \phi(t)\right], \tag{2.77}$$

$$\dot{x}(t) = -\omega_0 a(t)\sin\left[\omega_0 t + \phi(t)\right]. \tag{2.78}$$

Here $a(t)$ indicates the envelope and $\phi(t)$ is the phase of the response, which are slowly varying with respect to time if ϵ is small. Once we differentiate equation (2.77) with respect to time, we obtain

$$\dot{x}(t) = \dot{a}(t)\cos\left[\omega_0 t + \phi(t)\right] - a(t)\left\{\omega_0 t + \dot{\phi}(t)\right\}\sin\left[\omega_0 t + \phi(t)\right]. \tag{2.79}$$

This can be equated with equation (2.78) letting us have

$$\dot{a}(t)\cos\left[\omega_0 t + \phi(t)\right] - a(t)\dot{\phi}(t)\sin\left[\omega_0 t + \phi(t)\right] = 0. \tag{2.80}$$

In a similar fashion, we obtain the following expression by the second derivative of equation (2.78) with respect to time.

$$\begin{aligned}\ddot{x}(t) = & -\omega_0^2 a(t)\cos\left[\omega_0 t + \phi(t)\right] - \omega_0\dot{\phi}(t)a(t)\cos\left[\omega_0 t + \phi(t)\right], \\ & -\omega_0\dot{a}(t)\sin\left[\omega_0 t + \phi(t)\right].\end{aligned} \tag{2.81}$$

Once we plug all these results into the equation (2.76), and by rearranging, we obtain two equations for $\dot{a}(t)$ and $\dot{\phi}(t)$.

$$\frac{da(t)}{dt} = \frac{\epsilon^2}{\omega_0^2} g\Big(a(t)\cos\left[\omega_0 t + \phi(t)\right], -a(t)\omega_0 \sin\left[\omega_0 t + \phi(t)\right]\Big) \sin\left[\omega_0 t + \phi(t)\right] - \frac{\epsilon}{a(t)\omega_0} y(t) \sin\left[\omega_0 t + \phi(t)\right] \tag{2.82}$$

$$\frac{d\phi(t)}{dt} = \frac{\epsilon^2}{a(t)\omega_0^2} g\Big(a(t)\cos\left[\omega_0 t + \phi(t)\right], -a(t)\omega_0 \cos\left[\omega_0 t + \phi(t)\right]\Big) \sin\left[\omega_0 t + \phi(t)\right] - \frac{\epsilon}{a(t)\omega_0} y(t) \cos\left[\omega_0 t + \phi(t)\right] \tag{2.83}$$

We note that these two equations are referred to as the standard form, and this is equivalent with equation (2.76). From the above equations, one can obtain the transient probability density function, $f(a, \phi, t)$, by the FPK equation for the limiting Markov process [136].

Chapter 3

Moment-Equation-Copula-Closure Method for Nonlinear Vibrational Systems Subjected to Correlated Noise

3.1 Introduction

In numerous systems in engineering, uncertainty in the dynamics is as important as the known conservation laws. Such an uncertainty can be introduced by external stochastic excitations, e.g. energy harvesters or structural systems subjected to ocean waves, wind excitations, earthquakes, and impact loads [55, 143, 136, 140, 107, 144]. For these cases, deterministic models cannot capture or even describe the essential features of the response and to this end, understanding of the system dynamics and optimization of its parameters for the desired performance is a challenging task. On the other hand, a probabilistic perspective can, in principle, provide such information but then the challenge is the numerical treatment of the resulted descriptive equations, which are normally associated with prohibitive computational cost.

The focal point of this work is the development of a semi-analytical method for the inexpensive probabilistic description of nonlinear vibrational systems of low to moderate dimensionality subjected to correlated inputs. Depending on the system dimensionality and its dynamical characteristics, numerous techniques have been developed to quantify the response statistics, i.e. the probability density function (pdf) for the system state. For systems subjected to white noise, Fokker-Planck-Kolmogorov (FPK) equation provides a complete statistical description of the response statistics [155, 45, 43]. However, exact analytical solutions of the FPK equation are available only for a small class of systems. An alternative computational approach, the path integral solution (PIS) method, has been developed to provide the response pdf for general nonlinear systems at a specific time instant given the pdf of an earlier time instant. Many studies have been focused on the application of step-by-step PIS method numerically [154, 106, 42] and analytically [80, 81, 41] reporting its effectiveness on capturing the response statistics. On the other hand, for non-Markovian systems subjected to correlated excitations the joint response-excitation pdf method provides a computational framework for the full statistical solution [126, 153, 27]. However, such methodologies rely on the solution of transport equations for the pdf and they are associated with very high computational cost especially when it comes to the optimization of system parameters.

To avoid solving the transport equations for the pdf, semi-analytical approximative approaches with significantly reduced computational cost have been developed. Among them the most popular method in the context of structural systems is the statistical linearization method [24, 22, 73, 122, 137], which can also handle correlated excitations. The basic concept of this approach is to replace the original nonlinear equation of motion with a linear equation, which can be treated analytically, by minimizing the statistical difference between those two equations. Statistical linearization performs very well for systems with unimodal statistics, i.e. close to Gaussian. However, when the response is essentially nonlinear, e.g. as it is the case for a double-well oscillator, the application of statistical linearization is less straightforward and involves the ad-hoc selection of shape parameters for the response statistics [31].

An alternative class of methods relies on the derivation of moment equations, which describes the evolution of the the joint response-excitation statistical moments or (depending on the nature of the stochastic excitation) the response statistical moments [125, 19, 14]. The challenge with moment equations arises if the equation of motion of the system contains nonlinear terms in which case we have the well known closure problem. This requires the adoption of closure schemes, which essentially truncate the infinite system of moment equations to a finite one. The simplest approach along this line is the Gaussian closure [66] but nonlinear closure schemes have also been developed (see e.g. [33, 34, 92, 157, 62, 53, 59, 156, 54]). In most cases, these nonlinear approaches may offer some improvement compared with the stochastic linearization approach applied to nonlinear systems but the associated computational cost is considerably larger [109]. For strongly nonlinear systems, such as bistable systems, these improvements can be very small. Bistable systems, whose potential functions have bimodal shapes, have become very popular in energy harvesting applications [52, 58, 39, 56, 51, 60, 96, 9], where there is a need for fast and reliable calculations that will be able to resolve the underlying nonlinear dynamics in order to provide with optimal parameters of operation (see e.g. [70, 79]).

The goal of this work is the development of a closure methodology that can overcome the limitations of traditional closure schemes and can approximate the steady state statistical structure of bistable systems excited by correlated noise. We first formulate the moment equations for the joint pdf of the response and the excitation at two arbitrary time instants [4]. To close the resulted system of moment equations, we formulate a two-time representation of the joint response-excitation pdf using copula functions. We choose the representation so that the single time statistics are consistent in form with the Fokker-Planck-Kolmogorov solution in steady state, while the joint statistical structure between two different time instants is represented with a Gaussian copula density. Based on these two ingredients (dynamical information expressed as moment equations and assumed form of the response statistics), we for-

mulate a minimization problem with respect to the unknown parameters of the pdf representation so that both the moment equations and the closure induced by the representation are optimally satisfied. For the case of unimodal systems, the described approach reproduces the statistical linearization method while for bi-modal systems it still provides meaningful and accurate results with very low computational cost.

3.2 Description of the Method

In this section, we give a detailed description of the proposed method for the inexpensive computation of the response statistics for dynamical systems subjected to colored noise excitation. The computational approach relies on two basic ingredients:

- *Two-time statistical moment equations.* These equations will be derived directly from the system equation and they will express the dynamics that govern the two-time statistics. For systems excited by white-noise, single time statistics are sufficient to describe the response but for correlated excitation, this is not the case and it is essential to consider higher order moments. Note that higher (than two) order statistical moment equations may be used but in the context of this work two-time statistics would be sufficient.

- *Probability density function (pdf) representation for the joint response-excitation statistics.* This will be a family of probability density functions with embedded statistical properties such as multi-modality, tail decay properties, correlation structure between response and excitation, or others. The joint statistical structure will be represented using copula functions. We will use representations inspired by the analytical solutions of the dynamical system when this is excited by white noise. These representations will reflect features of the Hamiltonian structure of the system and will be used to derive appropriate closure schemes that will be combined with the moment equations.

Based on these two ingredients, we will formulate a minimization problem with respect to the unknown parameters of the pdf representation so that both the moment equations and the closure induced by the representation are optimally satisfied. We will see that for the case of unimodal systems the described approach reproduces the statistical linearization method while for bi-modal systems it still provides meaningful and accurate results with very low computational cost.

For the sake of simplicity, we will present our method through a specific system involving a nonlinear SDOF oscillator with a double well potential. This system has

been studied extensively in the context of energy harvesting especially for the case of white noise excitation [39, 38, 50, 48]. However, for realistic setups it is important to be able to optimize/predict its statistical properties under general (colored) excitation. More specifically we consider a nonlinear harvester of the form

$$\ddot{x} + \lambda\dot{x} + k_1 x + k_3 x^3 = \ddot{y}. \tag{3.1}$$

where x is the relative displacement between the harvester mass and the base, y is the base excitation representing a stationary stochastic process, λ is normalized (with respect to mass) damping coefficient, and k_1 and k_3 are normalized stiffness coefficients.

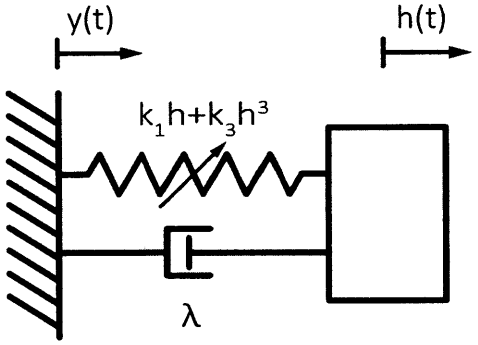

Figure 3-1: Nonlinear energy harvester with normalized system parameters.

3.3 Two-time Moment System

We consider two generic time instants, t and s. The two-time moment equations have been considered previously in [4] for the determination of the solution of a 'half' degree-of-freedom nonlinear oscillator by utilizing a Gaussian closure. We multiply the equation of motion at time t with the response displacement $x(s)$ and apply the mean value operator $\overline{\square}$ (ensemble average). This will give us an equation which contains an unknown term on the right hand side. To determine this term we repeat the same step but we multiply the equation of motion with $y(s)$. This gives us the following two-time moment equations:

$$\overline{\ddot{x}(t)y(s)} + \lambda\overline{\dot{x}(t)y(s)} + k_1\overline{x(t)y(s)} + k_3\overline{x(t)^3y(s)} = \overline{\ddot{y}(t)y(s)}, \tag{3.2}$$

$$\overline{\ddot{x}(t)x(s)} + \lambda\overline{\dot{x}(t)x(s)} + k_1\overline{x(t)x(s)} + k_3\overline{x(t)^3x(s)} = \overline{\ddot{y}(t)x(s)}. \tag{3.3}$$

Here the excitation is assumed to be a stationary stochastic process with zero mean and a given power spectral density; this can have an arbitrary form, e.g. monochromatic, colored, or white noise. Since the system is characterized by an odd restoring force, we expect that its response also has zero mean. Moreover, we assume that after an initial transient the system will be reaching a statistical steady state given the stationary character of the excitation. Based on properties of mean square calculus [136, 14], we interchange the differentiation and the mean value operators. Then the moment equations will take the form:

$$\frac{\partial^2}{\partial t^2}\overline{x(t)y(s)} + \lambda\frac{\partial}{\partial t}\overline{x(t)y(s)} + k_1\overline{x(t)y(s)} + k_3\overline{x(t)^3y(s)} = \frac{\partial^2}{\partial t^2}\overline{y(t)y(s)}, \tag{3.4}$$

$$\frac{\partial^2}{\partial t^2}\overline{x(t)x(s)} + \lambda\frac{\partial}{\partial t}\overline{x(t)x(s)} + k_1\overline{x(t)x(s)} + k_3\overline{x(t)^3x(s)} = \frac{\partial^2}{\partial t^2}\overline{y(t)x(s)}. \tag{3.5}$$

Expressing everything in terms of the covariance functions, above equations will result in:

$$\frac{\partial^2}{\partial t^2}C_{xy}^{ts} + \lambda\frac{\partial}{\partial t}C_{xy}^{ts} + k_1 C_{xy}^{ts} + k_3\overline{x(t)^3 y(s)} = \frac{\partial^2}{\partial t^2}C_{yy}^{ts}, \tag{3.6}$$

$$\frac{\partial^2}{\partial t^2}C_{xx}^{ts} + \lambda\frac{\partial}{\partial t}C_{xx}^{ts} + k_1 C_{xx}^{ts} + k_3\overline{x(t)^3 x(s)} = \frac{\partial^2}{\partial t^2}C_{yx}^{ts}, \tag{3.7}$$

where the covariance function is defined as

$$C_{xy}^{ts} = \overline{x(t)y(s)} = C_{xy}(t-s) = C_{xy}(\tau). \tag{3.8}$$

Taking into account the assumption for a stationary response (after the system has gone through an initial transient phase), the above moment equations can be rewritten in terms of the time difference $\tau = t - s$:

$$\frac{\partial^2}{\partial \tau^2}C_{xy}(\tau) + \lambda\frac{\partial}{\partial \tau}C_{xy}(\tau) + k_1 C_{xy}(\tau) + k_3\overline{x(t)^3 y(s)} = \frac{\partial^2}{\partial \tau^2}C_{yy}(\tau), \tag{3.9}$$

$$\frac{\partial^2}{\partial \tau^2}C_{xx}(\tau) + \lambda\frac{\partial}{\partial \tau}C_{xx}(\tau) + k_1 C_{xx}(\tau) + k_3\overline{x(t)^3 x(s)} = \frac{\partial^2}{\partial \tau^2}C_{xy}(-\tau). \tag{3.10}$$

Note that all the linear terms in the original equation of motion are expressed in terms of covariance functions, while the nonlinear (cubic) terms show up in the form of fourth order moments. To compute the latter we will need to adopt an appropriate closure scheme.

3.4 Two-time PDF Representations and Induced Closures

In the absence of higher-than-two order moments, the response statistics can be analytically obtained in a straightforward manner. However, for higher order terms it is necessary to adopt an appropriate closure scheme that closes the infinite system of moment equations. A standard approach in this case, which performs very well for unimodal systems, is the application of Gaussian closure which utilizes Isserlis' Theorem [63] to connect the higher order moments with the second order statistical quantities. Despite its success for unimodal systems, Gaussian closure does not provide accurate results for bistable systems. This is because in this case (i.e. bistable oscillators) the closure induced by the Gaussian assumption does not reflect the properties of the system attractor in the statistical steady state.

Here we aim to solve this problem by proposing a non-Gaussian representation for the joint response-response pdf at two different time instants and for the joint response-excitation pdf at two different time instants. These representations will:

- incorporate specific properties or information about the response pdf (single time statistics) in the statistical steady state,
- capture the correlation structure between the statistics of the response and/or excitation at different time instants by employing Gaussian copula density functions,
- have a consistent marginal with the excitation pdf (for the case of the joint response-excitation pdf).

3.4.1 Representation Properties for Single Time Statistics

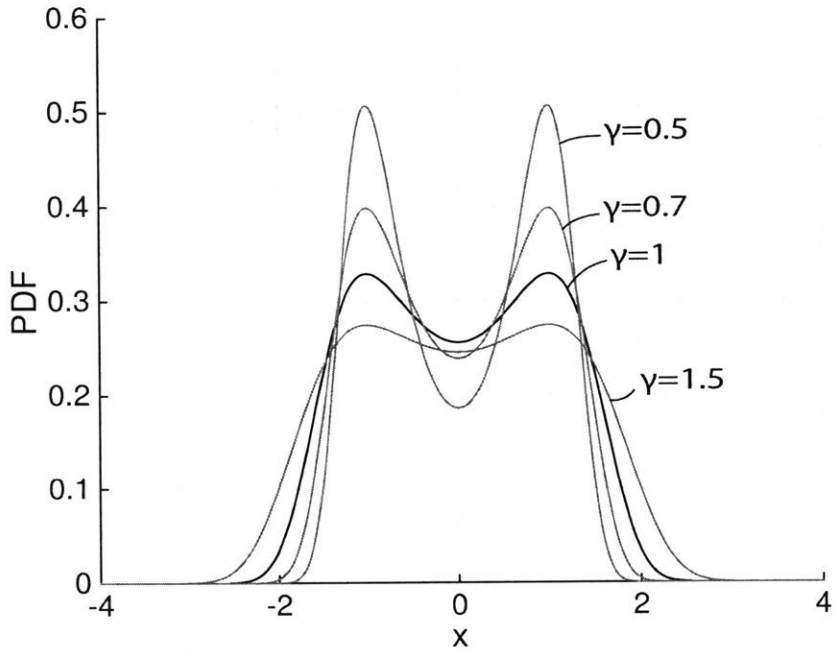

Figure 3-2: Representation of the steady state pdf for single time statistics of a system with double-well potential. The pdf is shown for different energy levels of the system.

We begin by introducing the pdf properties for the single time statistics. The selected representation will be based on the analytical solutions of the Fokker-Planck equation which are available for the case of white noise excitation [138, 136], and for vibrational systems that has an underlying Hamiltonian structure. Here we will leave the energy level of the system as a free parameter - this will be determined later. In particular, we will consider the following family of pdf solutions (figure 3-2):

$$f(x;\gamma) = \frac{1}{\mathcal{F}} \exp\{-\frac{1}{\gamma}U(x)\} = \frac{1}{\mathcal{F}} \exp\Big\{ -\frac{1}{\gamma}\Big(\frac{1}{2}k_1x^2 + \frac{1}{4}k_3x^4\Big)\Big\}, \tag{3.11}$$

where U is the potential energy of the oscillator, γ is a free parameter connected with the energy level of the system, and $\mathcal{F}$ is the normalization constant expressed as follows:

$$\mathcal{F} = \int_{-\infty}^{\infty} \exp\Big\{ -\frac{1}{\gamma}\Big(\frac{1}{2}k_1x^2 + \frac{1}{4}k_3x^4\Big)\Big\}dx. \tag{3.12}$$

3.4.2 Correlation Structure between Two-time Statistics

Representing the single time statistics is not sufficient since for non-Markovian systems (i.e. correlated excitation) the system dynamics can be effectively expressed only through (at least) two-time statistics. To represent the correlation between two different time instants we introduce Gaussian copula densities [108, 101]. A copula is a multivariate probability distribution with uniform marginals. It has emerged as an useful tool for modeling stochastic dependencies allowing the separation of dependence modeling from the given marginals [114]. Based on this formulation we obtain pdf representations for the joint response-response and response-excitation at different time instants.

Joint response-excitation pdf. We first formulate the joint response-excitation pdf at two different (arbitrary) time instants. In order to design the joint pdf based on the given marginals of response and excitation, we utilize a bivariate Gaussian copula whose density can be written as follows [101]:

$$C(u,v) = \frac{1}{\sqrt{1-c^2}} \exp\left(\frac{2c\Phi^{-1}(u)\,\Phi^{-1}(v) - c^2\left(\Phi^{-1}(u)^2 + \Phi^{-1}(v)^2\right)}{2(1-c^2)} \right), \tag{3.13}$$

where u and v indicate cumulative distribution functions and the standard cumulative distribution function is given as the following form:

$$\Phi(x) = \frac{1}{\sqrt{2\pi}} \int_{-\infty}^{x} \exp\left(-\frac{z^2}{2}\right) dz. \tag{3.14}$$

Denoting with x the argument that corresponds to the response at time t, with y the argument for the excitation at time $s = t - \tau$, and with $g(y)$ the (zero-mean) marginal

pdf for the excitation, we have the expression for the joint response-excitation pdf.

$$\begin{aligned} q(x,y) &= f(x)g(y)\mathcal{C}\left(F(x),G(y)\right), \\ &= f(x)g(y)\frac{1}{\sqrt{1-c^2}} \\ &\quad \times \exp\left(\frac{2c\Phi^{-1}\left(F(x)\right)\Phi^{-1}\left(G(y)\right) - c^2\left(\Phi^{-1}\left(F(x)\right)^2 + \Phi^{-1}\left(G(y)\right)^2\right)}{2(1-c^2)}\right), \end{aligned} \tag{3.15}$$

where c defines the correlation between the response and the excitation and has values $-1 \leq c \leq 1$ and $F(x)$ and $G(y)$ are the cumulative distribution functions obtained through the response marginal pdf, $f(x)$, and the excitation marginal pdf, $g(y)$, respectively. Note that the coefficient c depends on the time difference $\tau = t - s$ of the response and excitation. This dependence will be recovered through the resolved second-order moments (over time) between the response and excitation.

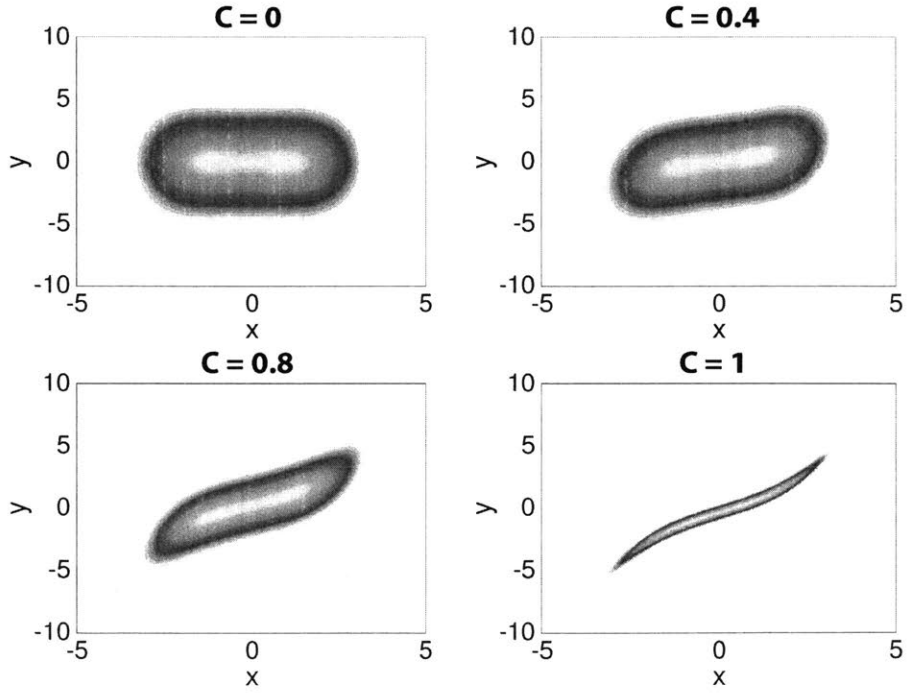

Figure 3-3: The joint response excitation pdf is also shown for different values of the correlation parameter c ranging from small values (corresponding to large values of $|\tau|$) to larger ones (associated with smaller values of $|\tau|$).

Joint response-response pdf. The joint pdf for two different time instants of the response, denoted as $p(x,z)$, is a special case of what has been presented. In order to avoid confusion, a different notation z is used to represent the response at a different time instant $s = t - \tau$. We have:

$$\begin{aligned} p(x,z) &= f(x)f(z)\mathcal{C}\left(F(x),F(z)\right), \\ &= f(x)f(z)\frac{1}{\sqrt{1-c^2}} \\ &\quad \times \exp\left(\frac{2c\Phi^{-1}\left(F(x)\right)\Phi^{-1}\left(F(z)\right) - c^2\left(\Phi^{-1}\left(F(x)\right)^2 + \Phi^{-1}\left(F(z)\right)^2\right)}{2(1-c^2)}\right), \end{aligned} \tag{3.16}$$

where c is a correlation constant (that depends on the time-difference τ). Note that the response z at the second time instant follows the same non-Gaussian pdf corresponding to the single time statistics of the response. In figure 3-3, we present the above joint pdf (equation (3.15)) with the marginal f (response) having a bimodal structure and the marginal g (excitation) having a Gaussian structure. For $c = 0$ we have independence, which essentially expresses the case of very distant two-time statistics, while as we increase c the correlation between the two variables increases referring to the case of small values of τ.

3.4.3 Induced Non-Gaussian Closures

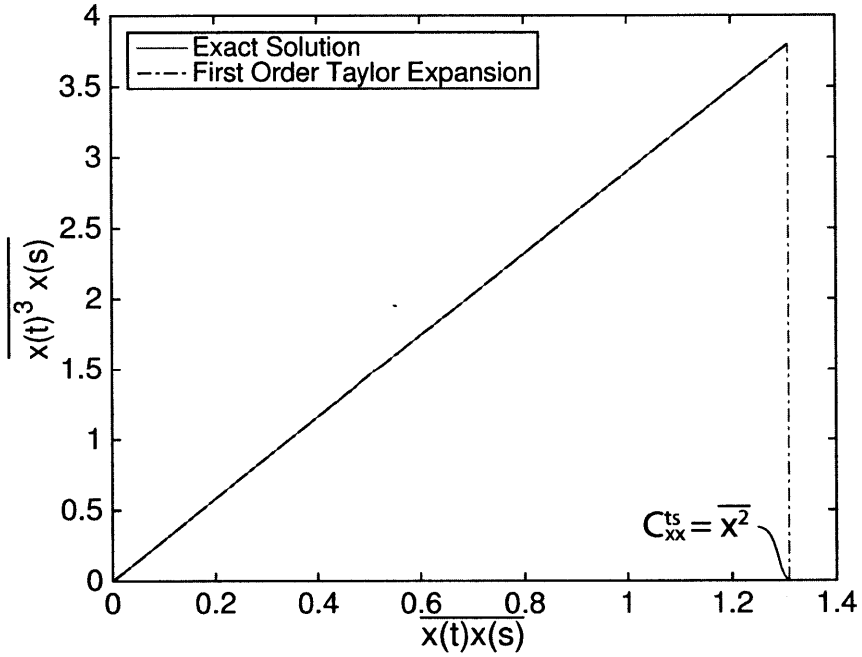

Figure 3-4: The relation between $\overline{x(t)^3 x(s)}$ and $\overline{x(t)x(s)}$. Exact relation is illustrated in red curve and approximated relation using non-Gaussian pdf representations is depicted in black curve.

Using these non-Gaussian pdf representations, we will approximate the fourth order moment terms that show up in the moment equations. We numerically observe that in the context of the pdf representations given above, the relation between $\overline{x(t)^3 x(s)}$ and $\overline{x(t)x(s)}$ is essentially linear (see figure 3-4). To this end, we choose a closure of the following form for both the response-response and the response-excitation terms:

$$\overline{x(t)^3 x(s)} = \rho_{x,x}\, \overline{x(t)x(s)}, \tag{3.17}$$

where $\rho_{x,x}$ is the closure coefficient for the joint response-response statistics. The value of $\rho_{x,x}$ is obtained by expanding both $\overline{x(t)^3 x(s)}$ and $\overline{x(t)x(s)}$ with respect to c keeping

up to the first order terms:

$$\begin{aligned}
\overline{xz} &= \iint xzp(x,z)dxdz \\
&= 2\Big\{\int xf(x)\,\mathrm{erf}^{-1}\left(2F(x)-1\right)dx\Big\}^2 c + \mathcal{O}(c^2), \qquad (3.18)\\
\overline{x^3z} &= \iint x^3zp(x,z)dxdz \\
&= 2\Big\{\int x^3f(x)\,\mathrm{erf}^{-1}\left(2F(x)-1\right)dx\Big\}\Big\{\int zf(z)\,\mathrm{erf}^{-1}\left(2F(z)-1\right)dz\Big\}c + \mathcal{O}(c^2), \qquad (3.19)
\end{aligned}$$

where the error function is given by:

$$\mathrm{erf}(x) = \frac{2}{\sqrt{\pi}}\int_0^x e^{-t^2}dt. \qquad (3.20)$$

Thus, we observe that the assumed copula function in combination with the marginal densities prescribe an explicit dependence between fourth- and second-order moments, expressed through the coefficient:

$$\rho_{x,x} = \frac{\int x^3f(x)\,\mathrm{erf}^{-1}\left(2F(x)-1\right)dx}{\int xf(x)\,\mathrm{erf}^{-1}\left(2F(x)-1\right)dx}. \qquad (3.21)$$

We emphasize that this closure coefficient does not depend on the time-difference τ but only on the single time statistics and in particular the energy level of the system, defined by γ. To this end, for any given marginal pdf f, we can analytically find what would be the closure coefficient under the assumptions of the adopted copula function.

The corresponding coefficient for the joint response-excitation statistics $\rho_{x,y}$ can be similarly obtained through a first order expansion of the moments:

$$\rho_{x,y} = \frac{\int x^3f(x)\,\mathrm{erf}^{-1}\left(2F(x)-1\right)dx}{\int xf(x)\,\mathrm{erf}^{-1}\left(2F(x)-1\right)dx}. \qquad (3.22)$$

The closure coefficient $\rho_{x,y}$ has exactly the same form with the closure coefficient $\rho_{x,x}$ and it does not depend on the statistical properties of the excitation nor on the time-

difference τ but only on the energy level γ. We will refer to equations (equation (3.21)) and (equation (3.22)) as the *closure constraints.* This will be one of the two sets of constraints that we will include in the minimization procedure for the determination of the solution.

3.4.4 Closed Moment Equations

The next step involves the application of above closure scheme on the derived two-time moment equations. By directly applying the induced closure schemes on equations (equation (3.9)) and (equation (3.10)), we have the linear set of moment equations for the second-order statistics:

$$\frac{\partial^2}{\partial\tau^2}C_{xy}(\tau) + \lambda\frac{\partial}{\partial\tau}C_{xy}(\tau) + (k_1 + \rho_{x,y}k_3)C_{xy}(\tau) = \frac{\partial^2}{\partial\tau^2}C_{yy}(\tau), \tag{3.23}$$

$$\frac{\partial^2}{\partial\tau^2}C_{xx}(\tau) + \lambda\frac{\partial}{\partial\tau}C_{xx}(\tau) + (k_1 + \rho_{x,x}k_3)C_{xx}(\tau) = \frac{\partial^2}{\partial\tau^2}C_{xy}(-\tau). \tag{3.24}$$

Using the Wiener-Khinchin theorem, we transform the above equations to the corresponding power spectral density equations:

$$\{(j\omega)^2 + \lambda(j\omega) + k_1 + \rho_{x,y}k_3\}S_{xy}(\omega) = (j\omega)^2 S_{yy}(\omega), \tag{3.25}$$

$$\{(j\omega)^2 - \lambda(j\omega) + k_1 + \rho_{x,x}k_3\}S_{xx}(\omega) = (j\omega)^2 S_{xy}(\omega). \tag{3.26}$$

These equations allow us to obtain an expression for the power spectral density of the response displacement in terms of the excitation spectrum:

$$S_{xx}(\omega) = \left|\frac{\omega^4}{\{k_1 + \rho_{x,y}k_3 - \omega^2 + j(\lambda\omega)\}\{k_1 + \rho_{x,x}k_3 - \omega^2 - j(\lambda\omega)\}}\right| S_{yy}(\omega). \tag{3.27}$$

Integration of the above equation will give us the variance of the response:

$$\begin{aligned}\overline{x^2} &= \int_0^\infty S_{xx}(\omega)d\omega \\ &= \int_0^\infty \left|\frac{\omega^4}{\{k_1 + \rho_{x,y}k_3 - \omega^2 + j(\lambda\omega)\}\{k_1 + \rho_{x,x}k_3 - \omega^2 - j(\lambda\omega)\}}\right| S_{yy}(\omega)d\omega.\end{aligned} \tag{3.28}$$

The last equation is the second constraint, the *dynamics constraint*, which expresses the second order dynamics of the system. Our goal is to optimally satisfy it together with the *closure constraints* defined by equations (equation (3.21)) and (equation (3.22)).

3.4.5 Moment Equation Copula Closure (MECC) Method

The last step is the minimization of the two set of constraints, the *closure constraints* and the *dynamics constraint*, which have been expressed in terms of the system response variance $\overline{x^2}$. The minimization will be done in terms of the unknown energy level γ and the closure coefficients $\rho_{x,x}$ and $\rho_{x,y}$. More specifically, we define the following cost function which incorporates our constraints:

$$\begin{aligned}\mathcal{J}(\gamma,\rho_{x,x},\rho_{x,y}) = &\left\{\overline{x^2} - \int_0^\infty |\frac{\omega^4 S_{yy}(\omega)}{\{k_1+\rho_{x,y}k_3-\omega^2+j(\lambda\omega)\}\{k_1+\rho_{x,x}k_3-\omega^2-j(\lambda\omega)\}}|d\omega\right\}^2 \\ &+\left\{\rho_{x,x} - \frac{\int x^3 f(x)\,\mathrm{erf}^{-1}\left(2F(x)-1\right)dx}{\int x f(x)\,\mathrm{erf}^{-1}\left(2F(x)-1\right)dx}\right\}^2 \\ &+\left\{\rho_{x,y} - \frac{\int x^3 f(x)\,\mathrm{erf}^{-1}\left(2F(x)-1\right)dx}{\int x f(x)\,\mathrm{erf}^{-1}\left(2F(x)-1\right)dx}\right\}^2. \end{aligned} \tag{3.29}$$

Note that in the context of statistical linearization only the first constraint is minimized while the closure coefficient is the one that follows exactly from a Gaussian representation for the pdf. In this context there is no attempt to incorporate in an equal manner the mismatch in the dynamics and the pdf representation. The minimization of this cost function essentially allows mismatch for the equation (expressed through the dynamic constraint) but also for the pdf representation (expressed through the closure constraints). For linear systems and an adopted Gaussian pdf for the response the above cost function vanishes identically.

Chapter 4

Applications of Moment-Equation-Copula-Closure Method

4.1 Formulation

In chapter 3, we have developed computational framework which allows for the inexpensive and accurate approximation of the second order statistics of the system even for oscillators associated with double-well potentials. In addition, it allows for the semi-analytical approximation of the full non-Gaussian joint response-excitation pdf in a post-processing manner.

In this chapter, we illustrate applications of the developed approach through nonlinear single-degree-of-freedom energy harvesters with double-well potentials subjected to correlated noise with Pierson-Moskowitz power spectral density. We also consider the case of bi-stable oscillators coupled with electromechanical energy harvesters (one and a half degrees-of-freedom systems), and we demonstrate how the proposed probabilistic framework can be used for performance optimization and parameters selection. In the later section, we extend the applicability of MECC method to a

general linear structure attached with a nonlinear energy harvesters. We consider two examples, the linear single-degree-of-freedom system and the linear undamped elastic rod, under stochastic forcing with Pierson-Moskowitz spectrum and provide the comparison of semi-analytical results and direct Monte-Carlo simulations. We note that, for all applications, it is assumed that the stationary stochastic excitation has a power spectral density given by the Pierson-Moskowitz spectrum, which is typical for excitation created by random water waves:

$$S(\omega) = q\ \frac{1}{\omega^5} \exp(-\frac{1}{\omega^4}), \tag{4.1}$$

where q controls the intensity of the excitation.

4.2 SDOF Bistable Oscillator Excited by Colored Noise

For the colored noise excitation that we just described, we apply the MECC method. We consider a set of system parameters that correspond to a double well potential. Depending on the intensity of the excitation (which is adjusted by the factor q), the response of the bistable system 'lives' in three possible regimes. If q is very low, the bistable system is trapped in either of the two wells while if q is very high the energy level is above the homoclinic orbit and the system performs cross-well oscillations. Between these two extreme regimes, the stochastic response exhibits combined features and characteristics of both energy levels and it has a highly nonlinear, multi-frequency character [47, 46].

Despite these challenges, the presented MECC method can inexpensively provide with a very good approximation of the system's statistical characteristics as it is shown in figure 4-1. In particular in figure 4-1, we present the response variance as the intensity of the excitation varies for two sets of the system parameters. We also compare our results with direct Monte-Carlo simulations and with a standard Gaussian closure method [136, 140, 55].

For the Monte-Carlo simulations the time series for the excitation has been generated as the sum of cosines over a range of frequencies. The amplitudes and the range of frequencies are determined through the power spectrum while the phases are assumed to be random variables which follow a uniform distribution. In the presented examples, the excitation has power spectral density that follows the Pierson-Moskowitz spectrum. Once each ensemble time series for the excitation has been computed, the governing ordinary differential equation is solved using a 4th/5th order Runge-Kutta method. For each realization the system is integrated for a sufficiently long time interval in order to guarantee that the response statistics have converged. For each problem, we generate 100 realizations in order to compute the second-order statistics. However,

for the computation of the full joint pdf, a significantly larger number of samples is needed reaching the order of 10^7.

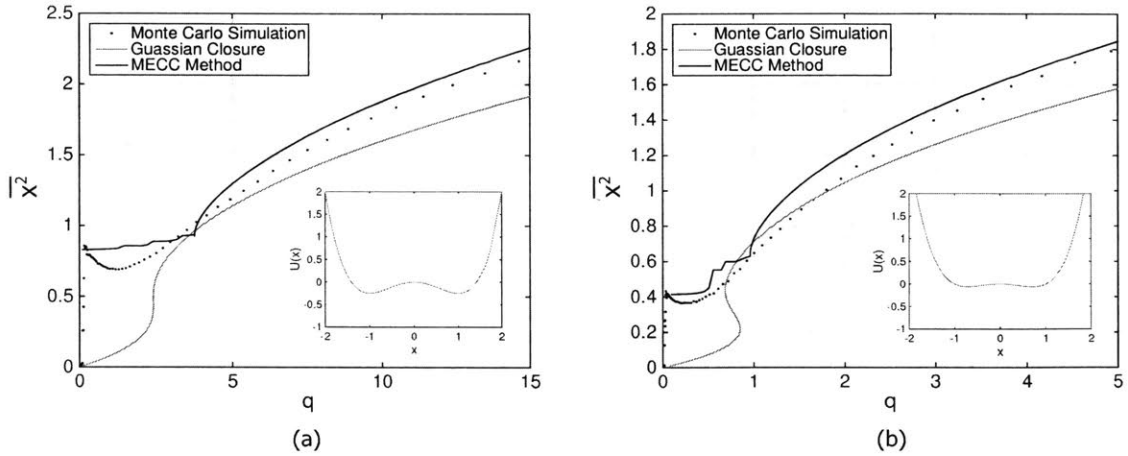

Figure 4-1: Mean square response displacement with respect to the amplification factor of Pierson-Moskowitz spectrum for the bistable system with two different sets of system parameters. (a) $\lambda = 1$, $k_1 = -1$, and $k_3 = 1$. (b) $\lambda = 0.5$, $k_1 = -0.5$, and $k_3 = 1$.

We observe that for very large values of q the computed approximation closely follows the Monte-Carlo simulation. On the other hand, the Gaussian closure method systematically underestimates the variance of the response. For lower intensities of the excitation, the exact (Monte-Carlo) variance presents a non-monotonic behavior with respect to q due to the co-existence of the cross- and intra-well oscillations. While the Gaussian closure has very poor performance on capturing this trend, the MECC method can still provide a satisfactory approximation of the dynamics. Note that the non-smooth transition observed in the MECC curve is due to the fact that for very low values of q the minimization of the cost function (equation (3.29)) does not reach a zero value while this is the case for larger values of q. In other words, in the strongly nonlinear regime neither the *dynamics constraint* nor the *closure constraint* is satisfied exactly, yet this optimal solution provides with a good approximation of the system dynamics.

After we have obtained the unknown parameters γ, $\rho_{x,x}$ and $\rho_{x,y}$ by minimizing the cost function for each given q, we can then compute the covariance functions and the joint

pdf in a post-process manner. More specifically, since a known γ corresponds to a specific $\rho_{x,y}$ (equation (equation (3.22))) we can immediately determine $C_{xy}(\tau)$ by taking the inverse Fourier transform of S_{xy} found through equation (equation (3.25)). The next step is the numerical integration of the closed moment equation (equation (3.24)) utilizing the determined value $\rho_{x,x}$ with initial conditions given by

$$C_{xx}(0) = \int x^2 f(x;\gamma)\, dx, \quad \textit{and} \quad \dot{C}_{xx}(0) = 0, \tag{4.2}$$

where the second condition follows from the symmetry properties of C_{xx}. Note that we integrate equation (equation (3.24)) instead of using the inverse Fourier transform as we did for $C_{xy}(\tau)$ so that we can impose the variance found in the last equation by integrating the resulted density for the determined γ. Using the correlation functions $C_{xx}(\tau)$ and $C_{xy}(\tau)$ we can also determine, for each case, the correlation coefficient c of the copula function for each time-difference τ. The detailed steps are given at the end of this subsection.

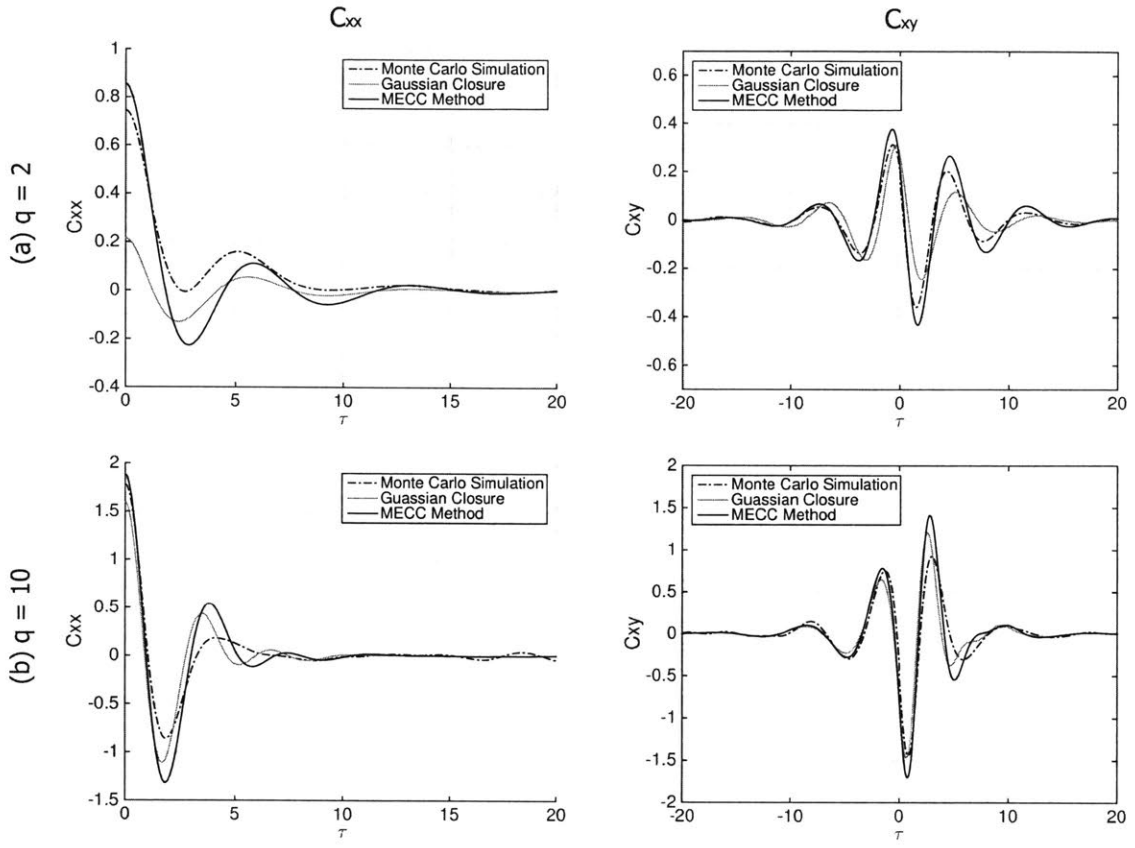

Figure 4-2: Correlation functions C_{xx} and C_{xy} of the bistable system with system parameters $\lambda = 1$, $k_1 = -1$, and $k_3 = 1$ subjected to Pierson-Moskowitz spectrum. (a) Amplification factor of $q = 2$. (b) Amplification factor of $q = 10$.

The results as well as a comparison with the Gaussian closure method and a direct Monte-Carlo simulation are presented in figure 4-2. We can observe that through the proposed approach we are able to satisfactorily approximate the correlation function even close to the non-linear regime $q = 2$, where the Gaussian closure method presents important discrepancies.

Finally, using the computed parameters γ and closure coefficients, $\rho_{x,x}$ and $\rho_{x,y}$, we can also construct the three-dimensional non-Gaussian joint pdf for the response-response-excitation at different time instants. This will be derived based on the three-

dimensional Gaussian copula density of the following form:

$$\mathcal{C}\left(F(x),F(z),G(y)\right)=\frac{1}{\sqrt{\det R}}\exp\left(-\frac{1}{2}\begin{bmatrix}\Phi^{-1}\left(F(x)\right)\\ \Phi^{-1}\left(F(z)\right)\\ \Phi^{-1}\left(G(y)\right)\end{bmatrix}^{T}\cdot\left(R^{-1}-\mathbf{I}\right)\cdot\begin{bmatrix}\Phi^{-1}\left(F(x)\right)\\ \Phi^{-1}\left(F(z)\right)\\ \Phi^{-1}\left(G(y)\right)\end{bmatrix}\right). \tag{4.3}$$

The three-dimensional non-Gaussian joint pdf for the response-response-excitation at different time instants can be expressed as follows:

$$\begin{aligned}f_{x(t),x(t+\tau),y(t+\tau)}(x,z,y)&=f(x)f(z)g(y)\mathcal{C}\left(F(x),F(z),G(y)\right)\\&=f(x)f(z)g(y)\frac{1}{\sqrt{\det R}}\\&\quad\times\exp\left(-\frac{1}{2}\begin{bmatrix}\Phi^{-1}\left(F(x)\right)\\ \Phi^{-1}\left(F(z)\right)\\ \Phi^{-1}\left(G(y)\right)\end{bmatrix}^{T}\cdot\left(R^{-1}-\mathbf{I}\right)\cdot\begin{bmatrix}\Phi^{-1}\left(F(x)\right)\\ \Phi^{-1}\left(F(z)\right)\\ \Phi^{-1}\left(G(y)\right)\end{bmatrix}\right).\end{aligned} \tag{4.4}$$

where R represents the $3\times\ 3$ correlation matrix with all diagonal elements equal to 1:

$$R=\begin{bmatrix}1 & c_{xz} & c_{xy}\\ c_{xz} & 1 & c_{zy}\\ c_{xy} & c_{zy} & 1\end{bmatrix}. \tag{4.5}$$

The time dependent parameters c_{xz}, c_{xy}, c_{zy} of the copula function can be found through the resolved moments, by expanding the latter as:

$$C_{xx}(\tau)=\iint xzf_{x(t),x(t+\tau),y(t+\tau)}(x,z,y)dxdydz=2\mathcal{F}^{2}c_{xz}+\mathcal{O}\left(c_{xz}^{2}\right), \tag{4.6}$$

$$C_{xy}(\tau)=\iint xyf_{x(t),x(t+\tau),y(t+\tau)}(x,z,y)dxdydz=2\mathcal{F}\mathcal{G}c_{xy}+\mathcal{O}\left(c_{xy}^{2}\right), \tag{4.7}$$

$$C_{xy}(0)=\iint zyf_{x(t),x(t+\tau),y(t+\tau)}(x,z,y)dxdydz=2\mathcal{F}\mathcal{G}c_{zy}+\mathcal{O}\left(c_{zy}^{2}\right). \tag{4.8}$$

where,

$$\mathcal{F} = \int x f(x) \operatorname{erf}^{-1}(2F(x) - 1)\, dx \quad \text{and} \quad \mathcal{G} = \int x g(x) \operatorname{erf}^{-1}(2G(x) - 1)\, dx.$$

If necessary higher order terms may be retained in the Taylor expansion although for the present problem a linear approximation was sufficient. The computed approximation is presented in figure 4-3 through two dimensional marginals as well as through isosurfaces of the full three-dimensional joint pdf. We compare with direct Monte-Carlo simulations and as we are able to observe, the computed pdf compares favorably with the expensive Monte-Carlo simulation. The joint statistics using the Monte-Carlo approach were computed using 10^7 number of samples while the computational cost of the MECC method involved the minimization of a three dimensional function.

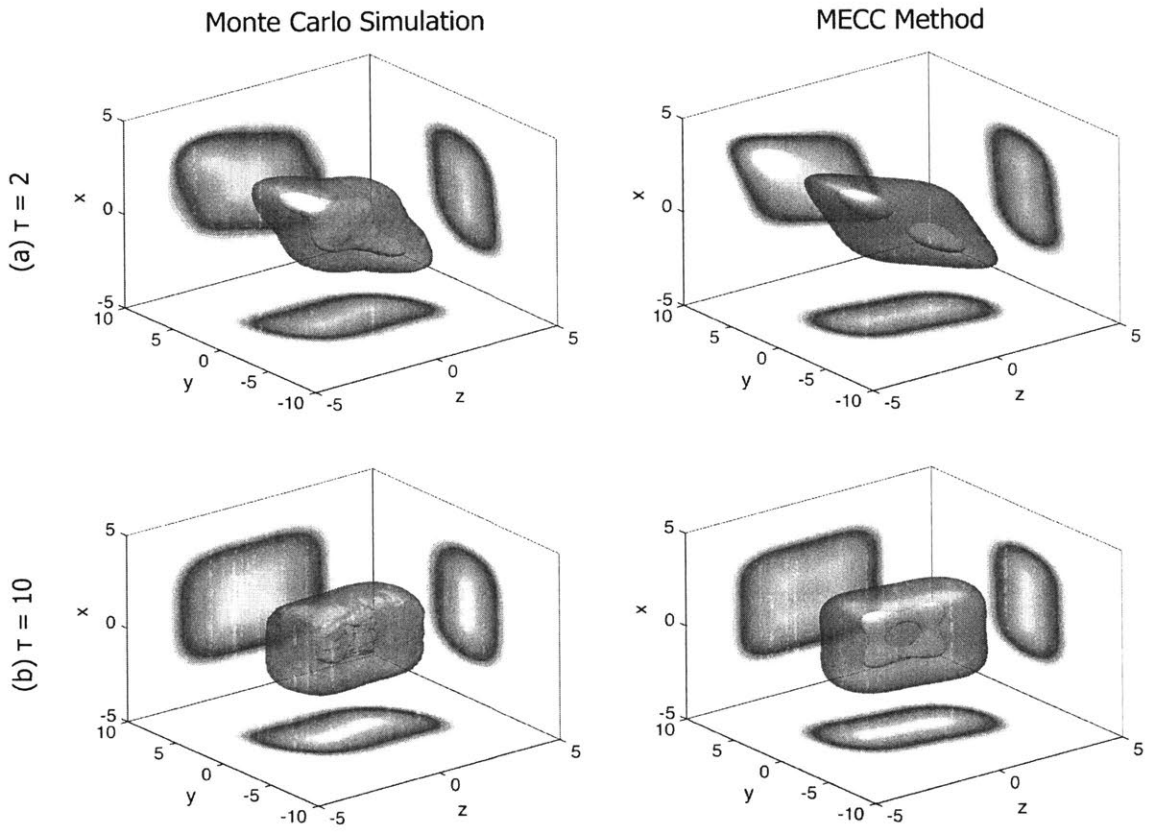

Figure 4-3: Joint pdf $f_{x(t)x(t+\tau)y(t+\tau)}(x, z, y)$ computed using direct Monte-Carlo simulation and the MECC method. The system parameters are given by $\lambda = 1$, $k_1 = -1$, and $k_3 = 1$ and the excitation is Gaussian following a Pierson-Moskowitz spectrum with $q = 10$. The pdf is presented through two dimensional marginals as well as through isosurfaces. (a) $\tau = 3$. (b) $\tau = 10$.

4.3 SDOF Bistable Oscillator Coupled to an Electromechanical Harvester

In practical configurations, energy harvesting occurs through a linear electromechanical transducer coupled to the nonlinear oscillator [56, 72, 99]. In this section, we assess how our method performs for a bistable nonlinear SDOF oscillator coupled to a linear electromechanical transducer. The equations of motion in this case take the form:

$$\ddot{x} + \lambda\dot{x} + k_1 x + k_3 x^3 + \alpha v = \ddot{y}, \tag{4.9}$$

$$\dot{v} + \beta v = \delta\dot{x}, \tag{4.10}$$

where x is the response displacement, y is a stationary stochastic excitation, v is the voltage across the load, λ is the normalized damping coefficient, k_1 and k_3 are the normalized stiffness coefficients, α and δ are the normalized coupling coefficients, and β is the normalized time coefficient for the electrical system. All the coefficients except k_1 are positive. Based on the linearity of the second equation, we express the voltage in an integral form:

$$v(t) = \delta \int_0^t \dot{x}(\zeta) e^{-\beta(t-\zeta)} d\zeta = \delta\dot{x}(t) * e^{-\beta t} u(t), \tag{4.11}$$

where $*$ indicates convolution and $u(t)$ represents the Heaviside step function. We then formulate the second-order moment equations following a similar approach with

the previous section.

$$\frac{\partial^2}{\partial t^2}\overline{x(t)y(s)} + \lambda\frac{\partial}{\partial t}\overline{x(t)y(s)} + k_1\overline{x(t)y(s)} + k_3\overline{x(t)^3y(s)} + \alpha\overline{v(t)y(s)} = \frac{\partial^2}{\partial t^2}\overline{y(t)y(s)}, \tag{4.12}$$

$$\frac{\partial^2}{\partial t^2}\overline{x(t)x(s)} + \lambda\frac{\partial}{\partial t}\overline{x(t)x(s)} + k_1\overline{x(t)x(s)} + k_3\overline{x(t)^3x(s)} + \alpha\overline{v(t)x(s)} = \frac{\partial^2}{\partial t^2}\overline{y(t)x(s)}, \tag{4.13}$$

$$\frac{\partial}{\partial t}\overline{v(t)v(s)} + \beta\overline{v(t)v(s)} = \delta\frac{\partial}{\partial t}\overline{x(t)v(s)}. \tag{4.14}$$

In this case, we estimate two additional covariance functions, $\overline{v(t)y(s)}$ and $\overline{v(t)x(s)}$ before applying MECC method:

$$\overline{v(t)y(s)} = \delta\int_0^t \overline{\dot{x}(\zeta)y(s)}e^{-\beta(t-\zeta)}d\zeta, \tag{4.15}$$

$$= \delta\int_0^t \frac{\partial}{\partial\zeta}C_{xy}(\zeta - s)e^{-\beta(t-\zeta)}d\zeta, \tag{4.16}$$

$$= \delta\frac{\partial}{\partial t}C_{xy}(t-s) * e^{-\beta t}u(t), \tag{4.17}$$

$$= \delta\frac{\partial}{\partial\tau}C_{xy}(\tau) * e^{-\beta t}u(t), \tag{4.18}$$

where $\tau = t - s$ is the time difference of two generic time instants t and s. Considering the power spectrum, the Fourier transform of the above gives:

$$\mathcal{F}\{\overline{v(t)y(s)}\} = S_{vy}(\omega) = \frac{j\delta\omega}{\beta + j\omega}S_{xy}(\omega). \tag{4.19}$$

Similarly, we also obtain for $\overline{v(t)x(s)}$:

$$\mathcal{F}\{\overline{v(t)x(s)}\} = S_{vx}(\omega) = \frac{j\delta\omega}{\beta + j\omega}S_{xx}(\omega). \tag{4.20}$$

By applying the previously described closure scheme on equations (equation (4.12)) and (equation (4.13)), we have a linear set of moment equations for the second-order

statistics:

$$\frac{\partial^2}{\partial\tau^2}C_{xy}(\tau)+\lambda\frac{\partial}{\partial\tau}C_{xy}(\tau)+(k_1+\rho_{x,y}k_3)C_{xy}(\tau)+\alpha\delta\frac{\partial}{\partial\tau}C_{xy}(\tau)*e^{-\beta t}u(t)=\frac{\partial^2}{\partial\tau^2}C_{yy}(\tau), \tag{4.21}$$

$$\frac{\partial^2}{\partial\tau^2}C_{xx}(\tau)+\lambda\frac{\partial}{\partial\tau}C_{xx}(\tau)+(k_1+\rho_{x,x}k_3)C_{xx}(\tau)+\alpha\delta\frac{\partial}{\partial\tau}C_{xx}(\tau)*e^{-\beta t}u(t)=\frac{\partial^2}{\partial\tau^2}C_{xy}(-\tau), \tag{4.22}$$

$$\frac{\partial}{\partial\tau}C_{vv}(\tau)+\beta C_{vv}(\tau)=\delta\frac{\partial}{\partial\tau}C_{vx}(-\tau). \tag{4.23}$$

Using the Wiener-Khinchin theorem, we transform the above equations to the corresponding power spectral density equations:

$$\{(j\omega)^2+\lambda(j\omega)+k_1+\rho_{x,y}k_3+\frac{j\alpha\delta\omega}{\beta+j\omega}\}S_{xy}(\omega)=(j\omega)^2S_{yy}(\omega), \tag{4.24}$$

$$\{(j\omega)^2-\lambda(j\omega)+k_1+\rho_{x,x}k_3-\frac{j\alpha\delta\omega}{\beta-j\omega}\}S_{xx}(\omega)=(j\omega)^2S_{xy}(\omega), \tag{4.25}$$

$$\{-(j\omega)+\beta\}S_{vv}(\omega)=-\delta(j\omega)S_{vx}(\omega). \tag{4.26}$$

These equations allow us to obtain an expression for the power spectral density of the response displacement and response voltage in terms of the excitation spectrum:

$$S_{xx}(\omega)=\left|\frac{\omega^4}{\{k_1+\rho_{x,y}k_3-\omega^2+j(\lambda\omega)+\frac{j\alpha\delta\omega}{\beta+j\omega}\}}\times\frac{1}{\{k_1+\rho_{x,x}k_3-\omega^2-j(\lambda\omega)-\frac{j\alpha\delta\omega}{\beta-j\omega}\}}\right|S_{yy}(\omega), \tag{4.27}$$

$$S_{vv}(\omega)=\left|\frac{\delta^2\omega^6}{\{\beta^2+\omega^2\}\{k_1+\rho_{x,y}k_3-\omega^2+j(\lambda\omega)+\frac{j\alpha\delta\omega}{\beta+j\omega}\}}\times\frac{1}{\{k_1+\rho_{x,x}k_3-\omega^2-j(\lambda\omega)-\frac{j\alpha\delta\omega}{\beta-j\omega}\}}\right|S_{yy}(\omega). \tag{4.28}$$

Integration of the above equation will give us the variance of the response displacement and voltage:

$$\overline{x^2} = \int_0^\infty \left| \frac{\omega^4}{\{k_1 + \rho_{x,y}k_3 - \omega^2 + j(\lambda\omega) + \frac{j\alpha\delta\omega}{\beta+j\omega}\}} \times \frac{1}{\{k_1 + \rho_{x,x}k_3 - \omega^2 - j(\lambda\omega) - \frac{j\alpha\delta\omega}{\beta-j\omega}\}} \right| S_{yy}(\omega)d\omega, \quad (4.29)$$

$$\overline{v^2} = \int_0^\infty \left| \frac{\delta^2\omega^6}{\{\beta^2+\omega^2\}\{k_1 + \rho_{x,y}k_3 - \omega^2 + j(\lambda\omega) + \frac{j\alpha\delta\omega}{\beta+j\omega}\}} \times \frac{1}{\{k_1 + \rho_{x,x}k_3 - \omega^2 - j(\lambda\omega) - \frac{j\alpha\delta\omega}{\beta-j\omega}\}} \right| S_{yy}(\omega)d\omega. \quad (4.30)$$

Equation (equation (4.29)) expresses the second order dynamics of the SDOF bistable oscillator coupled with an electromechanical harvester, and is the *dynamics constraint* for this system. We will minimize it together with the *closure constraints* defined by equations (equation (3.21)) and (equation (3.22)):

$$\begin{aligned} \mathcal{J}(\gamma, \rho_{x,x}, \rho_{x,y}) = & \left\{ \rho_{x,x} - \frac{\int x^3 f(x) \operatorname{erf}^{-1}(2F(x)-1)\,dx}{\int x f(x) \operatorname{erf}^{-1}(2F(x)-1)\,dx} \right\}^2 \\ & + \left\{ \rho_{x,y} - \frac{\int x^3 f(x) \operatorname{erf}^{-1}(2F(x)-1)\,dx}{\int x f(x) \operatorname{erf}^{-1}(2F(x)-1)\,dx} \right\}^2 \\ & + \left\{ \overline{x^2} - \int_0^\infty \left| \frac{\omega^4 S_{yy}(\omega)}{\{k_1 + \rho_{x,y}k_3 - \omega^2 + j(\lambda\omega) + \frac{j\alpha\delta\omega}{\beta+j\omega}\}} \times \frac{1}{\{k_1 + \rho_{x,x}k_3 - \omega^2 - j(\lambda\omega) - \frac{j\alpha\delta\omega}{\beta-j\omega}\}} \right| d\omega \right\}^2. \end{aligned} \quad (4.31)$$

In figure 4-4, we illustrate the variance of the response displacement and the voltage as the intensity of the excitation varies for two sets of the system parameters. For both sets of system parameters, we observe that for large intensity of the excitation, the MECC method computes the response variances (displacement and voltage) very accurately, while the Gaussian closure method systematically underestimates them.

For lower intensities of the excitation, the response displacement variance computed by the Monte-Carlo simulation presents a non-monotonic behavior with respect to q. While the Gaussian closure has very poor performance on capturing this trend, the MECC method can still provide a satisfactory approximation of the dynamics.

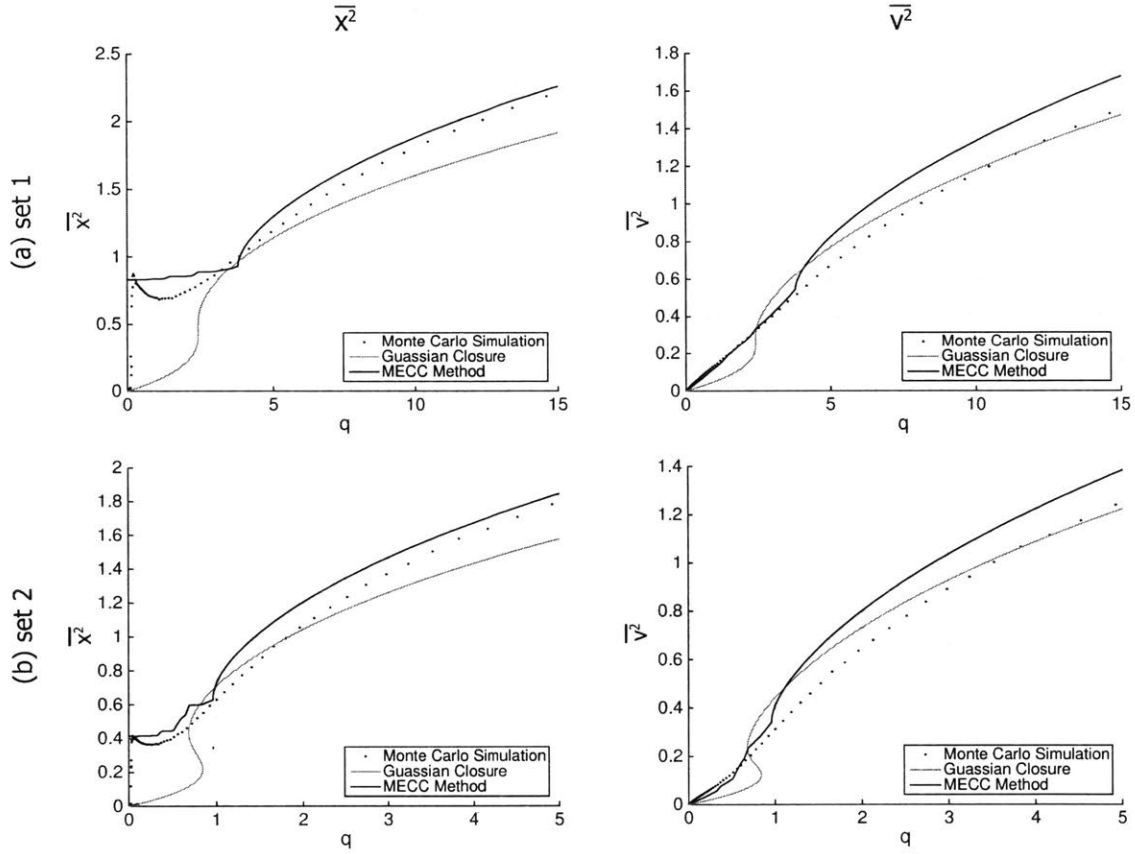

Figure 4-4: Mean square response displacement and mean square response voltage with respect to the amplification factor of Pierson-Moskowitz spectrum for bistable system with two different sets of system parameters. Electromechanical harvester parameters are $\alpha = 0.01$, $\beta = 1$, and $\delta = 1$. (a) $\lambda = 1$, $k_1 = -1$, and $k_3 = 1$. (b) $\lambda = 0.5$, $k_1 = -0.5$, and $k_3 = 1.0$.

Following similar steps with the previous section, we obtain the covariance functions of the response displacement and voltage and the joint pdf in a post-process manner. The results as well as a comparison with the Gaussian closure method and the Monte-Carlo simulation are illustrated in figure 4-5. We can observe that through the proposed approach we are able to satisfactorily approximate the correlation function even close to the non-linear regime $q = 2$, where the Gaussian closure method presents important discrepancies. In figure 4-6, we illustrate two dimensional marginal pdfs as well as isosurfaces of the full three-dimensional joint pdf. We compare with direct Monte-Carlo simulations and as we are able to observe, the computed pdf closely approximates the expensive Monte-Carlo simulation in statistical regimes which are far from Gaussian.

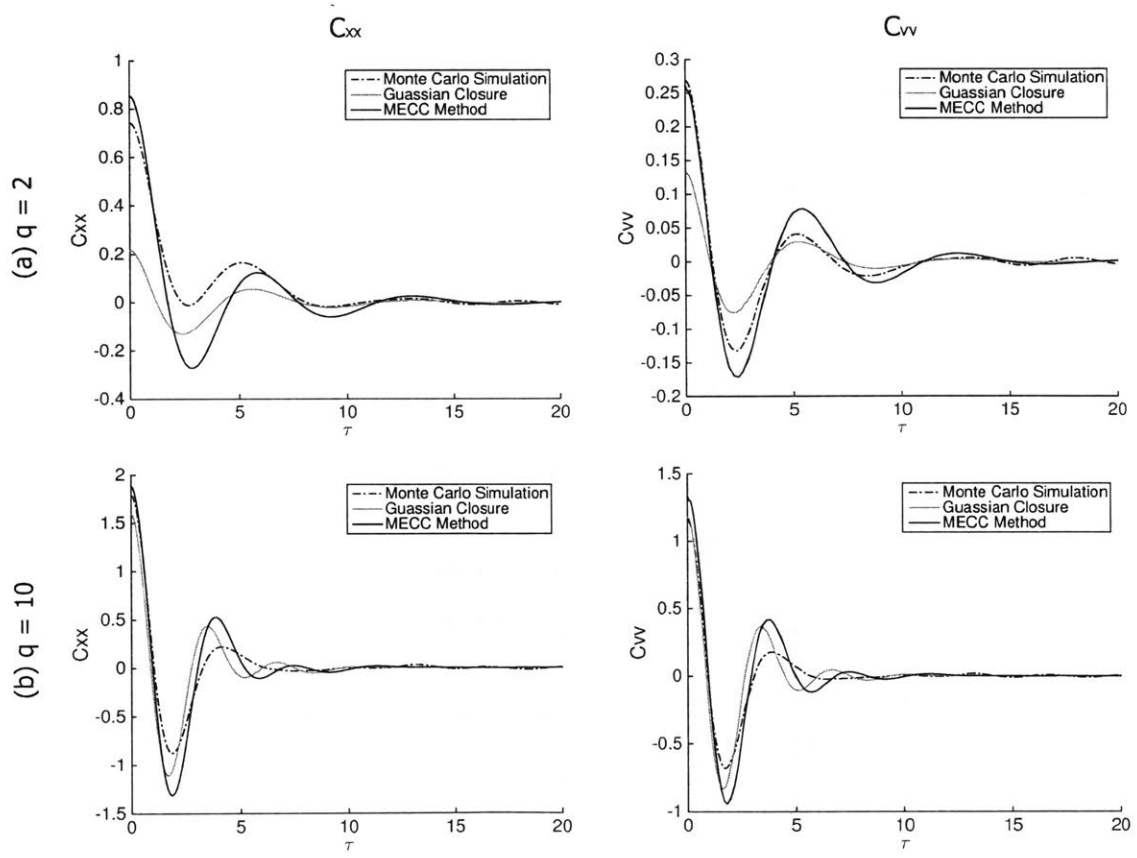

Figure 4-5: Correlation functions C_{xx} and C_{vv} of the bistable system with $\lambda = 1$, $k_1 = -1$, and $k_3 = 1$ subjected to Pierson-Moskowitz spectrum. Electromechanical harvester parameters are $\alpha = 0.01$, $\beta = 1$, and $\delta = 1$. (a) Amplification factor of $q = 2$. (b) Amplification factor of $q = 10$.

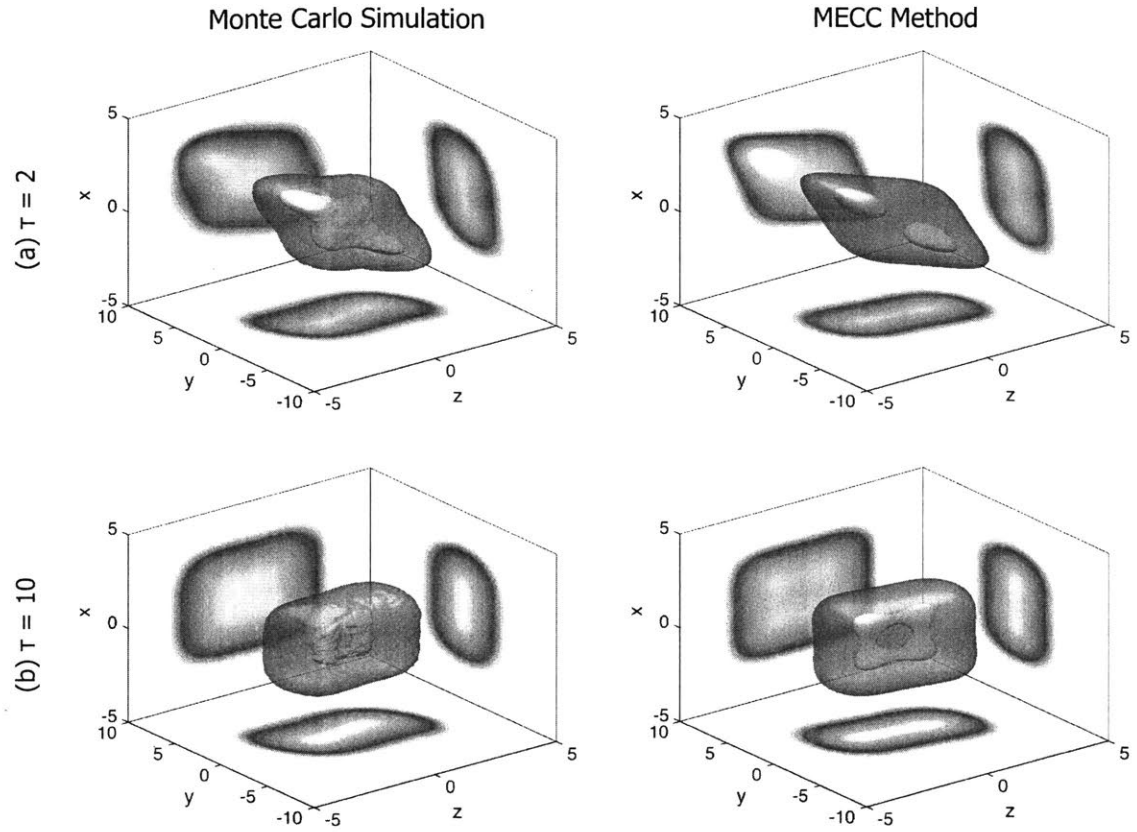

Figure 4-6: Joint pdf $f_{x(t)x(t+\tau)y(t+\tau)}(x, z, y)$ computed using direct Monte-Carlo simulation and the MECC method. The system parameters are given by $\lambda = 1$, $k_1 = -1$, and $k_3 = 1$ under Pierson-Moskowitz spectrum $q = 10$. Electromechanical harvester parameters are $\alpha = 0.01$, $\beta = 1$, and $\delta = 1$. The pdf is presented through two dimensional marginals as well as through isosurfaces. (a) $\tau = 3$. (b) $\tau = 10$.

Finally in figure 4-7, we demonstrate how the proposed MECC method can be used to study robustness over variations of the excitation parameters. In particular, we present the mean square response displacement and response voltage estimated for various amplification factors q and frequency-varied excitation spectra:

$$S_p(\omega) = S(\omega - \omega_0), \tag{4.32}$$

where ω_0 is the perturbation frequency. The comparison with direct Monte-Carlo simulation indicates the effectiveness of the presented method to capture accurately the response characteristics over a wide range of input parameters.

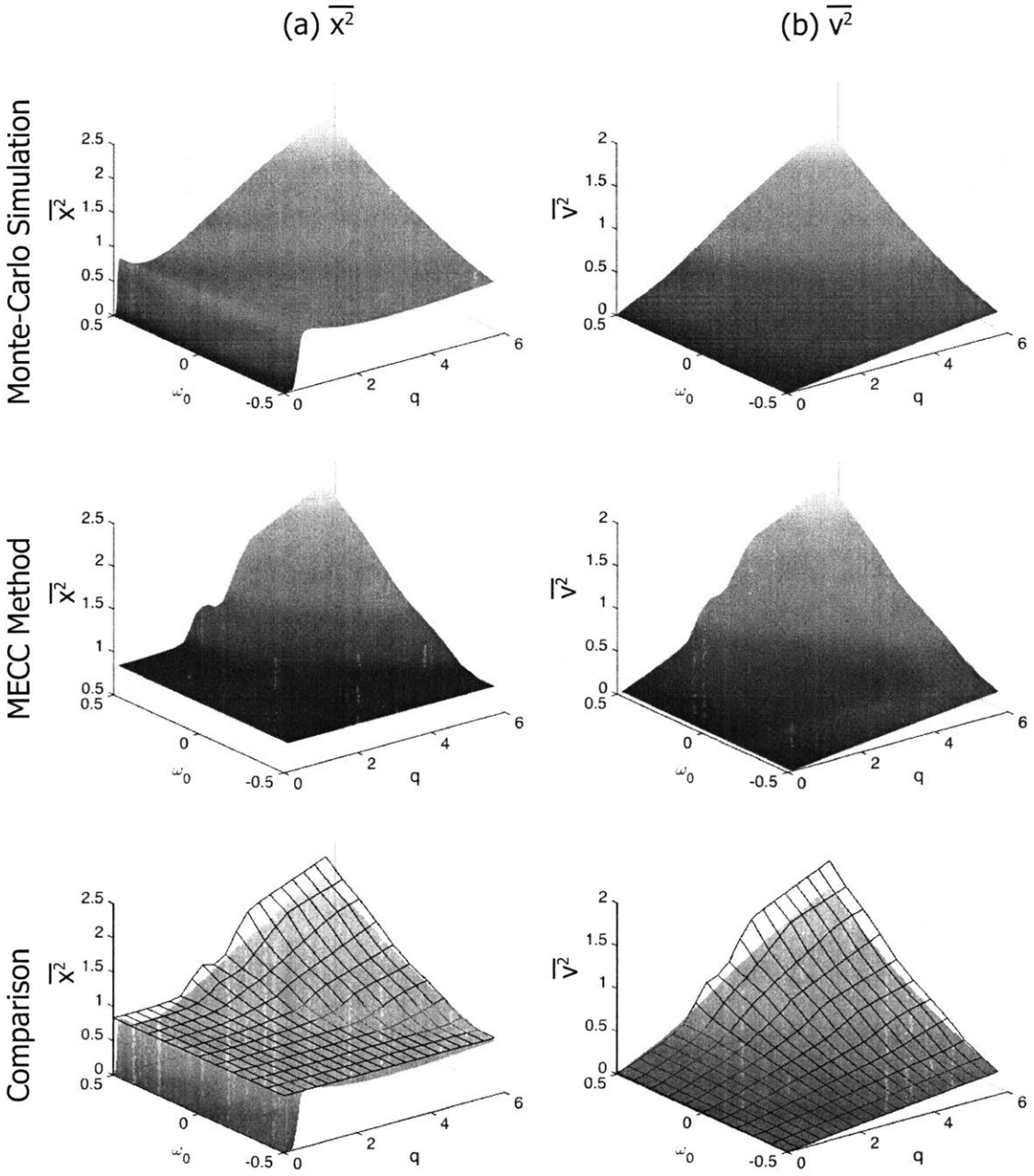

Figure 4-7: Performance comparison (mean square response displacement (a) and voltage (b)) between Monte-Carlo simulations (100 realizations) and MECC method. Results are shown in terms of the amplification factor q and the perturbation frequency ω_0 of the excitation spectrum (Pierson-Moskowitz) for the bistable system with $\lambda = 1$, $k_1 = -1$, and $k_3 = 1$. The electromechanical harvester parameters are $\alpha = 0.01$, $\beta = 1$, and $\delta = 1$.

4.4 General Linear Structure Attached with SDOF Bistable Oscillator

In this section we consider the bistable energy harvester attached to a general linear structure, and we apply the previously developed Moment Equation Copula Closure (MECC) method to obtain the response statistics. We first formulate the problem for a generalized dynamical configuration, and in the later subsections we provide two examples: one is single-degree-of-freedom system attached with a bistable energy harvester, and the other is continuous linear elastic rod attached with a bistable energy harvester. In this way we point out the applicability of the MECC method to an arbitrary linear structure for the purpose of energy harvesting with bistable oscillator.

4.4.1 General Linear Structure

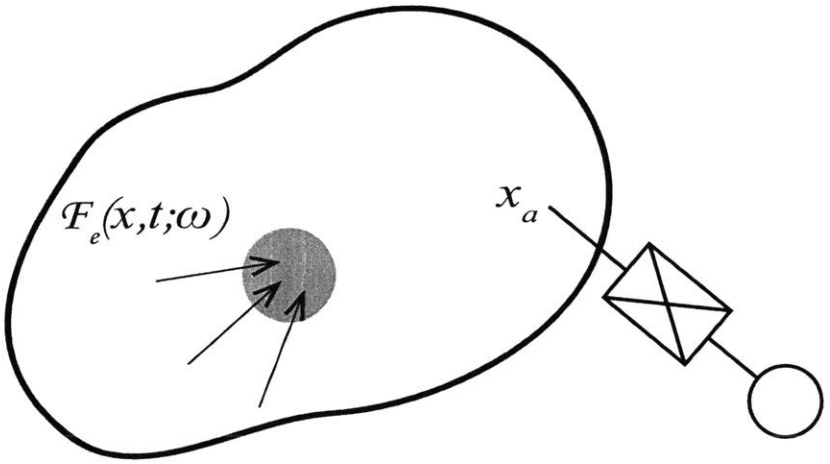

Figure 4-8: General linear structure attached with nonlinear (i.e. bistable) energy harvester.

We first formulate the problem with a general linear structure subject to an external forcing attached with an energy harvester. The way we set up the problem as well as definitions and notations are initially introduced in [128]. Here we adopt the same procedures by slightly modifying and adjusting to our problem. Interested readers should first refer to the original paper [128].

The dynamics of a linear structure can be formulated in terms of a linear operator.

$$\frac{\partial^2 u(x,t)}{\partial t^2} = \mathcal{L}[u(x,t)] + \mathcal{F}(x,t;\varpi), \qquad x \in \mathcal{D}, \varpi \in \Omega. \tag{4.33}$$

Here $u(x,t)$ indicates the response of the linear structure, x is an index taking values in a discrete or continuous set $\mathcal{D}$, and $\mathcal{F}$ describes all the stochastic and/or deterministic forcing acting on the linear structure. We consider a probability space Ω which contains the set of events $\varpi \in \Omega$. The boundary conditions and initial conditions can be expressed by

$$\mathcal{M}[u(x,t)] = h(x,t), \tag{4.34}$$

$$u(x,t_0) = f_0(x;\varpi), \quad u_t(x,t_0) = g_0(x;\varpi), \qquad x \in \mathcal{D}, \varpi \in \Omega, \tag{4.35}$$

where $\mathcal{M}[u(x,t)]$ is the operator for the boundary condition, f_0 and g_0 describe the initial conditions of displacement and velocity, respectively. In our problem the linear structure is coupled with a nonlinear (bistable) energy harvester connected to the linear structure at point x_a (figure 4-8). We consider the case of bimodal nonlinearity which can be characterized by negative linear stiffness $k_{1a} < 0$ and positive cubic stiffness $k_{3a} > 0$:

$$m_a\ddot{q} + \lambda_a(\dot{q} - u_t(x_a,t)) + k_{1a}(q - u(x_a,t)) + k_{3a}(q - u(x_a,t))^3 = 0, \tag{4.36}$$

$$q(t_0;\varpi) = q_0(\varpi), \qquad \dot{q}(t_0;\varpi) = \dot{q}_0(\varpi), \quad \varpi \in \Omega, \tag{4.37}$$

where m_a and λ_a are mass and damping coefficient of the attachment, respectively. We note that the coupling with the linear structure has been introduced through the relative displacement $q - u(x_a,t)$ across the nonlinear attachment. Considering the external force $\mathcal{F}_e(x,t;\varpi)$, we can split the force acting on the linear structure $\mathcal{F}(x,t;\varpi)$

as follows.

$$\mathcal{F}(x,t;\overline{\omega}) = \Big[\lambda_a(\dot{q} - u_t(x_a,t)) + k_{1a}(q - u(x_a,t)) + k_{3a}(q - u(x_a,t))^3\Big]\delta(x - x_a) + \mathcal{F}_e(x,t;\overline{\omega}). \tag{4.38}$$

Now we can characterize the response of the linear structure in terms of a Green's function [10]. Detailed derivation and proofs can be found in [128, 10].

$$u(x,t) = \int_{t_0}^{t}\int_D G(x,t|y,s)\mathcal{F}(y,s;\overline{\omega})dyds + \int_D \Big[G(x,t|y,t_0)g_0(y;\overline{\omega}) - G_t(x,t|y,t_0)f_0(y;\overline{\omega})\Big]dy. \tag{4.39}$$

By plugging equation (4.38) into the above, we obtain

$$\begin{aligned} u(x,t) = &\int_{t_0}^{t}\int_D G(x,t|y,s)\mathcal{F}_e(y,s;\overline{\omega})dyds \\ &+ \int_D \Big[G(x,t|y,t_0)g_0(y;\overline{\omega}) - G_t(x,t|y,t_0)f_0(y;\overline{\omega})\Big]dy \\ &+ \int_{t_0}^{t} G(x,t|x_a,s)\Big[\lambda_a(\dot{q} - u_t(x_a,s)) + k_{1a}(q - u(x_a,s)) + k_{3a}(q - u(x_a,s))^3\Big]ds. \end{aligned} \tag{4.40}$$

Based on these, we can simply replace the equation of motion for the nonlinear attachment in equation (4.37) as follows:

$$m_a\ddot{q} + \lambda_a(\dot{q} - \dot{\zeta}) + k_{1a}(q - \zeta) + k_{3a}(q - \zeta)^3 = 0, \tag{4.41}$$

$$q(t_0;\overline{\omega}) = q_0(\overline{\omega}), \qquad \dot{q}(t_0;\overline{\omega}) = \dot{q}_0(\overline{\omega}), \quad \overline{\omega} \in \Omega, \tag{4.42}$$

where we have defined

$$\zeta(t) = u(x_a,t) \tag{4.43}$$

$$= \mathcal{H}(t;\overline{\omega}) + \int_{t_0}^{t} G(x_a,t|x_a,s)\Big[\lambda_a(\dot{q} - \dot{\zeta}(s)) + k_{1a}(q - \zeta(s)) + k_{3a}(q - \zeta(s))^3\Big]ds. \tag{4.44}$$

The term $\mathcal{H}(t;\overline{\omega})$ consists of i) an external stochastic forcing on the linear structure and ii) a stochastic initial conditions.

$$\begin{aligned}\mathcal{H}(t;\overline{\omega}) = & \int_{t_0}^{t}\int_D G(x_a,t|y,s)\mathcal{F}_e(y,s;\overline{\omega})dyds \\ & + \int_D \Big[G(x_a,t|y,t_0)g_0(y;\overline{\omega}) - G_t(x_a,t|y,t_0)f_0(y;\overline{\omega})\Big]dy. \end{aligned} \tag{4.45}$$

We assume that

$$v = q + \zeta, \qquad w = q - \zeta, \tag{4.46}$$

which are equivalent with

$$q = \frac{1}{2}(v+w), \qquad \zeta = \frac{1}{2}(v-w). \tag{4.47}$$

By plugging above relations into equation (4.41) and equation (4.44), we obtain

$$\ddot{w} + \frac{2\lambda_a}{m_a}\dot{w} + \frac{2k_{1a}}{m_a}w + \frac{2k_{3a}}{m_a}w^3 = -\ddot{v}, \tag{4.48}$$

$$\begin{aligned} v(t) = & \, w(t) + 2\mathcal{H}(t;\overline{\omega}) \\ & + 2\int_{t_0}^{t} G(x_a,t|x_a,s)[\lambda_a\dot{w}(s) + k_{1a}w(s) + k_{3a}(w(s))^3]ds, \end{aligned} \tag{4.49}$$

$$w(t_0;\overline{\omega}) = q_0(\overline{\omega}), \qquad \dot{w}(t_0;\overline{\omega}) = \dot{q}_0(\overline{\omega}), \tag{4.50}$$

where we assumed $f_0(x_a,\overline{\omega}) = 0$ and $g_0(x_a;\overline{\omega}) = 0$ without loss of generality. Substituting $v(t)$ from the second equation into the first equation, we can combine the equations as

$$\begin{aligned} & \ddot{w} + \frac{\lambda_a}{m_a}\dot{w} + \frac{k_{1a}}{m_a}w + \frac{k_{3a}}{m_a}w^3 \\ & = -\ddot{\mathcal{H}}(t;\overline{\omega}) - \frac{d^2}{dt^2}\Big[\int_{t_0}^{t} G(x_a,t|x_a,s)[\lambda_a\dot{w}(s) + k_{1a}w(s) + k_{3a}(w(s))^3]ds\Big]. \end{aligned} \tag{4.51}$$

We note that above stochastic nonlinear integro-differential equation is the exact reformulation of the original problem we consider and no approximation has been

applied. The entire step we described here can be applied to any general linear structure under external forcing attached with bistable energy harvesters. More generalized formulation with multiple number of nonlinear attachments to a linear structure has been discussed in [128]. In the following subsections, we demonstrate how this approach can be repeated to the two specific linear structures (single-degree-of-freedom linear structure and continuous linear elastic rod) attached with the bistable energy harvester. We then describe how the developed MECC method can be utilized to estimate the response statistics. Semi-analytical results will be compared with direct Monte-Carlo simulations as well as the traditional Gaussian closure scheme.

4.4.2 Bistable Energy Harvester with Linear SDOF Structure

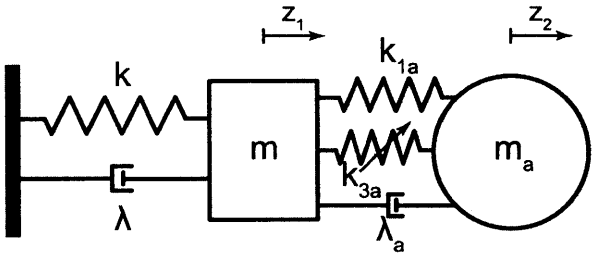

Figure 4-9: TDOF linear structure attached with nonlinear (bistable) energy harvester.

We first consider the example of linear single-degree-of-freedom system attached with essentially nonlinear bistable energy harvester (figure 4-9) whose equations of motion are:

$$m\ddot{\zeta} + \lambda\dot{\zeta} + k\zeta + \lambda_a(\dot{\zeta} - \dot{\eta}) + k_{1a}(\zeta - \eta) + k_{3a}(\zeta - \eta)^3 = \ddot{y}, \tag{4.52}$$

$$m_a\ddot{\eta} + \lambda_a(\dot{\eta} - \dot{\zeta}) + k_{1a}(\eta - \zeta) + k_{3a}(\eta - \zeta)^3 = 0, \tag{4.53}$$

where m, λ, and k are the mass, damping coefficient and stiffness of the linear structure while m_a, λ_a, k_{1a} and k_{3a} are the mass, damping coefficient, linear stiffness and cubic stiffness of the attachment. Here we note that in order to impose the bimodal nonlinearity we consider k_{1a} to be negative, $k_{1a} < 0$. Also ζ and η indicate the rela-

tive displacement of the linear structure and the attachment, respectively. y indicates the excitation displacement whose spectral density is in the Pierson-Moskowitz form (equation (4.1)). The coupling between the linear structure and the attachment has been introduced by the relative displacement of ζ and η. Thus by letting $x = \eta - \zeta$, we can re-write above governing equations as

$$m\ddot{\zeta} + \lambda\dot{\zeta} + k\zeta + m_a\ddot{x} + m_a\ddot{\zeta} = \ddot{y}, \tag{4.54}$$

$$m_a\ddot{x} + \lambda_a\dot{x} + k_{1a}x + k_{3a}x^3 = -m_a\ddot{\zeta}. \tag{4.55}$$

By letting the Fourier transform of $\zeta(t)$ is $Z(j\omega)$, we take the Fourier transform of the first equation of above:

$$\Big(m(j\omega)^2 + \lambda(j\omega) + k + m_a(j\omega)^2\Big)Z(j\omega) + m_a(j\omega)^2X(j\omega) = (j\omega)^2Y(j\omega), \tag{4.56}$$

then this follows:

$$Z(j\omega) = \frac{-m_a(j\omega)^2}{m(j\omega)^2 + \lambda(j\omega) + k + m_a(j\omega)^2}X(j\omega) + \frac{(j\omega)^2}{m(j\omega)^2 + \lambda(j\omega) + k + m_a(j\omega)^2}Y(j\omega), \tag{4.57}$$

$$(j\omega)^2Z(j\omega) = \frac{-m_a(j\omega)^4}{m(j\omega)^2 + \lambda(j\omega) + k + m_a(j\omega)^2}X(j\omega) + \frac{(j\omega)^4}{m(j\omega)^2 + \lambda(j\omega) + k + m_a(j\omega)^2}Y(j\omega). \tag{4.58}$$

Above second equation can be rewritten in time domain by taking inverse Fourier transformation:

$$\ddot{\zeta}(t) = \alpha(t) * x(t) + \beta(t) * y(t), \tag{4.59}$$

where

$$\mathcal{A}(j\omega) = \frac{-m_a(j\omega)^4}{m(j\omega)^2 + \lambda(j\omega) + k + m_a(j\omega)^2}, \tag{4.60}$$

$$\alpha(t) = \mathcal{F}^{-1}\Big(\frac{-m_a(j\omega)^4}{m(j\omega)^2 + \lambda(j\omega) + k + m_a(j\omega)^2}\Big), \tag{4.61}$$

and

$$\mathcal{B}(j\omega) = \frac{(j\omega)^4}{m(j\omega)^2 + \lambda(j\omega) + k + m_a(j\omega)^2}, \tag{4.62}$$

$$\beta(t) = \mathcal{F}^{-1}\Big(\frac{(j\omega)^4}{m(j\omega)^2 + \lambda(j\omega) + k + m_a(j\omega)^2}\Big). \tag{4.63}$$

We can plug this relation into the second equation of equation (4.55) which gives:

$$m_a\ddot{x} + \lambda_a\dot{x} + k_{1a}x + k_{3a}x^3 + m_a\alpha * x = -m_a\beta * y. \tag{4.64}$$

Again above stochastic nonlinear integro-differential equation (in terms of convolutions) is the exact reformulation of the original governing equations. Moreover the equation is in the similar form of what we have performed the MECC method in (section 4.2). We simply follow the same procedures to obtain the response spectral density function. First we compute the differential equations in terms of covariance functions by multiplying with x and y at different time instant s and by taking ensemble average.

$$\frac{\partial^2}{\partial\tau^2}C_{xy}(\tau) + \lambda_a\frac{\partial}{\partial\tau}C_{xy}(\tau) + (k_{1a} + \rho_{x,y}k_{3a} + m_aA(j\omega))C_{xy}(\tau) = -m_aB(j\omega)C_{yy}(\tau), \tag{4.65}$$

$$\frac{\partial^2}{\partial\tau^2}C_{xx}(\tau) + \lambda_a\frac{\partial}{\partial\tau}C_{xx}(\tau) + (k_{1a} + \rho_{x,x}k_{3a} + m_aA(j\omega))C_{xx}(\tau) = -m_aB(j\omega)C_{xy}(-\tau). \tag{4.66}$$

Using the Wiener-Khinchin theorem, we transform the above equations to the corresponding power spectral density equations:

$$\{m_a(j\omega)^2 + \lambda_a(j\omega) + k_{1a} + k_{3a}\rho_{x,y} + m_a\mathcal{A}(\omega)\}S_{xy}(\omega) = -m_aB(j\omega)S_{yy}(\omega), \tag{4.67}$$

$$\{m_a(j\omega)^2 - \lambda_a(j\omega) + k_{1a} + k_{3a}\rho_{x,x} + m_a\mathcal{A}(-\omega)\}S_{xx}(\omega) = -m_aB(j\omega)S_{xy}(\omega). \tag{4.68}$$

These equations can be combined into

$$S_{xx}(\omega) = \frac{m_a^2\mathcal{B}(\omega)\mathcal{B}(-\omega)}{\Big(m_a(j\omega)^2 + \lambda_a(j\omega) + k_{1a} + k_{3a}\rho_{x,y} + m_a\mathcal{A}(\omega)\Big)} \times \frac{1}{\Big(m_a(j\omega)^2 - \lambda_a(j\omega) + k_{1a} + k_{3a}\rho_{x,x} + m_a\mathcal{A}(-\omega)\Big)}S_{yy}(\omega) \tag{4.69}$$

Integration of the above equation will give us the variance.

$$\overline{x^2} = \int_0^\infty |\frac{m_a^2\mathcal{B}(\omega)\mathcal{B}(-\omega)S_{yy}(\omega)}{\Big(m_a(j\omega)^2 + \lambda_a(j\omega) + k_{1a} + k_{3a}\rho_{x,y} + m_a\mathcal{A}(\omega)\Big)} \times \frac{1}{\Big(m_a(j\omega)^2 - \lambda_a(j\omega) + k_{1a} + k_{3a}\rho_{x,x} + m_a\mathcal{A}(-\omega)\Big)}|d\omega. \tag{4.70}$$

As before, the last equation is the *dynamics constraint*, which expresses the second order dynamics of the system. We aim to optimally satisfy it together with the *closure constraints* defined by equations (equation (3.21)) and (equation (3.22)) by constructing and minimizing the following objective function in terms of the unknown energy

level γ and the closure coefficients $\rho_{x,x}$ and $\rho_{x,y}$:

$$\mathcal{J}(\gamma, \rho_{x,x}, \rho_{x,y}) = \left\{ \overline{x^2} - \int_0^\infty \left| \frac{m_a^2 \mathcal{B}(\omega)\mathcal{B}(-\omega) S_{yy}(\omega)}{\Big(m_a(j\omega)^2 + \lambda_a(j\omega) + k_{1a} + k_{3a}\rho_{x,y} + m_a\mathcal{A}(\omega)\Big)} \right.\right.$$
$$\left.\left. \times \frac{1}{\Big(m_a(j\omega)^2 - \lambda_a(j\omega) + k_{1a} + k_{3a}\rho_{x,x} + m_a\mathcal{A}(-\omega)\Big)} \right| d\omega \right\}^2$$
$$+ \left\{ \rho_{x,x} - \frac{\int x^3 f(x) \operatorname{erf}^{-1}(2F(x) - 1)\, dx}{\int x f(x) \operatorname{erf}^{-1}(2F(x) - 1)\, dx} \right\}^2$$
$$+ \left\{ \rho_{x,y} - \frac{\int x^3 f(x) \operatorname{erf}^{-1}(2F(x) - 1)\, dx}{\int x f(x) \operatorname{erf}^{-1}(2F(x) - 1)\, dx} \right\}^2. \tag{4.71}$$

We emphasize that in the context of statistical linearization only the first constraint is minimized while the closure coefficient is the one that follows exactly from a Gaussian representation for the pdf. In this case there is no attempt to incorporate in an equal manner the mismatch in the dynamics and the pdf representation. The minimization of this cost function essentially allows mismatch for the equation but also for the pdf representation. Once we have obtained the closure coefficients and the expression of response spectral density (for relative displacement x), one can easily obtain the response spectral density for the main linear structure (for the relative displacement ζ). From the equation (4.59), we have the following relations:

$$S_{\zeta\zeta}(\omega) = \frac{\mathcal{A}(\omega)}{(j\omega)^2} S_{x\zeta}(\omega) + \frac{\mathcal{B}(\omega)}{(j\omega)^2} S_{y\zeta}(\omega). \tag{4.72}$$

However two spectral densities $S_{x\zeta}$ and $S_{y\zeta}$ are unknowns for now, and we first compute $S_{x\zeta}(\omega)$ from

$$S_{\zeta x}(\omega) = \frac{\mathcal{A}(\omega)}{(j\omega)^2} S_{xx}(\omega) + \frac{\mathcal{B}(\omega)}{(j\omega)^2} S_{yx}(\omega). \tag{4.73}$$

Taking into account the second equation of equation (4.66), we obtain

$$S_{yx}(\omega) = -\frac{m_a(j\omega)^2 + \lambda_a(j\omega) + k_{1a} + k_{3a}\rho_{xx} + m_a\mathcal{A}(\omega)}{m_a\mathcal{B}(\omega)} S_{xx}(\omega). \tag{4.74}$$

Hence we obtain

$$S_{\zeta x}(\omega) = \left\{ \frac{\mathcal{A}(\omega)}{(j\omega)^2} - \frac{m_a(j\omega)^2 + \lambda_a(j\omega) + k_{1a} + k_{3a}\rho_{xx} + m_a\mathcal{A}(\omega)}{m_a(j\omega)^2} \right\} S_{xx}(\omega). \quad (4.75)$$

For brevity, we choose the following notation

$$T_1(\omega) = \frac{\mathcal{A}(\omega)}{(j\omega)^2} - \frac{m_a(j\omega)^2 + \lambda_a(j\omega) + k_{1a} + k_{3a}\rho_{xx} + m_a\mathcal{A}(\omega)}{m_a(j\omega)^2}, \quad (4.76)$$

and we simply rewrite into

$$S_{x\zeta}(\omega) = T_1(-\omega)S_{xx}(\omega). \quad (4.77)$$

Now we similarly obtain $S_{y\zeta}(\omega)$:

$$S_{\zeta y}(\omega) = \frac{\mathcal{A}(\omega)}{(j\omega)^2} S_{xy}(\omega) + \frac{\mathcal{B}(\omega)}{(j\omega)^2} S_{yy}(\omega). \quad (4.78)$$

Taking into account the first equation of equation (4.66), we obtain

$$S_{\zeta y}(\omega) = \left\{ - \frac{m_a\mathcal{A}(\omega)\mathcal{B}(\omega)}{(j\omega)^2\Big(m_a(j\omega)^2 + \lambda_a(j\omega) + k_{1a} + k_{3a}\rho_{xy} + m_a\mathcal{A}(\omega)\Big)} + \frac{\mathcal{B}(\omega)}{(j\omega)^2} \right\} S_{yy}(\omega). \quad (4.79)$$

We also choose the notation of

$$T_2(\omega) = - \frac{m_a\mathcal{A}(\omega)\mathcal{B}(\omega)}{(j\omega)^2\Big(m_a(j\omega)^2 + \lambda_a(j\omega) + k_{1a} + k_{3a}\rho_{xy} + m_a\mathcal{A}(\omega)\Big)} + \frac{\mathcal{B}(\omega)}{(j\omega)^2}, \quad (4.80)$$

then we get

$$S_{y\zeta}(\omega) = T_2(-\omega)S_{hh}(\omega). \quad (4.81)$$

Finally plugging equation (4.77) and equation (4.81) into equation (4.72), we obtain the spectral density function for ζ.

$$S_{\zeta\zeta}(\omega) = \frac{\mathcal{A}(\omega)}{(j\omega)^2} T_1(-\omega) S_{xx}(\omega) + \frac{\mathcal{B}(\omega)}{(j\omega)^2} T_2(-\omega) S_{yy}(\omega). \tag{4.82}$$

In figures 4-10 and 4-11, we illustrate the variance of the response displacements ζ and x as the intensity of the excitation varies for four different sets of the system parameters. Those system parameters are summarized in table 4.1, table 4.2, table 4.3, table 4.4, respectively. For all cases, we observe that the MECC method computes the response variances very accurately, while the Gaussian closure method systematically underestimates them. For lower intensities of the excitation, the response displacement variance computed by the Monte-Carlo simulation presents a non-monotonic behavior with respect to q. In this regime, the Gaussian closure has very poor performance on capturing this trend, however the MECC method provides a satisfactory approximation of the dynamics. Finally we point out that the same procedures can be applied to any linear multi-degree-of-freedom structures attached with bistable energy harvesters.

Table 4.1: System parameters for SDOF 1.

m	1	m_a	1
λ	0.1	λ_a	1
k	1	k_{1a}	-1
–	–	k_{3a}	1

Table 4.2: System parameters for SDOF 2.

m	1	m_a	1
λ	0.1	λ_a	0.5
k	1	k_{1a}	-0.5
–	–	k_{3a}	1

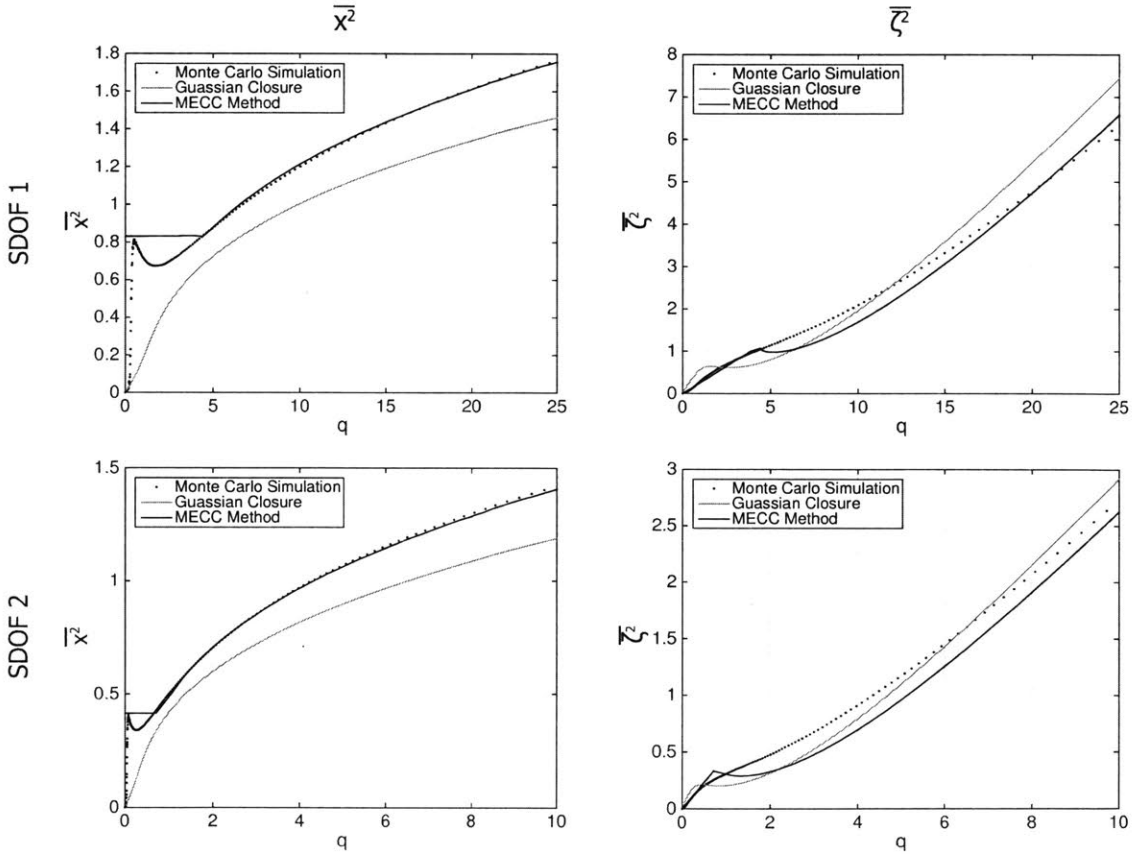

Figure 4-10: Mean square response displacements $\overline{x^2}$ and $\overline{\zeta^2}$ with respect to the amplification factor of Pierson-Moskowitz spectrum for SDOF 1 and 2 attached with the bistable system. System parameters can be found in 4.1 and 4.2.

Table 4.3: System parameters for SDOF 3.

m	1	m_a	0.1
λ	0.1	λ_a	0.05
k	1	k_{1a}	-0.05
–	–	k_{3a}	0.1

Table 4.4: System parameters for SDOF 4.

m	1	m_a	0.1
λ	0.1	λ_a	0.1
k	1	k_{1a}	-0.1
–	–	k_{3a}	0.1

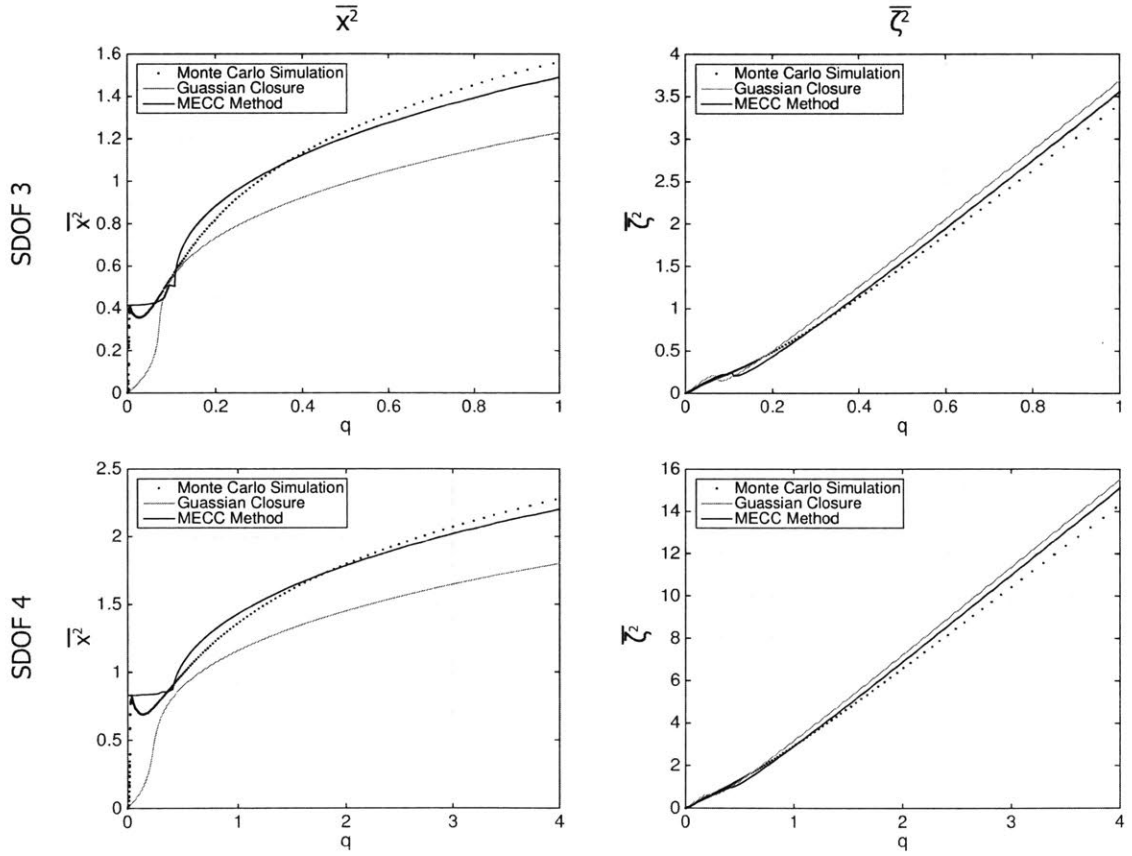

Figure 4-11: Mean square response displacements $\overline{x^2}$ and $\overline{\zeta^2}$ with respect to the amplification factor of Pierson-Moskowitz spectrum for SDOF 3 and 4 attached with the bistable system. System parameters can be found in 4.3 and 4.4.

4.4.3 Non-Gaussian Closure on Continuous System

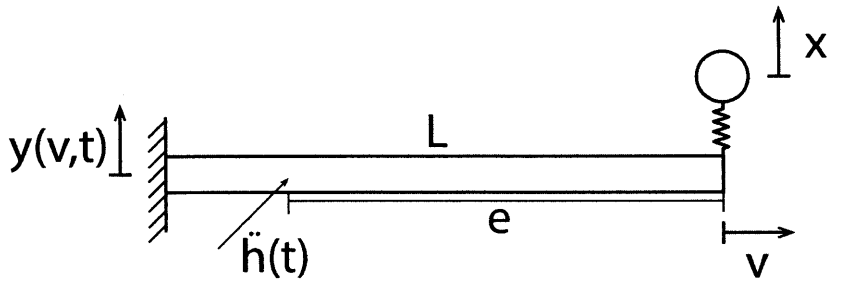

Figure 4-12: linear elastic rod attached with nonlinear (bistable) energy harvester.

The second example is a linear undamped elastic rod connected to a bistable nonlinear energy harvester by means of a weak linear stiffness. This problem setting has initially introduced in [149] considering the rod is subject to the impulse and step excitation. Interested readers should first refer to the original work [149]. The way of setting up the problem with elastic rod connected to an attachment has been adopted in this section, however we modify it to our problem by applying correlation excitation as well as attaching bimodal nonlinear oscillator.

We first specify the governing equations and boundary conditions for this problem (figure 4-12).

$$\frac{\partial^2}{\partial t^2}y(v,t) + \omega_0^2 y(v,t) - \frac{\partial^2}{\partial v^2}y(v,t) = \ddot{h}(t)\delta(v+e), \qquad -L \le v \le 0, \tag{4.83}$$

$$\ddot{x}(t) + \lambda\dot{x}(t) + \epsilon\Big(x(t) - y(\underline{v}_O,t)\Big) + k_1 x(t) + k_3 x^3(t) = 0, \tag{4.84}$$

$$\frac{\partial}{\partial v}y(0,t) + \epsilon\Big(x(t) - y(0,t)\Big) = 0, \tag{4.85}$$

$$y(-L,t) = 0, \quad y(v,0) = \frac{\partial}{\partial t}y(v,0) = x(0) = \dot{x}(0) = 0. \tag{4.86}$$

where L is the finite length of the linearly elastic rod on a continuous elastic foundation whose normalized stiffness is ω_0^2. We assume that all the geometric and material properties of the rod are uniform. Also the bistable oscillator is situated at the point of $\underline{v}_O(v=0)$, and the rod is subject to the excitation $\ddot{h}$ at the point of $v = -e > -L$. We consider the excitation has the power spectral density in the form of Pierson-

Moskowitz shape. The damping coefficient, linear and cubic stiffness of the attachment are denoted as λ, k_1, and k_3, respectively, and we note that $k_1 < 0$ in order to impose the bimodal nonlinearity. $0 < \epsilon \ll 1$ indicates the weak coupling stiffness between the elastic rod and the attachment. From the above, we consider the governing equation for the attachment (equation (4.84)), and we can rewrite as

$$\ddot{x}(t) + \lambda\dot{x}(t) + \epsilon x(t) + k_1 x(t) + k_3 x^3(t) = \epsilon y(\underline{v}_O, t), \tag{4.87}$$

Here the response of the main system (linear elastic rod) at point O ($y(\underline{v}_O, t)$) can be expressed in terms of the Green's functions g_{OO} and g_{OA} assuming the main linear structure (i.e. rod) is initially at rest and an excitation $\ddot{h}(t)$ is applied at point A, $\underline{v}_A(v = -e)$, at $t = 0$:

$$y(\underline{v}_O, t) = \int_{-\infty}^{t} \ddot{h}(\underline{v}_A, \tau) g_{OA}(t-\tau) d\tau - \int_{-\infty}^{t} \epsilon \left(y(\underline{v}_O, \tau) - x(\tau)\right) g_{OO}(t-\tau) d\tau, \tag{4.88}$$

$$= \ddot{h}(\underline{v}_A, t) * g_{OA}(t) + \epsilon x(t) * g_{OO}(t) - \epsilon y(\underline{v}_O, t) * g_{OO}(t). \tag{4.89}$$

Here the green function g_{OO} indicates the displacement at point O (in the direction of x) due to the unit impulse excitation at point O. Similarly g_{OA} indicates the displacement at point O due to the unit impulse excitation at point A. We note that $y(\underline{v}_O, t)$ in the left hand side equation (4.89) also appears in its right hand side giving us the recursive form. By plugging equation (4.89) into equation (4.87), we obtain

$$\ddot{x}(t) + \lambda\dot{x}(t) + \epsilon x(t) + k_1 x(t) + k_3 x^3(t)$$

$$= \epsilon\ddot{h}(\underline{v}_A, t) * g_{OA}(t) + \epsilon^2 x(t) * g_{OO}(t) - \epsilon^2 y(\underline{v}_O, t) * g_{OO}(t). \tag{4.90}$$

Considering the weak coupling between the rod and the attachment $\epsilon \ll 1$, we ignore the higher order terms ($O(\epsilon^2)$) with respect to ϵ:

$$\ddot{x}(t) + \lambda\dot{x}(t) + \epsilon x(t) + k_1 x(t) + k_3 x^3(t) = \epsilon\ddot{h}(\underline{v}_A, t) * g_{OA}(t) + O(\epsilon^2). \tag{4.91}$$

Now the Green's function describing the response of the rod at position v and time t

due to the unit impulse at $\overline{v}$ at $\overline{t}$ can be obtained by [149]

$$g_1(v-\overline{v},t-\overline{t}) = \mathcal{J}_0\Big(\omega_0\sqrt{(t-\overline{t})^2-(v-\overline{v})^2}\Big)u(t-\overline{t}-v+\overline{v}) \tag{4.92}$$

where $u(\cdot)$ is a step function and $\mathcal{J}_0(\cdot)$ is the Bessel function of zeroth order and first kind. Then the previous two Green's functions can be rewritten as:

$$g_{OO}(t) = \mathcal{J}_0\big(\omega_0 t\big)u(t), \qquad g_{OA}(t) = \mathcal{J}_0\Big(\omega_0\sqrt{t^2-e^2}\Big)u(t-e), \tag{4.93}$$

Withe these, we finally have

$$\ddot{x}+\ \lambda\dot{x}+\epsilon x+k_1x+k_3x^3 = \epsilon\ddot{h}*g_{OA}. \tag{4.94}$$

We point out that equation (4.94) is the exact reformulation of the original governing equations by means of green functions. Above nonlinear integro-differential equation can be utilized to obtain the response statistics of the attachment.

Interestingly the above equation is in the exactly same form of what we have worked on in the previous sections except we have additional small coupling stiffness ϵ term and the excitation is in a modified form. We can follow the same procedures for the above governing equation as in previous sections to derive the response power spectral density, however the analytical form of Fourier transform of g_{OA} is not readily available. Instead we assume that the excitation is

$$\ddot{z} = \ddot{h}*g_{OA}, \tag{4.95}$$

and numerically estimate the power spectral density of z. Since we have analytical expression for g_{OA} in time domain, we can compute the convolution with the original excitation displacement h, and by taking Fourier transformation of its covariance function $C_{zz}(\tau)$, we can derive $S_{zz}(\omega)$. Once we numerically estimate the modified spectral density $S_{zz}(\omega)$, we can follow the exactly same procedures in (section 4.2).

Examples of numerically estimated power spectral density $S_{zz}(\omega)$ has been illustrated in figure 4-13. For the completeness, we summarize the final equations. The power spectral density function for the relative displacement x is

$$S_{xx}(\omega) = \left| \frac{\omega^4}{\{k_1 + \epsilon + \rho_{x,z}k_3 - \omega^2 + j(\lambda\omega)\}} \right. \\ \left. \times \frac{1}{\{k_1 + \epsilon + \rho_{x,x}k_3 - \omega^2 - j(\lambda\omega)\}} \right| S_{zz}(\omega). \quad (4.96)$$

The integration gives the variance of the response.

$$\overline{x^2} = \int_0^\infty | \frac{\omega^4}{\{k_1 + \epsilon + \rho_{x,z}k_3 - \omega^2 + j(\lambda\omega)\}} \\ \times \frac{1}{\{k_1 + \epsilon + \rho_{x,x}k_3 - \omega^2 - j(\lambda\omega)\}} | d\omega \quad (4.97)$$

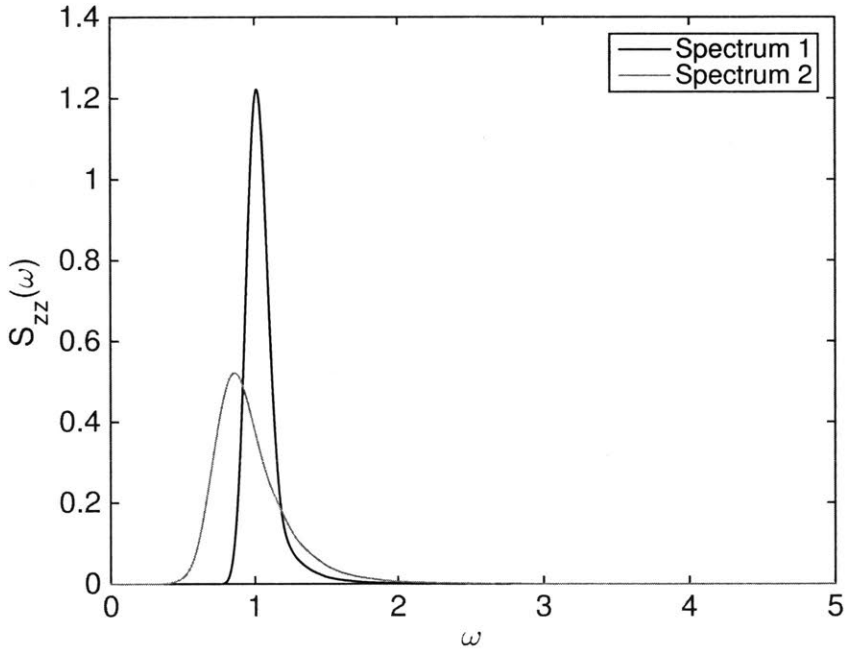

Figure 4-13: Spectrum 1 is $S_{zz}(\omega)$ with $e = 10, \omega_0^2 = 1$. Spectrum 2 is $S_{zz}(\omega)$ with $e = 50, \omega_0^2 = 0.5$.

The closure coefficient $\rho_{x,z}$ connects the fourth order of moment $\overline{x(t)^3 z(s)}$ and the second order of moment $\overline{x(t)z(s)}$ as follows:

$$\overline{x(t)^3 z(s)} = \rho_{x,z}\, \overline{x(t)z(s)}, \tag{4.98}$$

and as in equation (4.99), the coefficient can be obtained by

$$\rho_{x,z} = \frac{\int x^3 f(x) \operatorname{erf}^{-1}(2F(x)-1)\, dx}{\int x f(x) \operatorname{erf}^{-1}(2F(x)-1)\, dx}. \tag{4.99}$$

Please note that above relation does not depend on the excitation statistics, rather it only depends on the response statistics of displacement x, which indicates $\rho_{x,z}$ is essentially the same as $\rho_{x,y}$ in equation (3.22). In other words the closure coefficient $\rho_{x,y}$ stays the same regardless of the change in excitation.

Finally, we construct the minimization objective function as follows:

$$\begin{aligned}\mathcal{J}(\gamma, \rho_{x,x}, \rho_{x,z}) = &\left\{ \overline{x^2} - \int_0^\infty \left| \frac{\omega^4}{\{k_1 + \epsilon + \rho_{x,z} k_3 - \omega^2 + j(\lambda\omega)\}} \right.\right. \\ &\left.\left. \times \frac{1}{\{k_1 + \epsilon + \rho_{x,x} k_3 - \omega^2 - j(\lambda\omega)\}} \right| d\omega \right\}^2 \\ &+ \left\{ \rho_{x,x} - \frac{\int x^3 f(x) \operatorname{erf}^{-1}(2F(x)-1)\, dx}{\int x f(x) \operatorname{erf}^{-1}(2F(x)-1)\, dx} \right\}^2 \\ &+ \left\{ \rho_{x,z} - \frac{\int x^3 f(x) \operatorname{erf}^{-1}(2F(x)-1)\, dx}{\int x f(x) \operatorname{erf}^{-1}(2F(x)-1)\, dx} \right\}^2. \end{aligned} \tag{4.100}$$

The minimization will be performed with respect to the unknown energy level γ and the closure coefficients $\rho_{x,x}$ and $\rho_{x,z}$. In figure 4-14 and figure 4-15, we have also summarized the variance of the response displacement x with respect to various intensities of the excitation for four different cases. Associated parameters are summarized in table 4.5, table 4.6, table 4.7, and table 4.8, respectively. We observe that the MECC method computes the response variances very accurately, while the Gaussian closure method systematically underestimates them. For lower intensities of the excitation, the exact

(Monte-Carlo) variance presents a non-monotonic behavior with respect to q due to the co-existence of the cross- and intra-well oscillations. While the Gaussian closure has very poor performance on capturing this trend, the MECC method can still provide a satisfactory approximation of the dynamics.

Table 4.5: System parameters for linear elastic rod 1.

w_0^2	1	m_a	1
e	10	λ_a	1
ϵ	0.1	k_{1a}	-1
–	–	k_{3a}	1

Table 4.6: System parameters for linear elastic rod 2.

w_0^2	0.5	m_a	1
e	50	λ_a	1
ϵ	0.05	k_{1a}	-1
–	–	k_{3a}	1

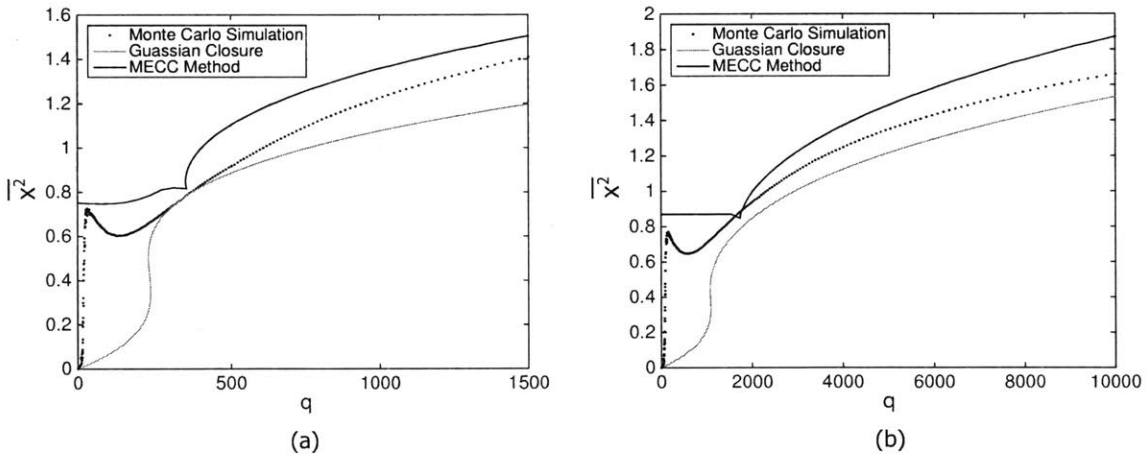

Figure 4-14: Mean square response displacement $\overline{x^2}$ with respect to the amplification factor of Pierson-Moskowitz spectrum for (a) Rod 1, and (b) Rod 2. Parameters are summarized in table 4.5 and table 4.6.

Table 4.7: System parameters for linear elastic rod 3.

w_0^2	1	m_a	1
e	10	λ_a	0.5
ϵ	0.1	k_{1a}	-0.5
–	–	k_{3a}	1

Table 4.8: System parameters for linear elastic rod 4.

w_0^2	0.5	m_a	1
e	50	λ_a	0.5
ϵ	0.05	k_{1a}	-0.5
–	–	k_{3a}	1

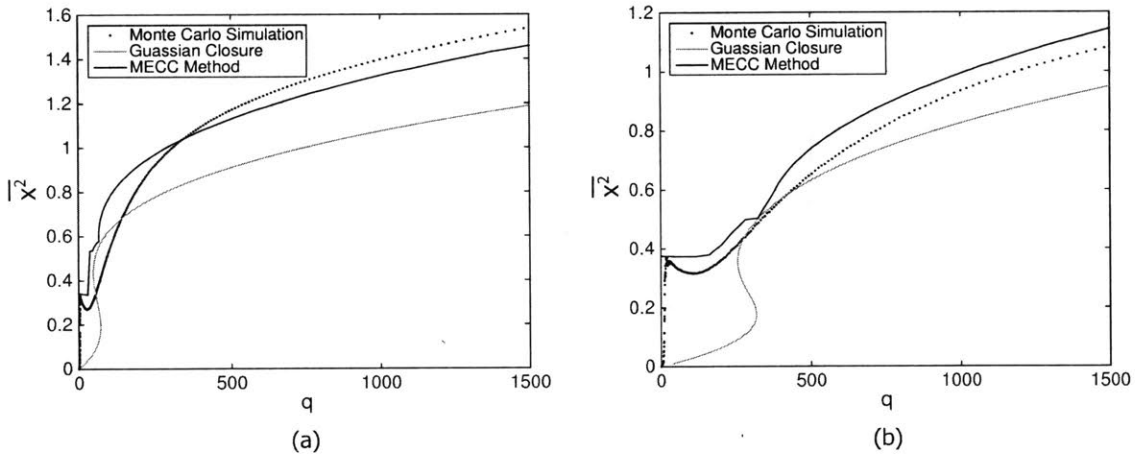

Figure 4-15: Mean square response displacement $\overline{x^2}$ with respect to the amplification factor of Pierson-Moskowitz spectrum for (a) Rod 3, and (b) Rod 4. Parameters are summarized in table 4.7 and table 4.8.

4.5 Summary

In chapter 3 and chapter 4, we have considered the problem of determining the non-Gaussian steady state statistical structure of bistable nonlinear vibrational systems subjected to colored noise excitation. We first derived moment equations that describe the dynamics governing the two-time statistics. We then combined those with a non-Gaussian pdf representation for the joint response-response and joint response-excitation statistics. This representation has i) single time statistical structure consistent with the analytical solutions of the Fokker-Planck equation, and ii) two-time statistical structure that follows from the adoption of a Gaussian copula function. The pdf representation takes the form of *closure constraints* while the moment equations have the form of a *dynamics constraint.* We formulated the two sets of constraints as a low-dimensional minimization problem with respect to the unknown parameters of the representation. The minimization of both the *dynamics constraint* and the *closure constraints* imposes an interplay between these two factors.

We then applied the presented method to two nonlinear oscillators in the context of vibration energy harvesting. One is a single degree of freedom (SDOF) bistable oscillator with linear damping while the other is a same SDOF bistable oscillator coupled with an electromechanical energy harvester. For both applications, it was assumed that the stationary stochastic excitation has a power spectral density given by the Pierson-Moskowitz spectrum. We have shown that the presented method can provide a very good approximation of second order statistics of the system, when compared with direct Monte-Carlo simulations, even in essentially nonlinear regimes, where Gaussian closure techniques fail completely to capture the dynamics. In addition, we can compute the full (non-Gaussian) probabilistic structure of the solution in a post-process manner. We emphasize that the computational cost associated with the new method is considerably smaller compared with methods that evolve the pdf of the solution since MECC method relies on the minimization of a function with a few unknown variables.

Finally the developed MECC method has been applied to a general linear structure attached with bistable nonlinear oscillator with the aim of energy harvesting. We first introduced the general framework of how the problem can be formulated in terms of bimodal nonlinearity, and then we demonstrated MECC method for two specific examples: linear single-degree-of-freedom system attached with bistable oscillator and undamped linear elastic rod connected to the bistable oscillator. We provided comparisons of the MECC results with direct Monte-Carlo simulations which presented a good agreement for the estimation of variance of the response statistics.

Chapter 5

Reliability of Linear Structural Systems Subjected to Extreme Forcing Events

5.1 Introduction

A large class of physical systems in engineering and science can be modeled by stochastic differential equations. For many of these systems, the dominant source of uncertainty is due to the forcing which can be described by a stochastic process. Applications include ocean engineering systems excited by water waves (such as ship motions in large waves [104, 13, 30, 29] or high speed crafts subjected to rough seas [120, 119]) and rare events in structural systems (such as beam buckling [1, 90], vibrations due to earthquakes [87, 20] and wind loads [89, 142]). For all of these cases, it is common that hidden in the otherwise predictable magnitude of the fluctuations are extreme events, i.e. abnormally large magnitude forces which lead to rare responses in the dynamics of the system (figure 5-1). Clearly these events must be adequately taken into account for the effective quantification of the reliability properties of the system. In this work, we develop an efficient method to fully describe the probabilistic response of linear structural systems under general time-correlated random excitations containing rare

and extreme events.

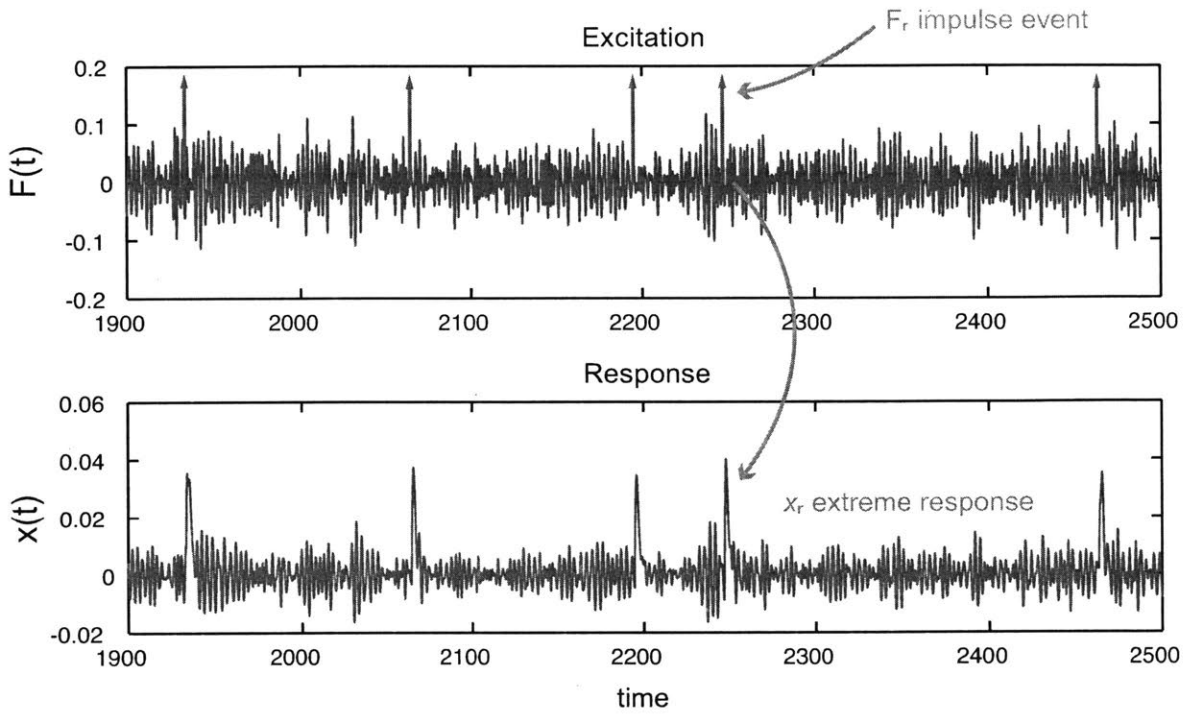

Figure 5-1: (Top) Background stochastic excitation including impulsive loads in (red) upward arrows. (Bottom) System response displacement.

Systems under forcing having these characteristics pose significant challenges for traditional uncertainty quantification schemes. While there is a large class of methods that can accurately resolve the statistics associated with random excitations (e.g. the Fokker-Planck equation [140, 136] for systems excited by white-noise and the joint response-excitation method [126, 153, 69, 5] for arbitrary stochastic excitation) these have important limitations for high dimensional systems. In addition, even for low-dimensional systems determining the part of the probability density function (pdf) associated with extreme events poses important numerical challenges. On the other hand, Gaussian closure schemes and moment equation or cumulant closure methods [15, 157] either cannot "see" the rare events completely or they are very expensive and require the solution of an inverse moment problem in order to determine the pdf of interest [3]. Similarly, approaches relying on polynomial-chaos expansions [159, 158] have been shown to have important limitations for systems with intermittent responses [94].

Another popular approach for the study of rare event statistics in systems under intermittent forcing is to represent extreme events in the forcing as identically distributed independent impulses arriving at random times. The generalized Fokker-Planck equation or Kolmogorov-Feller (KF) equation is the governing equation that solves for the evolution of the response pdf under Poisson noise [136]. However, exact analytical solutions are available only for a limited number of special cases [151]. Although alternative methods such as the path integral method [82, 65, 8] and the stochastic averaging method [161, 160] may be applied, solving the FP or KF equations is often very expensive [100, 40] even for very low dimensional systems.

Here we consider the problem of quantification of the response pdf and the pdf associated with local extrema of linear systems subjected to stochastic forcing containing extreme events based on the recently formulated probabilistic-decomposition synthesis (PDS) method [102, 103]. The approach relies on the decomposition of the statistics into a 'non-extreme core', typically Gaussian, and a heavy-tailed component. This decomposition is in full correspondence with a partition of the phase space into a 'stable' region where we do not have rare events and a region where non-linear instabilities or external forcing lead to rare transitions with high probability. We quantify the statistics in the stable region using a Gaussian approximation approach, while the non-Gaussian distribution associated with the intermittently unstable regions of phase space is performed taking into account the non-trivial character of the dynamics (either because of instabilities or external forcing). The probabilistic information in the two domains is analytically synthesized through a total probability argument.

We begin with the simplest case of a linear, single-degree-of-freedom (SDOF) system and then formulate the method for multi-degree-of-freedom systems. *The main result of our work is the derivation of analytic/semi-analytic approximation formulas for the response pdf and the pdf of the local extrema of intermittently forced systems that can accurately characterize the statistics many standard deviations away from the*

mean. Although the systems considered in this work are linear, the method is directly applicable for nonlinear structural systems as well. This approach circumvents the challenges that rare events pose for traditional uncertainty quantification schemes, in particular the computational burden associated with rare events in systems. We emphasize the statistical accuracy and the computational efficiency of the presented approach, which we rigorously demonstrate through extensive comparisons with direct Monte-Carlo simulations. In brief, the principal contributions of this chapter are:

- Analytical (under certain conditions) and semi-analytical (under no restrictions) pdf expressions for the response displacement, velocity and acceleration for single-degree-of-freedom systems under intermittent forcing.
- Semi-analytical pdf expressions for the value and the local extrema of the displacement, velocity and acceleration for multi-degree-of-freedom systems under intermittent forcing.

This chapter is structured as follows. In section 5.2, we provide a general formulation of the probabilistic decomposition-synthesis method for the case of structural systems under intermittent forcing. Next, in section 5.3, we apply the developed method analytically, which is possible for two limiting cases: underdamped systems with $\zeta \ll 1$ or overdamped with $\zeta \gg 1$, where ζ is the damping ratio . The system we consider is excited by a forcing term consisting of a background time-correlated stochastic process superimposed with a random impulse train (describing the rare and extreme component). We give a detailed derivation of the response pdf of the system (displacement, velocity and acceleration) and compare the results with expensive Monte-Carlo simulations. In section 5.4, we slightly modify the developed formulation to derive a semi-analytical scheme considering the same linear system but without any restriction on the damping ratio ζ, demonstrating global applicability of the approach. In section 5.5, we demonstrate applicability of our method for multiple-degree-of-freedom systems and in section 5.6 we present results for the local extrema of the response. Finally, we offer concluding remarks of this chapter in section 5.7.

5.2 The Probabilistic Decomposition-Synthesis Method for Intermittently Forced Systems

Here we provide a brief presentation of the recently developed probabilistic decomposition-synthesis method adapted for the case of intermittently forced linear systems [102]. We consider the following vibrational system,

$$M\ddot{\mathbf{x}}(t) + D\dot{\mathbf{x}}(t) + K\mathbf{x}(t) = \mathbf{F}(t), \quad \mathbf{x}(t) \in \mathbb{R}^n, \tag{5.1}$$

where M is a mass matrix, D is the damping matrix, and K is the stiffness matrix. We assume $\mathbf{F}(t)$ is a stochastic forcing with intermittent characteristics that can be expressed as

$$\mathbf{F}(t) = \mathbf{F}_b(t) + \mathbf{F}_r(t). \tag{5.2}$$

The forcing consists of background component $\mathbf{F}_b$ of characteristic magnitude σ_b and a *rare and extreme* component $\mathbf{F}_r$ with magnitude $\sigma_r \gg \sigma_b$. The components $\mathbf{F}_b$ and $\mathbf{F}_r$ may both be (weakly) stationary stochastic processes, while the sum of the two processes will in general be non-stationary.

This can be seen if we directly consider the sum of two (weakly) stationary processes x_1 and x_2, with time correlation functions $\mathrm{Corr}_{x_1}(\tau)$ and $\mathrm{Corr}_{x_2}(\tau)$, respectively. Then for the sum $z = x_1 + x_2$ we have

$$\mathrm{Corr}_z(t,\tau) = \mathrm{Corr}_{x_1}(\tau) + \mathbb{E}[x_1(t)x_2(t+\tau)] + \mathbb{E}[x_1(t+\tau)x_2(t)] + \mathrm{Corr}_{x_2}(\tau).$$

Therefore the process z is stationary if and only if the cross-covariance terms $\mathbb{E}[x_1(t)x_2(t+\tau)]$ and $\mathbb{E}[x_1(t+\tau)x_2(t)]$ are functions of τ or only if they are zero (i.e. x_1 and x_2 are not correlated).

To apply the PDS method we decompose the response into two terms

$$\mathbf{x}(t) = \mathbf{x}_b(t) + \mathbf{x}_r(t), \tag{5.3}$$

where $\mathbf{x}_b$ accounts for the background state (non-extreme) and $\mathbf{x}_r$ is the response of extreme responses (due to the intermittent forcing) - see figure figure 5-2. More precisely $\mathbf{x}_r$ is the system response under two conditions: (1) the forcing is given by $\mathbf{F} = \mathbf{F}_r$ and (2) the norm of the response is greater than a threshold value $\|\mathbf{x}\| > \gamma$, where γ is the rare event threshold level that is connected with the typical variance of the background response fluctuations. These rare transitions correspond with $\mathbf{F}_r$, *but also include a phase that relaxes the system back to the background state* $\mathbf{x}_b$. The background component $\mathbf{x}_b$ corresponds to system response without rare events $\mathbf{x}_b = \mathbf{x} - \mathbf{x}_r$, and in this regime the system is primarily governed by the background forcing term $\mathbf{F}_b$.

We require that rare events are statistically independent from each other. In the generic formulation of the PDS we also need to assume that rare events have negligible effects on the background state $\mathbf{x}_b$ but here this assumption is not necessary due to the linear character of the examples considered. However, in order to apply the method for general nonlinear structural systems we need to have this condition satisfied.

Next, we focus on the statistical characteristics of an individual mode $u(t) \in \mathbb{R}$ of the original system in equation (5.1). The first step of the PDS method is to quantify the conditional statistics of the rare event regime. When the system enters the rare event response at $t = t_0$ we will have an arbitrary background state u_b at t_0 and the problem will be formulated as:

$$\ddot{u}_r(t) + \lambda \dot{u}_r(t) + k u_r(t) = F_r(t), \qquad \text{with } u_r(t_0) = u_b \text{ and } F = F_r \text{ for } t > t_0. \tag{5.4}$$

Under the assumption of independent rare events we can use equation (5.4) as a basis to derive analytical or numerical estimates for the statistical response during the rare

event regime.

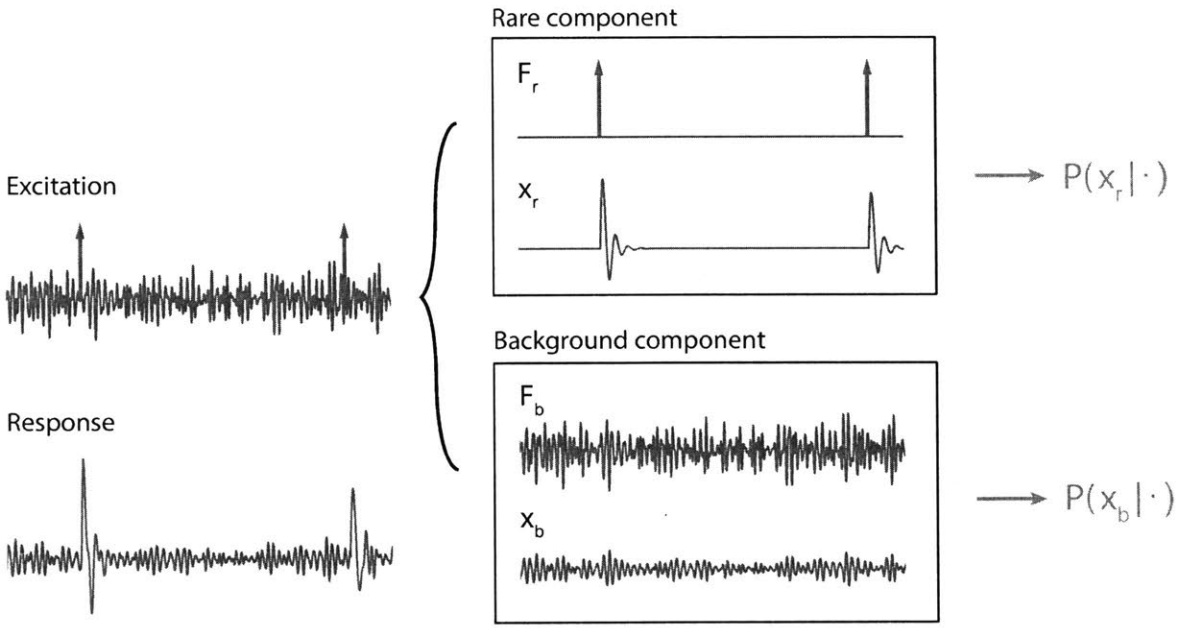

Figure 5-2: Schematic representation of the PDS method for an intermittently forced system.

The background component, on the other hand, can be studied through the equation,

$$M\ddot{\mathbf{x}}_b(t) + D\dot{\mathbf{x}}_b(t) + K\mathbf{x}_b(t) = \mathbf{F}_b(t). \tag{5.5}$$

Because of the non-intermittent character of the response in this regime, it is sufficient to obtain the low-order statistics of this system. For the case where $F_b(t)$ follows a Gaussian distribution the problem is straightforward. For non-Gaussian $F_b(t)$ other methods such as moment equations may be utilized. Consequently, this step provides us with the statistical steady state probability distribution for the mode of interest under the condition that the dynamics 'live' in the stochastic background.

Finally once the analysis of the two regimes is completed, we can synthesize the results

through a total probability argument

$$f(q) = \underbrace{f(q \mid \|u\| > \gamma, u \in u_b, F = F_r)}_{\text{rare events}} \mathbb{P}_r + \underbrace{f(q \mid F = F_b)}_{\text{background}} (1 - \mathbb{P}_r), \tag{5.6}$$

where q may be any function of interest involving the response. In the last equation, $\mathbb{P}_r$ denotes the rare event probability. This is defined as the probability of the response exceeding a threshold γ because of a rare event in the excitation:

$$\mathbb{P}_r \equiv \mathbb{P}(\|u\| > \gamma, F = F_r) = \frac{1}{T} \int_{t \in T} \mathbb{1}(\|u\| > \gamma, F = F_r)\, dt, \tag{5.7}$$

where $\mathbb{1}(\cdot)$ is the indicator function. The rare event probability measures the total duration of the rare events taking into account their frequency and duration. The utility of the presented decomposition is its flexibility in capturing rare responses, since we can account for the rare event dynamics directly and connect their statistical properties directly to the original system response.

5.2.1 Problem Formulation for Linear SDOF Systems

In order to demonstrate the method, we begin with a very simple example and we consider a single-degree-of-freedom linear system (see figure 5-3)

$$\ddot{x} + \lambda \dot{x} + kx = F(t), \tag{5.8}$$

where k is the stiffness, λ is the damping, $\zeta = \lambda / 2\sqrt{k}$ is the damping ratio, and $F(t)$ is a stochastic forcing term with intermittent characteristics, which can be written as

$$F(t) = F_b(t) + F_r(t). \tag{5.9}$$

Here F_b is the background forcing component that has a characteristic magnitude σ_b and F_r is a rare and large amplitude forcing component that has a characteristic magnitude σ_r, which is much larger than the magnitude of the background forcing, $\sigma_r \gg \sigma_b$. Despite the simplicity of the system, this may have a significantly complicated

statistical structure with heavy-tailed features. The basic principles of the PDS method can be directly demonstrated in this practical case and also generalized to more complex MDOF linear systems.

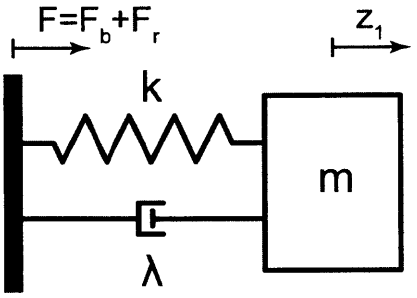

Figure 5-3: Prototype SDOF system.

For the concreteness, we consider a prototype system motivated from ocean engineering applications, modeling base excitation of a structural mode:

$$\ddot{x} + \lambda\dot{x} + kx = \ddot{h}(t) + \sum_{i=1}^{N(t)} \alpha_i \, \delta(t - \tau_i), \quad 0 < t \leq T. \tag{5.10}$$

Here $h(t)$ denotes the zero-mean background base motion term (having opposite sign from x) with a Pierson-Moskowitz spectrum:

$$S_{hh}(\omega) = q\frac{1}{\omega^5}\exp\left(-\frac{1}{\omega^4}\right), \tag{5.11}$$

where q controls the magnitude of the forcing.

The second forcing term in equation (5.10) describes rare and extreme events. In particular, we assume this component is a random impulse train ($\delta(\cdot)$ is a unit impulse), where $N(t)$ is a Poisson counting process that represents the number of impulses that arrive in the time interval $0 < t \leq T$, α is the impulse magnitude (characterizing the rare event magnitude σ_r), which we assume is normally distributed with mean μ_α and variance σ_α^2, and the constant arrival rate is given by ν_r (or by the mean arrival time $T_\alpha = 1/\nu_\alpha$ so that impulse arrival times are exponentially distributed $\tau \sim e^{T_\alpha}$).

We take the impulse magnitude as being m-times larger than the standard deviation of the excitation velocity $\dot{h}(t)$:

$$\mu_\alpha = m\sigma_{\dot{h}}, \text{ with } m > 1, \tag{5.12}$$

where $\sigma_{\dot{h}}$ is the standard deviation of $\dot{h}(t)$ which can be directly obtained from the background excitation term.

$$\sigma_{\dot{h}}^2 = \int_0^\infty \omega^2 S_{hh}(\omega) d\omega \tag{5.13}$$

This prototype system is widely applicable to other systems with similar features including structures under wind excitations, systems under seismic excitations, and vibrations of road vehicles [136, 140, 120].

5.3 Response PDF of SDOF Systems for Limiting Cases of Damping

We first apply the probabilistic decomposition-synthesis method for the special cases $\zeta \ll 1$ and $\zeta \gg 1$ to derive analytical approximations for the response pdfs for the displacement and velocity, and acceleration. We perform the analysis first for the response displacement and by way of a minor modification obtain the response velocity and acceleration, as well. Other than these two cases, completely analytical formulas do not exist (as they require transformations with no explicit solutions), and alternatively we propose a semi-analytical approach described in section 5.4, that removes the restriction on ζ and is applicable for any ζ value.

5.3.1 Background Response PDF

We first consider the statistical response of the system to the background forcing component,

$$\ddot{x}_b + \lambda \dot{x}_b + k x_b = \ddot{h}(t). \tag{5.14}$$

Due to the Gaussian character of the statistics, the response is fully characterized by the spectrum. The spectral density of the displacement, velocity and acceleration of this system are given by,

$$S_{x_b x_b}(\omega) = \left| \frac{\omega^4}{(k-\omega^2)^2 + \lambda^2 \omega^2} \right| S_{\dot{h}\dot{h}}(\omega), \tag{5.15}$$

$$S_{\dot{x}_b \dot{x}_b}(\omega) = \omega^2 S_{x_b x_b}(\omega), \tag{5.16}$$

$$S_{\ddot{x}_b \ddot{x}_b}(\omega) = \omega^4 S_{x_b x_b}(\omega). \tag{5.17}$$

Thus we can obtain the variance of response displacement, velocity and acceleration:

$$\sigma_{x_b}^2 = \int_0^\infty S_{x_b x_b}(\omega)\, d\omega, \tag{5.18}$$

$$\sigma_{\dot{x}_b}^2 = \int_0^\infty S_{\dot{x}_b \dot{x}_b}(\omega)\, d\omega, \tag{5.19}$$

$$\sigma_{\ddot{x}_b}^2 = \int_0^\infty S_{\ddot{x}_b \ddot{x}_b}(\omega)\, d\omega. \tag{5.20}$$

Moreover the envelopes are Rayleigh distributed [86]:

$$u_b \sim \mathcal{R}(\sigma_{x_b}), \tag{5.21}$$

$$\dot{u}_b \sim \mathcal{R}(\sigma_{\dot{x}_b}), \tag{5.22}$$

$$\ddot{u}_b \sim \mathcal{R}(\sigma_{\ddot{x}_b}), \tag{5.23}$$

where the Rayleigh distribution of $\mathcal{R}(\sigma)$ takes the following form of pdf:

$$f(x;\sigma) = \frac{x}{\sigma^2} \exp\left(-\frac{x^2}{2\sigma^2}\right), \quad x \geq 0. \tag{5.24}$$

5.3.2 Impulse Response of SDOF Systems

In order to derive the pdf of the rare component of equation (5.10), we consider the impulse response of a linear sdof system. Recalling basic results, the governing equation of the system can written as follows.

$$\ddot{x}_r(t) + \lambda \dot{x}_r(t) + k x_r(t) = 0, \tag{5.25}$$

under an impulse α at an arbitrary time t_0, say $t_0 = 0$, and given a zero background state ($(x_r, \dot{x}_r) = (0,0)$ at $t = 0^-$) are given by the following equations under the two limiting cases of interest (heavily damped and lightly damped systems).

Severely underdamped case $\zeta \ll 1$ With the approximation of $\zeta \ll 1$ (or $\omega_d \approx \omega_n$), we can simplify responses as

$$x_r(t) = \frac{\alpha}{\omega_d} e^{-\zeta\omega_n t} \sin \omega_d t, \tag{5.26}$$

$$\dot{x}_r(t) = \alpha e^{-\zeta\omega_n t} \cos \omega_d t; \tag{5.27}$$

$$\ddot{x}_r(t) = -\alpha\omega_d e^{-\zeta\omega_n t} \sin \omega_d t, \tag{5.28}$$

and the envelopes as

$$u_r(t) = \frac{\alpha}{\omega_d} e^{-\zeta\omega_n t}, \tag{5.29}$$

$$\dot{u}_r(t) = \alpha e^{-\zeta\omega_n t}, \tag{5.30}$$

$$\ddot{u}_r(t) = -\alpha\omega_d e^{-\zeta\omega_n t}. \tag{5.31}$$

Severely overdamped case $\zeta \gg 1$ Similarly, with the approximation of $\zeta \gg 1$ (or $\omega_o \approx \zeta\omega_n$), we can simplify responses as

$$x_r(t) = \frac{\alpha}{2\omega_o} e^{-(\zeta\omega_n - \omega_o)t}, \tag{5.32}$$

$$\dot{x}_r(t) = \alpha e^{-(\zeta\omega_n + \omega_o)t}, \tag{5.33}$$

$$\ddot{x}_r(t) = -(\zeta\omega_n + \omega_o)\alpha e^{-(\zeta\omega_n + \omega_o)t}. \tag{5.34}$$

Where above we adopted the standard definitions: $\omega_n = \sqrt{k}$, $\zeta = \lambda/(2\sqrt{k})$, $\omega_o = \omega_n\sqrt{\zeta^2 - 1}$, and $\omega_d = \omega_n\sqrt{1 - \zeta^2}$. The results above do not account for non-zero background initial conditions, i.e. $(x, \dot{x}) = (x_b, \dot{x}_b)$ at $t = 0^-$. Non-zero background initial conditions will modify the prefactor involving α and also adds additional terms to the results above. We will only take into consideration the leading order impact of the background state which contributes additionally to the impulse magnitude α in the leading order terms above and drop the other terms due to the non-zero initial conditions that do not involve α as they are negligible.

5.3.3 Extreme Event Response

In the severely underdamped case, the rare event responses can be considered by appropriately taking into account the background state

$$x_r(t) \sim \frac{\dot{x}_b + \alpha}{\omega_d} \mathrm{e}^{-\zeta\omega_n t} \sin \omega_d t, \tag{5.35}$$

$$\dot{x}_r(t) \sim (\dot{x}_b + \alpha) \mathrm{e}^{-\zeta\omega_n t} \cos \omega_d t, \tag{5.36}$$

$$\ddot{x}_r(t) \sim \omega_d (\dot{x}_b + \alpha) \mathrm{e}^{-\zeta\omega_n t} \sin \omega_d t, \tag{5.37}$$

The envelopes of the response during the rare event are,

$$u_r(t) \sim \frac{|\dot{x}_b + \alpha|}{\omega_d} \mathrm{e}^{-\zeta\omega_n t}, \tag{5.38}$$

$$\dot{u}_r(t) \sim |\dot{x}_b + \alpha| \mathrm{e}^{-\zeta\omega_n t}, \tag{5.39}$$

$$\ddot{u}_r(t) \sim \omega_d |\dot{x}_b + \alpha| \mathrm{e}^{-\zeta\omega_n t}. \tag{5.40}$$

In equation (5.38) the two contributions $\dot{x}_b$ and α in the term $\dot{x}_b + \alpha$ are both Gaussian distributed, and thus their sum is also Gaussian distributed:

$$\eta \equiv \dot{x}_b + \alpha \sim \mathcal{N}(\mu_\alpha, \sigma^2_{\dot{x}_b} + \sigma^2_\alpha). \tag{5.41}$$

Therefore, the distribution of the quantity $|\eta|$ is given by the following folded normal distribution:

$$f_{|\eta|}(n) = \frac{1}{\sigma_{|\eta|}\sqrt{2\pi}} \left\{ \exp\left(-\frac{(n-\mu_\alpha)^2}{2\sigma^2_{|\eta|}} \right) + \exp\left(-\frac{(n+\mu_\alpha)^2}{2\sigma^2_{|\eta|}} \right) \right\}, \quad 0 < n < \infty \tag{5.42}$$

where $\sigma_{|\eta|} = \sqrt{\sigma^2_{\dot{x}_b} + \sigma^2_\alpha}$. Note in the following subsections we proceed with the approximation of pdf for the system that is underdamped $\zeta \ll 1$, the general steps are exactly the same for the overdamped case, which we will summarize in the last subsection.

5.3.4 Rare Event Transition Probability

Next we compute the rare event transition probability defined in equation (5.7) by considering the time duration τ_e, a rare response takes to return back to the background state (see figure 5-4). In other words, τ_e represents the duration starting from the initial impulse event time to the point where the response has decayed back to 10% ($\rho_c = 0.1$) of its absolute maximum. We note that extremely underdamped systems exhibit oscillatory behaviors, and for these cases we define the rare event duration as the time starting from the event to the point where the *response envelope* has decayed back to 10% of its *response absolute maximum*:

$$u_r(\tau_e) = \rho_c \max\{|x_r|\} = \rho_c x_r\left(\frac{\pi}{2\omega_d}\right), \tag{5.43}$$

where the absolute maximum of x_r for heavily underdamped system takes place at $\frac{\pi}{2\omega_d}$. We solve the above using equations (5.26) and (5.29) to obtain

$$\tau_e = \frac{\pi}{2\omega_d} - \frac{1}{\zeta\omega_n}\log\rho_c. \tag{5.44}$$

Since the magnitude of the background excitation η only enters as a multiplicative constant in the analytical form of the rare response, *the end time τ_e is independent of its conditional background magnitude.* On the other hand, the response displacement, velocity, and acceleration are associated with different characteristic end times even under the same rare events. Accordingly, the rare event time duration τ_e needs to be defined separately, and these quantities are be differentiated by $\tau_{e,\text{dis}}$, $\tau_{e,\text{vel}}$, and $\tau_{e,\text{acc}}$. For simplicity in notation, we drop the additional subscript differentiating these different rare event end times, with it being implied that they are different depending on the quantity of interest. With the obtained value for τ_e we compute the desired probability of a rare event using the frequency ν_α (equal to $1/T_\alpha$) :

$$\mathbb{P}_r = \nu_\alpha \tau_e = \tau_e / T_\alpha. \tag{5.45}$$

We emphasize again that the probability of a rare event $\mathbb{P}_r$ takes different values for the response displacement, velocity, and acceleration and will be denoted by $\mathbb{P}_{r,\text{dis}}$, $\mathbb{P}_{r,\text{vel}}$, and $\mathbb{P}_{r,\text{acc}}$, respectively.

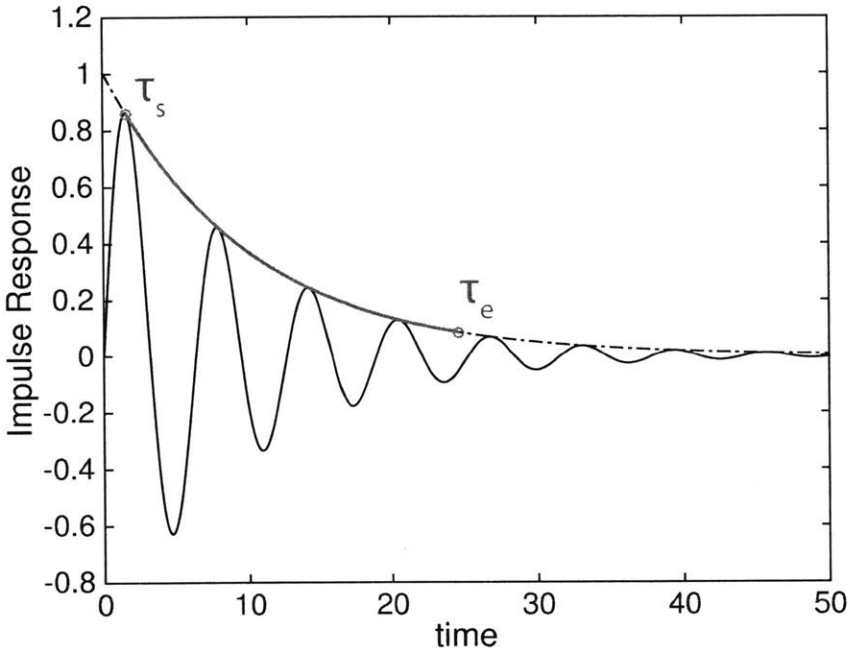

Figure 5-4: Rare event time duration τ_e and the time τ_s where the maximum magnitude of the response takes place.

5.3.5 Probability Density Function for Rare Events

We proceed with the derivation of the pdf in the rare event regime. Consider again the response displacement during a rare event,

$$u_r(t) \sim \frac{|\eta|}{\omega_d} \mathrm{e}^{-\zeta\omega_n t}, \tag{5.46}$$

here t is a random variable uniformly distributed between the initial time when the rare response has its maximum amplitude τ_s (to be defined later) and the end time τ_e (equation (5.44)) when the response has relaxed back to the background dynamics:

$$t \sim \text{Uniform}(\tau_s, \tau_e) \tag{5.47}$$

Note that the initial time instant τ_s is necessary based on the fact that the responses or response envelopes maximum value do not occur at the exact instant $\tau_s = 0$ that an impulse occurs; τ_s accounts for the actual maximum of the response in reference to the initial impulse time instant (see figure 5-4).

We condition the rare event distribution as follows,

$$f_{u_r}(r) = \int f_{u_r||\eta|}(r|n)\, f_{|\eta|}(n)\, dn, \tag{5.48}$$

where we have already derived the pdf for $f_{|\eta|}$ in equation (6.13), what remains is the derivation of the pdf for $f_{u_r||\eta|}$.

By conditioning on $|\eta| = n$, we find the derived distribution for the conditional pdf for u_r is given by

$$f_{u_r||\eta|}(r \mid n) = \frac{1}{r\zeta\omega_n\left(\tau_{e,\text{dis}} - \tau_s\right)}\left\{s\left(r - \frac{n}{\omega_d}\mathrm{e}^{-\zeta\omega_n\tau_{e,\text{dis}}}\right) - s\left(r - \frac{n}{\omega_d}\mathrm{e}^{-\zeta\omega_n\tau_s}\right)\right\} \tag{5.49}$$

where $s(x)$ denotes the step function which is equal to 1 when $x \geq 0$ and 0 otherwise. Detailed derivation is provided in appendix A.

Using the results equations (5.49) and (6.13) in equation (5.48) we obtain the final result for the rare event distribution for response displacement as

$$f_{u_r}(r) = \int f_{u_r||\eta|}(r \mid n) f_{|\eta|}(n)\, dn, \tag{5.50}$$

$$= \frac{1}{r\zeta\omega_n\sigma_{|\eta|}\sqrt{2\pi}\left(\tau_{e,\text{dis}} - \tau_s\right)}\int_0^\infty \left\{\exp\left(-\frac{(n-\mu_\alpha)^2}{2\sigma_{|\eta|}^2}\right) + \exp\left(-\frac{(n+\mu_\alpha)^2}{2\sigma_{|\eta|}^2}\right)\right\} \times \left\{s\left(r - \frac{n}{\omega_d}\mathrm{e}^{-\zeta\omega_n\tau_{e,\text{dis}}}\right) - s\left(r - \frac{n}{\omega_d}\mathrm{e}^{-\zeta\omega_n\tau_s}\right)\right\} dn, \tag{5.51}$$

The last quantity to be determined is τ_s, which represents the maximum magnitude of the response displacement. The maximum magnitude of the rare component of the

response displacement and acceleration (see equation (5.26)) occur at $\tau_s = \frac{2\pi}{\omega_d}\frac{1}{4} = \frac{\pi}{2\omega_d}$; similarly, for the velocity response the maximum occurs at $\tau_s = 0$.

5.3.6 Analytical PDF for the Underdamped Case $\zeta \ll 1$

Displacement Finally, combining the results of sections 5.3.1, 5.3.4, and 5.3.5 using the total probability law,

$$f_u(r) = f_{u_b}(r)(1 - \mathbb{P}_{r,\text{dis}}) + f_{u_r}(r)\mathbb{P}_{r,\text{dis}}, \tag{5.52}$$

we obtain the desired envelope distribution for the displacement of the response

$$\begin{aligned} f_u(r) = {} & \frac{r}{\sigma_{x_b}^2}\exp\left(-\frac{r^2}{2\sigma_{x_b}^2}\right)(1 - \nu_\alpha \tau_{e,\text{dis}}) \\ & + \frac{\nu_\alpha \tau_{e,\text{dis}}}{r\zeta\omega_n\sigma_{|\eta|}\sqrt{2\pi}\,(\tau_{e,\text{dis}} - \tau_s)}\int_0^\infty \left\{\exp\left(-\frac{(n-\mu_\alpha)^2}{2\sigma_{|\eta|}^2}\right) + \exp\left(-\frac{(n+\mu_\alpha)^2}{2\sigma_{|\eta|}^2}\right)\right\} \\ & \times \left\{s\left(r - \frac{n}{\omega_d}\mathrm{e}^{-\zeta\omega_n\tau_{e,\text{dis}}}\right) - s\left(r - \frac{n}{\omega_d}\mathrm{e}^{-\zeta\omega_n\tau_s}\right)\right\} dn, \end{aligned} \tag{5.53}$$

where $\tau_s = \frac{\pi}{2\omega_d}$ and $\tau_{e,\text{dis}} = \frac{\pi}{2\omega_d} - \frac{1}{\zeta\omega_n}\log\rho_c$.

Velocity Similarly, we also obtain the envelope distribution of the velocity of the system. The background dynamics distribution for velocity was obtained in equation (5.21). Noting that (5.38) $\dot{u}_r = \omega_d u_r$, the rare event pdf will be modified by a constant factor

$$f_{\dot{u}}(r) = f_{\dot{u}_b}(r)(1 - \mathbb{P}_{r,\text{vel}}) + \omega_d^{-1} f_{u_r}(r/\omega_d)\mathbb{P}_{r,\text{vel}}. \tag{5.54}$$

The final formula for the velocity envelope pdf is thus

$$f_{\dot{u}}(r) = \frac{r}{\sigma_{\dot{x}_b}^2}\exp\left(-\frac{r^2}{2\sigma_{\dot{x}_b}^2}\right)(1-\nu_\alpha\tau_{e,\text{vel}}) + \frac{\nu_\alpha\tau_{e,\text{vel}}}{r\zeta\omega_n\sigma_{|\eta|}\sqrt{2\pi}\tau_{e,\text{vel}}}\int_0^\infty\left\{\exp\left(-\frac{(n-\mu_\alpha)^2}{2\sigma_{|\eta|}^2}\right)+\exp\left(-\frac{(n+\mu_\alpha)^2}{2\sigma_{|\eta|}^2}\right)\right\} \times\left\{s\left(r-ne^{-\zeta\omega_n\tau_{e,\text{vel}}}\right)-s\left(r-n\right)\right\}dn, \quad (5.55)$$

where $\tau_s = 0$ and $\tau_{e,\text{vel}} = -\frac{1}{\zeta\omega_n}\log\rho_c$.

Acceleration Lastly we also obtain the envelope distribution of the acceleration. Noting that (5.38) $\ddot{u}_r = \omega_d^2 u_r$, the rare event pdf for acceleration will also be modified by a constant factor

$$f_{\ddot{u}}(r) = f_{\ddot{u}_b}(r)(1-\mathbb{P}_{r,\text{acc}}) + \omega_d^{-2} f_{u_r}(r/\omega_d^2)\mathbb{P}_{r,\text{acc}}. \quad (5.56)$$

The final formula for the acceleration envelope pdf is then

$$f_{\ddot{u}}(r) = \frac{r}{\sigma_{\ddot{x}_b}^2}\exp\left(-\frac{r^2}{2\sigma_{\ddot{x}_b}^2}\right)(1-\nu_\alpha\tau_{e,\text{acc}}) + \frac{\nu_\alpha\tau_{e,\text{acc}}}{r\zeta\omega_n\sigma_{|\eta|}\sqrt{2\pi}\left(\tau_{e,\text{acc}}-\tau_s\right)}\int_0^\infty\left\{\exp\left(-\frac{(n-\mu_\alpha)^2}{2\sigma_{|\eta|}^2}\right)+\exp\left(-\frac{(n+\mu_\alpha)^2}{2\sigma_{|\eta|}^2}\right)\right\} \times\left\{s\left(r-n\omega_d e^{-\zeta\omega_n\tau_{e,\text{acc}}}\right)-s\left(r-n\omega_d e^{-\zeta\omega_n\tau_s}\right)\right\}dn, \quad (5.57)$$

where $\tau_s = 0$ and $\tau_{e,\text{acc}} = \frac{\pi}{2\omega_d} - \frac{1}{\zeta\omega_n}\log\rho_c$.

5.3.6.1 Comparisons with Monte-Carlo Simulations

Next we compare the accuracy of the derived analytical results given in equations (5.53), (5.55), and (5.57) through comparisons to Monte-Carlo simulations. For the Monte-Carlo simulations the excitation time series is generated by superimposing the background and rare event components. The background excitation, described by a sta-

tionary stochastic process with a Pierson-Moskowitz spectrum (equation (6.7)), is simulated through a superposition of cosines over a range of frequencies with corresponding amplitudes and uniformly distributed random phases. The intermittent component is the random impulse train, and each impact is introduced as a velocity jump with a given magnitude at the point of the impulse impact.

For each of the comparisons performed in this work we generate 10 realizations of the excitation time series, each with a train of 100 impulses. Once each ensemble time series for the excitation is computed, the governing ordinary differential equations are solved using a 4th/5th order Runge-Kutta method (we carefully account for the modifications in the momentum that an impulse imparts by integrating up to each impulse time and modifying the initial conditions that the impulse imparts before integrating the system to the next impulse time). For each realization the system is integrated for a sufficiently long time so that we have converged response statistics for the displacement, velocity, and acceleration.

We utilize a shifted Pierson-Moskowitz spectrum $S_{hh}(\omega-1)$ in order to avoid resonance. The other parameters and resulted statistical quantities of the system are given in table 5.1. As it can be seen in figure 5-5 the analytical approximations compare favorably with the Monte-Carlo simulations many standard deviations away from zero. The results are robust to different parameters as far as we satisfy the assumption of independent (non-overlapping) random events.

Table 5.1: Parameters and relevant statistical quantities for SDOF system 1.

λ	0.01	k	1
T_α	5000	ζ	0.005
ω_n	1	ω_d	1
$\mu_\alpha = 7 \times \sigma_{\dot{h}}$	0.1	q	1.582×10^{-4}
$\sigma_\alpha = \sigma_{\dot{h}}$	0.0143	σ_h	0.0063
$\sigma_{\dot{x}_b}$	0.0179	σ_{x_b}	0.0082
$\sigma_{\lvert\eta\rvert}$	0.0229	$\mathbb{P}_{r,dis}$	0.0647
$\mathbb{P}_{r,vel}$	0.0614	$\mathbb{P}_{r,acc}$	0.0647

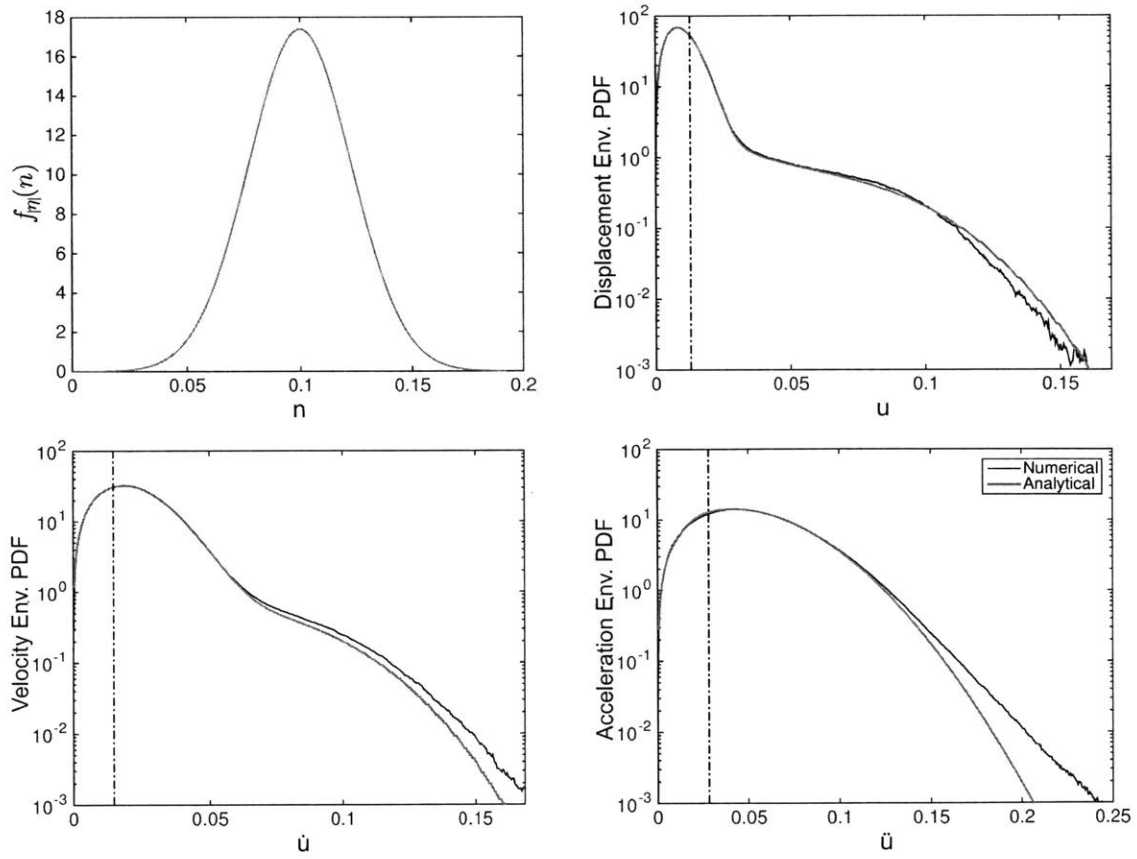

Figure 5-5: [Severely underdamped case] Comparison between direct Monte-Carlo simulation and the analytical pdf for the SDOF system 1. The pdf for the envelope of each stochastic process is presented. The dashed line indicates one standard deviation. Parameters and statistical quantities are summarized in table 5.1.

5.3.7 Analytical PDF for the Overdamped Case $\zeta \gg 1$

In the previous section, we illustrated the derivation of the analytical response pdfs under the assumption $\zeta \ll 1$. Here, we briefly summarize the results for the response pdfs for the case where $\zeta \gg 1$. One can follow the same steps starting from equation (5.32) to obtain these results. We note that for the overdamped case, the system does not exhibit oscillatory motion as opposed to the underdamped case, and hence we directly work on response pdfs instead of envelope pdfs, since there is no envelope in this case for the rare responses.

Displacement The total probability law becomes

$$f_x(r) = f_{x_b}(r)(1 - \mathbb{P}_{r,\text{dis}}) + f_{x_r}(r)\mathbb{P}_{r,\text{dis}}, \tag{5.58}$$

and we obtain the following pdf for the displacement of the system

$$\begin{aligned} f_x(r) = {} & \frac{1}{\sigma_{x_b}\sqrt{2\pi}} \exp\left(-\frac{r^2}{2\sigma_{x_b}^2}\right)(1 - \nu_\alpha \tau_{e,\text{dis}}) \\ & + \frac{\nu_\alpha \tau_{e,\text{dis}}}{r(\zeta\omega_n - \omega_o)\sigma_\eta\sqrt{2\pi}\,(\tau_{e,\text{dis}} - \tau_s)} \int_0^\infty \exp\left(-\frac{(n-\mu_\alpha)^2}{2\sigma_\eta^2}\right) \\ & \times \left\{ s\left(r - \frac{n}{2\omega_o}\mathrm{e}^{-(\zeta\omega_n - \omega_o)\tau_{e,\text{dis}}}\right) - s\left(r - \frac{n}{2\omega_o}\mathrm{e}^{-(\zeta\omega_n - \omega_o)\tau_s}\right)\right\} dn, \end{aligned} \tag{5.59}$$

where $\tau_s = 0$ and $\tau_{e,\text{dis}} = \frac{\pi}{2\omega_o} - \frac{1}{\zeta\omega_n - \omega_o}\log\rho_c$.

Velocity Similarly we derive the total probability law for the response velocity

$$f_{\dot{x}}(r) = f_{\dot{x}_b}(r)(1 - \mathbb{P}_{r,\text{vel}}) + f_{\dot{x}_r}(r)\mathbb{P}_{r,\text{vel}}. \tag{5.60}$$

The final result for the velocity pdf is

$$f_{\dot{x}}(r) = \frac{1}{\sigma_{\dot{x}_b}\sqrt{2\pi}} \exp\left(-\frac{r^2}{2\sigma_{\dot{x}_b}^2}\right)(1 - \nu_\alpha \tau_{e,\text{vel}}) + \frac{\nu_\alpha \tau_{e,\text{vel}}}{r(\zeta\omega_n + \omega_o)\sigma_\eta\sqrt{2\pi}\tau_{e,\text{vel}}} \int_0^\infty \exp\left(-\frac{(n-\mu_\alpha)^2}{2\sigma_\eta^2}\right) \times \left\{ s\left(r - n\mathrm{e}^{-(\zeta\omega_n+\omega_o)\tau_{e,\text{vel}}}\right) - s\left(r - n\right)\right\} dn, \quad (5.61)$$

where $\tau_s = 0$ and $\tau_{e,\text{vel}} = -\frac{1}{\zeta\omega_n+\omega_o}\log\rho_c$.

Acceleration The total probability law for the response acceleration is

$$f_{\ddot{x}}(r) = f_{\ddot{x}_b}(r)(1 - \mathbb{P}_{r,\text{acc}}) + f_{\ddot{x}_r}(r)\mathbb{P}_{r,\text{acc}}, \quad (5.62)$$

and this gives the following result for the acceleration pdf

$$f_{\ddot{x}}(r) = \frac{1}{\sigma_{\ddot{x}_b}\sqrt{2\pi}} \exp\left(-\frac{r^2}{2\sigma_{\ddot{x}_b}^2}\right)(1 - \nu_\alpha \tau_{e,\text{acc}}) + \frac{\nu_\alpha \tau_{e,\text{acc}}}{r(\zeta\omega_n + \omega_o)\sigma_\eta\sqrt{2\pi}\tau_{e,\text{acc}}} \int_0^\infty \exp\left(-\frac{(n-\mu_\alpha)^2}{2\sigma_\eta^2}\right) \times \left\{ s\left(r - n(\zeta\omega_n + \omega_o)\mathrm{e}^{-(\zeta\omega_n+\omega_o)\tau_{e,\text{acc}}}\right) - s\left(r - n\left(\zeta\omega_n + \omega_o\right)\right)\right\} dn, \quad (5.63)$$

where $\tau_s = 0$ and $\tau_{e,\text{acc}} = -\frac{1}{\zeta\omega_n+\omega_o}\log\rho_c$. Note that in this case we do not have the simple scaling, as in the underdamped case, for the conditionally rare pdf.

5.3.7.1 Comparisons with Monte-Carlo Simulations

We confirm the accuracy of the analytical results given in equations (5.59), (5.61), and (5.63) for the strongly overdamped case through comparison with direct Monte-Carlo simulations. The parameters and resulted statistical quantities of the system are given in table 5.2. The analytical estimates show favorable agreement with numerical simulations for this case (figure 5-6), just as in the previous underdamped case.

Table 5.2: Parameters and relevant statistical quantities for SDOF system 2.

λ	6	k	1
T_α	1000	ζ	3
ω_n	1	ω_d	2.828
$\mu_\alpha = 7 \times \sigma_{\dot{h}}$	0.1	q	1.582×10^{-4}
$\sigma_\alpha = \sigma_{\dot{h}}$	0.0143	σ_h	0.0063
$\sigma_{\dot{x}_b}$	0.0056	σ_{x_b}	0.0022
σ_η	0.0154	$\mathbb{P}_{r,dis}$	0.0140
$\mathbb{P}_{r,vel}$	0.0004	$\mathbb{P}_{r,acc}$	0.0004

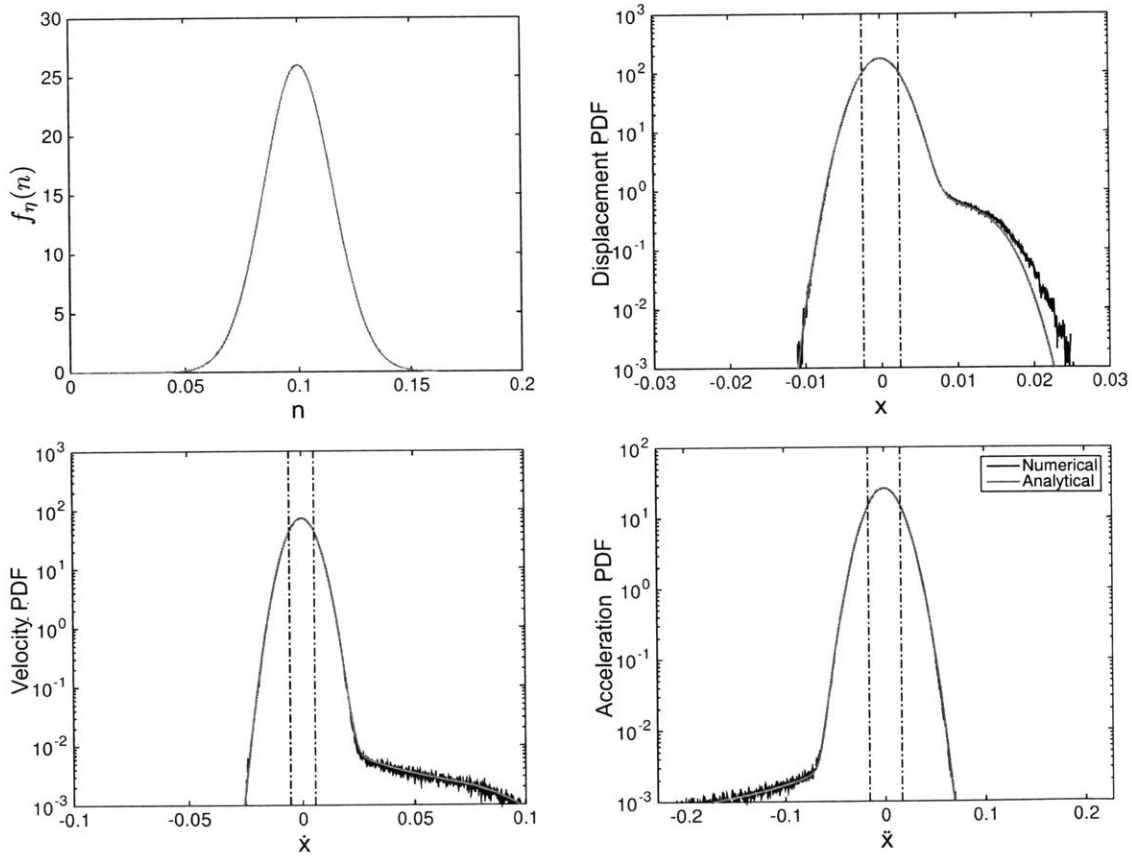

Figure 5-6: [Severely overdamped case] Comparison between direct Monte-Carlo simulation and the analytical pdf for SDOF system 2. The pdf for the value of each stochastic process is shown. The dashed line indicates one standard deviation. Parameters and statistical quantities are summarized in table 5.2.

5.4 Semi-analytical Quantification of Response PDFs in the General Case for Linear SDOF Systems

In the previous section we developed an analytical method to quantify response pdfs of single-degree-of-freedom linear systems under stochastic excitations containing rare events. However, explicit analytical expressions were only available for limited SDOF configurations, i.e. those with $\zeta \ll 1$ or $\zeta \gg 1$. Alternatively, here we propose a semi-analytical approach to quantify the response pdfs. We note that the semi-analytical method works for any SDOF system configuration including the severely underdamped or overdamped cases considered previously. The approach here adapts the numerical scheme described in [102] for systems undergoing internal instabilities.

We clarify that the scheme is *semi-analytical* in that

(i) it takes a numerical histogram of rare responses based on the exact solution of impulse response of the system, and

(ii) weights the conditional rare event distribution $f_{x_r|\eta}$ using the respective distribution for η, and

(iii) numerically estimates the absolute maximum of the response and computes the rare event duration τ_e.

We note that the essence of the algorithm remains the same as in section 5.3. Although the semi-analytical scheme includes numerical simulations, it still associates with significantly lower computational cost compared with numerical simulations, i.e. Monte-Carlo simulation. The reason for this is simple: we simulate and histogram the rare responses *directly* based on their analytical form. Furthermore, the beauty of the semi-analytical scheme is that it is easily extended to multi-degree-of-freedom systems. We illustrate the extension to MDOF systems in the next section.

5.4.1 Numerical Histogram of Rare Events

Consider the same SDOF system introduced in section 5.3. Recall that we have quantified the response pdfs by the PDS method using the total probability law

$$f_x(r) = f_{x_b}(r)(1 - \mathbb{P}_r) + f_{x_r}(r)\mathbb{P}_r. \tag{5.64}$$

In the previous section, the derivation consisted of estimating all three unknown quantities: the background distribution f_{x_b}, the rare event distribution f_{x_r}, and the rare event probability $\mathbb{P}_r$ analytically. However, in the semi-analytical scheme we will obtain the the rare event distribution f_{x_r} and rare event probability $\mathbb{P}_r$ by directly simulating the analytical form of the rare response and by taking a histogram of the numerically simulated analytical form of the rare response. The background distribution f_{x_b} can still be obtained analytically as in section 5.3.1.

Recall that the rare event distribution is given by

$$f_{x_r}(r) = \int f_{x_r|\eta}(r \mid n) f_\eta(n)\, dn, \tag{5.65}$$

where $f_\eta(n)$ is known analytically (section 5.3.2). It is the conditional pdf $f_{x_r|\eta}(r \mid n)$ that we estimate by a histogram:

$$f_{x_r|\eta}(r \mid n) = \text{Hist}\Big\{x_{r|\eta}(t \mid n)\Big\}, \quad t = [0, \tau_{e,\text{dis}}], \tag{5.66}$$

where we use the exact form of the conditional response:

$$x_{r|\eta}(t \mid n) = \frac{n}{2\omega_o}\left(\mathrm{e}^{-(\zeta\omega_n - \omega_o)t} - \mathrm{e}^{-(\zeta\omega_n + \omega_o)t}\right). \tag{5.67}$$

The histogram is taken from $t = 0$ till the end of the rare event at $t = \tau_e$. This gives the semi-analytical approach almost no additional computational costs over the previous analytical results in the previous section since we have the exact analytical form of rare responses and performing a histogram of this is a cheap operation. The

conditional distribution of rare event response for velocity and acceleration can be derived in similar fashion:

$$f_{\dot{x}_r|\eta}(r \mid n) = \text{Hist}\Big\{\dot{x}_{r|\eta}(t \mid n)\Big\}, \quad t = [0, \tau_{e,\text{vel}}] \tag{5.68}$$

$$f_{\ddot{x}_r|\eta}(r \mid n) = \text{Hist}\Big\{\ddot{x}_{r|\eta}(t \mid n)\Big\}, \quad t = [0, \tau_{e,\text{acc}}] \tag{5.69}$$

We note that, as opposed to the fully analytical scheme from before, here we do not need to approximate the initial instant τ_s (which was done in order to avoid overestimation of the magnitude of rare responses when using the envelope based approach for the underdamped system) because the semi-analytical approach is based on the exact impulse response.

5.4.2 Numerical Estimation of the Rare Event Transition Probability

In order to compute the histogram of a rare impulse event, the duration of a rare response needs to be obtained numerically. Recall that we have defined the duration of a rare responses by

$$x_r(\tau_e) = \rho_c \max\Big\{|x_r|\Big\}, \tag{5.70}$$

where $\rho_c = 0.1$. In the numerical computation of τ_e, the absolute maximum of the response needs to be estimated numerically in order to compute τ_e. Once the rare event duration has been specified, we can obtain the probability of a rare event by

$$\mathbb{P}_r = \nu_\alpha \tau_e = \tau_e / T_\alpha. \tag{5.71}$$

Again, this value is independent of the conditional background magnitude. The above procedure is applied for the rare event response displacement $\tau_{e,\text{dis}}$, velocity $\tau_{e,\text{vel}}$, and acceleration $\tau_{e,\text{acc}}$.

5.4.3 Semi-analytical Probability Density Functions

With the description above, we can easily compute the desired response pdfs and the final semi-analytical results. The only quantities that need numerical estimation are τ_e and $\text{Hist}\{q_{r|\eta}(t \mid n)\}$ (which is computed by simulating the analytical form of the rare response directly for $t \in [0, \tau_e]$ and by then taking a histogram), where q can be either x, $\dot{x}$, or $\ddot{x}$.

Displacement

$$f_x(r) = \frac{1 - \nu_\alpha \tau_{e,\text{dis}}}{\sigma_{x_b}\sqrt{2\pi}} \exp\left(-\frac{r^2}{2\sigma_{x_b}^2}\right) + \nu_\alpha \tau_{e,\text{dis}} \int_0^\infty \text{Hist}\{x_{r|\eta}(t \mid n)\} f_\eta(n)\, dn. \quad (5.72)$$

Velocity

$$f_{\dot{x}}(r) = \frac{1 - \nu_\alpha \tau_{e,\text{vel}}}{\sigma_{\dot{x}_b}\sqrt{2\pi}} \exp\left(-\frac{r^2}{2\sigma_{\dot{x}_b}^2}\right) + \nu_\alpha \tau_{e,\text{vel}} \int_0^\infty \text{Hist}\{\dot{x}_{r|\eta}(t \mid n)\} f_\eta(n)\, dn. \quad (5.73)$$

Acceleration

$$f_{\ddot{x}}(r) = \frac{1 - \nu_\alpha \tau_{e,\text{acc}}}{\sigma_{\ddot{x}_b}\sqrt{2\pi}} \exp\left(-\frac{r^2}{2\sigma_{\ddot{x}_b}^2}\right) + \nu_\alpha \tau_{e,\text{acc}} \int_0^\infty \text{Hist}\{\ddot{x}_{r|\eta}(t \mid n)\} f_\eta(n)\, dn. \quad (5.74)$$

5.4.3.1 Comparisons with Monte-Carlo Simulations

We now compare the derived semi-analytical scheme for the response pdfs of a general single-degree-of-freedom system with Monte-Carlo simulations. Details regarding the Monte-Carlos simulations are the same as before. For illustration, two SDOF configurations are considered with damping ratio values of $\zeta = 0.75$ and $\zeta = 1$. We note that these two regimes are where the analytical results derived in section 5.3 are not applicable and cannot be used.

The parameters and resulted statistical quantities of the sdof system 3 and 4 are given in table 5.3 and table 5.4, respectively. For both cases, analytical estimates show favorable agreement with numerical Monte-Carlo simulations for these case (figure 5-7 and figure 5-8). We emphasize that the computational cost of semi-analytical scheme for SDOF systems is *comparable with that of analytical method*, and both are *significantly lower* than the costs of Monte-Carlo simulations.

Table 5.3: Parameters and relevant statistical quantities for SDOF system 3.

λ	1.5	k	1
T_α	400	ζ	0.75
ω_n	1	ω_d	0.661
$\mu_\alpha = 7 \times \sigma_{\dot{h}}$	0.1	q	1.582×10^{-4}
$\sigma_\alpha = \sigma_{\dot{h}}$	0.0143	σ_h	0.0063
$\sigma_{\dot{x}_b}$	0.0137	σ_{x_b}	0.0060
σ_η	0.0198	$\mathbb{P}_{r,dis}$	0.0097
$\mathbb{P}_{r,vel}$	0.0090	$\mathbb{P}_{r,acc}$	0.0041

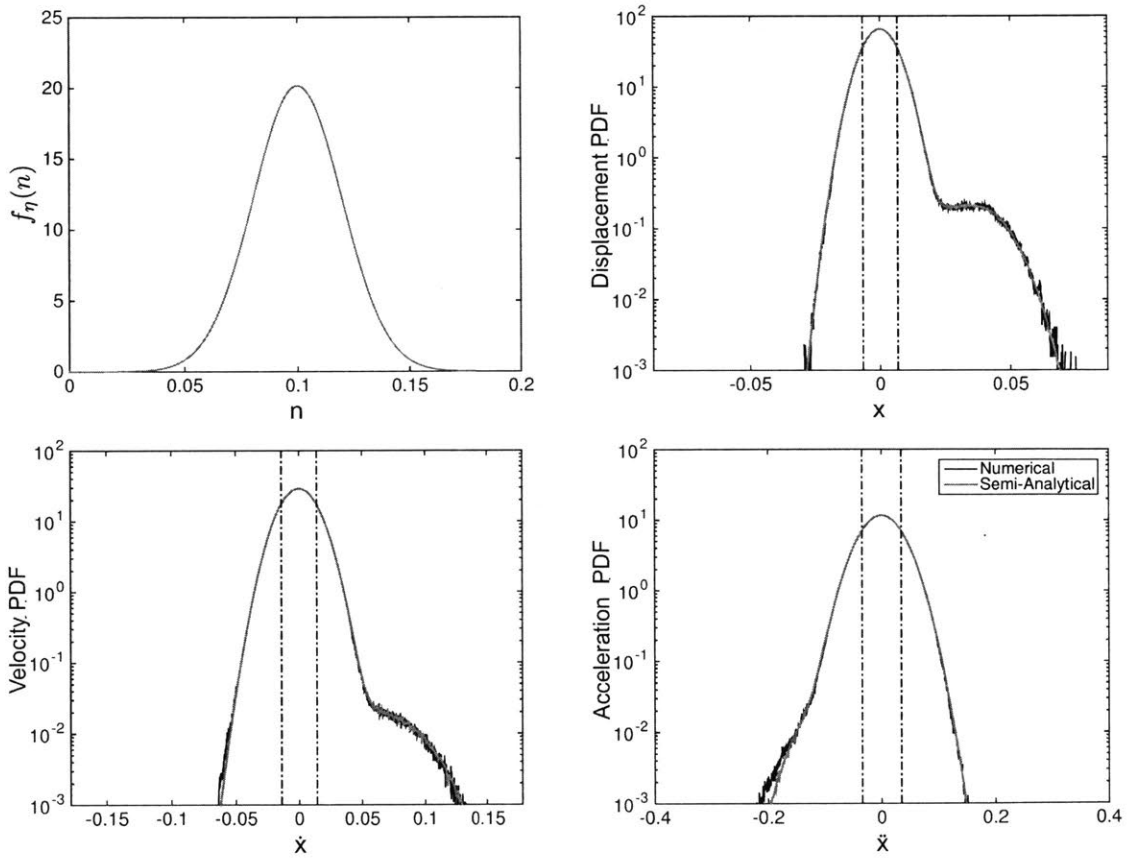

Figure 5-7: [Intermediate damped system] Comparison between direct Monte-Carlo simulations and the semi-analytical pdf for SDOF system 3. Dashed lines indicate one standard deviation. Parameters and statistical quantities are summarized in table 5.3.

Table 5.4: Parameters and relevant statistical quantities for SDOF system 4.

λ	2	k	1
T_α	400	ζ	1
ω_n	1	ω_d	0
$\mu_\alpha = 7 \times \sigma_{\dot{h}}$	0.1	q	1.582×10^{-4}
$\sigma_\alpha = \sigma_{\dot{h}}$	0.0143	σ_h	0.0063
$\sigma_{\dot{x}_b}$	0.0120	σ_{x_b}	0.0052
σ_η	0.0187	$\mathbb{P}_{r,dis}$	0.0122
$\mathbb{P}_{r,vel}$	0.0075	$\mathbb{P}_{r,acc}$	0.0032

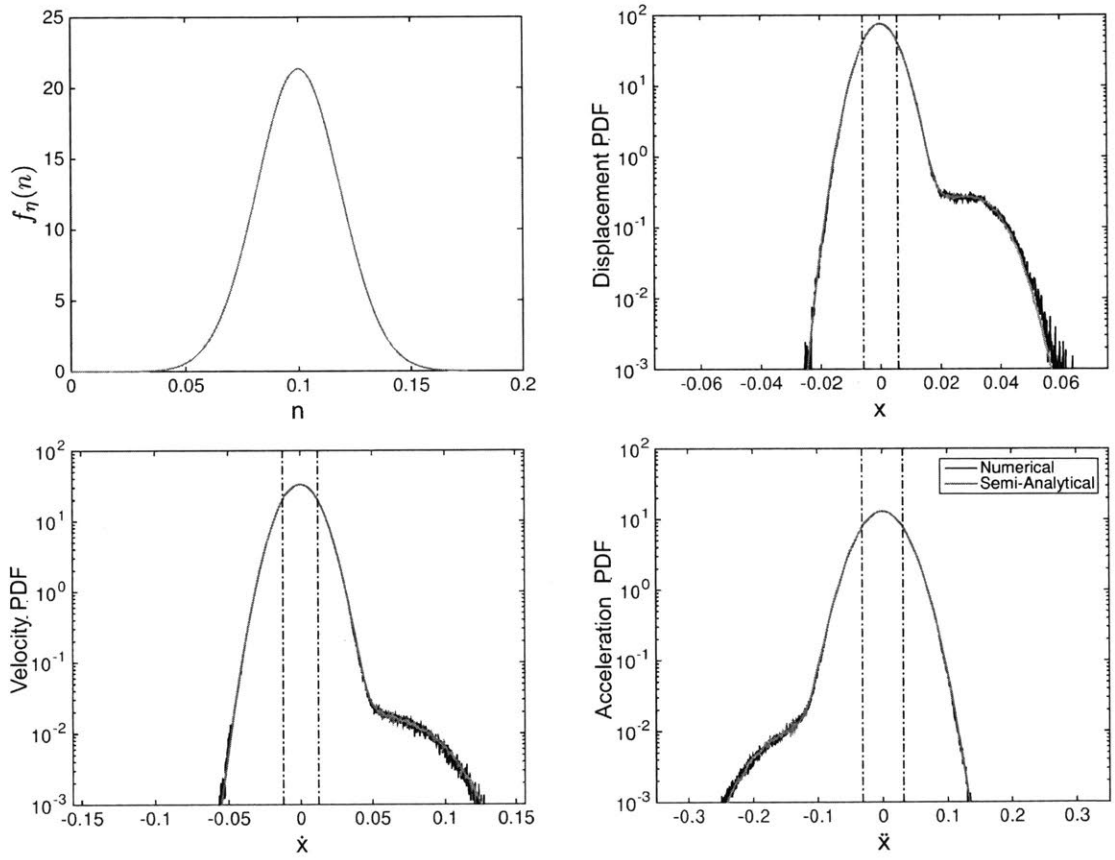

Figure 5-8: [Critical damped system] Comparison between direct Monte-Carlo simulations and the semi-analytical pdf for SDOF system 4. Dashed lines indicate one standard deviation. Parameters and statistical quantities are summarized in table 5.4.

We emphasize again that he described semi-analytical approach is applicable to single-degree-of-freedom systems with any damping ratio ζ. An an illustrative purpose, we revisit the SDOF system 1 which is heavily damped case and describe the semi-analytically obtained pdf as well as Monte-Carlo simulation result in figure 5-9. Note that although we have exactly same system parameters for SDOF 1, the relevant statistical quantities change since we utilize semi-analytical approach instead of analytical one here. We also point out that the response pdfs described in figure 5-9 are response displacement, velocity and acceleration, not response envelopes as in figure 5-5.

Table 5.5: Relevant statistical quantities for SDOF system 1 using semi-analytical method.

$\sigma_{\dot{x}_b}$	0.0179	σ_{x_b}	0.0082
σ_η	0.0229	$\mathbb{P}_{r,dis}$	0.0915
$\mathbb{P}_{r,vel}$	0.0918	$\mathbb{P}_{r,acc}$	0.0915

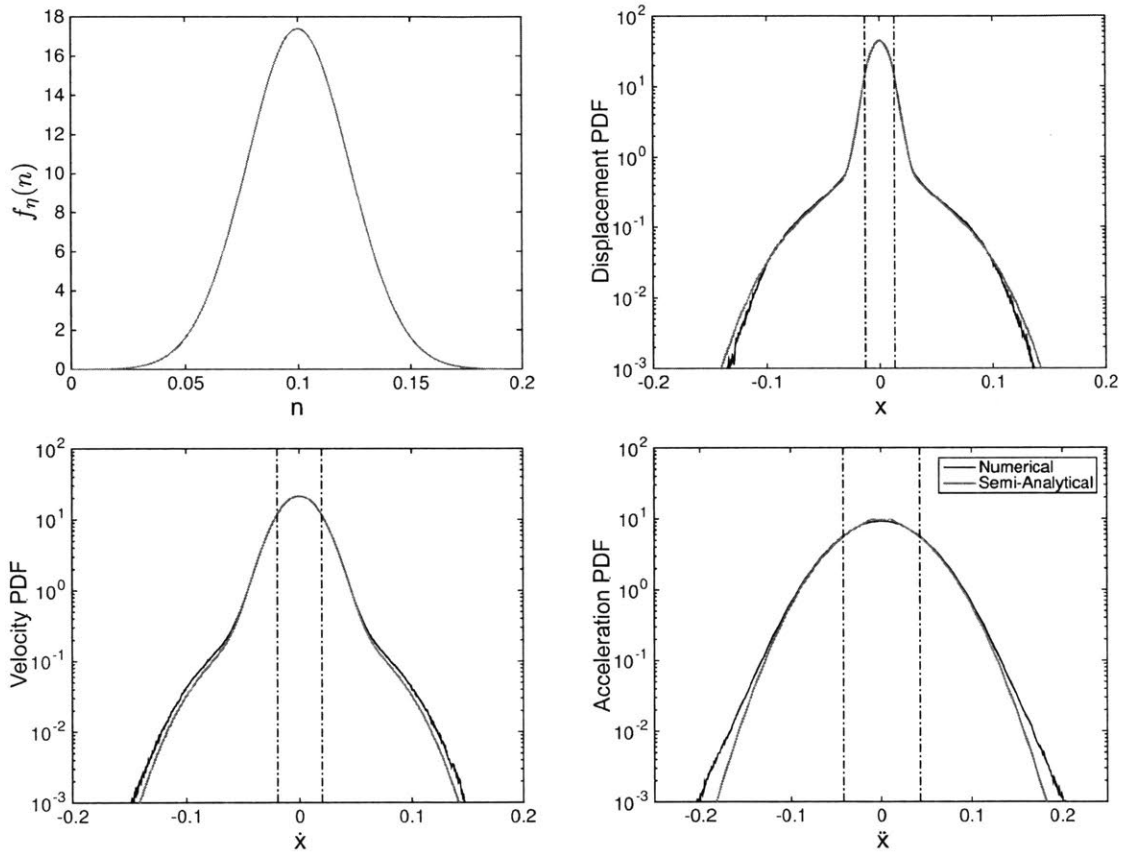

Figure 5-9: [Severely underdamped case; Semi-analytical Method] Comparison between direct Monte-Carlo simulation and the semi-analytical pdf for the SDOF system 1. The pdf for the envelope of each stochastic process is presented. The dashed line indicates one standard deviation. Statistical quantities are summarized in table 5.5. System parameters are the same as table 5.1.

5.5 Semi-analytical Quantification of Response PDFs for Intermittently Forced MDOF Prototype System

In the previous section we formulated the semi-analytical approach for obtaining response pdfs for SDOF linear systems under stochastic excitations containing rare events. The key advantage of the semi-analytical scheme is that the algorithm can be easily extended to MDOF linear systems with minor modifications (the basic principles behind the algorithm remain the same, but the details change). In this section we introduce how the extension can be made for a prototype TDOF linear system; in particular we consider the multi-degree-of-freedom extension of the considered prototype system in section 5.2 (see figure 5-10). In particular, the system is given by

$$m\ddot{x} + \lambda\dot{x} + kx + \lambda_a(\dot{x} - \dot{v}) + k_a(x - v) = F(t), \tag{5.75}$$

$$m_a\ddot{v} + \lambda_a(\dot{v} - \dot{x}) + k_a(v - x) = 0, \tag{5.76}$$

where the stochastic forcing $F(t) = F_b(t) + F_r(t)$ is applied to the first mass (mass m). As before, $F_b(t) = \ddot{h}(t)$ is the background component and $F_r(t) = \sum_{i=1}^{N(t)} \alpha_i \delta(t - \tau_i)$ is the rare event component. The backbone of the scheme, the PDS method with the total probability law composition, remains the same. We first quantify of background response statistics and then the rare event statistics and lastly show comparisons with numerical results.

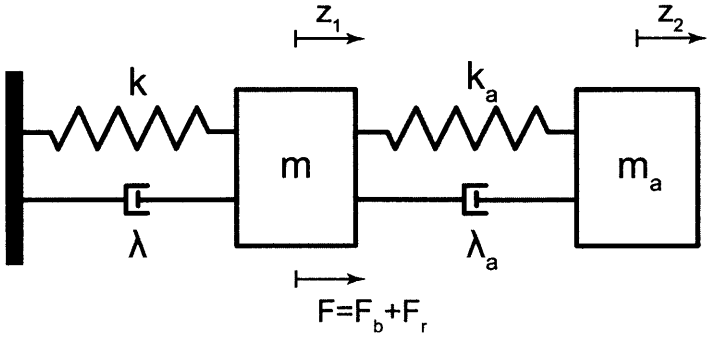

Figure 5-10: The considered TDOF system.

5.5.1 Background Response PDF Quantification

Consider the statistical response of the system to the background forcing component,

$$m\ddot{x}_b + \lambda\dot{x}_b + kx + \lambda_a(\dot{x}_b - \dot{v}_b) + k_a(x_b - v_b) = F_b(t), \tag{5.77}$$
$$m_a\ddot{v}_b + \lambda_a(\dot{v}_b - \dot{x}_b) + k_a(v_b - x_b) = 0.$$

The spectral density of responses are given by

$$S_{x_bx_b}(\omega) = \left|\frac{\omega^4}{\left\{\mathcal{A}(\omega) - \frac{\mathcal{B}(\omega)^2}{\mathcal{C}(\omega)}\right\}\left\{\mathcal{A}(-\omega) - \frac{\mathcal{B}(-\omega)^2}{\mathcal{C}(-\omega)}\right\}}\right| S_{F_b}(\omega), \tag{5.78}$$

$$S_{\dot{x}_b\dot{x}_b}(\omega) = \omega^2 S_{x_bx_b}(\omega), \tag{5.79}$$

$$S_{\ddot{x}_b\ddot{x}_b}(\omega) = \omega^4 S_{x_bx_b}(\omega), \tag{5.80}$$

$$S_{v_bv_b}(\omega) = \left|\frac{\omega^4}{\left\{\frac{\mathcal{A}(\omega)\mathcal{C}(\omega)}{\mathcal{B}(\omega)} - \mathcal{B}(\omega)\right\}\left\{\frac{\mathcal{A}(-\omega)\mathcal{C}(-\omega)}{\mathcal{B}(-\omega)} - \mathcal{B}(-\omega)\right\}}\right| S_{F_b}(\omega), \tag{5.81}$$

$$S_{\dot{v}_b\dot{v}_b}(\omega) = \omega^2 S_{v_bv_b}(\omega), \tag{5.82}$$

$$S_{\ddot{v}_b\ddot{v}_b}(\omega) = \omega^4 S_{v_bv_b}(\omega), \tag{5.83}$$

where

$$\mathcal{A}(\omega) = (\lambda_a + \lambda)(j\omega) + (k_a + k) - m\omega^2, \tag{5.84}$$

$$\mathcal{B}(\omega) = \lambda_a(j\omega) + k_a, \tag{5.85}$$

$$\mathcal{C}(\omega) = \lambda_a(j\omega) + k_a - m_a\omega^2. \tag{5.86}$$

Thus we can obtain the following conditionally background variances for the system:

$$\sigma^2_{x_b} = \int_0^\infty S_{x_bx_b}(\omega)\,d\omega, \quad \sigma^2_{\dot{x}_b} = \int_0^\infty S_{\dot{x}_b\dot{x}_b}(\omega)\,d\omega, \quad \sigma^2_{\ddot{x}_b} = \int_0^\infty S_{\ddot{x}_b\ddot{x}_b}(\omega)\,d\omega, \tag{5.87}$$

$$\sigma^2_{v_b} = \int_0^\infty S_{v_bv_b}(\omega)\,d\omega, \quad \sigma^2_{\dot{v}_b} = \int_0^\infty S_{\dot{v}_b\dot{v}_b}(\omega)\,d\omega, \quad \sigma^2_{\ddot{v}_b} = \int_0^\infty S_{\ddot{v}_b\ddot{v}_b}(\omega)\,d\omega. \tag{5.88}$$

5.5.2 Exact Solution under an Impulse Response

Next we derive the exact form of the system's response under an impulse:

$$m\ddot{x}_r + \lambda\dot{x}_r + kx + \lambda_a(\dot{x}_r - \dot{v}_r) + k_a(x_r - v_r) = 0, \tag{5.89}$$

$$m_a\ddot{v}_r + \lambda_a(\dot{v}_r - \dot{x}_r) + k_a(v_r - x_r) = 0. \tag{5.90}$$

where the system is subjected to an impulsive magnitude of $\eta = n$ at $t = 0$. Note that the rare event (impulse load) can be treated as the initial velocity of the first mass where the load is applied. We can rewrite the equations above in matrix form

$$\begin{bmatrix} m & 0 \\ 0 & m_a \end{bmatrix} \begin{bmatrix} \ddot{x}_r \\ \ddot{v}_r \end{bmatrix} + \begin{bmatrix} \lambda + \lambda_a & -\lambda_a \\ -\lambda_a & \lambda_a \end{bmatrix} \begin{bmatrix} \dot{x}_r \\ \dot{v}_r \end{bmatrix} + \begin{bmatrix} k + k_a & -k_a \\ -k_a & k_a \end{bmatrix} \begin{bmatrix} x_r \\ v_r \end{bmatrix} = \begin{bmatrix} 0 \\ 0 \end{bmatrix}. \tag{5.91}$$

Assuming solution of the form $x_r = A_1 e^{st}$ and $v_r = A_2 e^{st}$, we obtain

$$\begin{bmatrix} ms^2 + (\lambda + \lambda_a)s + k + k_a & -\lambda_a s - k_a \\ -\lambda_a s - k_a & m_a s^2 + \lambda_a s + k_a \end{bmatrix} \begin{bmatrix} A_1 \\ A_2 \end{bmatrix} = \begin{bmatrix} 0 \\ 0 \end{bmatrix}. \tag{5.92}$$

For a nontrivial response, the determinant of the coefficient matrix must vanish. Hence,

$$\begin{aligned} &\det \begin{bmatrix} ms^2 + (\lambda + \lambda_a)s + k + k_a & -\lambda_a s - k_a \\ -\lambda_a s - k_a & m_a s^2 + \lambda_a s + k_a \end{bmatrix} \\ &= (ms^2 + (\lambda + \lambda_a)s + k + k_a)(m_a s^2 + \lambda_a s + k_a) - (\lambda_a s + k_a)^2 = 0, \end{aligned} \tag{5.93}$$

where the fourth order polynomial have four roots, i.e s_1, s_2, s_3, and s_4 (in the non-degenerate case). Thus the impulse response of equation (5.91) is given by

$$\begin{bmatrix} x_r(t) \\ v_r(t) \end{bmatrix} = c_1 \begin{bmatrix} A_{11} \\ A_{21} \end{bmatrix} e^{s_1 t} + c_2 \begin{bmatrix} A_{12} \\ A_{22} \end{bmatrix} e^{s_2 t} + c_3 \begin{bmatrix} A_{13} \\ A_{23} \end{bmatrix} e^{s_3 t} + c_4 \begin{bmatrix} A_{14} \\ A_{24} \end{bmatrix} e^{s_4 t}, \tag{5.94}$$

where c_1, c_2, c_3, c_4 are constants that are determined from the initial conditions, and A_{1i} and A_{2i} can be estimated by

$$\frac{A_{2i}}{A_{1i}} = \frac{ms_i^2 + (\lambda + \lambda_a)s_i + k + k_a}{\lambda_a s_i + k_a}, \quad i = 1, \ldots, 4. \tag{5.95}$$

Assuming A_{1i} to be 1, we obtain 2 by 4 matrix $\mathcal{A}$ as

$$\mathcal{A} = \begin{bmatrix} 1 & \cdots & 1 \\ \frac{ms_1^2+(\lambda+\lambda_a)s_1+k+k_a}{\lambda_a s_1+k_a} & \cdots & \frac{ms_4^2+(\lambda+\lambda_a)s_4+k+k_a}{\lambda_a s_4+k_a} \end{bmatrix}, \tag{5.96}$$

and c_1, c_2, c_3, c_4 can be obtained by solving

$$\begin{bmatrix} 1 & \cdots & 1 \\ s_1 & \cdots & s_4 \\ \frac{ms_1^2+(\lambda+\lambda_a)s_1+k+k_a}{\lambda_a s_1+k_a} & \cdots & \frac{ms_4^2+(\lambda+\lambda_a)s_4+k+k_a}{\lambda_a s_4+k_a} \\ \frac{s_1(ms_1^2+(\lambda+\lambda_a)s_1+k+k_a)}{\lambda_a s_1+k_a} & \cdots & \frac{s_4(ms_4^2+(\lambda+\lambda_a)s_4+k+k_a)}{\lambda_a s_4+k_a} \end{bmatrix} \begin{bmatrix} c_1 \\ c_2 \\ c_3 \\ c_4 \end{bmatrix} = \begin{bmatrix} 0 \\ n \\ 0 \\ 0 \end{bmatrix}. \tag{5.97}$$

We note that one can apply the same procedures to any MDOF linear systems.

5.5.3 Semi-analytical Probability Density Function

Once the exact form of impulse response has been obtained, one can revisit sections 5.4.1 and 5.4.2 to numerically quantify the rare event distribution as well as the rare event duration. Here we simply state the final results.

Displacements The distribution for the displacements of the system are:

$$\begin{aligned} f_x(r) &= \frac{1 - \nu_\alpha \tau^x_{e,\text{dis}}}{\sigma_{x_b}\sqrt{2\pi}} \exp\left(-\frac{r^2}{2\sigma^2_{x_b}}\right) + \nu_\alpha \tau^x_{e,\text{dis}} \int_0^\infty \text{Hist}\Big\{x_{r|\eta}(t \mid n)\Big\} f_\eta(n)\, dn, \\ f_v(r) &= \frac{1 - \nu_\alpha \tau^v_{e,\text{dis}}}{\sigma_{v_b}\sqrt{2\pi}} \exp\left(-\frac{r^2}{2\sigma^2_{v_b}}\right) + \nu_\alpha \tau^v_{e,\text{dis}} \int_0^\infty \text{Hist}\Big\{v_{r|\eta}(t \mid n)\Big\} f_\eta(n)\, dn, \end{aligned} \tag{5.98}$$

where $\tau^x_{e,\text{dis}}$ and $\tau^v_{e,\text{dis}}$ are estimated numerically.

Velocities Similarly we derive the distribution of response velocities:

$$\begin{aligned} f_{\dot{x}}(r) &= \frac{1-\nu_\alpha \tau^x_{e,\text{vel}}}{\sigma_{\dot{x}_b}\sqrt{2\pi}} \exp\left(-\frac{r^2}{2\sigma^2_{\dot{x}_b}}\right) + \nu_\alpha \tau^x_{e,\text{vel}} \int_0^\infty \text{Hist}\Big\{\dot{x}_{r|\eta}(t \mid n)\Big\} f_\eta(n)\, dn, \\ f_{\dot{v}}(r) &= \frac{1-\nu_\alpha \tau^v_{e,\text{vel}}}{\sigma_{\dot{v}_b}\sqrt{2\pi}} \exp\left(-\frac{r^2}{2\sigma^2_{\dot{v}_b}}\right) + \nu_\alpha \tau^v_{e,\text{vel}} \int_0^\infty \text{Hist}\Big\{\dot{v}_{r|\eta}(t \mid n)\Big\} f_\eta(n)\, dn, \end{aligned} \tag{5.99}$$

where $\tau^x_{e,\text{vel}}$ and $\tau^v_{e,\text{vel}}$ are estimated numerically.

Accelerations The distribution of response accelerations are:

$$\begin{aligned} f_{\ddot{x}}(r) &= \frac{1-\nu_\alpha \tau^x_{e,\text{acc}}}{\sigma_{\ddot{x}_b}\sqrt{2\pi}} \exp\left(-\frac{r^2}{2\sigma^2_{\ddot{x}_b}}\right) + \nu_\alpha \tau^x_{e,\text{acc}} \int_0^\infty \text{Hist}\Big\{\ddot{x}_{r|\eta}(t \mid n)\Big\} f_\eta(n)\, dn, \\ f_{\ddot{v}}(r) &= \frac{1-\nu_\alpha \tau^v_{e,\text{acc}}}{\sigma_{\ddot{v}_b}\sqrt{2\pi}} \exp\left(-\frac{r^2}{2\sigma^2_{\ddot{v}_b}}\right) + \nu_\alpha \tau^v_{e,\text{acc}} \int_0^\infty \text{Hist}\Big\{\ddot{v}_{r|\eta}(t \mid n)\Big\} f_\eta(n)\, dn, \end{aligned} \tag{5.100}$$

where $\tau^x_{e,\text{acc}}$ and $\tau^v_{e,\text{acc}}$ are estimated numerically.

5.5.3.1 Comparisons with Monte-Carlo Simulations

Here compare the derived formulas in equations (5.98) to (5.100) for the response pdfs for the two-degree-of-freedom system in equation (6.2) with Monte-Carlo simulations. Details regarding the Monte-Carlos simulations are the same as described in section 5.3.6.1. Results are shown for three different sets of system parameters, and response pdfs for the displacements, velocities and accelerations for both masses are compared. Three tdof systems are chosen such that i) symmetric masses with two dependent modes, ii) symmetric masses with two independent mode, and iii) asymmetric masses.

The parameters and resulted statistical quantities of the TDOF 1, 2 and 3 are given in table 5.6, table 5.7 and table 5.8 , respectively. The results of this comparison demonstrate the accuracy of the proposed semi-analytical method, and agree closely with the numerical simulations in both the presented cases (see figures 5-11 to 5-13). Further simulations using different system parameters were also performed and we obtained similar agreement demonstrating the robustness of the proposed method.

Table 5.6: Parameters and relevant statistical quantities for the TDOF system 1.

m	1	m_a	1
λ	0.01	k	1
λ_a	1	k_a	0.1
T_α	1000	σ_η	0.0199
μ_α	0.1	q	1.582×10^{-4}
σ_α	0.0143	σ_{F_b}	0.0351
$\mathbb{P}^x_{r,dis}$	0.0177	$\mathbb{P}^v_{r,dis}$	0.0190
$\mathbb{P}^x_{r,vel}$	0.0098	$\mathbb{P}^v_{r,vel}$	0.0209
$\mathbb{P}^x_{r,acc}$	0.0066	$\mathbb{P}^v_{r,acc}$	0.0082

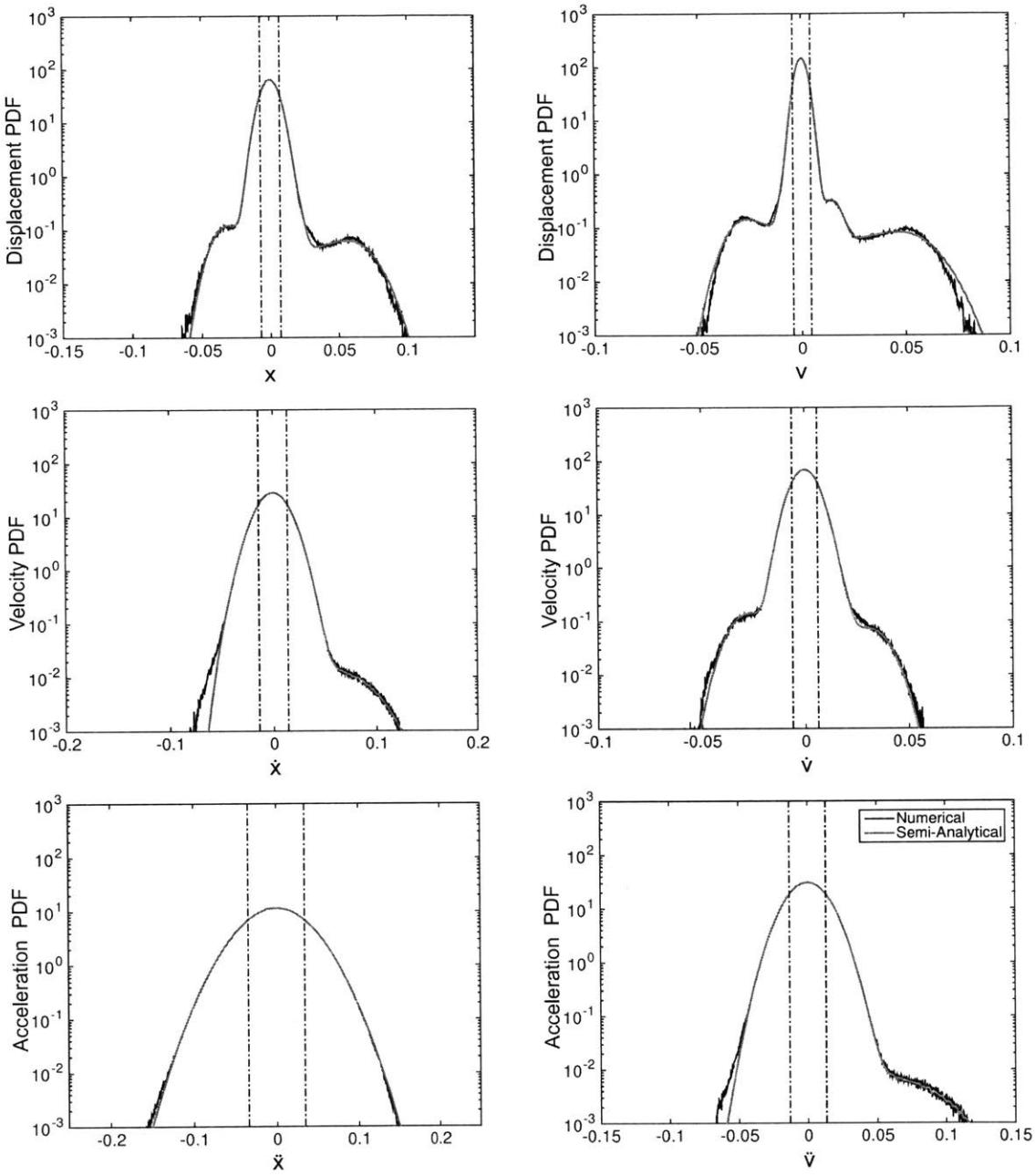

Figure 5-11: [Two DOF System 1] Comparison between direct Monte-Carlo simulation and the semi-analytical approximation. The pdf for the value of the time series are presented. Dashed line indicates one standard deviation. Parameters and statistical quantities are summarized in table 5.6.

Table 5.7: Parameters and relevant statistical quantities for the TDOF system 2.

m	1	m_a	1
λ	0.1	k	1
λ_a	0.1	k_a	1
T_α	5000	σ_η	0.0323
μ_α	0.1	q	1.582×10^{-4}
σ_α	0.0143	σ_{F_b}	0.0351
$\mathbb{P}^x_{r,dis}$	0.0198	$\mathbb{P}^v_{r,dis}$	0.0218
$\mathbb{P}^x_{r,vel}$	0.0100	$\mathbb{P}^v_{r,vel}$	0.0205
$\mathbb{P}^x_{r,acc}$	0.0049	$\mathbb{P}^v_{r,acc}$	0.0126

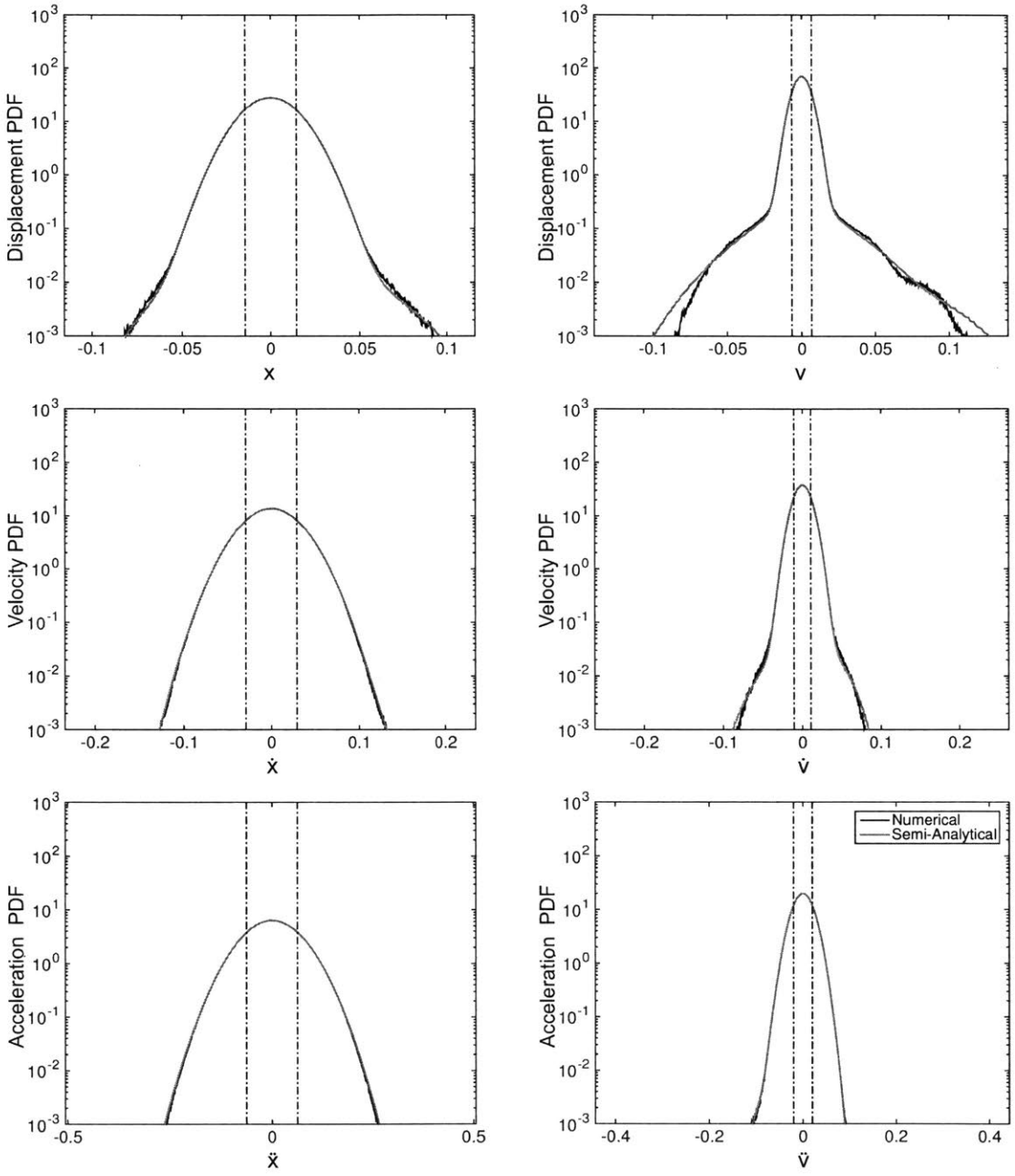

Figure 5-12: [Two DOF System 2] Comparison between direct Monte-Carlo simulation and the semi-analytical approximation. The pdf for the value of the time series are presented. Dashed line indicates one standard deviation. Parameters and statistical quantities are summarized in table 5.7.

Table 5.8: Parameters and relevant statistical quantities for the TDOF system 3.

m	1	m_a	0.05
λ	0.05	k	1
λ_a	0.1	k_a	0.1
T_α	5000	σ_η	0.0225
μ_α	0.1	q	1.582×10^{-4}
σ_α	0.0143	σ_{F_b}	0.0351
$\mathbb{P}^x_{r,dis}$	0.0145	$\mathbb{P}^v_{r,dis}$	0.0153
$\mathbb{P}^x_{r,vel}$	0.0135	$\mathbb{P}^v_{r,vel}$	0.0150
$\mathbb{P}^x_{r,acc}$	0.0138	$\mathbb{P}^v_{r,acc}$	0.0102

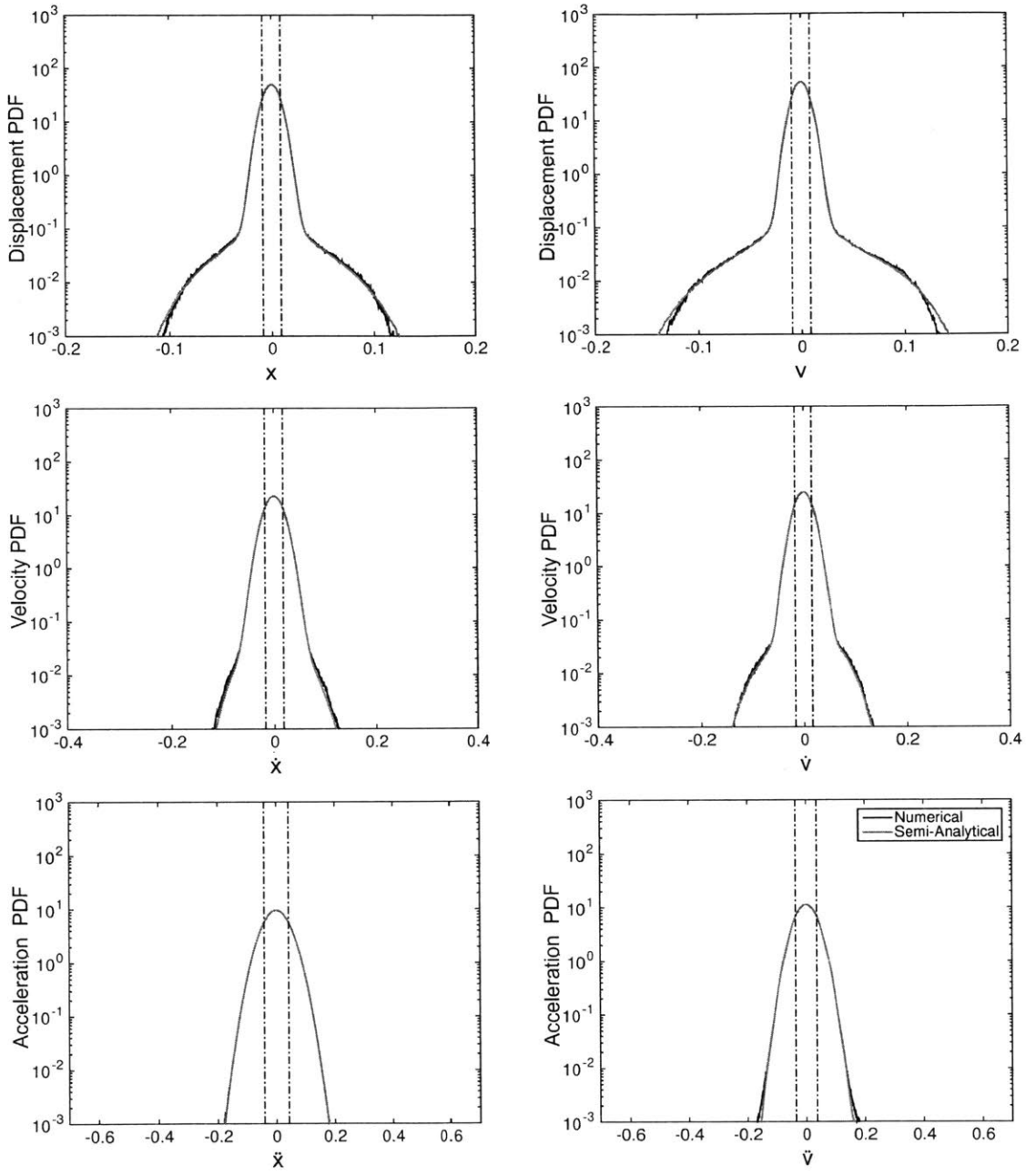

Figure 5-13: [Two DOF System 3] Comparison between direct Monte-Carlo simulation and the semi-analytical approximation. The pdf for the value of the time series are presented. Dashed line indicates one standard deviation. Parameters and statistical quantities are summarized in table 5.8.

5.6 Semi-analytical Quantification of Peak PDFs for Intermittently Forced MDOF Prototype System

In previous sections, we have formulated the semi-analytical approach for quantifying response pdfs for MDOF linear systems under stochastic excitations containing rare events. One important extension of semi-analytical scheme is the quantification of local extrema distribution. The local extrema distributions of stochastic responses play the critical role in fatigue and reliability analysis problems. In this section, we briefly introduce how the semi-analytical scheme for response pdf quantification can be easily extended to estimate local extrema distributions. We then demonstrate the semi-analytical quantification of local extrema distributions for single-degree-of-freedom system as well as two-degree-of-freedom system, and the results will be compared with Monte-Carlo simulations. We first quantify of background local extrema statistics and then the rare event statistics and lastly show comparisons with numerical results.

5.6.1 Background Peak PDF Quantification

For the gaussian process with arbitrary spectral bandwidth ϵ, the probability density function of positive maxima can be described as follows [110, 71]:

$$f_{m^+}(\zeta) = \frac{\epsilon}{\sqrt{2\pi}} e^{-\zeta^2/2\epsilon^2} + \sqrt{1-\epsilon^2}\zeta e^{-\zeta^2/2}\Phi\left(\frac{\sqrt{1-\epsilon^2}}{\epsilon}\zeta\right), \qquad -\infty \leq \zeta \leq \infty, \quad (5.101)$$

where $\zeta = \frac{x}{\sqrt{m_0}}$, x is the magnitude of the maxima, spectral bandwidth $\epsilon = \sqrt{1 - \frac{m_2^2}{m_0 m_4}}$, and $\Phi(\cdot)$ is the standard normal cumulative distribution function.

$$\Phi(x) = \frac{1}{\sqrt{2\pi}} \int_{-\infty}^{x} e^{-u^2/2} du. \quad (5.102)$$

Spectral moments for the background response displacement x_b are given as

$$m_0 = \int_0^\infty S_{x_b x_b}(\omega) d\omega, \tag{5.103}$$

$$m_2 = \int_0^\infty \omega^2 S_{x_b x_b}(\omega) d\omega, \tag{5.104}$$

$$m_4 = \int_0^\infty \omega^4 S_{x_b x_b}(\omega) d\omega, \tag{5.105}$$

where $S_{x_b x_b}(\omega)$ is the one-sided spectral density function of the background response displacement. In the above we can observe that for an infinitely narrow-banded signal ($\epsilon = 0$), the pdf becomes Rayleigh distribution. On the other hand for an infinitely broad-banded signal ($\epsilon = 1$), the distribution converges to the Gaussian pdf. For a signal with in-between spectral bandwidth ($0 \leq \epsilon \leq 1$), the pdf has a complex structure with the form in equation (5.101). Those cases are illustrated in figure 5-14. Considering the asymmetric structure of the response under intermittent forcing, we focus on the positive and negative maxima of the background response, and the pdf can be written as follows:

$$f_{\hat{x}_b}(x) = \frac{1}{2\sqrt{m_0}} \left\{ f_{m^+}\left(\frac{x}{m_0}\right) + f_{m^+}\left(-\frac{x}{m_0}\right) \right\}, \qquad -\infty \leq x \leq \infty. \tag{5.106}$$

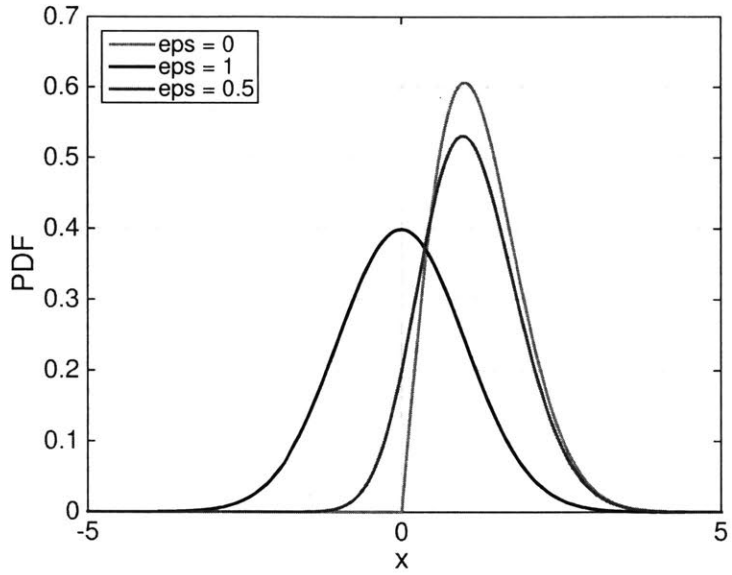

Figure 5-14: The probability density function of positive maxima with three different spectral bandwidth ($\epsilon = 0$, $\epsilon = 1$, $\epsilon = 0.5$).

5.6.2 Numerical Histogram of Peaks within Rare Events

Previously we have quantified response pdfs by the PDS method using the total probability law, and the same approach applies for the quantification of local extrema (positive/negative maxima) distributions.

$$f_{\hat{x}}(r) = f_{\hat{x}_b}(r)(1 - \mathbb{P}_r) + f_{\hat{x}_r}(r)\mathbb{P}_r. \tag{5.107}$$

where $f_{\hat{x}_b}(r)$ is the background local extrema distribution, $f_{\hat{x}_r}(r)$ is the rare event local extrema distribution, $\mathbb{P}_s$ is the background probability, and $\mathbb{P}_r$ is the rare event probability. The rare event local extrema distribution can be decomposed into the conditional rare event local extrema distribution under the given impulse magnitude $\eta = n$.

$$f_{\hat{x}_r}(r) = \int f_{\hat{x}_r|\eta}(r \mid n) f_\eta(n)\, dn, \tag{5.108}$$

where $f_\eta(n)$ is known analytically (section 5.3.2). Now we quantify the conditional local extrema pdf $f_{\hat{x}_r|\eta}(r \mid n)$ by a histogram:

$$f_{\hat{x}_r|\eta}(r \mid n) = \text{Hist}\Big\{\mathcal{M}\left(x_{r|\eta}(t \mid n)\right)\Big\}, \quad t = [0, \tau_{e,\text{dis}}], \tag{5.109}$$

where $\mathcal{M}(\cdot)$ is an operator which finds all the positive/negative maxima. The positive/negative maxima are defined as where its derivative becomes zero. For a given impulse magnitude $\eta = n$, it finds all the positive/negative maxima between $t \in [0, \tau_{e,dis}]$.

5.6.3 Semi-analytical Probability Density Function

With the description above, we can obtain the desired positive/negative maxima pdfs and the final semi-analytical results. Note that all the quantities (i.e. probability of rare event $\mathbb{P}_r$ and rare event time duration τ_e) stay the same as in the response pdf cases. The only modifications are i) background peak pdf $f_{\hat{x}_b}(r)$, and ii) numerical histogram of positive/negative maxima of the impulse response. In below, we show the full semi-analytical expression of local extrema pdfs for single-degree-of-freedom case.

Displacement

$$f_{\hat{x}}(r) = (1 - \nu_\alpha \tau_{e,\text{dis}})\, f_{\hat{x}_b}(r) + \nu_\alpha \tau_{e,\text{dis}} \int_0^\infty \text{Hist}\Big\{\mathcal{M}\left(x_{r|\eta}(t \mid n)\right)\Big\} f_\eta(n)\, dn. \tag{5.110}$$

Velocity

$$f_{\hat{\dot{x}}}(r) = (1 - \nu_\alpha \tau_{e,\text{vel}})\, f_{\hat{\dot{x}}_b}(r) + \nu_\alpha \tau_{e,\text{vel}} \int_0^\infty \text{Hist}\Big\{\mathcal{M}\left(\dot{x}_{r|\eta}(t \mid n)\right)\Big\} f_\eta(n)\, dn. \tag{5.111}$$

Acceleration

$$f_{\hat{\ddot{x}}}(r) = (1 - \nu_\alpha \tau_{e,\text{acc}})\, f_{\hat{\ddot{x}}_b}(r) + \nu_\alpha \tau_{e,\text{acc}} \int_0^\infty \text{Hist}\Big\{\mathcal{M}\left(\ddot{x}_{r|\eta}(t \mid n)\right)\Big\} f_\eta(n)\, dn. \tag{5.112}$$

In the case of multi-degree-of-freedom systems, we can follow the same steps to obtain the full semi-analytical expressions. In below we summarize the expressions for TDOF

system.

Displacements

$$f_{\hat{x}}(r) = \left(1 - \nu_\alpha \tau^x_{e,\text{dis}}\right) f_{\hat{x}_b}(r) + \nu_\alpha \tau^x_{e,\text{dis}} \int_0^\infty \text{Hist}\Big\{\mathcal{M}\left(x_{r|\eta}(t \mid n)\right)\Big\} f_\eta(n)\, dn, \quad (5.113)$$

$$f_{\hat{v}}(r) = \left(1 - \nu_\alpha \tau^v_{e,\text{dis}}\right) f_{\hat{v}_b}(r) + \nu_\alpha \tau^v_{e,\text{dis}} \int_0^\infty \text{Hist}\Big\{\mathcal{M}\left(v_{r|\eta}(t \mid n)\right)\Big\} f_\eta(n)\, dn. \quad (5.114)$$

Velocities

$$f_{\hat{\dot{x}}}(r) = \left(1 - \nu_\alpha \tau^x_{e,\text{vel}}\right) f_{\hat{\dot{x}}_b}(r) + \nu_\alpha \tau^x_{e,\text{vel}} \int_0^\infty \text{Hist}\Big\{\mathcal{M}\left(\dot{x}_{r|\eta}(t \mid n)\right)\Big\} f_\eta(n)\, dn, \quad (5.115)$$

$$f_{\hat{\dot{v}}}(r) = \left(1 - \nu_\alpha \tau^v_{e,\text{vel}}\right) f_{\hat{\dot{v}}_b}(r) + \nu_\alpha \tau^v_{e,\text{vel}} \int_0^\infty \text{Hist}\Big\{\mathcal{M}\left(\dot{v}_{r|\eta}(t \mid n)\right)\Big\} f_\eta(n)\, dn. \quad (5.116)$$

Accelerations

$$f_{\hat{\ddot{x}}}(r) = \left(1 - \nu_\alpha \tau^x_{e,\text{acc}}\right) f_{\hat{\ddot{x}}_b}(r) + \nu_\alpha \tau^x_{e,\text{acc}} \int_0^\infty \text{Hist}\Big\{\mathcal{M}\left(\ddot{x}_{r|\eta}(t \mid n)\right)\Big\} f_\eta(n)\, dn, \quad (5.117)$$

$$f_{\hat{\ddot{v}}}(r) = \left(1 - \nu_\alpha \tau^x_{e,\text{acc}}\right) f_{\hat{\ddot{v}}_b}(r) + \nu_\alpha \tau^v_{e,\text{acc}} \int_0^\infty \text{Hist}\Big\{\mathcal{M}\left(\ddot{v}_{r|\eta}(t \mid n)\right)\Big\} f_\eta(n)\, dn. \quad (5.118)$$

5.6.3.1 Comparisons with Monte-Carlo Simulations

We compare the derived schemes for the local extrema distribution quantification for the single-degree-of-freedom system and the two-degree-of-freedom system with Monte-Carlo simulations. Details regarding the Monte-Carlos simulations are the same as described in section 5.3.6.1 except 100 realizations with 100 impulses are utilized. For illustration, results are shown for SDOF 3, SDOF 4 and TDOF 1, and local extrema pdfs for the displacements, velocities and accelerations are compared. Note that the relevant statistical quantities do not change, and one can refer table 5.3, table 5.4 and table 5.6, respectively. The results of the comparison demonstrate the accuracy of the proposed semi-analytical method, and agree closely with the numerical simulations in all the presented cases. Throughout the comparison the semi-analytical scheme demonstrates accurate estimation of heavy tail trends, and the non-Gaussian/non-Rayleigh structure of background peak distribution has been also captured properly.

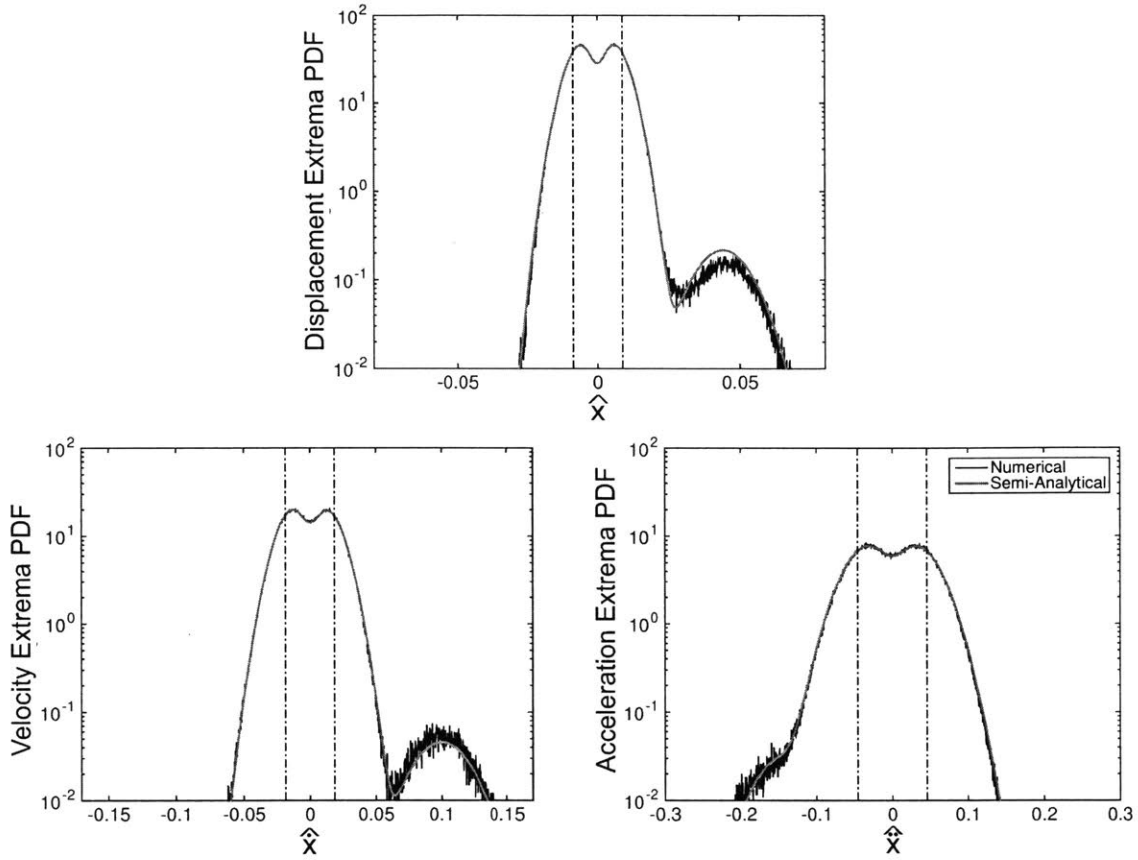

Figure 5-15: [Local extrema for SDOF 3] Comparison between direct Monte-Carlo simulation and the semi-analytical approximation. The pdf for the local extrema of the response are presented. Dashed line indicates one standard deviation.

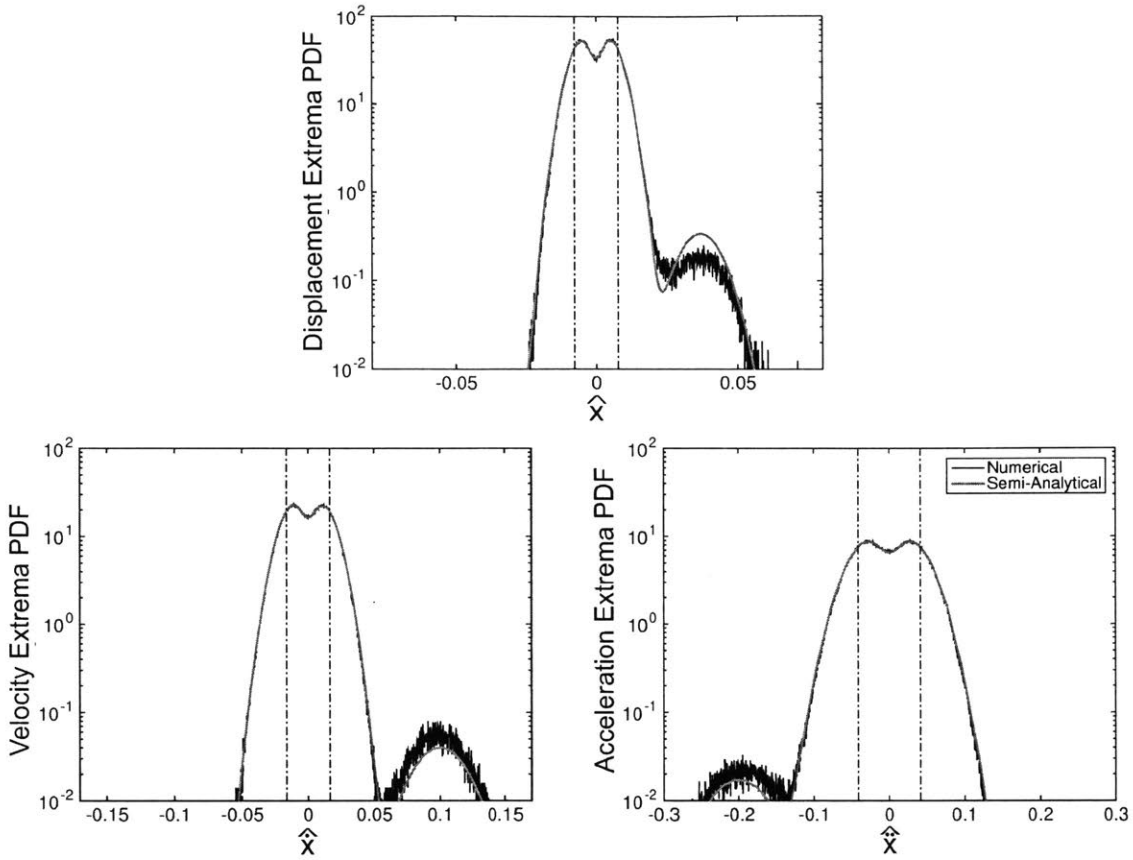

Figure 5-16: [Local extrema for SDOF 4] Comparison between direct Monte-Carlo simulation and the semi-analytical approximation. The pdf for the local extrema of the response are presented. Dashed line indicates one standard deviation.

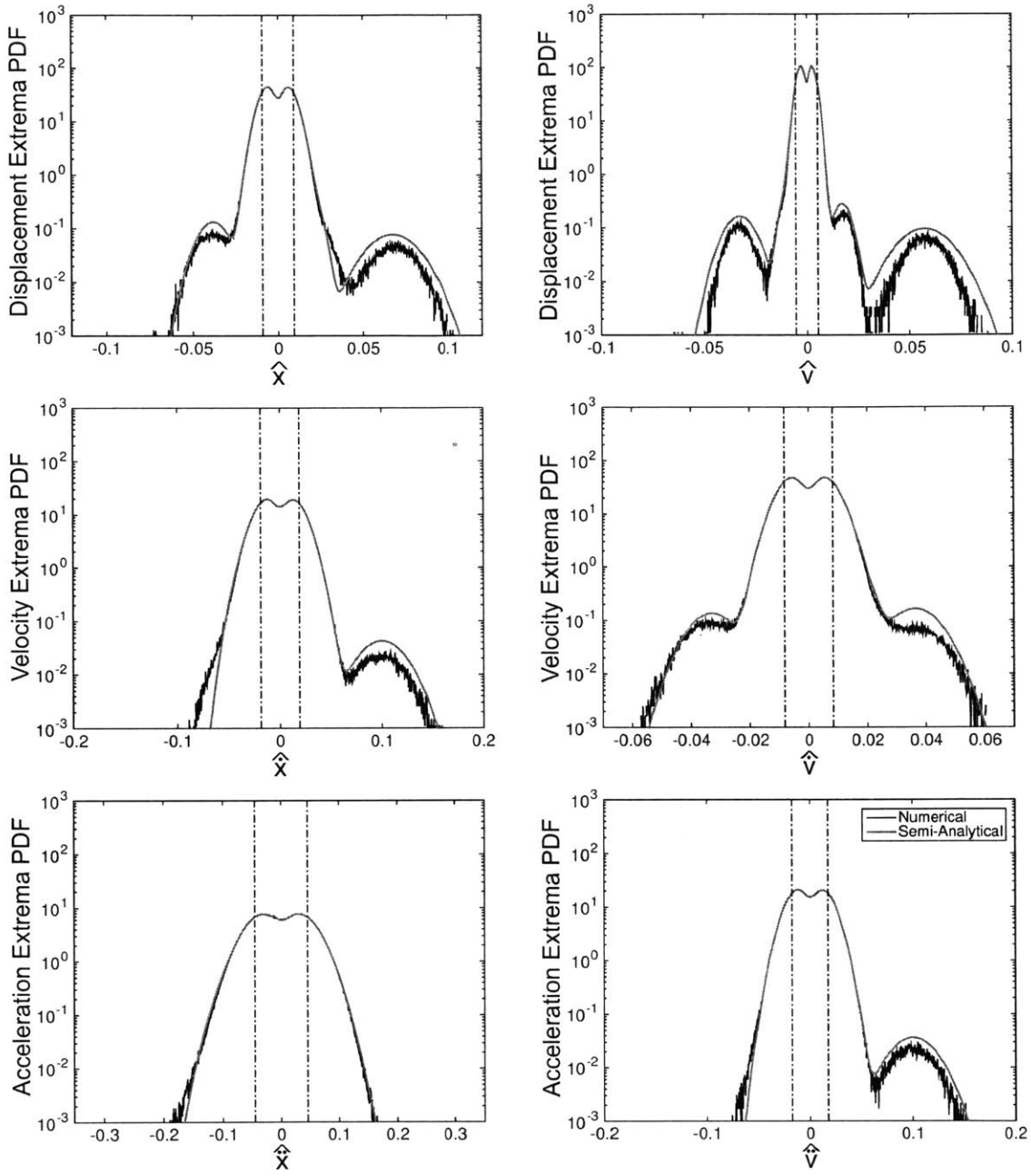

Figure 5-17: [Local extrema for TDOF 1] Comparison between direct Monte-Carlo simulation and the semi-analytical approximation. The pdf for the local extrema of the response are presented. Dashed line indicates one standard deviation.

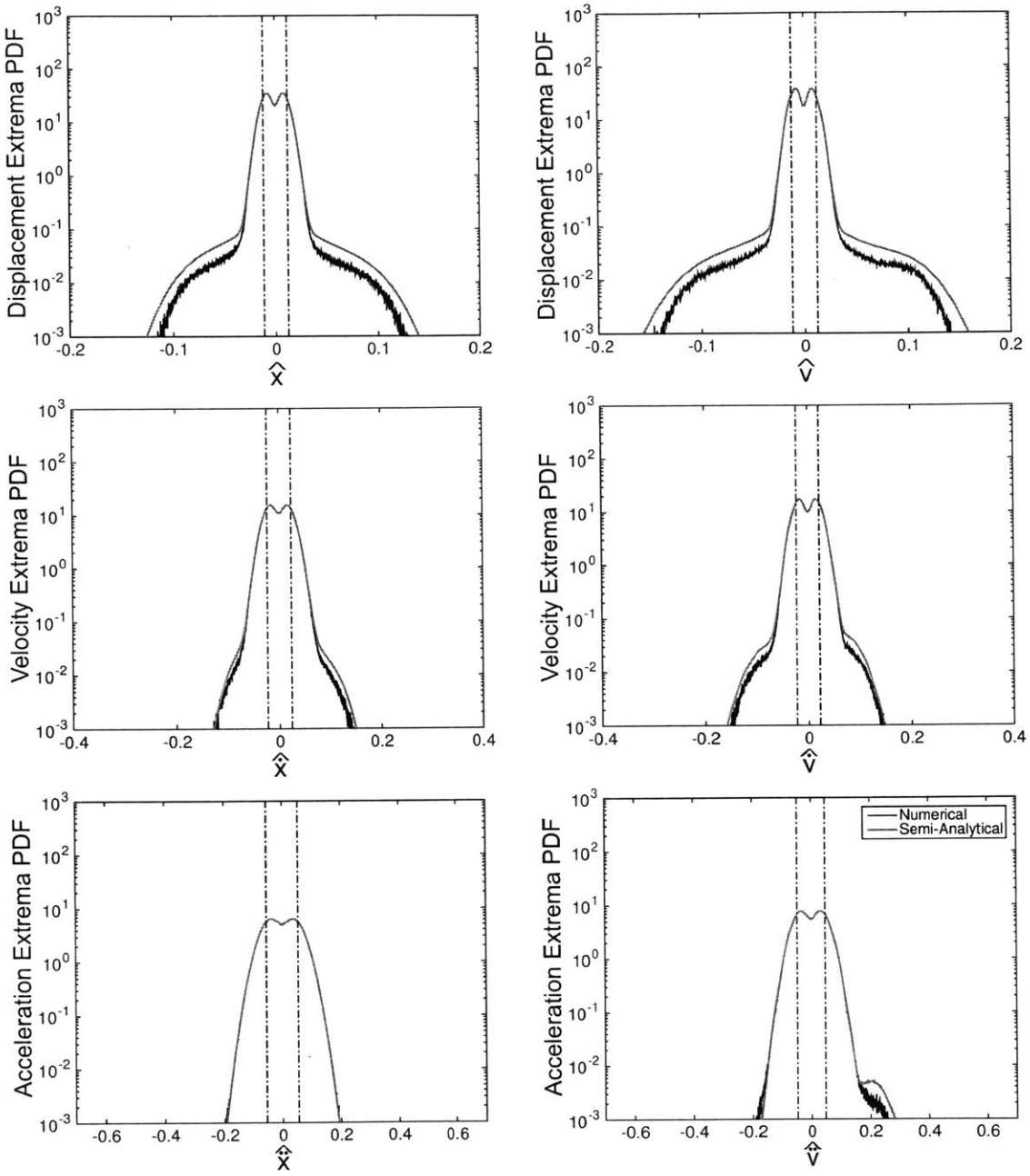

Figure 5-18: [Local extrema for TDOF 3] Comparison between direct Monte-Carlo simulation and the semi-analytical approximation. The pdf for the local extrema of the response are presented. Dashed line indicates one standard deviation.

5.7 Summary

We have formulated a robust approximation method to quantify the probabilistic response of structural systems subjected to stochastic excitation containing intermittent components. The foundation of our approach is the recently developed probabilistic decomposition-synthesis method for the quantification of rare events due to internal instabilities to the problem where extreme responses are triggered by external forcing. The intermittent forcing is represented as a background component, modeled through a colored processes with energy distributed across a range of frequencies, and additionally a rare/extreme component that can be represented by impulses that are Poisson distributed with large inter-arrival time. Owing to the nature of the forcing, even the probabilistic response of a linear system can be highly complex with asymmetry and complicated tail behavior that is far from Gaussian, which is the expected form of the response pdf if the forcing did not contain an intermittently extreme component.

Table 5.9: Summary of the of developed analytical/semi-analytical response pdfs.

DOF	Damping ratio ζ	Analytical scheme	Semi-analytical scheme
SDOF	$\zeta \ll 1$	section 5.3 (5.3.6)	section 5.4
	$\zeta < 1$	—	
	$\zeta = 1$		
	$\zeta > 1$		
	$\zeta \gg 1$	section 5.3 (5.3.7)	
MDOF	—	—	section 5.5

The main result of this work is the derivation of analytical/semi-analytical expressions for the pdf of the response and its local extrema for structural systems (including the response displacement, velocity, and acceleration pdf). These expressions decompose the pdf into a probabilistic core, capturing the statistics under background excitation, as well as a heavy tail component associated with the extreme transitions resulting by the rare impacts. We have performed a thorough analysis for linear SDOF sys-

tems under various system parameters and also derived analytical formulas for two special cases of parameters (lightly damped or heavily damped systems). The general semi-analytical decomposition is applicable for any arbitrary set of system parameters and we have demonstrated its validity through comprehensive comparisons with Monte-Carlo simulations. The general framework is also directly applicable to MDOF systems, as well as systems with nonlinearities and we have assessed its performance through a 2DOF linear system of two coupled oscillators excited through the first mass. Modifications of the method to compute statistics of local extrema have also been presented. The derived methodologies are summarized in table 5.9. We emphasize that the developed approach allows for computation of the response pdf of structural systems many orders of magnitude faster than a direct Monte-Carlo simulation, which is currently the only reliable tool for such computations.

Chapter 6

Extreme events and their optimal mitigation in nonlinear structural systems excited by stochastic loads

6.1 Introduction

For a plethora of structural systems it is essential to specify their reliability under uncertain environmental loading conditions and most importantly provide design guidelines using knowledge of their response characteristics. This involves accurate estimation of the structural systems probabilistic response. Environmental loads are typically random by nature and are likely to include intermittently occurring components of an extreme magnitude, representing abnormal environmental events or conditions. Although extreme loadings occur with lower probability than typical conditions, their impact is significant and cannot be neglected since these events determine the systems behavior away from the average operating conditions, which are precisely the conditions that are important to quantify for safe assessment and design. Important examples include mechanical and ocean engineering systems. High speed crafts in rough seas [120, 119], wave impacts on fixed or floating offshore platforms and ship capsize events [104, 13, 105, 91, 84], vibrations of buildings or bridge structures due

to earthquakes or strong wind excitations [87, 20, 89, 142] are just a few examples where extreme responses occur infrequently but are critical in determining the overall systems reliability.

Numerous research endeavors have been dedicated on the effective suppression and rapid dissipation of the energy associated with extreme impacts on structures. Many of these schemes rely on linear configurations, known as tuned mass damper (TMD) and result in a halving of the resonance frequency. Although the mitigation performance is highly effective when most of the energy is concentrated at the characteristic frequency of the system, their effectiveness drastically drops if there is a mistuning in frequency. Moreover, it is not clear how these configurations perform in the presence of rare impulsive loads. Many of these limitations can be overcome by utilizing small attachments coupled with the primary system through nonlinear springs, also known as nonlinear energy sinks (NES). If carefully chosen these nonlinear attachments can lead to robust, irreversible energy transfer from the primary structure to the attachment and dissipation there [146, 147]. The key mechanism behind the efficient energy dissipation in this case is the targeted energy transfer phenomenon which is an essentially nonlinear mechanism and relies primarily on the energy level of the system, rather then the resonant frequency [148, 75]. Such configurations have been proven to be successful on the mitigation of deterministic impulsive loads on large structures [134, 135, 93] and their performance has been measured through effective nonlinear measures such as effective damping and stiffness [127, 115].

Despite their success, nonlinear configurations have been primarily developed for deterministic impulsive loads. To quantify and optimize their performance in the realistic settings mentioned previously it is essential to understand their effects on the statistics of the response and in particular in the heavy tails of the probability distribution function (PDF). However, quantifying the PDF of nonlinear structures under random forcing containing impulsive-type extreme events, poses many challenges for traditional methods. Well established approaches for determining the statistics of

nonlinear dynamical systems include the Fokker-Planck equation [140, 136], the joint response-excitation method [126, 153, 69, 5], Gaussian closure schemes, moment equation or cumulant closure methods [15, 157], the Polynomial-Chaos approach [159], and stochastic averaging methods [161]. For systems associated with heavy tails, however, these methods either cannot capture the statistics of rare and extreme type events due to inherent limitations [94] or are far too computationally expensive in practice, even for low-dimensional systems [100, 40]. Alternatively, one can study the statistics of the extreme events alone (by ignoring the background 'non-extreme' forcing fluctuations) through a Poisson process representation and then analyze the response using the generalized Fokker-Planck or Kolmogorov-Feller equations [136], which governs the evolution of the corresponding PDF, or by applying the path integral formalism [82, 65], or even through special stochastic averaging techniques [160]. While attractive, these ideas lead, in general, to analytical results for a very limited number of special cases. Besides, it is still an important aspect to account for the background random fluctuations in the forcing term in order to fully characterize the systems overall probabilistic properties (e.g. this is important in order to fully determine all the moments of the response). Moreover, even though the background forcing component does not directly correspond to extreme events, the background term may have important consequences for the initiation of intermittent type extreme responses [102].

In this work we consider the problem of nonlinear structural systems under general time-correlated stochastic forcing that includes extreme, impulsive type random events. We address two important challenges related to this problem. The first is the development of a fast and accurate estimation method for the response statistics, expressed through the PDF, with emphasis on the accurate estimation of the tail form (events far away from the mean). The second is the design and parameter optimization of small attachments that can mitigate or suppress the effects of the extreme forcing events on the system response while they also improve the system behavior during the regular regime. The two problems are connected since extreme event suppression is directly reliant upon a fast and accurate estimation method for the response pdf

under different designs or parameters. Indeed, without a fast and reliable method to evaluate response statistics, in particular tail statistics, optimization cannot be performed because of the inherent computational cost associated with typical quantification methods such as Monte-Carlo. This aspect highlights the practical utility of the proposed fast PDF estimation scheme. We will illustrate the pdf estimation method and shock mitigation design analysis throughout the manuscript with a practical motivating prototype system related to high speed vehicle motion in rough seas, however we emphasize the proposed method broad applicability.

The probabilistic quantification scheme formulated here is based on the most general probabilistic decomposition-synthesis framework [102, 103], that has recently been applied in linear systems subjected to stochastic forcing containing extreme events [68] and can be used to efficiently estimate the PDF for the response displacement, velocity, and acceleration. We begin by formulating the response pdf quantification method (developed for linear multi-degree-of-freedom (MDOF) systems in [68]) for the case of nonlinear MDOF systems. This is achieved by combining the probabilistic decomposition-synthesis framework [102, 103] with the statistical linearization method [122]. The scheme circumvents the rare-event problem and enables rapid design and optimization in the presence of extreme events. We emphasize the statistical accuracy of the derived scheme, which we have validated through extensive comparisons with direct Monte-Carlo simulations. Next, we consider two prototype ocean engineering systems and perform a quantitative comparison of the performance of TMD and NES, evaluating their effectiveness at shock suppression under stochastic excitation containing extreme events. Finally, we perform optimization on a very generic, possibly asymmetric family of piecewise linear springs. Previous endeavors in the context of single-sided vibro-impact NES have shown that asymmetries in the NES can improve the shock mitigation properties (see [135]). In agreement with these results, our optimization scheme leads to the derivation of a new asymmetric NES which significantly improves the shock mitigation properties of the system in the realistic setting of stochastic excitation.

The chapter is structured as follows. In section 6.2 we describe the prototype models for high speed craft motion that we utilize throughout the work as practically relevant example. Next, in section 6.3 we provide a brief review of the probabilistic decomposition-synthesis (PDS) framework for the response pdf quantification of a linear single-degree-of-freedom system subject to a random forcing term containing extreme impulse type events. Section 6.4 describes the proposed general semi-analytical PDF estimation method for nonlinear MDOF structures and also includes a section on quantifying the conditionally rare response via the effective stiffness and damping framework. In section 6.5 we present the mitigation of extreme events analysis on the prototype high speed craft designs for both TMD and cubic NES attachments. Next, in section 6.6 we propose a new piecewise linear and asymmetric NES design that we optimize for extreme event mitigation. Finally in section 6.7 we offer concluding remarks.

6.2 Prototype models for high speed vehicle motion in rough seas

Here we describe the prototype models that we apply the quantification method for extreme event analysis and optimization. Specifically, we model the motion of a high-speed craft in random seas through two prototype systems: one being a two-degree-of-freedom system consisting of a suspended seat attached to the hull and the second being a three-degree-of-freedom system where the seat is attached to a suspended deck, which is attached on the hull; both prototypes contain a small linear or nonlinear energy sink (NES) vibration absorber.

6.2.1 2DOF Suspended seat system

In figure 6-1 we illustrate the first model consisting of a linear primary structure under base excitation that is attached to a small oscillator connected through a nonlinear spring (with cubic nonlinearity). This is a prototype system modeling the suspended seat of a high speed craft [111, 28]. The vibration absorber is attached to the seat with the aim to minimize ocean wave impacts on the operator of the vehicle and naturally we require that the attachment mass is much lower than the seat mass (i.e. $m_a < 0.1m_s$). The equation of motion for this two-degree-of-freedom system is given by:

$$m_s\ddot{x} + \lambda_s\dot{x} + k_s x + \lambda_a(\dot{x} - \dot{v}) + k_a(x - v) + c_a(x - v)^3 = -m_s\ddot{\xi}(t), \tag{6.1}$$

$$m_a\ddot{v} + \lambda_a(\dot{v} - \dot{x}) + k_a(v - x) + c_a(v - x)^3 = -m_a\ddot{\xi}(t), \tag{6.2}$$

where x, v are the relative displacements of the seat response and attachment response, respectively, with reference to the base motion $\xi(t)$ (that is, $x = \hat{x} - \xi$ and $v = \hat{v} - \xi$).

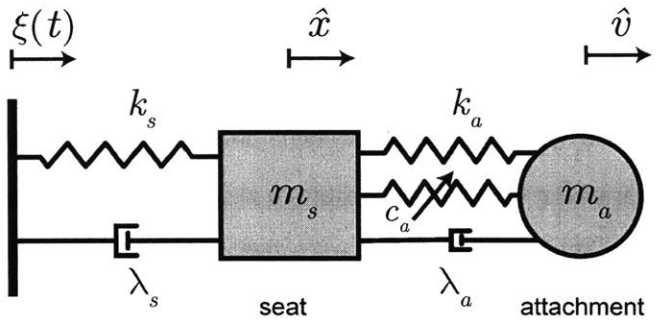

Figure 6-1: [**Suspended seat**] Mechanical model for the suspended seat problem with a small attachment (vibration absorber).

6.2.2 3DOF Suspended deck-seat system

The second prototype system is a suspended deck design for a high speed craft [145, 116, 78] and is illustrated in figure 6-2. In this case, the vibration absorber is attached to the suspended deck. The attachment mass is comparable to the seat mass and both are considerably smaller than the deck (i.e. $m_a \simeq m_s < 0.1m_h$). The governing equations for this three-degree-of-freedom system are given by:

$$m_h\ddot{y} + \lambda_h\dot{y} + k_h y + \lambda_s(\dot{y} - \dot{x}) + k_s(y - x) + \lambda_a(\dot{y} - \dot{v}) + k_a(y - v) + c_a(y - v)^3 = -m_h\ddot{\xi}(t) \quad (6.3)$$

$$m_s\ddot{x} + \lambda_s(\dot{x} - \dot{y}) + k_s(x - y) = -m_s\ddot{\xi}(t) \quad (6.4)$$

$$m_a\ddot{v} + \lambda_a(\dot{v} - \dot{y}) + k_a(v - y) + c_a(v - y)^3 = -m_a\ddot{\xi}(t), \quad (6.5)$$

where, again, x, y, v are the relative displacements of the seat response, the deck response and the attachment response, respectively, with reference to the base motion $\xi(t)$.

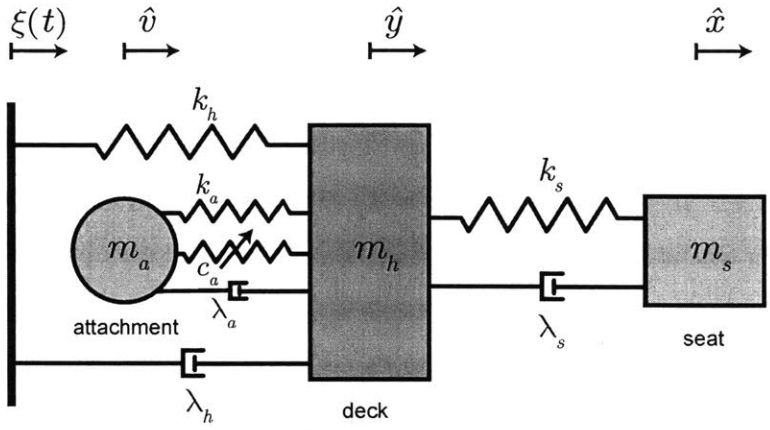

Figure 6-2: [**Suspended deck-seat**] Mechanical model for the suspended deck-seat problem with a small attachment (vibration absorber).

In both prototypes the aim of the vibration mitigating attachment is to minimize extreme impacts on the seat attachment as this represents an operator on the vehicle. We first examine the case of tuned-mass damper vibration absorber $k_a \neq 0, c_a = 0$ and the essentially nonlinear energy sink absorber $k_a = 0, c_a \neq 0$, that has been studied extensively in the context of shock mitigation [147]. In the last section we will examine the performance of an asymmetric, piecewise linear, spring.

6.2.3 The structure of the intermittently extreme stochastic forcing

Motivated by the ocean engineering systems in section 6.2, we consider base motion of the form,

$$\ddot{\xi}(t) = \ddot{h}(t) + \sum_{i=1}^{N(t)} \alpha_i \, \delta(t - \tau_i), \quad 0 < t \leq T, \tag{6.6}$$

In the expression above, $h(t)$ denotes a zero-mean smooth motion characterized by a Pierson-Moskowitz spectrum,

$$S_{hh}(\omega) = q \frac{1}{\omega^5} \exp\left(-\frac{1}{\omega^4}\right), \tag{6.7}$$

where q controls the magnitude of the motion. The second term in equation (6.6) describes rare and extreme impulses in terms of a random impulse train ($\delta(\,\cdot\,)$ is

a unit impulse), occurring due to slamming events. For this component, $N(t)$ is a Poisson counting process that represents the number of impulses that arrive in the time interval $0 < t \leq T$, α is the impulse magnitude, which we assume is normally distributed with mean μ_α and variance σ_α^2, and the constant arrival rate is given by ν_r. We take the impulse magnitude as being β-times larger than the standard deviation of the excitation velocity $\dot{h}(t)$: $\mu_\alpha = \beta\ \sigma_{\dot{h}}$, with $\beta\ > 1$.

6.3 Review of the probabilistic decomposition-synthesis (PDS) method

We first provide a brief review of the semi-analytical response quantification method for a linear single-degree-of-freedom system [68] subjected to stochastic excitation containing rare events. The purpose of this section is to provide a self-contained review of the core ideas, since the scheme for nonlinear structural systems that is described in the following section depends upon these concepts. Interested readers should first read chapter 5 where we discuss the semi-analytical response quantification method with full details.

Consider the following linear system

$$\ddot{x} + \lambda\dot{x} + kx = \ddot{\xi}(t), \tag{6.8}$$

k is the stiffness, λ is the damping, and $\zeta = \lambda/2\sqrt{k}$ is the damping ratio. Despite the simplicity of this system, the structure of the statistical response may be significantly complex and posses heavy-tails.

The framework to estimate the response PDF of equation (6.8) is the probabilistic decomposition-synthesis (PDS) method [102]. The basic idea is to decouple the rare events regime from the background fluctuations and then quantify the statistics of the two components separately. The results are then synthesized to obtain the full response PDF by using the total probability law:

$$f_x(r) = f_{x_b}(r)(1 - \mathbb{P}_r) + f_{x_r}(r)\mathbb{P}_r, \tag{6.9}$$

where $f_{x_b}(r)$ is the conditional PDF due to the smooth motion of the base, $f_{x_r}(r)$ is the conditional PDF due to the extreme impacts and $\mathbb{P}_r$ is the overall probability that the system operates in the extreme events regime.

6.3.1 Background response PDF

We first obtain the statistical response of the system under the condition that only the background (smooth) forcing component is acting. We have,

$$\ddot{x}_b + \lambda \dot{x}_b + k x_b = \ddot{h}(t). \tag{6.10}$$

In this case the analysis is particularly simple since the system is linear and time-invariant and the response PDF, f_{x_b}, is a zero-mean Gaussian. The spectral density of the response displacement and the variance are given by:

$$S_{x_b x_b}(\omega) = \frac{\omega^4 S_{hh}(\omega)}{\left(k - \omega^2\right)^2 + (\lambda\omega)^2}, \quad \sigma_{x_b}^2 = \int_0^\infty S_{x_b x_b}(\omega)\, d\omega. \tag{6.11}$$

The computations for the response velocity and acceleration can be similarly obtained.

6.3.2 Numerical histogram for rare events

The next step is to compute the rare event distribution f_{x_r} and the rare event probability $\mathbb{P}_r$. Specifically, the rare event distribution can be written as,

$$f_{x_r}(r) = \int f_{x_r|\eta}(r \mid n) f_\eta(n)\, dn, \tag{6.12}$$

where $f_\eta(n)$ is the distribution of the impulse magnitude, and $f_{x_r|\eta}$ is the conditional PDF of the response for an impact of magnitude η.

It is important to note that once an impulse of magnitude α hits the system, the momentum of the system right after the impact would be $\dot{x}_b + \alpha$, since the momentum of the system right before the impact is $\dot{x}_b$. As these two variables are both Gaussian distributed and independent, their sum is also Gaussian distributed and is given by,

$$\eta \equiv \dot{x}_b + \alpha \sim \mathcal{N}(\mu_\alpha,\, \sigma_{\dot{x}_b}^2 + \sigma_\alpha^2). \tag{6.13}$$

We estimate the conditional PDF $f_{x_r|\eta}(r \mid n)$ by the numerically computed histogram:

$$f_{x_r|\eta}(r \mid n) = \text{Hist}\Big\{x_{r|\eta}(t \mid n)\Big\}, \quad t \in [0, \tau_e], \tag{6.14}$$

where τ_e is the typical duration of the rare event (see next subsection) and the conditional response $x_{r|\eta}$ is given by,

$$x_{r|\eta}(t \mid n) = \frac{n}{2\omega_o}\left(\mathrm{e}^{-(\zeta\omega_n - \omega_o)t} - \mathrm{e}^{-(\zeta\omega_n + \omega_o)t}\right). \tag{6.15}$$

The conditionally extreme event distribution for velocity and acceleration are derived in a similar fashion.

6.3.3 Numerical estimation of the rare event probability

In order to compute the histogram of a rare impulse event, the duration of a rare response needs to be obtained numerically. We define the typical duration of a rare response by

$$x_r(\tau_e) = \rho_c \max\Big\{|x_r|\Big\}, \tag{6.16}$$

where $\rho_c = 0.1$, or in other words, the histogram is taken over the time it takes for the system response to decay to 10% of its maximum value. The absolute value of the maximum of the response needs to be estimated numerically.

Once this rare event duration has been specified, we can also obtain the probability of a rare event by

$$\mathbb{P}_r = \nu_\alpha \tau_e = \tau_e / T_\alpha. \tag{6.17}$$

Note that the extreme event duration for the displacement τ_e^x, velocity $\tau_e^{\dot{x}}$, and acceleration $\tau_e^{\ddot{x}}$ are in generally different.

6.3.4 Semi-analytical response probability distributions

With the description above, we obtain the response PDF using the total probability law. The resulting response PDF takes the form,

$$f_z(r) = \frac{1 - \nu_\alpha \tau_e^z}{\sigma_{z_b}\sqrt{2\pi}} \exp\left(-\frac{r^2}{2\sigma_{z_b}^2}\right) + \nu_\alpha \tau_e^z \int_0^\infty \text{Hist}\Big\{z_{r|\eta}(t \mid n)\Big\} f_\eta(n)\, dn, \tag{6.18}$$

where the argument z is either x, $\dot{x}$, or $\ddot{x}$. The validity of this approximation has been thoroughly verified in [68].

6.4 PDF quantification method for nonlinear MDOF systems

Here we formulate the probabilistic-decomposition method for multi-degree-of-freedom, nonlinear mechanical systems. There are some important differences with respect to the case of linear systems studied in [68]. Firstly, for the background component the system nonlinearities can be important and to this end we must utilize an appropriate statistical quantification method. Here we employ the statistical linearization approach [124]. Secondly, to characterize the statistics in the rare event regime it is even more crucial to take into account the nonlinear properties of the system, since these control the shock mitigation capabilities of the attachment.

To achieve this we use two alternative approaches. The first one is based on the direct simulation of the system for a range of initial conditions corresponding to all possible impact magnitudes. The second is based on the notion of effective stiffness and damping [127], which are measures that characterize the system response under various excitation magnitudes taking into account the presence of the nonlinear attachment. We provide comparisons with direct Monte-Carlo simulations to demonstrate the accuracy of both approaches. We first present the analysis for the background component

6.4.1 Quantification of the response pdf for the background component

For the background regime, we must account for nonlinearities and their interaction with the background part of the excitation. We use the statistical linearization method, since we are only interested in resolving the low-order statistics of the background response of the system (the rare events component defines the tails of the PDF).

Consider the response of the suspended seat problem, equation (6.2), under the exci-

tation term $\ddot{h}(t)$:

$$m_s\ddot{x} + \lambda_s\dot{x} + k_s x + \lambda_a(\dot{x}-\dot{v}) + k_a(x-v) + c_a(x-v)^3 = -m_s\ddot{h}(t), \tag{6.19}$$

$$m_a\ddot{v} + \lambda_a(\dot{v}-\dot{x}) + k_a(v-x) + c_a(v-x)^3 = -m_a\ddot{h}(t). \tag{6.20}$$

We first multiply the above two equations by $x(s)$, $v(s)$, $h(s)$ at different time instant $s \neq t$, and take ensemble averages to write the resulting equations in terms of covariance functions.

$$m_s C''_{xx} + \lambda_s C'_{xx} + k_s C_{xx} + \lambda_a\left(C'_{xx} - C'_{vx}\right) + k_a\left(C_{xx} - C_{vx}\right) + c_a\overline{(x(t)-v(t))^3 x(s)} = -m_s C''_{hx}, \tag{6.21}$$

$$m_s C''_{xv} + \lambda_s C'_{xv} + k_s C_{xv} + \lambda_a\left(C'_{xv} - C'_{vv}\right) + k_a\left(C_{xv} - C_{vv}\right) + c_a\overline{(x(t)-v(t))^3 v(s)} = -m_s C''_{hv}, \tag{6.22}$$

$$m_s C''_{xh} + \lambda_s C'_{xh} + k_s C_{xh} + \lambda_a\left(C'_{xh} - C'_{vh}\right) + k_a\left(C_{xh} - C_{vh}\right) + c_a\overline{(x(t)-v(t))^3 h(s)} = -m_s C''_{hh}, \tag{6.23}$$

$$m_a C''_{vx} + \lambda_a\left(C'_{vx} - C'_{xx}\right) + k_a\left(C_{vx} - C_{xx}\right) + c_a\overline{(v(t)-x(t))^3 x(s)} = -m_a C''_{hx}, \tag{6.24}$$

$$m_a C''_{vv} + \lambda_a\left(C'_{vv} - C'_{xv}\right) + k_a\left(C_{vv} - C_{xv}\right) + c_a\overline{(v(t)-x(t))^3 v(s)} = -m_a C''_{hv}, \tag{6.25}$$

$$m_a C''_{vh} + \lambda_a\left(C'_{vh} - C'_{xh}\right) + k_a\left(C_{vh} - C_{xh}\right) + c_a\overline{(v(t)-x(t))^3 h(s)} = -m_a C''_{hh}. \tag{6.26}$$

Here $'$ indicates the partial differentiation with respect to the time difference $\tau = t - s$. We then apply Isserlis' theorem based on the Gaussian process approximation for

response to express the fourth-order moments in terms of second-order moments [63].

$$\overline{(x(t)-v(t))^3 x(s)} = \left(3\sigma_x^2 - 6\sigma_{xv} + 3\sigma_v^2\right) C_{xx} - \left(3\sigma_x^2 - 6\sigma_{xv} + 3\sigma_v^2\right) C_{vx}, \quad (6.27)$$

$$\overline{(x(t)-v(t))^3 v(s)} = \left(3\sigma_x^2 - 6\sigma_{xv} + 3\sigma_v^2\right) C_{xv} - \left(3\sigma_x^2 - 6\sigma_{xv} + 3\sigma_v^2\right) C_{vv}, \quad (6.28)$$

$$\overline{(x(t)-v(t))^3 h(s)} = \left(3\sigma_x^2 - 6\sigma_{xv} + 3\sigma_v^2\right) C_{xh} - \left(3\sigma_x^2 - 6\sigma_{xv} + 3\sigma_v^2\right) C_{vh}. \quad (6.29)$$

This leads to a set of linear equations in terms of the covariance functions. Thus, the Wiener-Khinchin theorem can be applied to write the equations in terms of the power spectrum, giving

$$S_{xx}(\omega;\sigma_x^2,\sigma_{xv},\sigma_v^2) = \frac{\left(m_s + m_a\frac{\mathcal{B}(\omega)}{\mathcal{C}(\omega)}\right)\left(m_s + m_a\frac{\mathcal{B}(-\omega)}{\mathcal{C}(-\omega)}\right)\omega^4}{\left(\mathcal{A}(\omega) - \frac{\mathcal{B}(\omega)^2}{\mathcal{C}(\omega)}\right)\left(\mathcal{A}(-\omega) - \frac{\mathcal{B}(-\omega)^2}{\mathcal{C}(-\omega)}\right)} S_{hh}(\omega), \quad (6.30)$$

$$S_{vv}(\omega;\sigma_x^2,\sigma_{xv},\sigma_v^2) = \frac{\left(m_s + m_a\frac{\mathcal{A}(\omega)}{\mathcal{B}(\omega)}\right)\left(m_s + m_a\frac{\mathcal{A}(-\omega)}{\mathcal{B}(-\omega)}\right)\omega^4}{\left(\frac{\mathcal{A}(\omega)\mathcal{C}(\omega)}{\mathcal{B}(\omega)} - \mathcal{B}(\omega)\right)\left(\frac{\mathcal{A}(-\omega)\mathcal{C}(-\omega)}{\mathcal{B}(-\omega)} - \mathcal{B}(-\omega)\right)} S_{hh}(\omega), \quad (6.31)$$

$$S_{xv}(\omega;\sigma_x^2,\sigma_{xv},\sigma_v^2) = \frac{\left(m_s + m_a\frac{\mathcal{B}(\omega)}{\mathcal{C}(\omega)}\right)\left(m_s + m_a\frac{\mathcal{A}(-\omega)}{\mathcal{B}(-\omega)}\right)\omega^4}{\left(\mathcal{A}(\omega) - \frac{\mathcal{B}(\omega)^2}{\mathcal{C}(\omega)}\right)\left(\frac{\mathcal{A}(-\omega)\mathcal{C}(-\omega)}{\mathcal{B}(-\omega)} - \mathcal{B}(-\omega)\right)} S_{hh}(\omega), \quad (6.32)$$

$$S_{xh}(\omega;\sigma_x^2,\sigma_{xv},\sigma_v^2) = \frac{\left(m_s + m_a\frac{\mathcal{B}(\omega)}{\mathcal{C}(\omega)}\right)\omega^2}{\left(\mathcal{A}(\omega) - \frac{\mathcal{B}(\omega)^2}{\mathcal{C}(\omega)}\right)} S_{hh}(\omega), \quad (6.33)$$

$$S_{vh}(\omega;\sigma_x^2,\sigma_{xv},\sigma_v^2) = \frac{\left(m_s + m_a\frac{\mathcal{A}(\omega)}{\mathcal{B}(\omega)}\right)\omega^2}{\left(\frac{\mathcal{A}(\omega)\mathcal{C}(\omega)}{\mathcal{B}(\omega)} - \mathcal{B}(\omega)\right)} S_{hh}(\omega), \quad (6.34)$$

where,

$$\mathcal{A}(\omega;\sigma_x^2,\sigma_{xv},\sigma_v^2) = -m_s\omega^2 + (\lambda_s + \lambda_a)(j\omega) + k_s + k_a + c_a(3\sigma_x^2 - 6\sigma_{xv} + 3\sigma_v^2), \quad (6.35)$$

$$\mathcal{B}(\omega;\sigma_x^2,\sigma_{xv},\sigma_v^2) = \lambda_a(j\omega) + k_a + c_a(3\sigma_x^2 - 6\sigma_{xv} + 3\sigma_v^2), \quad (6.36)$$

$$\mathcal{C}(\omega;\sigma_x^2,\sigma_{xv},\sigma_v^2) = -m_a\omega^2 + \lambda_a(j\omega) + k_a + c_a(3\sigma_x^2 - 6\sigma_{xv} + 3\sigma_v^2). \quad (6.37)$$

At this point σ_x^2, σ_v^2, and σ_{xv} are still unknown, but can be determined by integrating

both sides of equations (6.30) to (6.32) and forming the following system of equations:

$$\sigma_x^2 = \int_0^\infty S_{xx}(\omega; \sigma_x^2, \sigma_{xv}, \sigma_v^2) d\omega, \tag{6.38}$$

$$\sigma_{xv} = \int_0^\infty S_{xv}(\omega; \sigma_x^2, \sigma_{xv}, \sigma_v^2) d\omega, \tag{6.39}$$

$$\sigma_v^2 = \int_0^\infty S_{vv}(\omega; \sigma_x^2, \sigma_{xv}, \sigma_v^2) d\omega. \tag{6.40}$$

By solving the above we find σ_x^2, σ_v^2, and σ_{xv}. This procedure determines the Gaussian PDF approximation for the background regime response. Further details regarding the special case of a linear attachment and the analysis for the suspended deck-seat problem can be found in appendix B.

6.4.2 Quantification of the response pdf for the extreme event component

We are going to utilize two alternative methods for the quantification of the statistics in the extreme event regime. The first approach is to obtain the conditional statistics based on direct simulations of the system response. The second method is utilizing effective measures [127] that also characterize the system nonlinear response in the presence of attachments.

6.4.2.1 Rare response PDF using direct simulations of the system under impulsive excitation

To compute the conditionally extreme distribution p_{x_r} and the probability of rare events $\mathbb{P}_r$ we follow the steps described in algorithm 1, which provides a high-level description for a single mode. The procedure is repeated for each degree of freedom of interest (in this case it is more efficient to simply store all the impulse realizations and then run the procedure for each degree of freedom of interest). We emphasize that the numerical simulation of impulse response for nonlinear systems is efficient, since the integrations are necessarily short due the impulsive nature of the forcing and

the condition on the rare event end time in equation (6.16). Moreover, throughout these simulations we do not take into account the background excitation since this is negligible compared with the effect of the initial conditions induced by the impact.

Algorithm 1 Calculation of $\mathbb{P}_r$ and $f_{x_r}(r) = \int f_{x_r|\eta}(r \mid n) f_\eta(n)\, dn$.

1: discretize $f_\eta(n)$
2: **for all** n values over the discretization f_η **do**
3: solve ODE system for $x^n(t)$ under impulse n, neglecting $\ddot{h}$
4: ${\tau_e}^n \leftarrow \{t_e \mid \rho_c \max_t |x^n(t)| = x^n(t_e)\}$ ▷ we set $\rho_c = 0.1$
5: $p^n_{x_r|\eta} \leftarrow \text{Hist}\Big\{x^n(t) \;\Big|\; t \in [0, {\tau_e}^n]\Big\}$
6: **end for**
7: $p_{x_r} \leftarrow \int p^n_{x_r|\eta}\, p^n_\eta$
8: $\tau_e \leftarrow \int {\tau_e}^n\, p^n_\eta$
9: $\mathbb{P}_r \leftarrow \nu_\alpha \tau_e$
10: **output:** $\mathbb{P}_r, p_{x_r}$

Comparison with Monte-Carlo Simulations

The full response PDF is composed using the total probability law,

$$f_z(r) = \frac{1 - \nu_\alpha \tau^z_{e,\text{dis}}}{\sigma_{z_b}\sqrt{2\pi}} \exp\left(-\frac{r^2}{2\sigma^2_{z_b}}\right) + \nu_\alpha \tau^z_{e,\text{dis}} \int_0^\infty \text{Hist}\Big\{z_{r|\eta}(t \mid n)\Big\} f_\eta(n)\, dn, \qquad (6.41)$$

where z is either the displacement, velocity or acceleration of the seat/attachment response. We utilize a shifted Pierson-Moskowitz spectrum $S_{hh}(\omega - 1)$ for the background forcing term in order to avoid system resonance.

For the Monte-Carlo simulations the excitation time series is generated by superimposing the background and rare event components. The background excitation, described by a stationary stochastic process with a Pierson-Moskowitz spectrum (equation (6.7)), is simulated through a superposition of cosines over a range of frequencies with corresponding amplitudes and uniformly distributed random phases. The intermittent

component is the random impulse train, and each impact is introduced as a velocity jump at the point of the impulse. For each of the comparisons performed in this work we generated 10 realizations of the excitation time series, each with a train of 100 impulses. Once each ensemble for the excitation is computed, the governing ordinary differential equations are solved using a 4th/5th order Runge-Kutta method (we carefully account for the modifications in the momentum that an impulse imparts by integrating up to each impulse time and modifying the initial conditions that the impulse imparts before integrating the system to the next impulse time). We verified that this number of ensembles and their durations leads to converged response statistics for the displacement, velocity, and acceleration.

In figure 6-3 we show comparisons for the suspended seat problem with parameters and relevant statistical quantities given in table 6.1. In figure 6-5 we also show comparisons for the suspended deck-seat problem with parameters and relevant statistical quantities in table 6.2. For both cases the adopted quantification scheme is able to compute the distributions for the quantities of interest extremely fast (less than a minute on a laptop), while the corresponding Monte-Carlo simulations take order of hours to complete.

Note that our method is able to capture the complex heavy tail structure many standard deviations away from the mean (dashed vertical line denotes 1 standard deviation). We emphasize that similar accuracy is observed for a variety of system parameters that satisfy the assumptions on the forcing. The close agreement validates that the proposed scheme is applicable and can be accurately used for system optimization and design.

Table 6.1: Parameters and relevant statistical quantities for the suspended seat system.

m_s	1	m_a	0.05
λ_s	0.01	λ_a	0.021
k_s	1	k_a	0
—	—	c_a	3.461
T_α	5000	σ_η	0.0227
$\mu_\alpha = 7 \times \sigma_{\dot{h}}$	0.1	q	1.582×10^{-4}
$\sigma_\alpha = \sigma_{\dot{h}}$	0.0141	σ_h	0.0063
$\mathbb{P}_r^x$	0.0214	$\mathbb{P}_r^v$	0.0107
$\mathbb{P}_r^{\dot{x}}$	0.0210	$\mathbb{P}_r^{\dot{v}}$	0.0100
$\mathbb{P}_r^{\ddot{x}}$	0.0212	$\mathbb{P}_r^{\ddot{v}}$	0.0096

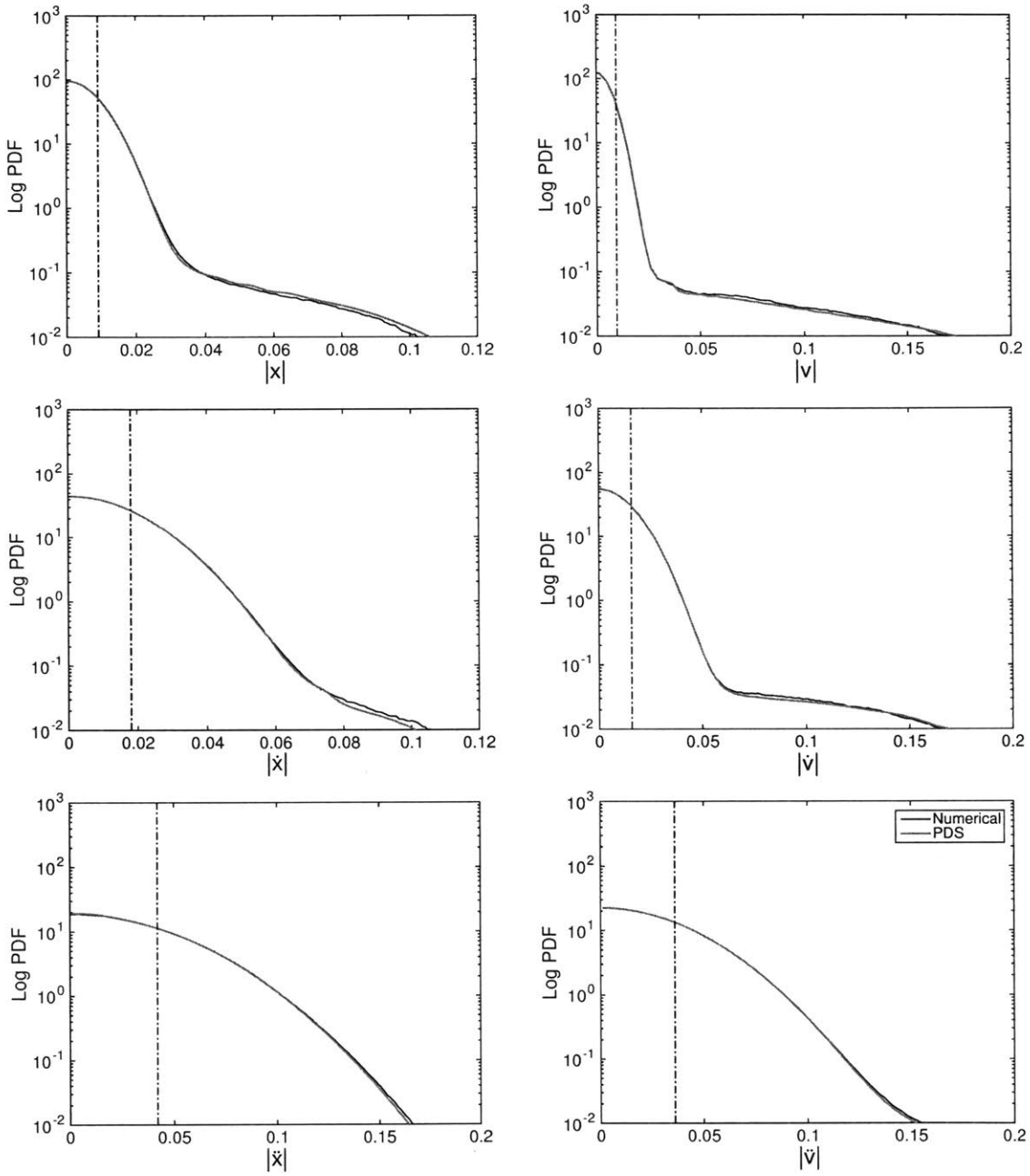

Figure 6-3: Suspended seat with a NES attached; Comparison between PDS method and Monte-Carlo simulations, with parameters given in table 6.1. Left column: seat response. Right column: NES response.

Table 6.2: Parameters and relevant statistical quantities for the suspended deck-seat system.

m_h	1	m_s	0.05	m_a	0.05
λ_h	0.01	λ_s	0.1	λ_a	0.035
k_h	1	k_s	1	k_a	0
—	—	—	—	c_a	5.860
T_α	5000	$\mu_\alpha = 7 \times \sigma_{\dot{h}}$	0.1	q	1.582×10^{-4}
σ_η	0.0232	$\sigma_\alpha = \sigma_{\dot{h}}$	0.0141	σ_h	0.0063
$\mathbb{P}_r^y$	0.0245	$\mathbb{P}_r^x$	0.0247	$\mathbb{P}_r^v$	0.0162
$\mathbb{P}_r^{\dot{y}}$	0.0234	$\mathbb{P}_r^{\dot{x}}$	0.0202	$\mathbb{P}_r^{\dot{v}}$	0.0161
$\mathbb{P}_r^{\ddot{y}}$	0.0238	$\mathbb{P}_r^{\ddot{x}}$	0.0081	$\mathbb{P}_r^{\ddot{v}}$	0.0146

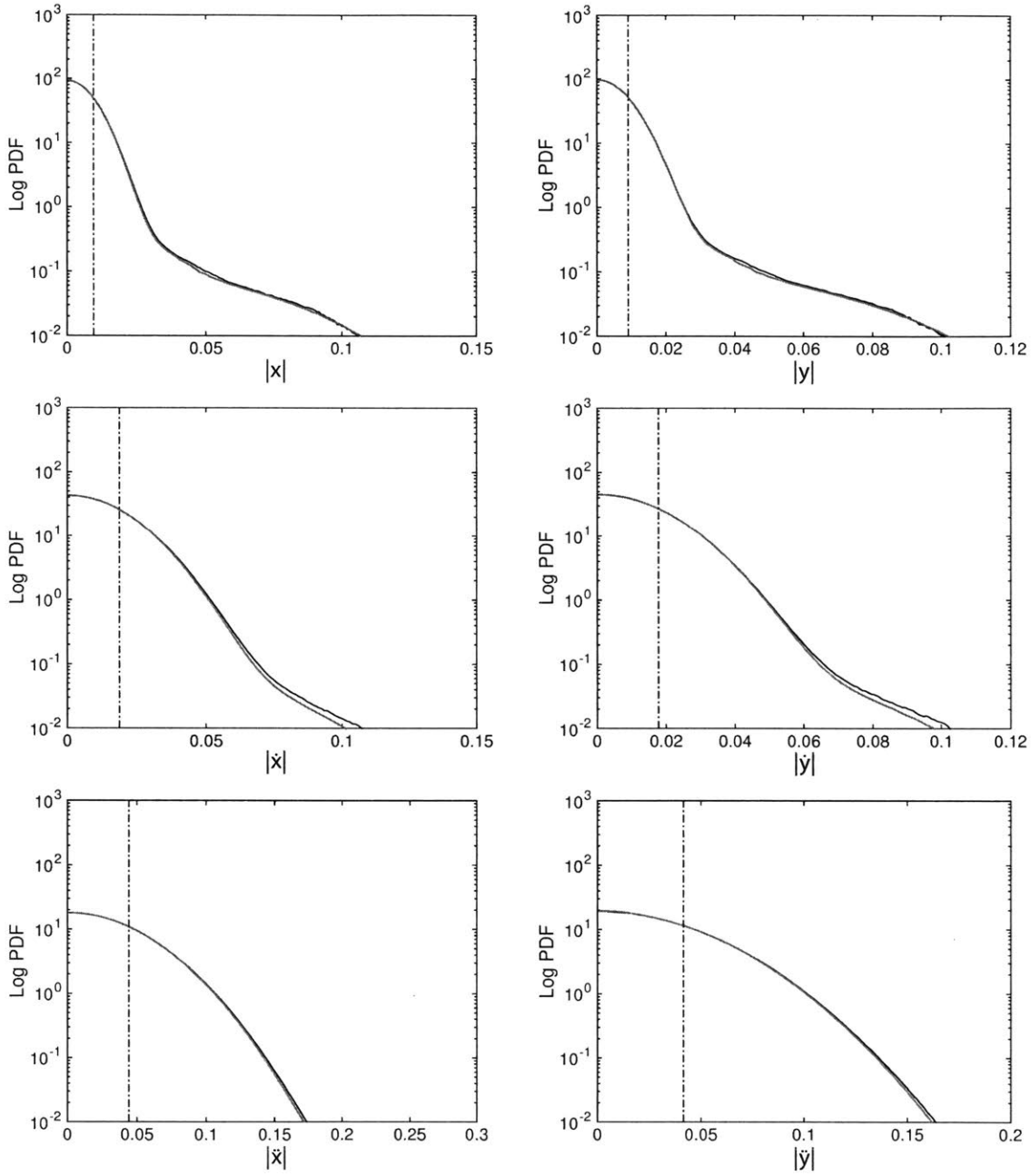

Figure 6-4: Suspended deck-seat with an NES attached; Comparison between the PDS method and Monte-Carlo simulations, with parameters given in table 6.2. Left column: seat response. Right column: deck response.

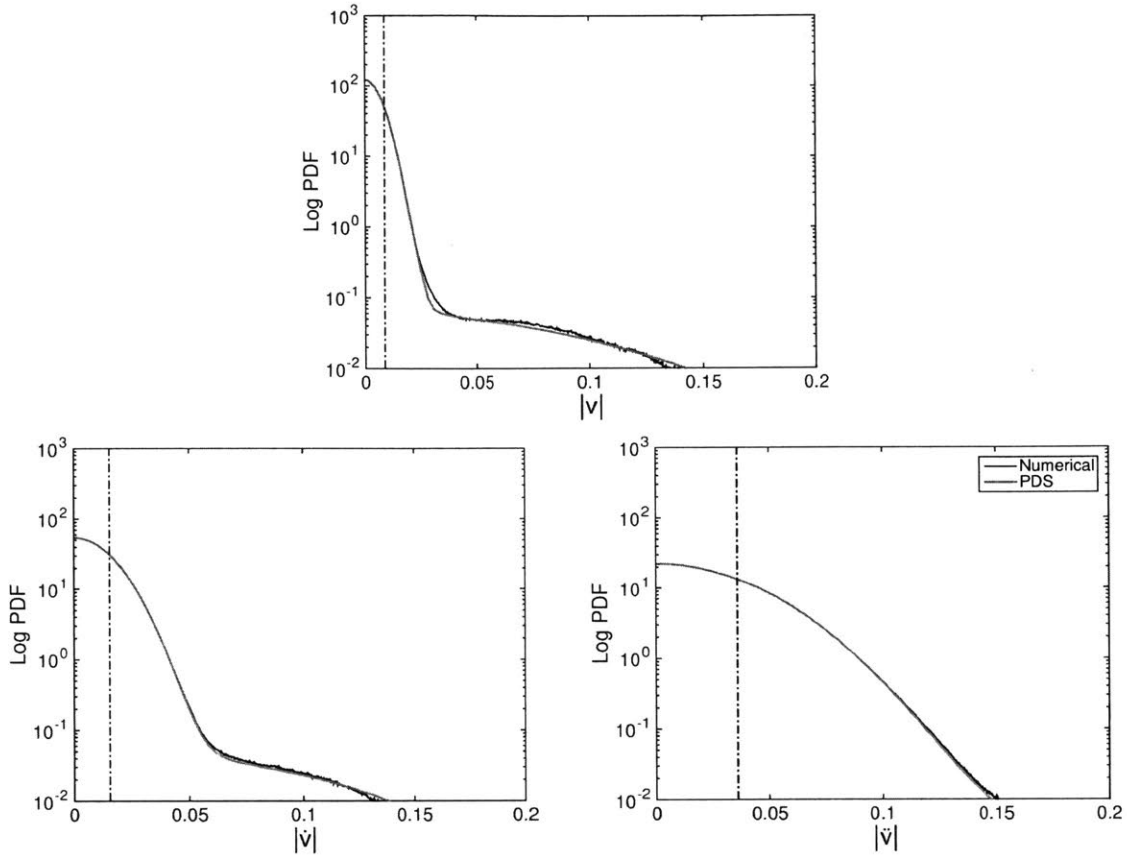

Figure 6-5: Suspended deck-seat with an NES attached (Continued); Comparison between the PDS method and Monte-Carlo simulations, with parameters given in table 6.2. NES response.

6.4.3 Rare response PDF using effective measures

Here we describe an alternative technique to quantify the rare event PDF component using the effective stiffness and damping framework described in [127]. These effective measures express any degree-of-freedom of the coupled *nonlinear* system, for a given initial energy level, as an equivalent *linear* single-degree-of-freedom system. Specifically, these effective measures correspond to the values of damping and stiffness for a linear system that has (for the same initial conditions) a response that is as close as possible to that of the original system, in the mean square sense.

We focus on the suspended seat problem to illustrate this strategy. It should be pointed out that the accuracy and applicability of this approach has some limitations:

- The accurate estimation of the PDF requires the knowledge of the effective measures over a sufficiently large range of initial impulses.
- The motion of the system should have an oscillatory character so that it can be captured by effective measures.
- The statistics of the attachment motion cannot be obtained directly from the effective measures.

To derive the PDF in the rare event regime we reduce the system to an effective linear system for the degree-of-freedome of interest. Consider the suspended seat system under an impulse,

$$\begin{aligned} m_s\ddot{x} &+ \lambda_s\dot{x} + k_s x + \lambda_a(\dot{x}-\dot{v}) + k_a(x-v) + c_a(x-v)^3 = 0 \\ m_a\ddot{v} &+ \lambda_a(\dot{v}-\dot{x}) + k_a(v-x) + c_a(v-x)^3 = 0 \end{aligned} \tag{6.42}$$

with initial conditions, at an arbitrary time say $t_0 = 0$,

$$x = 0, \quad \dot{x} = n, \quad v = 0, \quad \dot{v} = 0. \tag{6.43}$$

To determine the effective *linear* system for this system, we follow the strategy in [127] and compute the effective stiffness and damping:

$$k_{\text{eff}}(t;n) = \frac{2\langle \frac{1}{2}m_s\dot{x}^2\rangle_t}{\langle x^2\rangle_t}, \quad \lambda_{\text{eff}}(t;n) = -\frac{2\frac{d}{dt}\langle \frac{1}{2}m_s\dot{x}^2\rangle_t}{\langle \dot{x}^2\rangle_t}, \tag{6.44}$$

where $\langle\cdot\rangle$ denotes spline interpolation of the local maxima of the time series. We can then compute the weighted-average effective stiffness and damping:

$$\overline{k}_{\text{eff}}(n) = \frac{2\int_0^\infty \langle \frac{1}{2}m_s\dot{x}^2\rangle_s\, ds}{\int_0^\infty \langle x^2\rangle_s\, ds}, \qquad \overline{\lambda}_{\text{eff}}(n) = -2\frac{\int_0^\infty \frac{d}{ds}\langle \frac{1}{2}m_s\dot{x}^2\rangle_s\, ds}{\int_0^\infty \langle \dot{x}^2\rangle_s\, ds}. \tag{6.45}$$

With the weighted-average effective measures we rewrite the original two-degree-of-freedom system during rare events into an equivalent linear single-degree-of-freedom system with coefficients that depend on the initial impact (or the initial energy level

of the system):

$$\ddot{x} + \overline{\lambda}_{\text{eff}}(n)\,\dot{x} + \overline{k}_{\text{eff}}(n)\,x = 0 \tag{6.46}$$

Using the effective system in equation (6.46) we can obtain the conditionally rare PDF using the analysis for the linear system in section 6.3.1. The damping ratio and natural frequency now become functions of the initial impact, n:

$$\omega_n(n) = \sqrt{\overline{k}_{\text{eff}}(n)}, \quad \zeta(n) = \frac{\overline{\lambda}_{\text{eff}}(n)}{2\sqrt{\overline{k}_{\text{eff}}(n)}}, \quad \omega_o(n) = \omega_n(n)\sqrt{\zeta(n)^2 - 1}. \tag{6.47}$$

Subsequently, the PDF is obtained by taking a histogram of

$$x_{r|\eta}(t \mid n) = \frac{n}{2\omega_o(n)}\left(\mathrm{e}^{-(\zeta(n)\omega_n(n)-\omega_o(n))t} - \mathrm{e}^{-(\zeta(n)\omega_n(n)+\omega_o(n))t}\right). \tag{6.48}$$

In figure 6-6 (top) we present the suppression of the probability for large motions of the primary structure due to the presence of the NES (parameters given in table 6.1). This suppression is fully expressed in terms of the effective damping measure shown in the lower plot. Note that the suppression of the tail begins when the effective damping attains values larger than one.

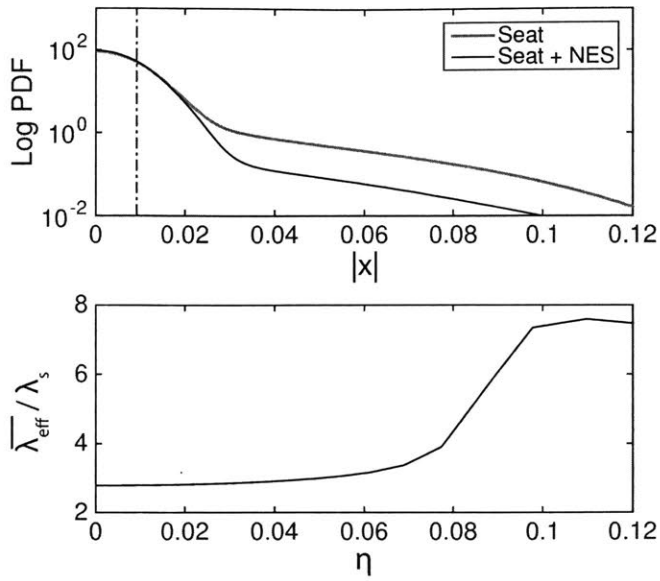

Figure 6-6: (Top) Suspended seat problem without and with a NES attached; (Bottom) Normalized weighted-averaged effective damping $\overline{\lambda}_{\text{eff}}(n)/\lambda_s$ as a function of impulse magnitudes η.

We emphasize that in the context of effective measures the motion of the system is assumed oscillatory. Motions with radically different characteristics will not be captured accurately from the last representation and the resulted histograms will not lead to an accurate representation of the tail. This problem is, in general, circumvented if we employ the first approach for the computation of the conditional PDF during extreme impacts. On the other hand, the advantage of the second approach is that we can interpret the form of the tail in the various regimes with respect to the properties of the effective measures (figure 6-6). This link between dynamics (effective measures) and statistics (heavy tail form) is important for the design process of the NES.

Comparison with Monte-Carlo simulations

Here we compare the PDS method combined with the effective measures with direct Monte-Carlo simulations. In figure 6-7 we show the response PDF for the primary structure for parameters given in table 6.1. Details regarding the Monte-Carlo computations are provided in section 6.4.2.1. We observe that the PDS method utilizing effective measures performs satisfactorily over a wide range similarly with the first

general scheme, based on individual trajectories computation.

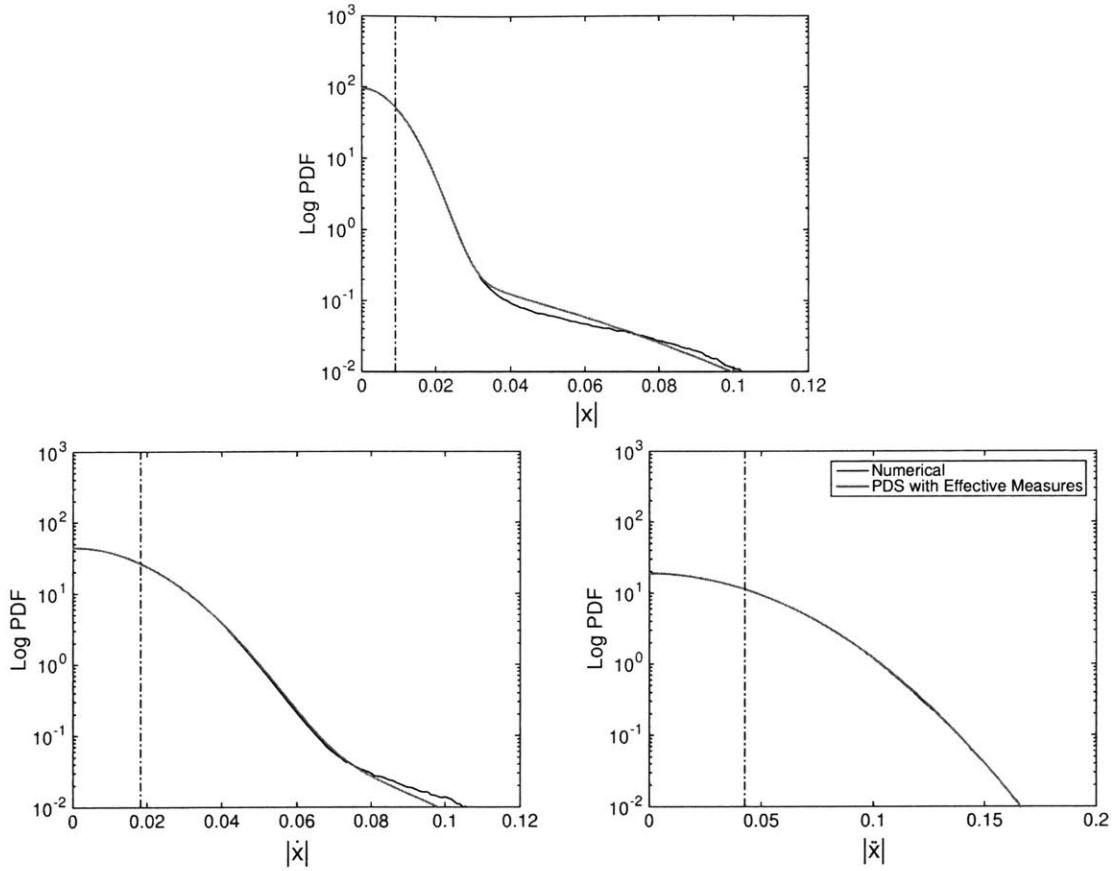

Figure 6-7: Suspended seat problem with an NES attached; Comparison between PDS estimate using effective measures and Monte-Carlo simulations. System parameters are given in table 6.1.

6.4.4 Quantification of the absolute response pdf

The developed PDF quantification schemes provide statistical description for relative quantities (with respect to the base), that is $x = \hat{x} - \xi, y = \hat{y} - \xi$ and $v = \hat{v} - \xi$. However, for the prototype systems that we consider we are more interested for the suppression of absolute quantities, instead of relative ones. As we illustrate below, the absolute response PDF can be derived from the relative response PDF in a straightforward manner .

Background component

For the background regime, we the absolute motion is expressed as:

$$\hat{x}_b = x_b + h. \tag{6.49}$$

As the relative motion and base motion $h(t)$ are both Gaussian distributed (but not independent), their sum is also Gaussian distributed and it is given by,

$$\mathcal{N}(\mu_{\hat{x}}, \sigma^2_{\hat{x}}) = \mathcal{N}(0, \sigma^2_x + \sigma^2_h + 2\sigma_{xh}). \tag{6.50}$$

In the previous section we have derived both σ^2_x and σ^2_h, and what remains is the covariance term σ_{xh} whose spectral density function is given in equation (6.32). This is given by:

$$\sigma_{xh} = \int_0^\infty S_{xh}(\omega; \sigma^2_x, \sigma_{xv}, \sigma^2_v) d\omega. \tag{6.51}$$

Extreme event component

For the extreme event component the motion of the motion is assumed very small (compared with the magnitude of the impact), in which case we have:

$$\hat{x}_r = x_r. \tag{6.52}$$

The estimation of the conditional PDF for x_r has already been described in section 6.4.2.

Comparison with Monte-Carlo Simulations

The full absolute response PDF is expressed using eq. (6.41), where z is either relative or absolute displacement, velocity or acceleration of the seat/attachment response. We compare the PDS method with direct Monte-Carlo simulations for the case of absolute motions. In figure 6-8 we show the absolute response PDF for the primary structure

for parameters given in table 6.1. Details regarding the Monte-Carlo computations are provided in section 6.4.2.1.

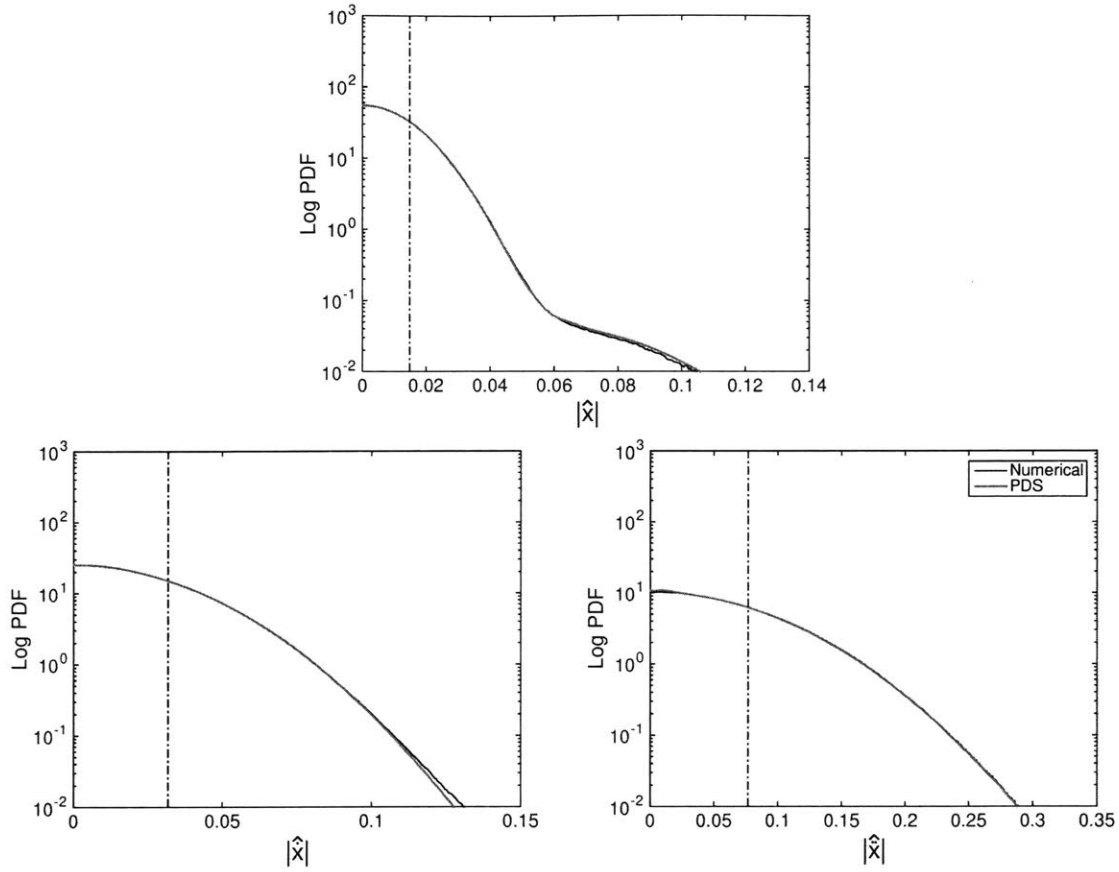

Figure 6-8: Suspended seat problem with an NES attached; Comparison between PDS method and Monte-Carlo simulations. System parameters are given in table 6.1.

6.5 System optimization for extreme event mitigation

We now consider the problem of optimization in the presence of stochastic excitation containing extreme events. The developed method provides a rapid and accurate semi-analytic estimation scheme for the statistical response of the nonlinear structural system. In particular, we can efficiently obtain the response statistics of the primary structure (the seat) for any given shock mitigating attachment and accurately capture the heavy-tailed structure of the distribution. This allows us to explore rare event mitigation performance characteristics of different attachment parameters and perform optimization. Such analysis is not practically feasible via a direct Monte-Carlo approach since a single parameter set takes on the order of hours to compute the resulting response PDF with converged tail statistics.

We consider the prototype systems described in section 6.2 with the aim to suppress the large energy delivered to the passenger (i.e. the seat). In all cases we optimize the attachment parameters, while the parameters of the primary structure are assumed to be fixed.

6.5.1 Optimization objective

We adopt the forth-order moment as our measure to reflect the severity of extreme events on the seat:

$$\overline{\hat{z}^4} = \int \hat{z}^4 f_{\hat{z}}(r)\, dr, \tag{6.53}$$

where the argument $\hat{z}$ can be either absolute displacement of the seat or absolute velocity depending on the optimization objective. The goal here is to minimize this measure and analyze the performance characteristics of the attachment when its parameters are varied.

We illustrate the results of the optimization using the following normalized measure:

$$\gamma = \overline{\hat{z}_a^4}/\overline{\hat{z}_o^4} \tag{6.54}$$

where $\hat{z}_a$ is either $\hat{x}$ or $\hat{\ddot{x}}$, and z_o is the corresponding quantity without any attachment. Values of this measure which are less than 1 ($\gamma < 1$) denote effective extreme event suppression.

6.5.2 Optimization of NES and TMD parameters

Results are shown for the suspended seat problem with an attachment mass $m_a = 0.05$. For a NES attachment ($k_a = 0$) we optimize over c_a and λ_a, while for a TMD ($c_a = 0$) we vary k_a and λ_a (figure 6-9). The resulted response PDF that minimize the displacement moments are illustrated in figure 6-10. The same analysis is performed for the suspended deck-seat problem with the same attachment mass $m_a = 0.05$ for both systems (figure 6-11). The resulted response PDF are illustrated in figure 6-12.

In both cases of systems we observe that the TMD and the optimal cubic NES can improve significantly the behavior of the primary structure in terms of reducing the displacement during impacts, with a reduction of 66-68% of the fourth-order moment. We also observe that the NES design is more robust to variations in the attachment parameters over the TMD design, which requires more stringent attachment parameter values for best performance with respect to γ. This is in line with the fact that the NES attachment performs better over a broader excitation spectrum than the TMD configuration, which requires carefully tuning. Note that for the case of the deck-seat problem (figure 6-11) we can achieve much larger mitigation of the absolute velocity at the order of 32-34% compared with the simpler system of the seat attached to the hull directly (figure 6-9), where the suppression is much smaller, 2-4%.

We performed the grid search for demonstration purposes to illustrate the performance characteristics as the stiffness and damping are varied; clearly, if we are only interested

in the optimal attachment the use of an appropriate global optimizer (such a particle swarm optimizer) would be more appropriate. All the results shown where computed using the proposed PDF estimation method. As a further check and validation, we benchmarked the semi-analytical PDF estimates and compare them with Monte-Carlo results for the extremity measure γ over a coarse grid of the attachment parameters.

Table 6.3: Suspended seat system parameters.

m_s	1	m_a	0.05
λ_s	0.01	k_s	1
T_α	5000	–	–
$\mu_\alpha = 7 \times \sigma_{\dot{h}}$	0.1	q	1.582×10^{-4}
$\sigma_\alpha = \sigma_{\dot{h}}$	0.0141	σ_h	0.0063

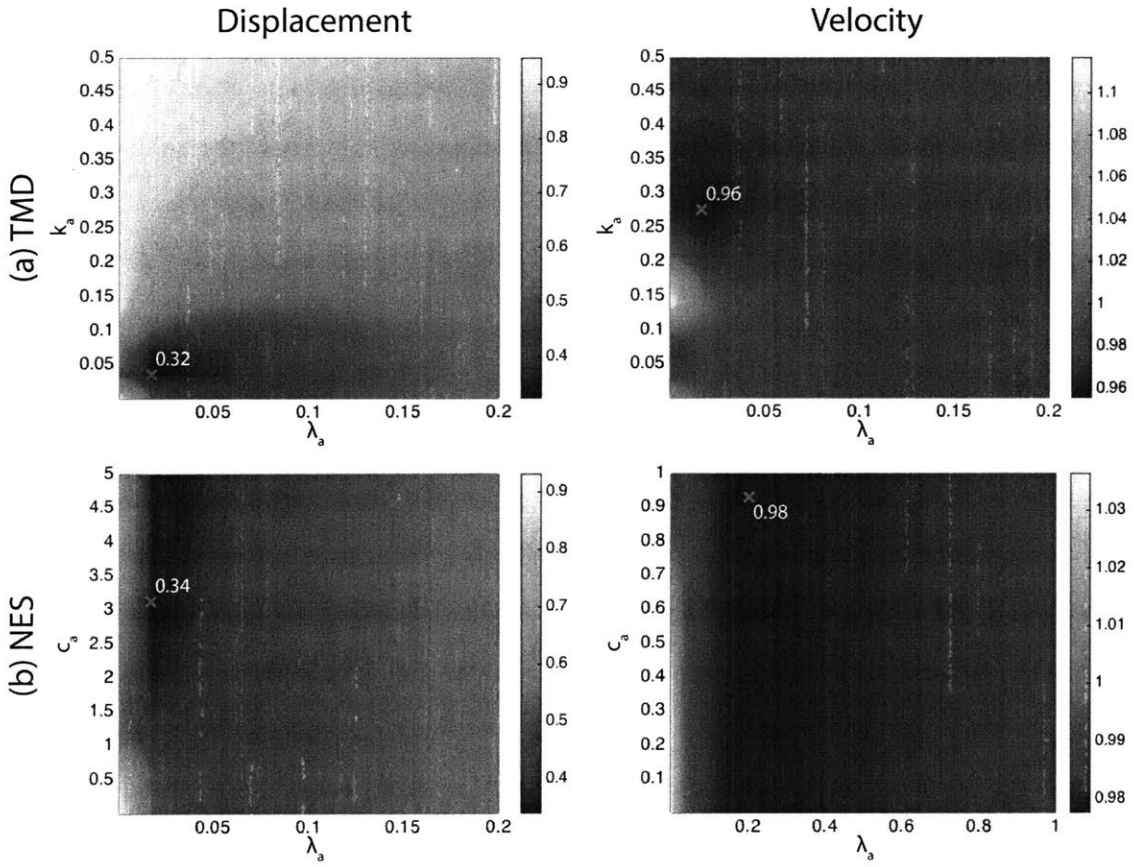

Figure 6-9: [**Suspended seat**] The result of the parametric grid search optimization of the suspended seat attached with (a) TMD ($c_a = 0$) and (b) NES ($k_a = 0$). Optimization has been performed with respect to the stiffness (linear/nonlinear) and damping coefficients of the attachment, and the optimal solutions are marked by a red cross ($\times$) along with the numeric value of the optimal measure γ. Optimization of the response displacement (left subplots) and velocity (right subplots) are presented. Parameters without attachment are shown in table 6.3.

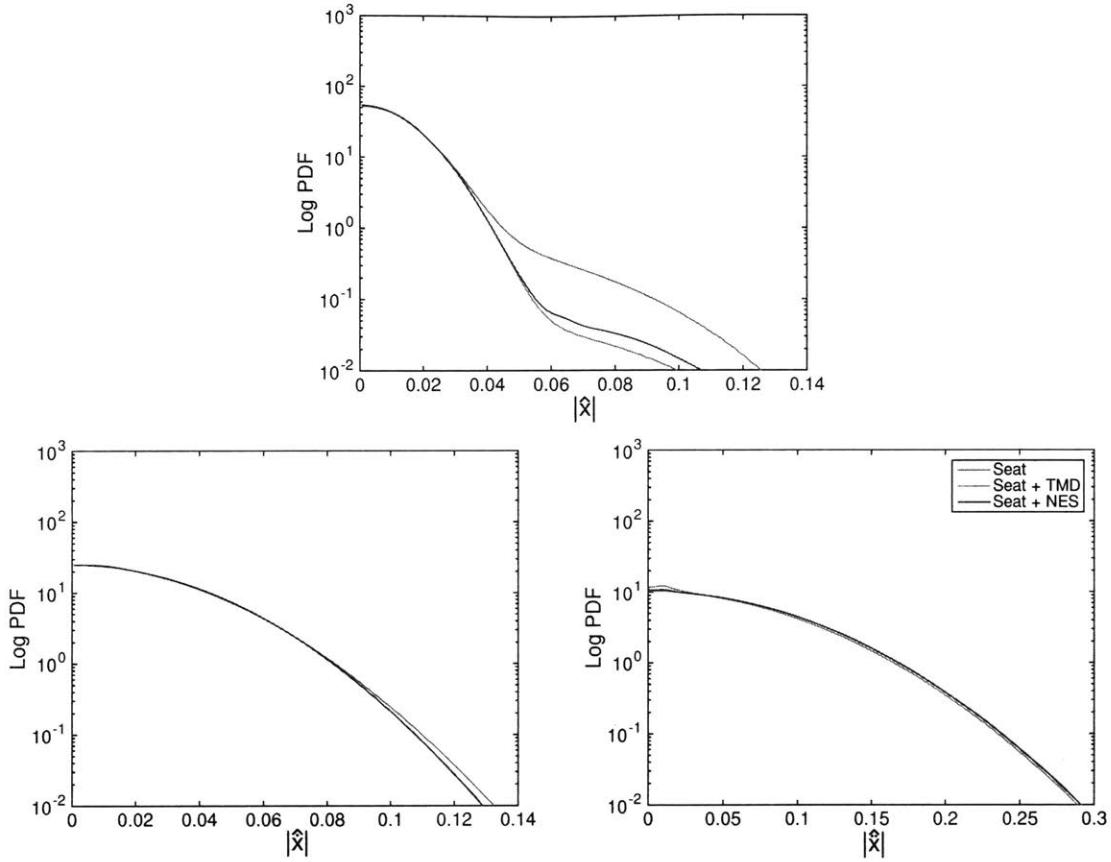

Figure 6-10: [**Suspended seat**] Comparison of the response PDF for optimization of the displacement fourth-order moment. Red curve: without any attachment; Green curve: TMD ($\lambda_a = 0.018$, $k_a = 0.036$); Blue curve: optimal NES ($\lambda_a = 0.018$, $c_a = 3.121$).

Table 6.4: Suspended deck-seat system parameters.

m_h	1	m_s	0.05
m_a	0.05	λ_h	0.01
k_h	1	λ_s	0.1
k_s	1	T_α	5000
$\mu_\alpha = 7 \times \sigma_{\dot{h}}$	0.1	q	1.582×10^{-4}
$\sigma_\alpha = \sigma_{\dot{h}}$	0.0141	σ_h	0.0063

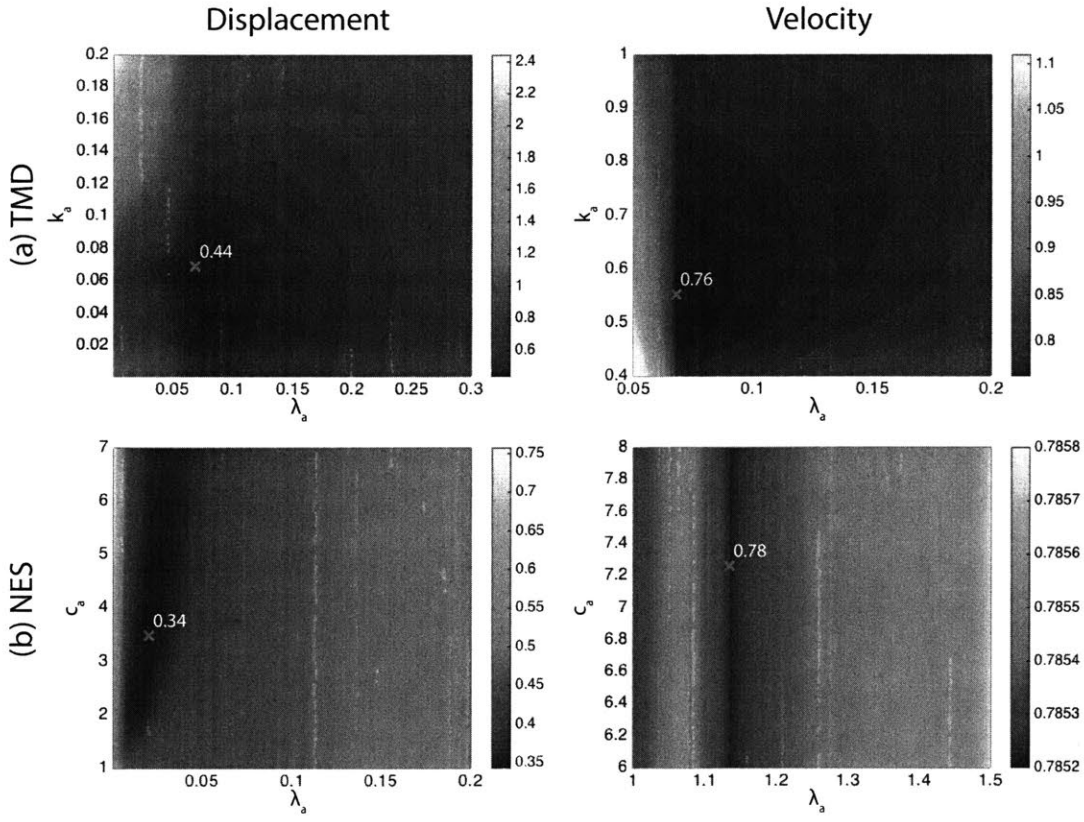

Figure 6-11: [**Suspended deck-seat**] The result of parametric grid search optimization of the suspended deck-seat attached with (a) TMD ($c_a = 0$) and (b) NES ($k_a = 0$). Optimization has been performed with respect to the stiffness (linear/nonlinear) and damping coefficients of the attachment and the optimal solutions are marked by a red cross ($\times$) along with the numeric value of the optimal measure γ. Optimization of the response displacement (left figures) and velocity (right figures) are presented. Parameters without attachment are shown in table 6.4.

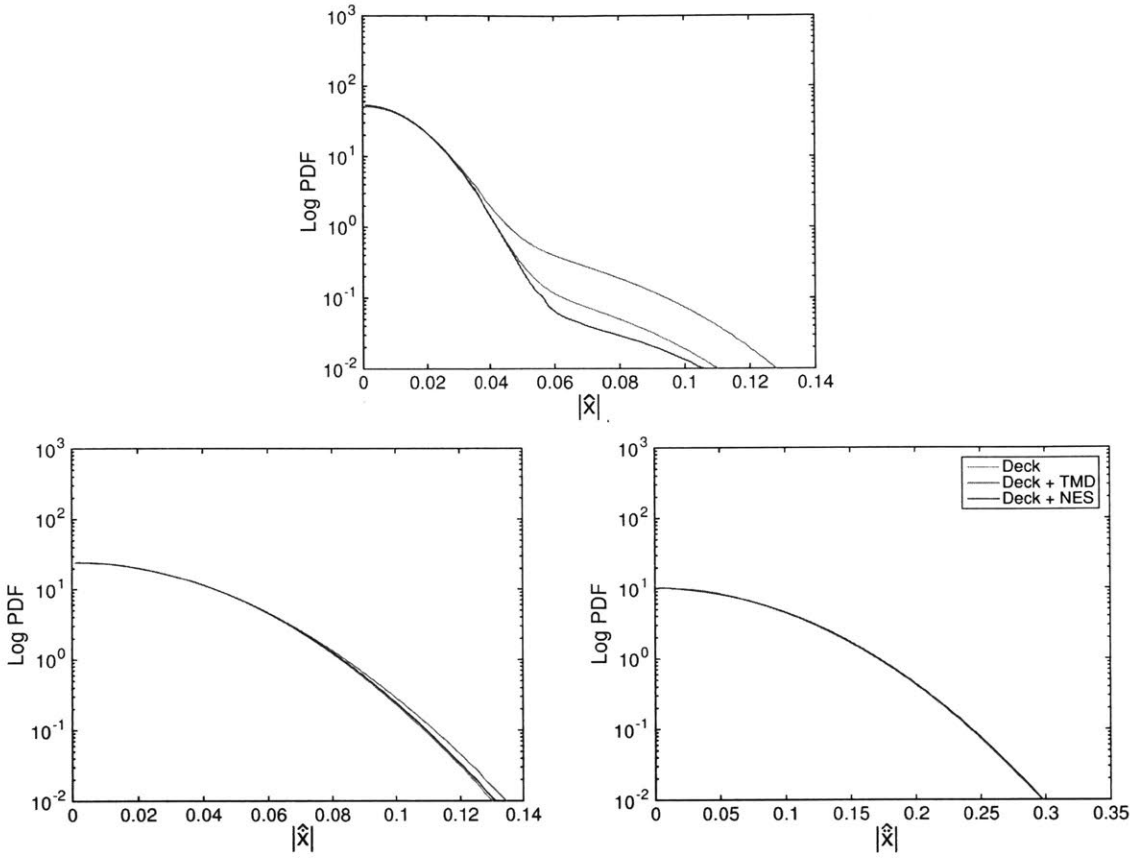

Figure 6-12: [**Suspended deck-seat**] Comparison of the response PDF for optimization of the displacement fourth-order moment. Red curve: without any attachment; Green curve: TMD ($\lambda_a = 0.069$, $k_a = 0.069$); Blue curve: optimal NES ($\lambda_a = 0.021$, $c_a = 3.484$).

6.6 Design and optimization of a piecewise linear NES

To further improve the shock mitigation properties of the attachment, we utilize a more generic form of NES consisting of a possibly asymmetric, piecewise linear spring. Similarly with the cubic NES and TMD attachments, we perform parameter optimization on the NES spring restoring characteristics and obtain a new optimal design that outperforms the TMD and cubic NES for the considered problems.

Here, we focus on suppressing large displacements of the seat, although velocity or acceleration would also be appropriate depending on the desired objectives. The general form of the considered spring consists of a linear regime with slope equal to that of the optimal TMD within a range of 4 standard deviations of the expected seat motion (e.g. when the TMD is employed). For motions (displacements) outside this range the spring has also a linear structure but with different slopes, α_{-1} for negative displacements (beyond 4 standard deviations) and α_1 for positive displacements (beyond 4 standard deviations). Therefore, the optimal linear stiffness operates for small to moderate displacement values and outside this regime, when the response is very large, we allow the stiffness characteristics to vary. The objective is to determine the optimal values for the curve in the extreme motion regime with respect to optimization criterion.

Therefore, the analytical form of the piecewise linear spring is given by:

$$f(x) = \begin{cases} \alpha_1 x + \beta_1, & x \geq 4\sigma_\zeta, \\ k_o x, & -4\sigma_\zeta \leq x \leq 4\sigma_\zeta, \\ \alpha_{-1} x + \beta_{-1}, & x \leq -4\sigma_\zeta, \end{cases} \tag{6.55}$$

where, σ_ζ is the standard deviation of the relative displacement $\zeta = x - v$ between the primary structure (the seat) and the attachment for the case of a TMD attachment.

The parameters, $\alpha_1 \geq 0$ and $\alpha_{-1} \geq 0$ define the slopes in the positive and negative extreme response regimes, which we seek to optimize. Moreover, the values for β_1 and β_{-1} are obtained by enforcing continuity:

$$\beta_1 = 4(k_o - \alpha_1)\sigma_\zeta, \tag{6.56}$$

$$\beta_{-1} = -4(k_o - \alpha_{-1})\sigma_\zeta. \tag{6.57}$$

The value of the stiffness in the center regime, k_o, is chosen using the optimal TMD attachment.

6.6.1 Application to the suspended seat and deck-seat problem and comparisons

We illustrate the optimization using the fourth-order moment of the seat response, employing the following measure:

$$\gamma' = \overline{\hat{z}_n^4}/\overline{\hat{z}_t^4} \tag{6.58}$$

where $\hat{z}_t$ is the system response with the optimal TMD attachment (from the previous parametric grid search optimization) and $\hat{z}_n$ is the response of the system with the piecewise linear NES attachment. Parameters corresponding to values less than 1 ($\gamma' < 1$) denote additional extreme event suppression, compared with the utilization of optimal TMD.

The result of the optimization for *minimum fourth-order moment for the displacement*, on the suspended seat problem, is shown in figure 6-13 while the corresponding PDF for the displacement, velocity and acceleration are shown in figure 6-14. We note the strongly asymmetric character of the derived piecewise linear spring. This is directly related with the asymmetric character of the impulsive excitation, which is in general positive. The performance of the optimized piecewise linear spring is radically improved compared with the optimal cubic NES and TMD as it is shown in the PDF

comparisons. Specifically, for rare events (probability of 1%) we observe a reduction of the motion amplitude by 50%, while for the velocity the reduction is smaller. A representative time series illustrating the performance of the optimal design for the suspended seat problem is shown in figure 6-15. The PDF for the acceleration for this set of parameters is not changing significantly. Our results are in agreement with previous studies involving single-sided vibro-impact NES that have been shown to improve shock mitigation properties in deterministic setups [135].

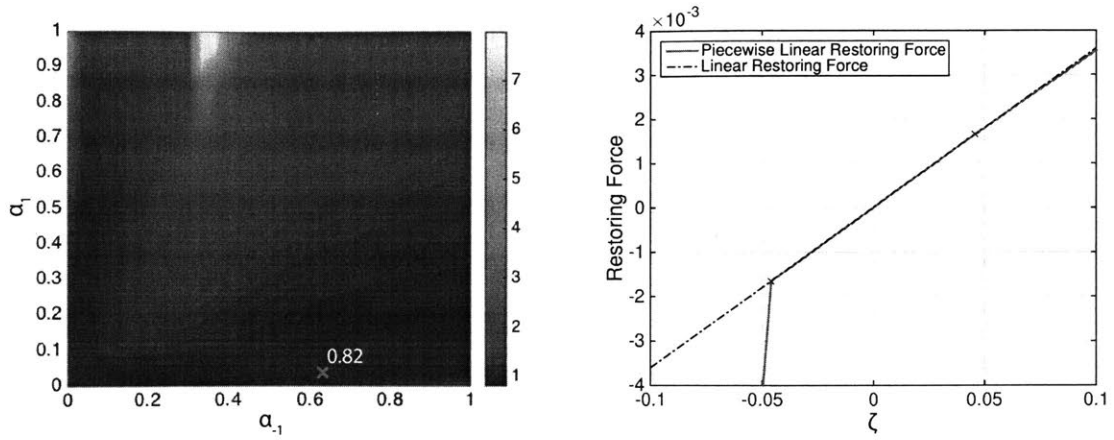

Figure 6-13: [**Suspended seat**] Left: fourth-order measure γ' for the seat absolute displacement as a function of the design variables α_{-1} and α_1. Right: corresponding optimal restoring curve ($\alpha_1 = 0.035$, $\alpha_{-1} = 0.634$).

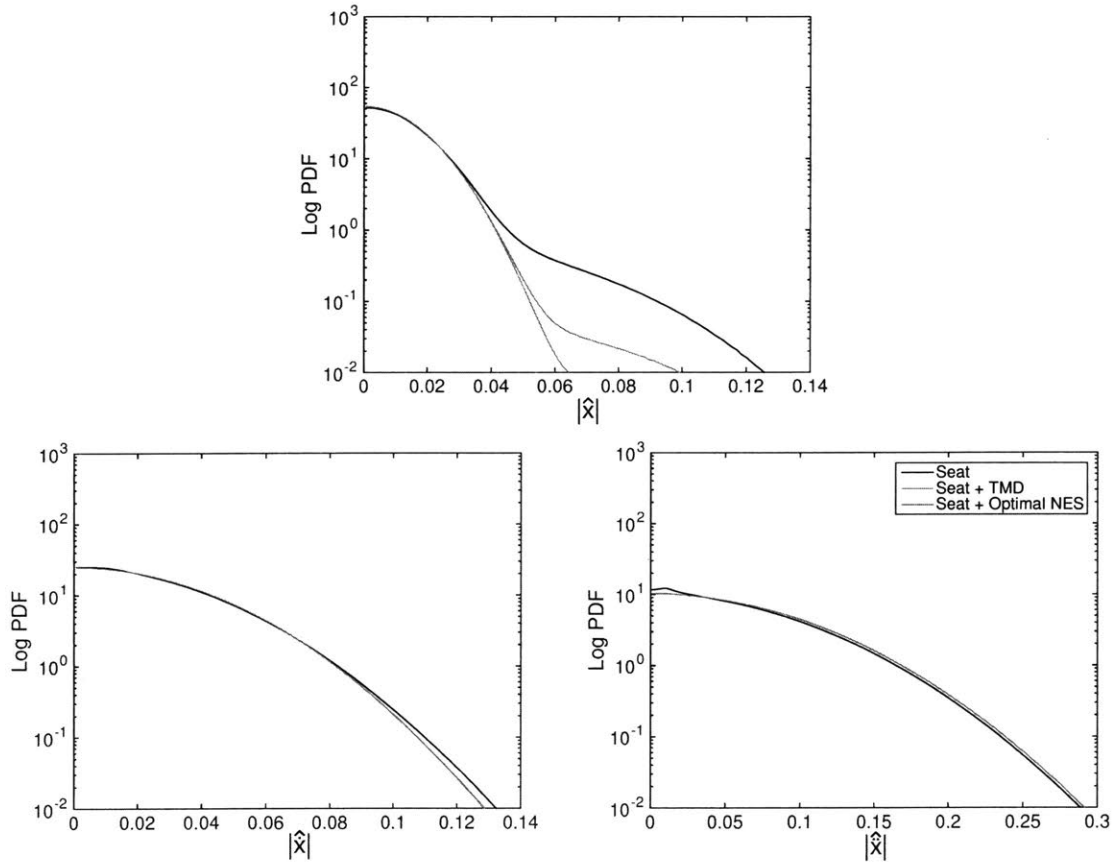

Figure 6-14: [**Suspended seat**] Comparison of the response PDF when the system is tuned for optimal displacement of the seat. Black curve: no attachment. Green curve: optimal TMD design ($\lambda_a = 0.018$, $k_a = 0.036$). Red curve: proposed optimal piecewise linear NES design.

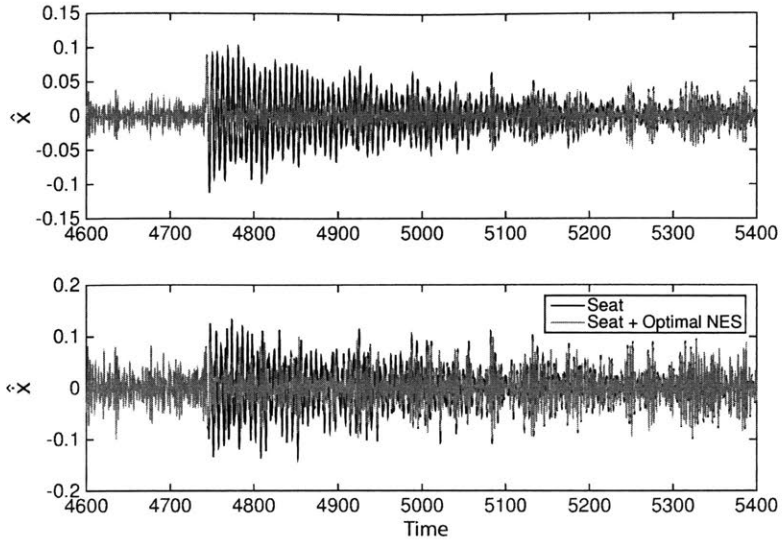

Figure 6-15: Representative time series segment for the absolute displacement and velocity for the suspended seat problem. Black curve: without attachment. Red curve: with optimal piece-wise linear NES. This is the result of design optimization performed in figure 6-13, with response PDF shown in figure 6-14.

The result of the optimization for the suspended deck-seat problem is shown in figure 6-16 and the corresponding PDF are shown in figure 6-17. Similarly with the previous problem, the optimization in this case as well leads to a strongly asymmetric piecewise linear spring. The reduction on the amplitude of the displacement during extreme events is radical (with an additional reduction of 32%) while the corresponding effects for the velocity and acceleration are negligible. This small improvement for the velocity is attributed to the fact that we have focused on minimizing the fourth-order moments for the displacement.

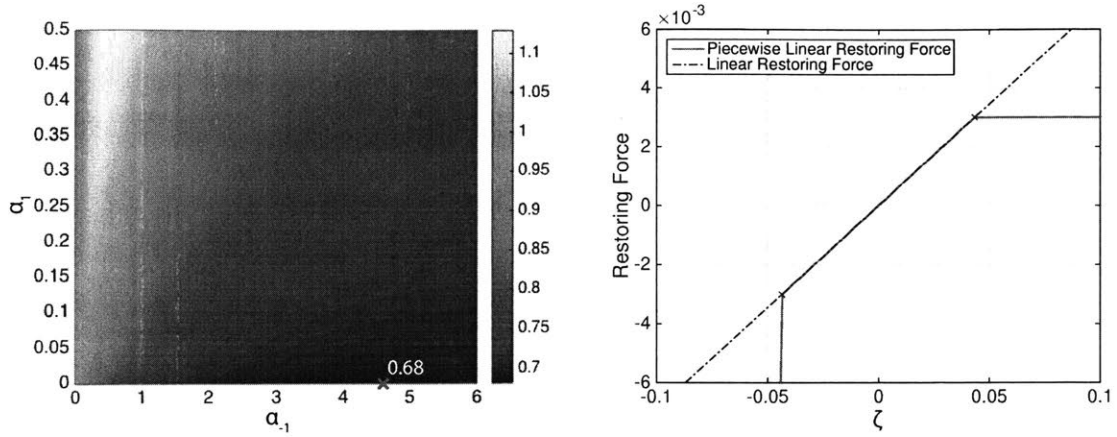

Figure 6-16: [**Suspended deck-seat**] Left: fourth-order measure γ' for the seat absolute displacement as a function of the design variables α_{-1} and α_1. Right: corresponding optimal restoring curve ($\alpha_1 = 0$, $\alpha_{-1} = 4.605$).

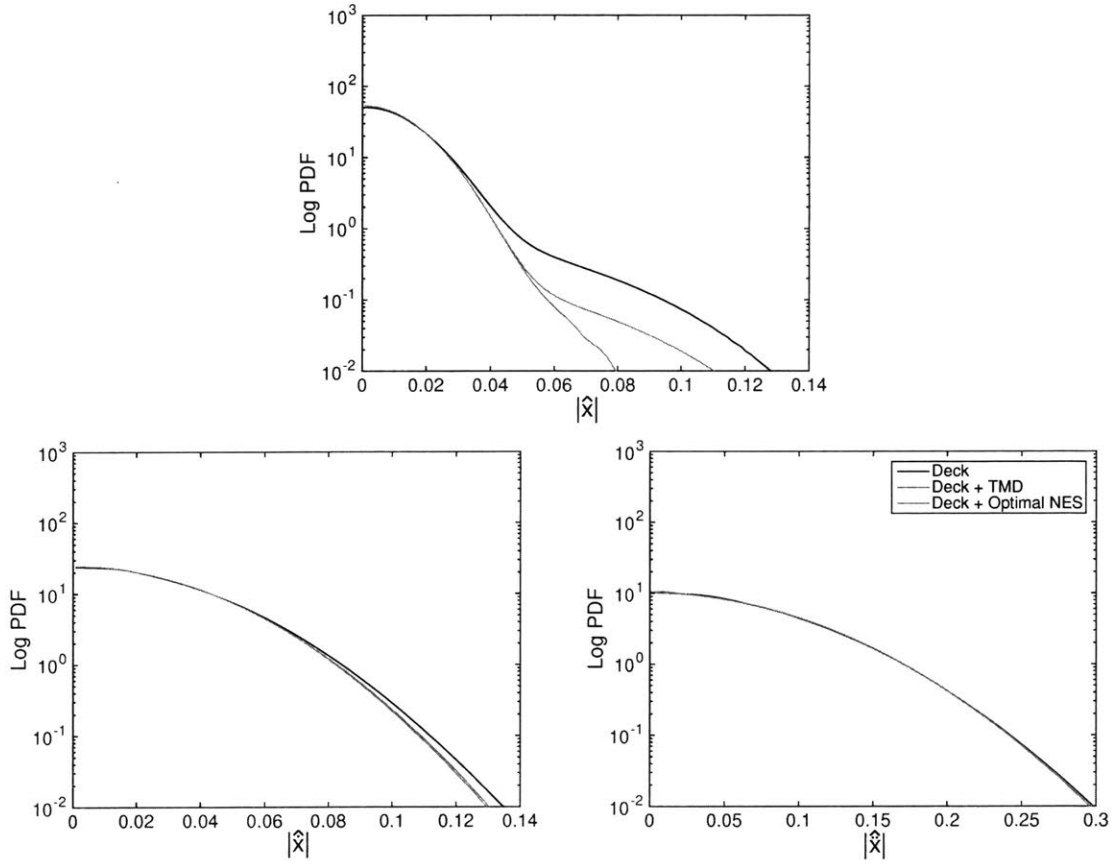

Figure 6-17: [**Suspended deck-seat**] Comparison of the response PDF when the system is tuned for optimal displacement of the seat. Black curve: no attachment. Green curve: optimal TMD design ($\lambda_a = 0.069$, $k_a = 0.069$). Red curve: proposed optimal piecewise linear NES design.

6.7 Summary

We have formulated a parsimonious and accurate quantification method for the heavy-tailed response statistics of nonlinear multi-degree-of-freedom systems under extreme forcing events. The computational core of our approach is the probabilistic decomposition-synthesis method which is formulated for nonlinear MDOF systems under stochastic excitations containing extreme events. Specifically, the excitation is modeled as a superposition of a Poisson distributed impulse train (with extreme magnitude and large inter-arrival times) and a background (smooth) component, modeled by a correlated stochastic excitation with broadband spectral density. This algorithm takes the form of a semi-analytical formula for the response PDF, allowing us to evaluate response statistics (having complex tail structure) on the order of seconds for the nonlinear dynamical structures considered.

Based on this computational statistical framework, we proceed with the design and optimization of small attachments that can optimally mitigate and suppress the extreme forcing events delivered to the primary system. We performed the suppression of extreme responses on prototype ocean engineering dynamical structures, *the suspended seat* and *the suspended deck-seat* of high speed crafts, via optimal TMD and cubic NES attachments through parametric optimization. As an optimization criterion we selected the forth-order moments of the response displacement, which is a measure of the severity of large deviations from the mean. Quantitative comparisons of TMD and cubic NES were presented, evaluating the effectiveness and robustness in terms of extreme event suppression. We then proposed a new piecewise linear NES with asymmetries, for extreme event mitigation. The optimization of the new design led to a strongly asymmetric spring that far outperforms the optimal cubic NES and TMD for the considered problem.

We emphasize the statistical accuracy of the PDF estimation schemes, which we demonstrated through comparisons with direct Monte-Carlo simulations. The pre-

sented schemes are generic, easy to implement, and can profitably be applied to a variety of different problems in structural engineering where similar characteristics are present, i.e. structures excited by extreme forcing events represented by impulsive-like terms that emerge from an otherwise random excitation background of moderate magnitude.

Chapter 7

Conclusions

In this chapter we summarize the results and contributions obtained throughout the thesis. In chapter 3, we considered the problem of non-Gaussian steady state statistics of nonlinear systems under correlated excitation. We first derived two-times moment equations, and these were then combined with a non-Gaussian pdf representation for the joint response-excitation statistics. This representation fulfill two properties: the single time statistical structure is consistent with the analytical solution of the corresponding Fokker-Planck equation, and the two-time statistical structure has Gaussian characteristics. Based on the pdf representation, we obtained a *closure constraint* and a *dynamics constraint*, which describes the nonlinear dynamics of the system. We then formulated these constraints as a minimization problem and performed the minimization to obtain a solution that satisfies both constraints as accurately as possible.

We then applied the developed method to nonlinear oscillators in the context of vibration energy harvesting in chapter 4. We first considered the case of a single-degree-of-freedom bistable oscillator with linear damping and the same single-degree-of-freedom bistable oscillator coupled with an electromechanical energy harvester, assuming the stationary stochastic excitation follows a Pierson-Moskowitz spectrum. Through comparisons with direct Monte-Carlo simulations, we have showed the method can provide a very good approximation of second order statistics of the system, even in essentially nonlinear regimes where the traditional Gaussian closure method or statistical lineariza-

tion fails to capture the dynamics. Additionally, we obtained the full non-Gaussian probabilistic structure of the response. Finally, the developed scheme was demonstrated to more generic structures, such as linear undamped elastic rods coupled with bistable nonlinear elements. The developed method provides with an efficient way to quantify the strongly non-Gaussian statistics for mechanical systems subjected to correlated excitation. These results have been published in [69].

In chapter 5, we formulated a robust approximation method to quantify the probabilistic response of structural systems subjected to stochastic excitation containing extreme forcing components. We achieved this by representing the stochastic excitation as the superposition of a background component, which is modeled by a stationary stochastic process, and a rare/extreme component, that can be modeled by Poisson distributed extreme impulses with large inter-arrival time. We then derived the analytical (under special conditions) and the generalized semi-analytical expressions for the pdf of response and its local extrema for structural systems. These expressions decompose the pdf into a probabilistic core, capturing the statistics under background excitation, as well as a heavy- tailed component associated with the extreme transitions due to the rare impacts. We have demonstrated the validity of the analytical and generalized semi-analytical schemes through comprehensive comparisons with Monte-Carlo simulations for numerous structural systems.

In chapter 6, we generalized the method for the case of nonlinear multi-degree-of-freedom systems under extreme forcing events. The developed approach allowed us to evaluate response statistics (of complex non-trivial tail structures) on the order of seconds for the nonlinear dynamical structures. With the developed scheme, we conducted design and optimization of small linear and nonlinear attachments that can optimally mitigate and suppress the extreme forcing events delivered to a primary system. We performed the suppression of extreme responses on two prototype dynamical structures found in ocean engineering: *the suspended seat* and *the suspended seat-deck* of a high speed craft. We employed optimal TMD and cubic NES attachments by per-

forming parametric optimization through the minimization of the forth-order moments of the response. We then developed a new design of NES that far outperforms the optimal cubic NES for the considered problem. We emphasized the statistical accuracy of the pdf estimation through comparisons with direct Monte-Carlo simulations.

7.1 Future Directions

The developed computational framework is the first, to the best of our knowledge, that provides with a feasible way to perform optimization with respect to the statistical properties of the response. This is an important step ahead from the standard paradigm followed in mechanics, where optimization is performed with respect to deterministic features of the dynamics, since stochastic simulations (especially focused on extreme events) are very expensive. Our schemes can be applied on a wide range of engineering problems where nonlinearity in the dynamics or non-stationarity in the excitation are important. For many systems in this category the designs have been restricted by the analysis/optimization tools available. To this end, future work includes the design, study and optimization of strongly nonlinear configurations with the aim of optimal and robust energy harvesting and impact mitigation. Areas that can benefit from the developed computational framework include Mechanical, Ocean, Civil, and Aerospace Engineering. We believe that the developed schemes are well suited to a large number of problems involving vibrations in these settings and can prove to be an important engineering method for design and reliability assessment. Appropriate experimental schemes should also be developed for the assessment of the predicted statistical features and this is also an interesting area for future work.

Appendix A

Probability Distribution of an Arbitrarily Exponentially Decaying Function

In this appendix, we provide the detailed derivation of pdf of an arbitrary exponentially decaying function considered in section 5.3.5. Please consider an arbitrary time series in the following form.

$$x(t) = A\mathrm{e}^{-\alpha t}, \quad \text{where } t \sim \text{Uniform}\,(\tau_1, \tau_2)\,, \tag{A.1}$$

where A and $\alpha > 0$ are constants, and we let $\tau_1 < \tau_2$ so that the time t is uniformly distributed between τ_1 and τ_2. In this case, the cumulative distribution function (cdf) of $x(t)$ can be derived as

$$\begin{aligned} F_x(x) &= \mathbb{P}(A\mathrm{e}^{-\alpha t} < x), && \text{(A.2)} \\ &= \mathbb{P}\Big(t > \frac{1}{\alpha}\log(A/x)\Big), && \text{(A.3)} \\ &= 1 - \mathbb{P}\Big(t < \frac{1}{\alpha}\log(A/x)\Big), && \text{(A.4)} \\ &= 1 - \int_{-\infty}^{\frac{1}{\alpha}\log(A/x)} f_T(t)\,dt. && \text{(A.5)} \end{aligned}$$

Please note that $f_T(t)$ is the uniform pdf for time t which can be expressed by step functions $s(\cdot)$.

$$f_T(t) = \frac{1}{\tau_2 - \tau_1}\Big\{s(t-\tau_1) - s(t-\tau_2)\Big\}, \quad \tau_1 < \tau_2. \tag{A.6}$$

Then the pdf of the response $x(t)$ can then be derived by differentiation.

$$\begin{aligned} f_x(x) =& \frac{d}{dx}F_x(x), && \text{(A.7)} \\ =& \frac{1}{\alpha x} f_T\Big(\frac{1}{\alpha}\log(Ax)\Big), && \text{(A.8)} \\ =& \frac{1}{\alpha x(\tau_2 - \tau_1)}\Big\{s(x - A\mathrm{e}^{-\alpha\tau_2}) - s(x - A\mathrm{e}^{-\alpha\tau_1})\Big\}. && \text{(A.9)} \end{aligned}$$

We utilize the above formula for deriving analytical response pdfs in section 5.3.5. We further note that the step function with respect to x can be derived from the following relations.

$$\tau_1 < t < \tau_2, \tag{A.10}$$

$$-\alpha\tau_2 < -\alpha t < -\alpha\tau_1, \tag{A.11}$$

$$A\mathrm{e}^{-\alpha\tau_2} < x < A\mathrm{e}^{-\alpha\tau_1}. \tag{A.12}$$

Appendix B

Statistical Linearization of the Background Regime

In this appendix, we provide the detailed derivation of statistical linearization of the background regime in the context of high speed craft problem, the suspended seat design and the suspended deck design, in chapter 6.

Suspended seat system with a linear attachment

For the special case of a linear attachment, $c_a = 0$, the operators for the suspended seat problem, $\mathcal{A}$, $\mathcal{B}$, and $\mathcal{C}$ in equations (6.35) to (6.37) reduce to

$$\mathcal{A}(\omega) = -m_s\omega^2 + (\lambda_s + \lambda_a)(j\omega) + k_s + k_a, \tag{B.1}$$

$$\mathcal{B}(\omega) = \lambda_a(j\omega) + k_a, \tag{B.2}$$

$$\mathcal{C}(\omega) = -m_a\omega^2 + \lambda_a(j\omega) + k_a. \tag{B.3}$$

In this case, we can directly integrate equations (6.30) to (6.32) to obtain the second order response statistics.

Suspended deck-seat system

For the suspended deck-seat design the background response is governed by the following system

$$m_h\ddot{y} + \lambda_h\dot{y} + k_h y + \lambda_s(\dot{y}-\dot{x}) + k_s(y-x) + \lambda_a(\dot{y}-\dot{v}) + k_a(y-v) + c_a(y-v)^3 = -m_h\ddot{h}(t), \quad \text{(B.4)}$$

$$m_s\ddot{x} + \lambda_s(\dot{x}-\dot{y}) + k_s(x-y) = -m_s\ddot{h}(t), \quad \text{(B.5)}$$

$$m_a\ddot{v} + \lambda_a(\dot{v}-\dot{y}) + k_a(v-y) + c_a(v-y)^3 = -m_a\ddot{h}(t). \quad \text{(B.6)}$$

As before we first multiply the above two equations by $y(s)$, $x(s)$, $v(s)$, $h(s)$ at different time instant $s \neq t$, and take ensemble averages to write the resulting equations in terms of covariance functions.

$$m_h C''_{y\eta} + \lambda_h C'_{y\eta} + k_h C_{y\eta} + \lambda_s\left(C'_{y\eta} - C'_{x\eta}\right) + k_s\left(C_{y\eta} - C_{x\eta}\right) + \lambda_a\left(C'_{y\eta} - C'_{v\eta}\right) + k_a\left(C_{y\eta} - C_{v\eta}\right) + c_a\overline{(y(t)-v(t))^3\,\eta(s)} = -m_h C''_{h\eta}, \quad \text{(B.7)}$$

$$m_s C''_{x\eta} + \lambda_s\left(C'_{x\eta} - C'_{y\eta}\right) + k_s\left(C_{x\eta} - C_{y\eta}\right) = -m_s C''_{h\eta}, \quad \text{(B.8)}$$

$$m_a C''_{v\eta} + \lambda_a\left(C'_{v\eta} - C'_{y\eta}\right) + k_a\left(C_{v\eta} - C_{y\eta}\right) + c_a\overline{(v(t)-y(t))^3\,\eta(s)} = -m_a C''_{h\eta}, \quad \text{(B.9)}$$

where η can be either y, x, v, or h, and $'$ indicates the partial differentiation with respect to the time difference $\tau = t - s$. We then apply Isserlis' theorem based on the Gaussian process approximation for response to express the fourth-order moments in terms of second-order moments [63].

$$\overline{(y(t)-v(t))^3\,\eta(s)} = \left(3\sigma_y^2 - 6\sigma_{yv} + 3\sigma_v^2\right)C_{y\eta} - \left(3\sigma_y^2 - 6\sigma_{yv} + 3\sigma_v^2\right)C_{v\eta}. \quad \text{(B.10)}$$

This leads to a set of linear equations in terms of covariance functions and thus the Wiener-Khinchin theorem can be applied to write the equations in terms of the power

spectrum. The spectral equations in this case are given by

$$S_{yy}(\omega;\sigma_y^2,\sigma_{yv},\sigma_v^2) = \frac{\left(m_h + m_a\frac{\mathcal{B}(\omega)}{\mathcal{C}(\omega)} + m_s\frac{\mathcal{D}(\omega)}{\mathcal{E}(\omega)}\right)}{\left(\mathcal{A}(\omega) - \frac{\mathcal{D}(\omega)^2}{\mathcal{E}(\omega)} - \frac{\mathcal{B}(\omega)^2}{\mathcal{C}(\omega)}\right)} \times \frac{\left(m_h + m_a\frac{\mathcal{B}(-\omega)}{\mathcal{C}(-\omega)} + m_s\frac{\mathcal{D}(-\omega)}{\mathcal{E}(-\omega)}\right)\omega^4\, S_{hh}(\omega)}{\left(\mathcal{A}(-\omega) - \frac{\mathcal{D}(-\omega)^2}{\mathcal{E}(-\omega)} - \frac{\mathcal{B}(-\omega)^2}{\mathcal{C}(-\omega)}\right)}, \quad \text{(B.11)}$$

$$S_{xx}(\omega;\sigma_y^2,\sigma_{yv},\sigma_v^2) = \frac{\left(m_h + m_s\frac{\mathcal{A}(\omega)}{\mathcal{D}(\omega)} - m_s\frac{\mathcal{B}(\omega)^2}{\mathcal{C}(\omega)\mathcal{D}(\omega)} - m_a\frac{\mathcal{B}(\omega)}{\mathcal{C}(\omega)}\right)}{\left(\frac{\mathcal{A}(\omega)\mathcal{E}(\omega)}{\mathcal{D}(\omega)} - \mathcal{D}(\omega) - \frac{\mathcal{B}(\omega)^2\mathcal{E}(\omega)}{\mathcal{D}(\omega)\mathcal{C}(\omega)}\right)} \quad \text{(B.12)}$$

$$\times \frac{\left(m_h + m_s\frac{\mathcal{A}(-\omega)}{\mathcal{D}(-\omega)} - m_s\frac{\mathcal{B}(-\omega)^2}{\mathcal{C}(-\omega)\mathcal{D}(-\omega)} - m_a\frac{\mathcal{B}(-\omega)}{\mathcal{C}(-\omega)}\right)\omega^4\, S_{hh}(\omega)}{\left(\frac{\mathcal{A}(-\omega)\mathcal{E}(-\omega)}{\mathcal{D}(-\omega)} - \mathcal{D}(-\omega) - \frac{\mathcal{B}(-\omega)^2\mathcal{E}(-\omega)}{\mathcal{D}(-\omega)\mathcal{C}(-\omega)}\right)}, \quad \text{(B.13)}$$

$$S_{vv}(\omega;\sigma_y^2,\sigma_{yv},\sigma_v^2) = \frac{\left(m_h + m_a\frac{\mathcal{A}(\omega)}{\mathcal{B}(\omega)} + m_s\frac{\mathcal{D}(\omega)}{\mathcal{E}(\omega)} - m_a\frac{\mathcal{D}(\omega)^2}{\mathcal{E}(\omega)\mathcal{B}(\omega)}\right)}{\left(\frac{\mathcal{A}(\omega)\mathcal{C}(\omega)}{\mathcal{B}(\omega)} - \frac{\mathcal{D}(\omega)^2\mathcal{C}(\omega)}{\mathcal{B}(\omega)\mathcal{E}(\omega)} - \mathcal{B}(\omega)\right)} \quad \text{(B.14)}$$

$$\times \frac{\left(m_h + m_a\frac{\mathcal{A}(-\omega)}{\mathcal{B}(-\omega)} + m_s\frac{\mathcal{D}(-\omega)}{\mathcal{E}(-\omega)} - m_a\frac{\mathcal{D}(-\omega)^2}{\mathcal{E}(-\omega)\mathcal{B}(-\omega)}\right)\omega^4\, S_{hh}(\omega)}{\left(\frac{\mathcal{A}(-\omega)\mathcal{C}(-\omega)}{\mathcal{B}(-\omega)} - \frac{\mathcal{D}(-\omega)^2\mathcal{C}(-\omega)}{\mathcal{B}(-\omega)\mathcal{E}(-\omega)} - \mathcal{B}(-\omega)\right)}, \quad \text{(B.15)}$$

$$S_{yv}(\omega;\sigma_y^2,\sigma_{yv},\sigma_v^2) = \frac{\left(m_h + m_a\frac{\mathcal{B}(\omega)}{\mathcal{C}(\omega)} + m_s\frac{\mathcal{D}(\omega)}{\mathcal{E}(\omega)}\right)}{\left(\mathcal{A}(\omega) - \frac{\mathcal{D}(\omega)^2}{\mathcal{E}(\omega)} - \frac{\mathcal{B}(\omega)^2}{\mathcal{C}(\omega)}\right)} \quad \text{(B.16)}$$

$$\times \frac{\left(m_h + m_a\frac{\mathcal{A}(-\omega)}{\mathcal{B}(-\omega)} + m_s\frac{\mathcal{D}(-\omega)}{\mathcal{E}(-\omega)} - m_a\frac{\mathcal{D}(-\omega)^2}{\mathcal{E}(-\omega)\mathcal{B}(-\omega)}\right)\omega^4\, S_{hh}(\omega)}{\left(\frac{\mathcal{A}(-\omega)\mathcal{C}(-\omega)}{\mathcal{B}(-\omega)} - \frac{\mathcal{D}(-\omega)^2\mathcal{C}(-\omega)}{\mathcal{B}(-\omega)\mathcal{E}(-\omega)} - \mathcal{B}(-\omega)\right)}, \quad \text{(B.17)}$$

$$S_{yh}(\omega;\sigma_y^2,\sigma_{yv},\sigma_v^2) = \frac{\left(m_h + m_a\frac{\mathcal{B}(\omega)}{\mathcal{C}(\omega)} + m_s\frac{\mathcal{D}(\omega)}{\mathcal{E}(\omega)}\right)\omega^2\, S_{hh}(\omega)}{\left(\mathcal{A}(\omega) - \frac{\mathcal{D}(\omega)^2}{\mathcal{E}(\omega)} - \frac{\mathcal{B}(\omega)^2}{\mathcal{C}(\omega)}\right)}, \quad \text{(B.18)}$$

$$S_{xh}(\omega;\sigma_y^2,\sigma_{yv},\sigma_v^2) = \frac{\left(m_h + m_s\frac{\mathcal{A}(\omega)}{\mathcal{D}(\omega)} - m_s\frac{\mathcal{B}(\omega)^2}{\mathcal{C}(\omega)\mathcal{D}(\omega)} - m_a\frac{\mathcal{B}(\omega)}{\mathcal{C}(\omega)}\right)\omega^2\, S_{hh}(\omega)}{\left(\frac{\mathcal{A}(\omega)\mathcal{E}(\omega)}{\mathcal{D}(\omega)} - \mathcal{D}(\omega) - \frac{\mathcal{B}(\omega)^2\mathcal{E}(\omega)}{\mathcal{D}(\omega)\mathcal{C}(\omega)}\right)}, \quad \text{(B.19)}$$

$$S_{vh}(\omega;\sigma_y^2,\sigma_{yv},\sigma_v^2) = \frac{\left(m_h + m_a\frac{\mathcal{A}(\omega)}{\mathcal{B}(\omega)} + m_s\frac{\mathcal{D}(\omega)}{\mathcal{E}(\omega)} - m_a\frac{\mathcal{D}(\omega)^2}{\mathcal{E}(\omega)\mathcal{B}(\omega)}\right)\omega^2\, S_{hh}(\omega)}{\left(\frac{\mathcal{A}(\omega)\mathcal{C}(\omega)}{\mathcal{B}(\omega)} - \frac{\mathcal{D}(\omega)^2\mathcal{C}(\omega)}{\mathcal{B}(\omega)\mathcal{E}(\omega)} - \mathcal{B}(\omega)\right)}, \quad \text{(B.20)}$$

where

$$\mathcal{A}(\omega;\sigma_y^2,\sigma_{yv},\sigma_v^2) = -m_h\omega^2 + (\lambda_h+\lambda_s+\lambda_a)(j\omega) + k_h + k_s + k_a + c_a(3\sigma_y^2 - 6\sigma_{yv} + 3\sigma_v^2), \tag{B.21}$$

$$\mathcal{B}(\omega;\sigma_y^2,\sigma_{yv},\sigma_v^2) = \lambda_a(j\omega) + k_a + c_a(3\sigma_y^2 - 6\sigma_{yv} + 3\sigma_v^2), \tag{B.22}$$

$$\mathcal{C}(\omega;\sigma_y^2,\sigma_{yv},\sigma_v^2) = -m_a\omega^2 + \lambda_a(j\omega) + k_a + c_a(3\sigma_y^2 - 6\sigma_{yv} + 3\sigma_v^2), \tag{B.23}$$

$$\mathcal{D}(\omega) = \lambda_s(j\omega) + k_s, \tag{B.24}$$

$$\mathcal{E}(\omega) = -m_s\omega^2 + \lambda_a(j\omega) + k_s. \tag{B.25}$$

Now σ_y^2, σ_v^2, and σ_{yv} are still unknown, but can be determined by integrating both sides of equations (B.11), (B.13), (B.15), and (B.17) and forming the following system of equations,

$$\sigma_y^2 = \int_0^\infty S_{xx}(\omega;\sigma_y^2,\sigma_{yv},\sigma_v^2)d\omega, \tag{B.26}$$

$$\sigma_{yv} = \int_0^\infty S_{yv}(\omega;\sigma_y^2,\sigma_{yv},\sigma_v^2)d\omega, \tag{B.27}$$

$$\sigma_v^2 = \int_0^\infty S_{vv}(\omega;\sigma_y^2,\sigma_{yv},\sigma_v^2)d\omega, \tag{B.28}$$

from which we obtain $\sigma_y^2, \sigma_{yv}, \sigma_v^2$.

Suspended deck-saet system with a linear attachment

If the attachment is linear $c_a = 0$, $\mathcal{A}$, $\mathcal{B}$, and $\mathcal{C}$ in equations (B.21), (B.22), and (B.25) reduce to

$$\mathcal{A}(\omega) = -m_h\omega^2 + (\lambda_h+\lambda_s+\lambda_a)(j\omega) + k_h + k_s + k_a, \tag{B.29}$$

$$\mathcal{B}(\omega) = \lambda_a(j\omega) + k_a, \tag{B.30}$$

$$\mathcal{C}(\omega) = -m_a\omega^2 + \lambda_a(j\omega) + k_a, \tag{B.31}$$

which can be directly integrated to obtain the second order response statistics.

Bibliography

[1] A. M. Abou-Rayan and A. H. Nayfeh. "Stochastic response of a buckled beam to external and parametric random excitations". In: *In: AIAA/ASME/ASCE/AHS/ASC Structures* (1993), pp. 1030–1040.

[2] T. S. Atalik and S. Utku. "Stochastic linearization of multi-degree-of-freedom non-linear systems". In: *Earthquake Engineering & Structural Dynamics* 4.4 (1976), pp. 411–420.

[3] G. A. Athanassoulis and P. N. Gavriliadis. "The truncated Hausdorff moment problem solved by using kernel density functions". In: *Probabilistic Engineering Mechanics* 17.3 (July 2002), pp. 273–291.

[4] G. A. Athanassoulis, I. C. Tsantili, and Z. G. Kapelonis. "Two-time, response-excitation moment equations for a cubic half-oscillator under Gaussian and cubic-Gaussian colored excitation. Part 1: The monostable case". In: *arXiv preprint arXiv:1304.2195* (2013).

[5] G. Athanassoulis, I.C. Tsantili, and Z.G. Kapelonis. "Beyond the Markovian assumption: Response-excitation probabilistic solution to random nonlinear differential equations in the long time". In: *Proceedings of the Royal Society A* 471 (2016), p. 20150501.

[6] J. D. Atkinson. "Eigenfunction expansions for randomly excited non-linear systems". In: *Journal of Sound and Vibration* 30.2 (1973), pp. 153–172.

[7] J. D. Atkinson and T. K. Caughey. "Spectral density of piecewise linear first order systems excited by white noise". In: *International Journal of Non-Linear Mechanics* 3.2 (1968), pp. 137–156.

[8] G. Barone, G. Navarra, and A. Pirrotta. "Probabilistic response of linear structures equipped with nonlinear damper devices (PIS method)". In: *Probabilistic engineering mechanics* 23.2 (2008), pp. 125–133.

[9] D. A. W. Barton, S. G. Burrow, and L. R. Clare. "Energy harvesting from vibrations with a nonlinear oscillator". In: *Journal of Vibration and Acoustics* 132.2 (2010), p. 021009.

[10] G. Barton. *Elements of Green's functions and propagation: potentials, diffusion, and waves.* Oxford University Press, 1989.

[11] J. J. Beaman and J. K. Hedrick. "Improved statistical linearization for analysis and control of nonlinear stochastic systems: Part I: An extended statistical linearization technique". In: *Journal of Dynamic Systems, Measurement, and Control* 103.1 (1981), pp. 14–21.

[12] R. F. Beck, W. E. Cummins, J. F. Dalzell, P. Mandel, and W. C. Webster. "Motions in waves". In: *Principles of naval architecture* 3 (1989), p. 2.

[13] V. L. Belenky and N. B. Sevastianov. *Stability and Safety of Ships: Risk of Capsizing.* The Society of Naval Architects and Marine Engineers, 2007.

[14] J. Beran. *Statistics for long-memory processes.* Vol. 61. CRC Press, 1994.

[15] M. Beran. *Statistical Continuum Theories.* Interscience Publishers, 1968.

[16] G. W. Bluman. "Similarity solutions of the one-dimensional Fokker-Planck equation". In: *International Journal of Non-linear Mechanics* 6.2 (1971), pp. 143–153.

[17] N. N. Bogolyubov and Y. A. Mitropolskii. *Asymptotic methods in the theory of nonlinear oscillations.* Tech. rep. DTIC Document, 1955.

[18] R. C. Booton, M. V. Mathews, and W. W. Seifert. *Nonlinear Servomechanisms with Random Inputs.* MIT Dynamic Analysis and Control Laboratory, 1953.

[19] D. C. C. Bover. "Moment equation methods for nonlinear stochastic systems". In: *Journal of Mathematical Analysis and Applications* 65.2 (1978), pp. 306–320.

[20] L. J. Branstetter, G. D. Jeong, J. T.P. Yao, Y.K. Wen, and Y.K. Lin. "Mathematical modelling of structural behaviour during earthquakes". In: *Probabilistic Engineering Mechanics* 3.3 (Sept. 1988), pp. 130–145.

[21] A. Bruckner and Y. K. Lin. "Application of complex stochastic averaging to non-linear random vibration problems". In: *International journal of non-linear mechanics* 22.3 (1987), pp. 237–250.

[22] T. K. Caughey. "Equivalent linearization techniques". In: *The Journal of the Acoustical Society of America* 35.11 (1963), pp. 1706–1711.

[23] T. K. Caughey. "On the response of a class of nonlinear oscillators to stochastic excitation". In: *Proceedings Collog. Int. du Centre National de la Recherche Scientifique* 148 (1964), pp. 392–402.

[24] T. K. Caughey. "Response of a nonlinear string to random loading". In: *Journal of Applied Mechanics* 26.3 (1959), pp. 341–344.

[25] T. K. Caughey and J. K. Dienes. "Analysis of a nonlinear first-order system with a white noise input". In: *Journal of Applied Physics* 32.11 (1961), pp. 2476–2479.

[26] T. K. Caughey and F. Ma. "The exact steady-state solution of a class of nonlinear stochastic systems". In: *International Journal of Non-Linear Mechanics* 17.3 (1982), pp. 137–142.

[27] H. Cho, D. Venturi, and George E. Karniadakis. "Adaptive discontinuous Galerkin method for response-excitation PDF equations". In: *SIAM Journal on Scientific Computing* 35.4 (2013), B890–B911.

[28] T. E. Coe, J. T. Xing, R. A. Shenoi, and D. Taunton. "A simplified 3-D human body–seat interaction model and its applications to the vibration isolation design of high-speed marine craft". In: *Ocean Engineering* 36.9 (2009), pp. 732–746.

[29] W. Cousins and T. P. Sapsis. "Quantification and prediction of extreme events in a one-dimensional nonlinear dispersive wave model". In: *Physica D* 280 (2014), pp. 48–58.

[30] W. Cousins and T. P. Sapsis. "Reduced order precursors of rare events in unidirectional nonlinear water waves". In: *Journal of Fluid Mechanics* 790 (2016), pp. 368–388.

[31] D. Crandall, P. Felzenszwalb, and D. Huttenlocher. "Spatial priors for part-based recognition using statistical models". In: *Computer Vision and Pattern Recognition, 2005. CVPR 2005. IEEE Computer Society Conference on.* Vol. 1. IEEE. 2005, pp. 10–17.

[32] S. H. Crandall. "Heuristic and equivalent linearization techniques for random vibration of nonlinear oscillators". In: *8th International Conference on Nonlinear Oscillations.* Vol. 1. 1979, pp. 211–226.

[33] S. H. Crandall. "Non-Gaussian closure for random vibration of non-linear oscillators". In: *International Journal of Non-Linear Mechanics* 15.4 (1980), pp. 303–313.

[34] S. H. Crandall. "Non-Gaussian closure techniques for stationary random vibration". In: *International journal of non-linear mechanics* 20.1 (1985), pp. 1–8.

[35] S. H. Crandall. "Perturbation techniques for random vibration of nonlinear systems". In: *The Journal of the Acoustical Society of America* 35.11 (1963), pp. 1700–1705.

[36] S. H. Crandall, G. R. Khabbaz, and J. E. Manning. "Random vibration of an oscillator with nonlinear damping". In: *The Journal of the Acoustical Society of America* 36.7 (1964), pp. 1330–1334.

[37] I. G. Cumming. "Derivation of the moments of a continuous stochastic system". In: *International Journal of Control* 5.1 (1967), pp. 85–90.

[38] M. F. Daqaq. "On intentional introduction of stiffness nonlinearities for energy harvesting under white Gaussian excitations". In: *Nonlinear Dynamics* 69.3 (2012), pp. 1063–1079.

[39] M. F. Daqaq. "Transduction of a bistable inductive generator driven by white and exponentially correlated Gaussian noise". In: *Journal of Sound and Vibration* 330.11 (2011), pp. 2554–2564.

[40] A. Di Matteo, M. Di Paola, and A. Pirrotta. "Probabilistic characterization of nonlinear systems under Poisson white noise via complex fractional moments". In: *Nonlinear Dynamics* 77.3 (2014), pp. 729–738.

[41] A. Di Matteo, I. A. Kougioumtzoglou, A. Pirrotta, T. D. Spanos, and M. Di Paola. "Stochastic response determination of nonlinear oscillators with fractional derivatives elements via the Wiener path integral". In: *Probabilistic Engineering Mechanics* 38 (2014), pp. 127–135.

[42] M. Di Paola and R. Santoro. "Path integral solution for non-linear system enforced by Poisson white noise". In: *Probabilistic Engineering Mechanics* 23.2 (2008), pp. 164–169.

[43] M. Di Paola and A. Sofi. "Approximate solution of the Fokker-Planck-Kolmogorov equation". In: *Probabilistic Engineering Mechanics* 17.4 (2002), pp. 369–384.

[44] M. F. Dimentberg. "An exact solution to a certain non-linear random vibration problem". In: *International Journal of Non-Linear Mechanics* 17.4 (1982), pp. 231–236.

[45] J. F. Dunne and M. Ghanbari. "Extreme-value prediction for non-linear stochastic oscillators via numerical solutions of the stationary FPK equation". In: *Journal of Sound and Vibration* 206.5 (1997), pp. 697–724.

[46] M. I. Dykman, R. Mannella, R. V. E. McClintock, F. Moss, and S. M. Soskin. "Spectral density of fluctuations of a double-well Duffing oscillator driven by white noise". In: *Physical Review A* 37.4 (1988), p. 1303.

[47] M. I. Dykman, S. M. Soskin, and M. A. Krivoglaz. "Spectral distribution of a nonlinear oscillator performing Brownian motion in a double-well potential". In: *Physica A: Statistical Mechanics and its Applications* 133.1 (1985), pp. 53–73.

[48] M. Ferrari, V. Ferrari, M. Guizzetti, B. Andò, S. Baglio, and C. Trigona. "Improved energy harvesting from wideband vibrations by nonlinear piezoelectric converters". In: *Sensors and Actuators A: Physical* 162.2 (2010), pp. 425–431.

[49] A. D. Fokker. "Dissertation Leiden". In: *Ann. d. Physik* 43 (1914), p. 812.

[50] L. Gammaitoni, I. Neri, and H. Vocca. "Nonlinear oscillators for vibration energy harvesting". In: *Applied Physics Letters* 94.16 (2009), p. 164102.

[51] P. L. Green, E. Papatheou, and N. D. Sims. "Energy harvesting from human motion and bridge vibrations: An evaluation of current nonlinear energy harvesting solutions". In: *Journal of Intelligent Material Systems and Structures* (2013).

[52] P. L. Green, K. Worden, K. Atallah, and N. D. Sims. "The benefits of Duffing-type nonlinearities and electrical optimisation of a mono-stable energy harvester under white Gaussian excitations". In: *Journal of Sound and Vibration* 331.20 (2012), pp. 4504–4517.

[53] M. Grigoriu. "A consistent closure method for non-linear random vibration". In: *International journal of non-linear mechanics* 26.6 (1991), pp. 857–866.

[54] M. Grigoriu. "Moment closure by Monte Carlo simulation and moment sensitivity factors". In: *International journal of non-linear mechanics* 34.4 (1999), pp. 739–748.

[55] M. Grigoriu. *Stochastic calculus: applications in science and engineering.* Springer, 2002.

[56] E. Halvorsen. "Fundamental issues in nonlinear wideband-vibration energy harvesting". In: *Physical Review E* 87.4 (2013), p. 042129.

[57] N. C. Hampl. "Non-Gaussian stochastic analysis of nonlinear systems". In: *Proceedings of the second international workshop on stochastic methods in structural mechanics.* 1986, pp. 277–288.

[58] R. L. Harne and K. W. Wang. "A review of the recent research on vibration energy harvesting via bistable systems". In: *Smart Materials and Structures* 22.2 (2013), p. 023001.

[59] A. M. Hasofer and M. Grigoriu. "A new perspective on the moment closure method". In: *Journal of applied mechanics* 62.2 (1995), pp. 527–532.

[60] Q. He and M. F. Daqaq. "New Insights into Utilizing Bi-stability for Energy Harvesting under White Noise". In: *Journal of Vibration and Acoustics* (2014).

[61] R. A. Ibrahim and A. Soundararajan. "Non-linear parametric liquid sloshing under wide band random excitation". In: *Journal of Sound and Vibration* 91.1 (1983), pp. 119–134.

[62] R. A. Ibrahim, A. Soundararajan, and H. Heo. "Stochastic response of nonlinear dynamic systems based on a non-Gaussian closure". In: *Journal of applied mechanics* 52.4 (1985), pp. 965–970.

[63] L. Isserlis. "On a formula for the product-moment coefficient of any order of a normal frequency distribution in any number of variables". In: *Biometrika* (1918), pp. 134–139.

[64] W. D. Iwan and I. M. Yang. "Application of statistical linearization techniques to nonlinear multidegree-of-freedom systems". In: *Journal of Applied Mechanics* 39.2 (1972), pp. 545–550.

[65] R. Iwankiewicz and S. R. K. Nielsen. "Solution techniques for pulse problems in non-linear stochastic dynamics". In: *Probabilistic engineering mechanics* 15.1 (2000), pp. 25–36.

[66] R. N. Iyengar and P. K. Dash. "Study of the random vibration of nonlinear systems by the Gaussian closure technique". In: *Journal of Applied Mechanics* 45.2 (1978), pp. 393–399.

[67] H. K. Joo, M. A. Mohamad, and T. P. Sapsis. "Extreme events and their optimal mitigation in nonlinear structural systems excited by stochastic loads: Application to ocean engineering systems". In: *Submitted* (2017).

[68] H. K. Joo, M. A. Mohamad, and T. P. Sapsis. "Heavy-tailed response of structural systems subjected to stochastic excitation containing extreme forcing events". In: *Submitted* (2016).

[69] H. K. Joo and T. P. Sapsis. "A moment-equation-copula-closure method for nonlinear vibrational systems subjected to correlated noise". In: *Probabilistic Engineering Mechanics* (2016).

[70] H. K. Joo and T. P. Sapsis. "Performance measures for single-degree-of-freedom energy harvesters under stochastic excitation". In: *Journal of Sound and Vibration* 333.19 (2014), pp. 4695–4710.

[71] H. Karadeniz. *Stochastic analysis of offshore steel structures: an analytical appraisal.* Springer Science & Business Media, 2012.

[72] M. A. Karami and D. J. Inman. "Powering pacemakers from heartbeat vibrations using linear and nonlinear energy harvesters". In: *Applied Physics Letters* 100.4 (2012), p. 042901.

[73] I. E. Kazakov. "An approximate method for the statistical investigation of nonlinear systems". In: *Trudy VVIA im Prof. NE Zhukovskogo* 394 (1954), pp. 1–52.

[74] I. E. Kazakov. *Approximate probability analysis of the operational precision of essentially nonlinear feedback control systems.* 1956.

[75] G. Kerschen, Y. S. Lee, A. F. Vakakis, D. M. McFarland, and L. A. Bergman. "Irreversible passive energy transfer in coupled oscillators with essential nonlinearity". In: *SIAM Journal on Applied Mathematics* 66.2 (2005), pp. 648–679.

[76] G. R. Khabbaz. "Power spectral density of the response of a nonlinear system to random excitation". In: *The Journal of the Acoustical Society of America* 38.5 (1965), pp. 847–850.

[77] R. Z. Khasminskii. "A limit theorem for the solutions of differential equations with random right-hand sides". In: *Theory of Probability & Its Applications* 11.3 (1966), pp. 390–406.

[78] D. J. Kim, W. Vorus, A. TroeshROESH, and R. Gollwitzer. "Coupled hydrodynamic impact and elastic response". In: (1996).

[79] J. M. Kluger, T. P. Sapsis, and A. H. Slocum. "Robust energy harvesting from walking vibrations by means of nonlinear cantilever beams". In: *Journal of Sound and Vibration* (2015).

[80] I. A. Kougioumtzoglou and P. D. Spanos. "An analytical Wiener path integral technique for non-stationary response determination of nonlinear oscillators". In: *Probabilistic Engineering Mechanics* 28 (2012), pp. 125–131.

[81] I. A. Kougioumtzoglou and P. D. Spanos. "Nonstationary stochastic response determination of nonlinear systems: A Wiener path integral formalism". In: *Journal of Engineering Mechanics* 140.9 (2014), p. 04014064.

[82] H. U. Köylüoglu, S. R. K. Nielsen, and R. Iwankiewicz. "Response and reliability of Poisson-driven systems by path integration". In: *Journal of engineering mechanics* 121.1 (1995), pp. 117–130.

[83] H. A. Kramers. "Brownian motion in a field of force and the diffusion model of chemical reactions". In: *Physica* 7.4 (1940), pp. 284–304.

[84] E. Kreuzer and W. Sichermann. "The effect of sea irregularities on ship rolling". In: *Computing in Science & Engineering* 8.3 (2006), pp. 26–34.

[85] P. R. Kry. "Third Canadian geotechnical colloquium: Ice forces on wide structures". In: *Canadian Geotechnical Journal* 17.1 (1980), pp. 97–113.

[86] R. S. Langley. "On various definitions of the envelope of a random process." In: *Journal of Sound and Vibration* 105.3 (1986), pp. 503–512.

[87] Y. K. Lin. "Application of nonstationary shot noise in the study of system response to a class of nonstationary excitations". In: *Journal of Applied Mechanics* 30.4 (1963), pp. 555–558.

[88] Y. K. Lin. *Probabilistic theory of structural dynamics.* Krieger Publishing Company, 1976.

[89] Y. K. Lin. "Stochastic stability of wind-excited long-span bridges". In: *Probabilistic Engineering Mechanics* 11.4 (Oct. 1996), pp. 257–261.

[90] Y. K. Lin and C. Q. Cai. *Probabilistic structural dynamics: advanced theory and applications.* Mcgraw-hill Professional Publishing, 1995.

[91] P. C. Liu. "A chronology of freaque wave encounters". In: *Geofizika* 24 (1) (2007).

[92] Q. Liu and H. G. Davies. "Application of non-Gaussian closure to the nonstationary response of a Duffing oscillator". In: *International journal of non-linear mechanics* 23.3 (1988), pp. 241–250.

[93] J. Luo, N. E. Wierschem, S. A. Hubbard, L. A. Fahnestock, D. D. Quinn, F. D. Michael, B. F. Spencer, A. F. Vakakis, and L. A. Bergman. "Large-scale experimental evaluation and numerical simulation of a system of nonlinear energy sinks for seismic mitigation". In: *Engineering Structures* 77 (2014), pp. 34–48.

[94] A. J. Majda and M. Branicki. "Lessons in Uncertainty Quantification for Turbulent Dynamical Systems". In: *Discrete and Continuous Dynamical Systems* 32 (2012), pp. 3133–3221.

[95] A. K. Malhotra and J. Penzien. "Nondeterministic analysis of offshore structures". In: *Journal of the Engineering Mechanics Division* 96.6 (1970), pp. 985–1003.

[96] B. P. Mann and N. D. Sims. "Energy harvesting from the nonlinear oscillations of magnetic levitation". In: *Journal of Sound and Vibration* 319.1 (2009), pp. 515–530.

[97] J. E. Manning. "Response spectra for nonlinear oscillators". In: *Journal of Engineering for Industry* 97.4 (1975), pp. 1223–1226.

[98] C. S. Manohar. "Methods of nonlinear random vibration analysis". In: *Sadhana* 20.2-4 (1995), pp. 345–371.

[99] R. Masana and M. F. Daqaq. "Response of duffing-type harvesters to band-limited noise". In: *Journal of Sound and Vibration* 332.25 (2013), pp. 6755–6767.

[100] A. Masud and L. A. Bergman. "Solution of the four dimensional Fokker-Planck Equation: Still a challenge". In: *ICOSSAR 2005* (2005), pp. 1911–1916.

[101] C. Meyer. "The bivariate normal copula". In: *Communications in Statistics-Theory and Methods* 42.13 (2013), pp. 2402–2422.

[102] M. A. Mohamad, W. Cousins, and T. P. Sapsis. "A probabilistic decomposition-synthesis method for the quantification of rare events due to internal instabilities". In: *Journal of Computational Physics* 322 (2016), pp. 288–308.

[103] M. A. Mohamad and T. P. Sapsis. "Probabilistic description of extreme events in intermittently unstable systems excited by correlated stochastic processes". In: *SIAM/ASA J. of Uncertainty Quantification* 3.1 (2015), pp. 709–736.

[104] M. A. Mohamad and T. P. Sapsis. "Probabilistic response and rare events in Mathieu's equation under correlated parametric excitation". In: *Ocean Engineering Journal* 120 (2016), pp. 289–297.

[105] P. Müller, C. Garrett, and A. Osborne. "Rogue waves". In: *Oceanography* 18.3 (2005), p. 66.

[106] A. Naess and J. M. Johnsen. "Response statistics of nonlinear, compliant offshore structures by the path integral solution method". In: *Probabilistic Engineering Mechanics* 8.2 (1993), pp. 91–106.

[107] A. Naess and T. Moan. *Stochastic dynamics of marine structures.* Cambridge University Press, 2012.

[108] R. B. Nelsen. *An introduction to copulas.* Springer Science & Business Media, 2007.

[109] M. N. Noori, A. Saffar, and H. Davoodi. "A comparison between non-Gaussian closure and statistical linearization techniques for random vibration of a non-linear oscillator". In: *Computers & structures* 26.6 (1987), pp. 925–931.

[110] K. Ochi M. *Applied probability and stochastic processes: In Engineering and Physical Sciences.* Vol. 226. Wiley-Interscience, 1990.

[111] K. Olausson and K. Garme. "Prediction and evaluation of working conditions on high-speed craft using suspension seat modeling". In: *Proceedings of the Institution of Mechanical Engineers, Part M: Journal of Engineering for the Maritime Environment* 229.3 (2015), pp. 281–290.

[112] M. Onorato, A. R. Osborne, M. Serio, and S. Bertone. "Freak waves in random oceanic sea states". In: *Physical Review Letters* 86.25 (2001), p. 5831.

[113] H. C. Öttinger. *Stochastic processes in polymeric fluids: tools and examples for developing simulation algorithms.* Springer Science & Business Media, 2012.

[114] L. Qu and W. Yin. "Copula density estimation by total variation penalized likelihood with linear equality constraints". In: *Computational Statistics & Data Analysis* 56.2 (2012), pp. 384–398.

[115] D. D. Quinn, S. Hubbard, N. Wierschem, M. A. Al-Shudeifat, R. J. Ott, J. Luo, B. F. Spencer, D. M. McFarland, A. F. Vakakis, and L. A. Bergman. "Equivalent modal damping, stiffening and energy exchanges in multi-degree-of-freedom systems with strongly nonlinear attachments". In: *Proceedings of the Institution of Mechanical Engineers, Part K: Journal of Multi-body Dynamics* 226.2 (2012), pp. 122–146.

[116] K. P. Ranieri, R. M. Berman, S. D. Wood, R. J. Garelick, C. J. Hauck, and M. G. Stoddard. *Active deck suspension system.* US Patent 6,763,774. 2004.

[117] J. W. S. B. Rayleigh. *The theory of sound.* Vol. 2. Macmillan, 1896.

[118] J. R. Red-Horse and P. D. Spanos. "A Closed Form Solution for a Class of Non-Stationary Nonlinear Random Vibration Problems". In: *Nonlinear Stochastic Dynamic Engineering Systems.* Springer, 1988, pp. 393–403.

[119] M. R. Riley and T. W. Coats. "A Simplified Approach for Analyzing Accelerations Induced by Wave- Impacts in High-Speed Planing Craft". In: *3rd Chesapeake Power Boat Symposium* June (2012), pp. 14–15.

[120] M. R. Riley, T. Coats, K. Haupt, and D. Jacobson. "Ride Severity Index - A New Approach to Quantifying the Comparison of Acceleration Responses of High-Speed Craft". In: *FAST 2011 11th International Conference on Fast Sea Transportation* September (2011), pp. 693–699.

[121] J. B. Roberts. "The energy envelope of a randomly excited non-linear oscillator". In: *Journal of Sound and Vibration* 60.2 (1978), pp. 177–185.

[122] J. B. Roberts and P. D. Spanos. *Random vibration and statistical linearization.* Courier Dover Publications, 2003.

[123] J. B. Roberts and P. D. Spanos. "Stochastic averaging: an approximate method of solving random vibration problems". In: *International Journal of Non-Linear Mechanics* 21.2 (1986), pp. 111–134.

[124] J. Roberts and P. Spanos. *Random Vibration and Statistical Linearization.* Dover Publications, 2003.

[125] N. G. F. Sancho. "Technique for finding the moment equations of a nonlinear stochastic system". In: *Journal of Mathematical Physics* 11.3 (1970), pp. 771–774.

[126] T. P. Sapsis and G. A. Athanassoulis. "New partial differential equations governing the joint, response-excitation, probability distributions of nonlinear systems, under general stochastic excitation". In: *Probab. Eng. Mech.* 23.2-3 (2008), pp. 289–306.

[127] T. P. Sapsis, D. Dane Quinn, Alexander F. Vakakis, and Lawrence A. Bergman. "Effective stiffening and damping enhancement of structures with strongly nonlinear local attachments". In: *Journal of vibration and acoustics* 134.1 (2012), p. 011016.

[128] T. P. Sapsis, A. F. Vakakis, and L. A. Bergman. "Effect of stochasticity on targeted energy transfer from a linear medium to a strongly nonlinear attachment". In: *Probabilistic Engineering Mechanics* 26.2 (2011), pp. 119–133.

[129] Y. Sawaragi. *Statistical Studies on non-linear control systems.* Nippon Print. and Pub. Co., 1962.

[130] G. I. Schuëller and C. G. Bucher. "Nonlinear damping and its effects on the reliability estimates of structural stystems". In: *Random Vibration-Status and Recent Developments: The Stephen Harry Crandall Festschrift* 14 (1986), p. 389.

[131] P. R. Sethna. "An extension of the method of averaging". In: *Quarterly of Applied Mathematics* 25.2 (1967), pp. 205–211.

[132] P. R. Sethna and S. Orey. "Some asymptotic results for a class of stochastic systems with parametric excitations". In: *International Journal of Non-Linear Mechanics* 15.6 (1980), pp. 431–441.

[133] T. Shimogo. "Nonlinear Vibrations of Systems under Random Loading". In: *Bulletin of JSME* 6.21 (1963), pp. 44–52.

[134] M. A. AL-Shudeifat, A. F. Vakakis, and L. A. Bergman. "Shock Mitigation by Means of Low- to High-Frequency Nonlinear Targeted Energy Transfers in a Large-Scale Structure". In: *Journal of Computational and Nonlinear Dynamics* 11.2 (2015).

[135] M. A. AL-Shudeifat, N. Wierschem, D. D. Quinn, A. F. Vakakis, L. A. Bergman, and B. F. Spencer. "Numerical and experimental investigation of a highly effective single-sided vibro-impact non-linear energy sink for shock mitigation". In: *International Journal of Non-Linear Mechanics* 52 (2013), pp. 96–109.

[136] K. Sobczyk. *Stochastic differential equations: with applications to physics and engineering.* Vol. 40. Springer, 2001.

[137] L. Socha. *Linearization methods for stochastic dynamic systems.* Vol. 730. Springer, 2008.

[138] C. Soize. *The Fokker-Planck equation for stochastic dynamical systems and its explicit steady state solutions.* Vol. 17. World Scientific, 1994.

[139] S. R. Soni and K. Surendran. "Transient response of nonlinear systems to stationary random excitation". In: *Journal of Applied Mechanics* 42.4 (1975), pp. 891–893.

[140] T. T. Soong and M. Grigoriu. "Random vibration of mechanical and structural systems". In: *NASA STI/Recon Technical Report A* 93 (1993), p. 14690.

[141] T. D. Spanos. "Formulation of stochastic linearization for symmetric or asymmetric MDOF nonlinear systems". In: *Journal of Applied Mechanics* 47.1 (1980), pp. 209–211.

[142] S. Spence and M. Gioffrè. "Large scale reliability-based design optimization of wind excited tall buildings". In: *Probabilistic Engineering Mechanics* 28 (2012), pp. 206–215.

[143] R. L. Stratonovich and R. A. Silverman. "Topics in the Theory of Random Noise. Volume II". In: (1967).

[144] C. W. S. To. *Nonlinear random vibration: Analytical techniques and applications.* CRC Press, 2011.

[145] N. C. Townsend, T. E. Coe, P. A. Wilson, and R. A. Shenoi. "High speed marine craft motion mitigation using flexible hull design". In: *Ocean Engineering* 42 (2012), pp. 126–134.

[146] A. F. Vakakis. "Inducing passive nonlinear energy sinks in vibrating systems". In: *Journal of Vibration and Acoustics* 123.3 (2001), pp. 324–332.

[147] A. F. Vakakis, O. V. Gendelman, L. A. Bergman, D. M. McFarland, G. Kerschen, and Y. S. Lee. *Nonlinear targeted energy transfer in mechanical and structural systems.* Vol. 156. Springer Science & Business Media, 2008.

[148] A. F. Vakakis, L. I. Manevitch, O. V. Gendelman, and L. A. Bergman. "Dynamics of linear discrete systems connected to local, essentially non-linear attachments". In: *Journal of Sound and Vibration* 264.3 (2003), pp. 559–577.

[149] A. F. Vakakis, L. I. Manevitch, A. I. Musienko, G. Kerschen, and L. A. Bergman. "Transient dynamics of a dispersive elastic wave guide weakly coupled to an essentially nonlinear end attachment". In: *Wave Motion* 41.2 (2005), pp. 109–132.

[150] W. E. Vander Velde. *Multiple-input describing functions and nonlinear system design.* New York: McGraw-Hill, 1968.

[151] M. Vasta. "Exact stationary solution for a class of non-linear systems driven by a non-normal delta-correlated process". In: *International journal of non-linear mechanics* 30.4 (1995), pp. 407–418.

[152] A. E. P. Veldman, R. Luppes, T. Bunnik, R. H. M. Huijsmans, B. Duz, B. Iwanowski, R. Wemmenhove, M. J. A. Borsboom, P. R. Wellens, H. J. L. Van Der Heiden, et al. "Extreme wave impact on offshore platforms and coastal constructions". In: *ASME 2011 30th International Conference on Ocean, Offshore and Arctic Engineering.* American Society of Mechanical Engineers. 2011, pp. 365–376.

[153] D. Venturi, T. P. Sapsis, H. Cho, and G. E. Karniadakis. "A computable evolution equation for the joint response-excitation probability density function of stochastic dynamical systems". In: *Proceedings of the Royal Society A: Mathematical, Physical and Engineering Science* 468.2139 (2012), pp. 759–783.

[154] M. F. Wehner and W. G. Wolfer. "Numerical evaluation of path-integral solutions to Fokker-Planck equations". In: *Physical Review A* 27.5 (1983), p. 2663.

[155] S. F. Wojtkiewicz, E. A. Johnson, L. A. Bergman, M. Grigoriu, and B. F. Spencer Jr. "Response of stochastic dynamical systems driven by additive Gaussian and Poisson white noise: Solution of a forward generalized Kolmogorov equation by a spectral finite difference method". In: *Computer methods in applied mechanics and engineering* 168.1 (1999), pp. 73–89.

[156] S. F. Wojtkiewicz, B. F. Spencer Jr, and L. A. Bergman. "On the cumulant-neglect closure method in stochastic dynamics". In: *International journal of non-linear mechanics* 31.5 (1996), pp. 657–684.

[157] W. F. Wu and Y. K. Lin. "Cumulant-neglect closure for non-linear oscillators under random parametric and external excitations". In: *International Journal of Non-Linear Mechanics* 19.4 (1984), pp. 349–362.

[158] D. Xiu and G. Karniadakis. "Modeling uncertainty in flow simulations via generalized polynomial chaos". In: *J. Comp. Phys.* 187 (2003), pp. 137–167.

[159] D. Xiu and G. Karniadakis. "The Wiener-Askey polynomial chaos for stochastic differential equations". In: *SIAM Journal on Scientific Computing* 24 (2002), pp. 619–644.

[160] Y. Zeng and W. Q. Zhu. "Stochastic averaging of strongly nonlinear oscillators under Poisson white noise excitation". In: *IUTAM symposium on nonlinear stochastic dynamics and control*. Springer. 2011, pp. 147–155.

[161] W. Q. Zhu. "Stochastic averaging methods in random vibration". In: *Applied Mechanics Reviews* 41.5 (1988), pp. 189–199.

[162] W. Q. Zhu. "Stochastic averaging of the energy envelope of nearly Lyapunov systems". In: *Random Vibrations and Reliability, Proceedings of the IUTAM Symposium, Akademie, Berlin.* 1983, pp. 347–357.

[163] W. Q. Zhu and J. S. Yu. "On the response of the Van der Pol oscillator to white noise excitation". In: *Journal of sound and vibration* 117.3 (1987), pp. 421–431.